

DEPARTMENT OF CHEMISTRY, UNIVERSITY OF JYVÄSKYLÄ
RESEARCH REPORT No. 204

**EXPERIMENTAL AND COMPUTATIONAL STUDIES OF
UNCONVENTIONAL MAIN GROUP COMPOUNDS: STABLE
RADICALS AND REACTIVE INTERMEDIATES**

BY

JUHA HURMALAINEN

Academic Dissertation for the Degree of
Doctor of Philosophy

*To be presented, by permission of the Faculty of Mathematics and Science of the
University of Jyväskylä, for public examination in Auditorium KEM4, on October 27th,
2017 at 12 noon.*



UNIVERSITY OF JYVÄSKYLÄ

Copyright ©, 2017
University of Jyväskylä
Jyväskylä, Finland
ISBN 978-951-39-7184-7 (print)
ISBN 978-951-39-7185-4 (electronic)
ISSN 0357-346X

ABSTRACT

Hurmalainen, Juha

Experimental and computational studies of unconventional main group compounds: stable radicals and reactive intermediates

Jyväskylä: University of Jyväskylä, 2017, 89 p.

(Department of Chemistry, University of Jyväskylä Research Report Series

ISSN: 0357-346X)

ISBN: 978-951-39-7184-7 (print), 978-951-39-7185-4 (electronic)

Ever since their discovery, radicals have intrigued the minds of experimental and theoretical chemists alike. While the vast majority of radicals are transient species, a large number of stable and persistent radicals are also known. This has enabled the use of radicals in different applications. For example, radicals are highly useful in chemical synthesis due to their selectivity and functional group tolerance. Detailed knowledge of the electronic structure of synthetic intermediates, both radical and non-radical, enables chemists to improve existing synthesis routes and to design completely new ones.

This thesis is divided into two parts. The first part begins with an introduction to the chemistry of stable and persistent radicals and presents some seminal discoveries in the field. A brief review of the role of radicals in synthetic chemistry is then given. This is followed by an overview of reactive intermediates in main group chemistry. Some novel methods used in the characterisation of such intermediates are presented along with selected examples of notable results.

The second part outlines the most significant findings reported in the five research papers associated with this thesis. The discussion begins with a comprehensive analysis of structural effects induced by redox processes in a 2,2'-biquinoline complex of boron. A new synthetic route to neutral phenothiazinyl radicals via Smiles rearrangement is then presented. This is followed by a discussion of radical intermediates in homocoupling reactions of benzo[*b*]furans and benzo[*b*]thiophenes. The role of perfluoroarylboranes in the activation of silane Si-H bonds in hydrosilylation reactions is then presented. Finally, the importance of a thorough structural characterisation is illustrated by a complete scrutiny of a putative intermediate in the formation of tetra-*n*-butylammonium bicarbonate. Overall, the reported results advance our knowledge of stable main group radicals and provide new insight about reactive intermediates in quintessential chemical reactions.

Keywords: main group chemistry, stable radicals, reactive intermediates, synthesis, X-ray crystallography, EPR spectroscopy, computational chemistry

Author's address Juha Hurmalainen
Department of Chemistry
P.O. Box 35
FI-40014 University of Jyväskylä
Finland
juha.p.hurmalainen@jyu.fi

Supervisors Professor Heikki M. Tuononen
Department of Chemistry
University of Jyväskylä
Jyväskylä, Finland

Professor Jason A.C. Clyburne
Department of Chemistry
Saint Mary's University
Halifax, NS, Canada

Senior Lecturer Jari Konu
Department of Chemistry
University of Jyväskylä
Jyväskylä, Finland

Reviewers Professor Paul J. Ragona
Department of Chemistry
The University of Western Ontario
London, ON, Canada

Doctor Raija Oilunkaniemi
Department of Chemistry
University of Oulu
Oulu, Finland

Opponent Associate Professor Jaclyn L. Brusso
Department of Chemistry
University of Ottawa
Ottawa, ON, Canada

PREFACE

The work presented in this dissertation was carried out at the Department of Chemistry at the University of Jyväskylä and at Saint Mary's University in Halifax, Canada, between 2012 and 2016.

I wish to express my deepest gratitude to my supervisor, Prof. Heikki M. Tuononen, for the opportunity to join his research group and for his support and guidance throughout this intriguing and challenging project. I also wish to thank my co-supervisor, Senior Lecturer Jari Konu, for his invaluable help and assistance, especially at the beginning of this project when he introduced me to Schlenk chemistry. Furthermore, I am ever so grateful to Prof. Jason A.C. Clyburne for his guidance and hospitality during my research visit in Canada.

The reviewers of this dissertation, Prof. Paul J. Ragogna and Dr. Raija Oilunkaniemi, are gratefully acknowledged for their invaluable comments and suggestions.

I wish to express my sincere gratitude to my fellow co-workers, both past and present, for insightful conversations and advice, as well as for the companionship they have shown over the years. I am especially indebted to Dr. Ian S. Morgan and Dr. Aaron Mailman for their help and advice in the laboratory. I also wish to thank M.Sc. Akseli Mansikkamäki and Dr. Anssi Peuronen for their help with computational chemistry and X-ray crystallography, respectively.

This work would not have been possible without the help and support of my beloved family. Thank you for being a part of my life and encouraging me to go forward. Similarly, I wish to thank my friends for allowing me to get my mind off work from time to time and for helping me to get through the harder times during this project.

The financial support from the University of Jyväskylä, Academy of Finland, Emil Aaltonen Foundation and the Finnish Chemical Society's Foundation for the Finnish Chemical Congress is gratefully acknowledged.

Jyväskylä, September 2017

Juha Hurmalainen

LIST OF ORIGINAL PUBLICATIONS

This dissertation is based on the following original research papers, which are hereafter referred to by their Roman numerals.

- I** Hurmalainen, J.; Mansikkamäki, A.; Morgan, I. S.; Peuronen, A.; Tuononen, H. M. **Synthesis and characterisation of p-block complexes of biquinoline at different ligand charge states**, *Dalton Trans.* **2017**, *46*, 1377-1381.
- II** Vasko, P.; Hurmalainen, J.; Mansikkamäki, A.; Peuronen, A.; Mailman, A.; Tuononen, H. M. **Synthesis of new hybrid 1,4-thiazinyl-1,2,3-dithiazolyl radicals via Smiles rearrangement**, *Dalton Trans.* **2017**, *in press*, DOI: 10.1039/c7dt03243a
- III** Wirtanen, T.; Muuronen, M.; Hurmalainen, J.; Tuononen, H. M.; Nieger, M.; Helaja, J. **Intermolecular oxidative dehydrogenative 3,3'-coupling of benzo[*b*]furans and benzo[*b*]thiophenes promoted by DDQ/H⁺: total synthesis of shandougenine B**, *Org. Chem. Front.* **2016**, *3*, 1738-1745.
- IV** Houghton, A. Y.; Hurmalainen, J.; Mansikkamäki, A.; Piers, W. E.; Tuononen, H. M. **Direct observation of a borane-silane complex involved in frustrated Lewis-pair-mediated hydrosilylations**, *Nature Chem.* **2014**, *6*, 983-988.
- V** Hurmalainen, J.; Land, M. A.; Robertson, K. N.; Roberts, C. J.; Morgan, I. S.; Tuononen, H. M.; Clyburne, J. A. C. **Comment on "Crystallographic Snapshot of an Arrested Intermediate in the Biomimetic Activation of CO₂"**, *Angew. Chem. Int. Ed.* **2015**, *54*, 7484-7487.

Author's contribution

The author of the present dissertation has performed all experimental work for the original research Paper I. He has performed synthetic work for Paper V and has taken part in the syntheses for Paper II. He has also carried out EPR- and cyclic voltammetry studies for Paper III. The author has performed quantum chemical calculations for the research Papers I, II and IV. He has written the original manuscript draft for Paper I and has participated in the writing of manuscript drafts for Papers II - V.

Other contributions

The following is a list of the author's other publications related to the topic but not included in this dissertation:

- i** Taponen, A; Lehmann, A; Hurmalainen, J.; Rautiainen, J. M.; Hänninen, M. H.; Mailman, A.; Tuononen, H. M. **Isolation and Characterization of the First Example of a Triazonyl Anion Radical and in situ Generation of New Ruthenium Complexes**, *manuscript in preparation*.
- ii** Barry, B.M.; Soper, R. G.; Hurmalainen, J.; Mansikkamäki, A.; Robertson, K. N.; McClennan, W. L.; Veinot, A. J.; Roemmele, T. L.; Werner-Zwanziger, U.; Boéré, R. T.; Tuononen, H. M.; Clyburne, J. A. C.; Masuda, J. D. **Mono- and Bis-Imidazolidinium Ethynyl Cations and the Reduction of the Latter to give an Extended Bis-1,4-([3]Cumulene)-Carbo-Quinoid System**, *manuscript in preparation*.

CONTENTS

ABSTRACT

PREFACE

LIST OF ORIGINAL PUBLICATIONS

CONTENTS

ABBREVIATIONS

1	INTRODUCTION	11
1.1	Aim of the work	12
2	STABLE AND TRANSIENT MAIN GROUP RADICALS	13
2.1	Stable and persistent radicals.....	13
2.1.1	Features affecting the stability of radicals	13
2.1.2	Radicals derived from hydrocarbons.....	14
2.1.3	Hydrazyl radicals.....	19
2.1.4	Nitroxides and nitronyl nitroxides.....	20
2.1.5	Sulphur-nitrogen radicals	22
2.1.6	Sulphur radicals	24
2.1.7	Inorganic main group radicals	25
2.1.8	Biradicals and biradicaloids	30
2.2	Transient radicals in organic synthesis.....	33
3	REACTIVE INTERMEDIATES	39
3.1	Characterisation of reactive species	39
3.1.1	Mass spectrometric studies of chemical intermediates	39
3.1.2	Diffusion-ordered NMR in the characterisation of reaction intermediates	43
3.1.3	Isolated and characterised intermediates	45
4	RESULTS AND DISCUSSION	53
4.1	Experimental methods	53
4.2	Computational methods	54
4.3	Stable main group radicals	54
4.3.1	p-Block complexes of 2,2'-biquinoline.....	54
4.3.2	Hybrid 1,4-thiazine-1,2,3-dithiazolyl radicals.....	58
4.4	Reactive intermediates	63
4.4.1	DDQ-generated radical intermediate.....	63
4.4.2	Borane-silane complex involved in metal-free hydrosilylations.....	68
4.4.3	Structure elucidation of a purported reactive intermediate ...	72
5	CONCLUSIONS	77
	REFERENCES.....	79

ABBREVIATIONS

biq	2,2'-biquinoline
bpy	2,2'-bipyridine
CB	cyclobutanediyl
CP(1,3)	cyclopentane-1,3-diyl
DCE	dichloroethane
DCM	dichloromethane
DDQ	2,3-dichloro-5,6-cyano-1,4-quinone
DESI	desorption electrospray ionisation
DFT	density functional theory
Dipp	2,6-diisopropylphenyl
DOSY	diffusion-ordered spectroscopy
DPPH	<i>N,N'</i> -diphenyl- <i>N'</i> -picrylhydrazyl
DTDA	1,2,3,5-dithiadiazolyl
ECC	external calibration curve
EPR	electron paramagnetic resonance
EWG	electron-withdrawing group
ESI-MS	electrospray ionisation mass spectrometry
FLP	frustrated Lewis pair
HFCC	hyperfine coupling constant
HOMO	highest occupied molecular orbital
ICC	internal calibration curve
LUMO	lowest unoccupied molecular orbital
MCR	multicomponent reaction
Mes	mesityl; 1,3,5-trimethylphenyl
MS	mass spectrometry
MsOH	methanesulphonic acid
NBO	natural bond orbital
NHC	<i>N</i> -heterocyclic carbene
NMR	nuclear magnetic resonance
Otf	triflate; trifluoromethanesulfonate
PRE	persistent radical effect
PSI	pressurised sample infusion
SCE	saturated calomel electrode
SET	single electron transfer
SOMO	singly occupied molecular orbital
SR	Smiles rearrangement
TEMPO	(2,2,6,6-tetramethyl-piperidin-1-yl)oxyl
TFA	trifluoroacetic acid
THF	tetrahydrofuran
TME	tetramethyleneethane
TMM	trimethylenemethane
TS	transition state

1 INTRODUCTION

Modern understanding of the chemistry of organic compounds started to evolve during the nineteenth century. Disputes surrounding the existence of free radicals were not insubstantial when Moses Gomberg published his seminal paper on the synthesis of a triphenylmethyl radical in 1900.¹ Gomberg's discovery had a significant impact on the chemical community and, after a tight scrutiny, his landmark result was globally accepted, setting the stage for the flourishing development of chemistry of odd-electron species.

A radical is a compound that has at least one unpaired electron. In other words, radicals are subvalent compounds with at least one bond less than could be expected by simple valency considerations. Typically, this causes radicals to be transient species that keenly react with other compounds or with themselves, forming dimers or polymers. A plethora of chemical reactions progress via radical intermediates, and radicals are also found in living organisms in which they control various vital processes.

There are, however, a great number of radicals that defy the common conception of odd-electron species existing only for a fleeting moment. Some radicals have lifetimes long enough so that they can be observed by conventional characterisation methods while others are so stable that they can be isolated as pure compounds. There are even radicals that are unreactive towards both oxygen and water and thus can exist indefinitely under ambient conditions. Indeed, there are nowadays many families of stable radicals of which several have been known for decades.

In many instances, the driving force behind radical research comes from fundamental considerations, that is, from the desire to understand the structure, bonding and reactivity of open shell compounds. However, the combination of stability and unpaired electrons has generated significant interest in developing novel applications that take advantage of these attributes. Stable radicals have a history of being used as reporter molecules to acquire structural information via EPR spectroscopy. More recently, a lot of attention has been focused on developing magnetic and conducting materials that exploit radicals as building blocks, either as pure substances or as ligands in metal complexes. Stable radi-

als are also used in a variety of chemical reactions such as in catalysis and polymer synthesis.

While the number of stable radicals is steadily growing, the majority of known open shell compounds are highly reactive species, an attribute they have in common with reaction intermediates, which are chemical entities that precede the formation of final products. Reaction intermediates are typically highly reactive, be they open or closed shell species, which shortens their lifetime and hinders their characterisation by conventional characterisation methods. However, as these fleeting chemical entities play a key role in chemical processes, their characterisation and even isolation is crucial in the quest to enhance our knowledge of chemistry.

In many instances, reactive intermediates can only be characterised using fast time-resolved spectroscopic methods. However, ever so often it happens that a highly reactive species can be isolated under some specific conditions, which enables characterisation by conventional methods. Gaining an in-depth knowledge of the molecular structure and properties of reactive intermediates greatly enhances our knowledge of chemical reactivity as it allows fine-tuning of existing synthesis methods as well as the design of new ones that offer paths to possibly hitherto unknown compounds.

1.1 Aim of the work

The goal of this research project was twofold: first, to develop new stable main group radicals and study their chemical and structural properties; and second, to investigate selected chemical reactions and characterise their reactive intermediates. Schlenk techniques played a key role in the synthetic work, whereas X-ray crystallography, EPR spectroscopy and computational chemistry were the primary tools used to investigate the characteristics of synthesised compounds and reaction intermediates.

The synthesis of new radical species was accomplished via two routes. The first route involved the stabilisation of an anionic biquinoline radical via coordination with a main group element centre.^I The second route took advantage of fusing the reactive phenothiazinyl radical with the well-known 1,2,3-dithiazolyl moiety to generate new hybrid 1,4-thiazinyl-1,2,3-dithiazolyl radicals via Smiles rearrangement.^{II}

The characterisation of important reaction intermediates was achieved in three instances. First, the role of radical intermediates in oxidative dehydrogenative coupling reactions was examined.^{III} Second, the intermediates in frustrated Lewis-pair-mediated hydrosilylation reactions were characterised computationally and the results substantiated with subsequent crystallographic studies.^{IV} Third, the recent claims of characterising a novel intermediate in biomimetic activation of CO₂ were examined in detail to correctly identify the species in question.^V

2 STABLE AND TRANSIENT MAIN GROUP RADICALS

This chapter aims to introduce the reader to the chemistry of radicals. The realm of odd-electron main group species is vast and diverse, so rather than providing a comprehensive review of the field, the focus will be on selected significant breakthroughs and seminal discoveries that have taken place during the past century. The first part of this chapter focuses on the chemistry of “organic” main group radicals, that is, radicals containing atoms C, N, O and S. “Inorganic” radicals based on other main group elements are then covered, followed by a brief look at the distinctive chemistry of diradicals. At the end of the chapter, a short overview of radicals as reaction intermediates and other transient species is given.

2.1 Stable and persistent radicals

Many radicals are highly reactive chemical species and, thus, short-lived. For the more longer-lived radicals, the terms *stable* and *persistent* are used rather subjectively. Griller and Ingold proposed the pragmatic approach of calling a radical stable if it can be isolated and handled as a pure compound under ambient conditions but calling a radical persistent if it cannot be isolated but can be detected by spectroscopic methods.² In this work, the description *stable* will be confined to radicals that can be isolated and stored without decomposition, either indefinitely or for long periods of time, at room temperature under an inert atmosphere. Griller and Ingold’s definition of *persistent* radicals will be employed as originally described.

2.1.1 Features affecting the stability of radicals

There are a few essential methods that can be used to stabilise radical species.^{3,4} One of the most profound ones is the steric protection of the reactive moiety

with the help of bulky substituents, which contributes to both kinetic and thermodynamic stability. Such a method does have its drawbacks, however, as many of the applications for which radicals are used require the unpaired electron to be able to interact with its surroundings. In other words, by employing bulky substituents, the stability of a radical species can be increased, but its ability to interact with its surroundings is simultaneously suppressed.

Other methods to stabilise radical species involve modifications to the electronic structure of the subvalent compound in question. A large number of stable radicals are heteroatom based. Nitrogen, oxygen and sulphur are especially good spin carriers. There are effectively two factors contributing to this phenomenon. The atoms N, O and S are lone-pair rich, which increases Pauli repulsion when two or more of these atoms are catenated, thus making catenation thermodynamically unfavoured.⁴ These same heteroatoms are also some of the most electronegative ones, which leads to lesser reactivity towards oxygen than, for example, that observed for typical carbon-centred radicals.

Another method to stabilise radicals is to delocalise the unpaired electron throughout the molecular framework. The majority of stable main group radicals are so-called π -radicals, which enables spin delocalisation over any section of the compound that is part of the same π -system. This, in turn, decreases the spin density on any one atom, thereby lowering the reactivity at that particular site. However, to say that more delocalisation is always better would be a great oversimplification as that would ignore the fact that spin localisation on certain heteroatom centres provides stabilisation as well.

Other factors governing the stability of radicals have received less attention but should, nevertheless, not be overlooked. For example, major changes in charge distribution can affect the stability drastically, which poses important restrictions on what substituents a particular radical framework can incorporate. Furthermore, certain classes of compounds can be used to stabilise radicals as they are able to withdraw spin density rather effectively. In this context, *N*-heterocyclic carbenes (NHCs) have recently been employed in stabilising new odd-electron species via delocalisation of electron density to their formally empty p-orbital through π -backbonding interactions.⁵

2.1.2 Radicals derived from hydrocarbons

Gomberg's synthesis of the triphenylmethyl radical is considered to be the starting point of free radical chemistry.^{1,6} Specifically, he reacted triphenylmethyl chloride with metallic silver or zinc to obtain a coloured solution which was identified to contain the triphenylmethyl radical **1** (Figure 1). Much controversy surrounded the identity of **1** over the following years. The dispute ended in 1910 when Wilhelm Schlenk and co-workers managed to synthesise tris(4-biphenyl)methyl **2** (Figure 1).⁷ The deeply coloured solid contained a dimer of **2** which, however, was almost completely dissociated in solution, thereby confirming the identity of **1**.

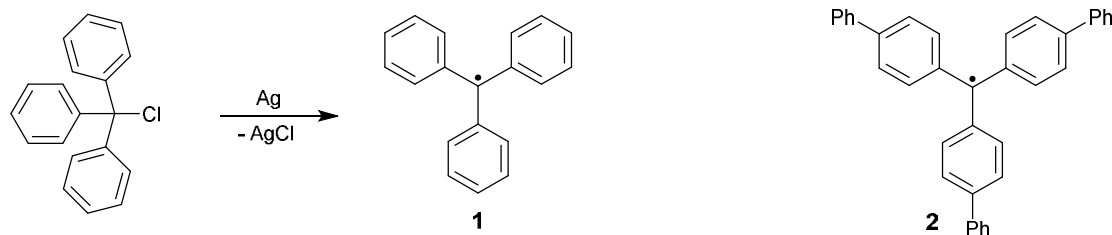


Figure 1. Synthesis of triphenylmethyl radical **1**¹ (left) and the structure of tris(4-biphenyl)methyl radical **2**⁷ (right).

In dilute and deoxygenated solutions, **1** exists in equilibrium with the dimeric form **3** (Figure 2). Thus, radical **1** cannot be isolated and it is best described as persistent rather than stable. The correct structure of the dimer **3**, a σ -bond between the central carbon of one radical and a para carbon of another, was confirmed only decades after Gomberg's initial discovery.⁸ The intermolecular bond is fairly weak,⁹ roughly 46 kJ mol⁻¹. The persistent nature of **3** is shared by many of its substituted derivatives and it is mostly ascribed to the steric protection afforded by the bulky phenyl substituents, giving the molecule a propeller-like structure with the three rings twisted out of plane by roughly 30°.^{10,11} Only a small amount of spin density can be found on the phenyl substituents, the majority being located on the central carbon atom.^{9,12,13} The π -type SOMO (singly occupied molecular orbital) has contributions from the p-orbitals of every other carbon atom, which rationalises the formation and structure of **3**.

The majority of heteroaromatic analogues of **1** show stability and chemical behaviour comparable to the parent compound.⁴ Different substituents can, however, inhibit the radical's ability to dimerise. An extreme example of the effect that the substituents have on the stability and chemical properties of triphenylmethyl is the perchlorinated derivative **4** (Figure 2), which is reactive only under extremely harsh conditions.¹⁴ The remarkable stability of **4** results mainly from the shielding of the central carbon atom by the six chlorine atoms at the ortho positions. The additional steric bulk twists the propeller-like structure out of plane by roughly 50°,¹⁵ which results in pronounced localisation of the spin density to the central carbon atom.¹⁶

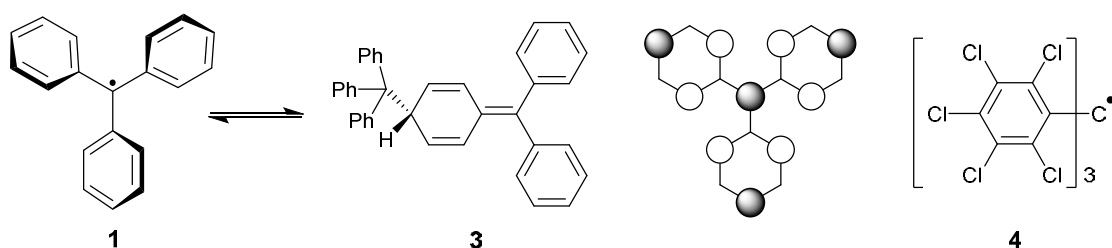


Figure 2. Dimerization of triphenylmethyl radical **1** to **3** (left), the π -type SOMO of **1** (second from right) and perchlorinated trimethylphenyl radical **4**¹⁴ (right).

A number of remarkably stable polychlorinated triphenylmethyl derivatives have also been synthesised.¹⁷ The study of these partially

chlorinated species has revealed that not all of the chlorine substituents are required to achieve stability comparable to that of **4**. It seems that the six chlorines at the ortho positions are sufficient to provide stability, which also suggests that steric effects are more crucial for the stability of these types of triphenylmethyl derivatives than electronic ones.^{18–20}

One notable organic radical that has garnered attention over the years from experimentalists and theoreticians alike is the phenalenyl **5** (Figure 3a). It was reported by Reid²¹ and independently prepared by Sogo *et al.*²² Several derivatives were soon synthesised; the older literature has been reviewed by Reid in 1965.²³ Typically, phenalenyl and its derivatives are oxygen sensitive radicals. They exist in equilibrium with their dimer **6** (Figure 3a), and in dilute and deoxygenated solutions, they are persistent either indefinitely or for a very long period of time.

Phenalenyl radicals are an excellent example of organic radicals benefiting from the stabilizing effect of electron delocalisation. The majority of spin density in **5** is located on the six α -carbon atoms; the six most important resonance structures are shown in Figure 3b. The three β -carbon atoms do possess a small amount of spin density, which arises from spin polarisation effects. The spin distribution can be rationalised by looking at the SOMO of **5**, which is a π -orbital that has significant coefficients only on the α -carbon atoms. Closer analysis of the electronic structure of **5** reveals a nodal plane between the central p-orbital and the p-orbitals of the peripheral carbons. This effectively prevents the delocalisation of spin density to the central carbon, leaving the unpaired electron to the peripheral orbitals.²⁴

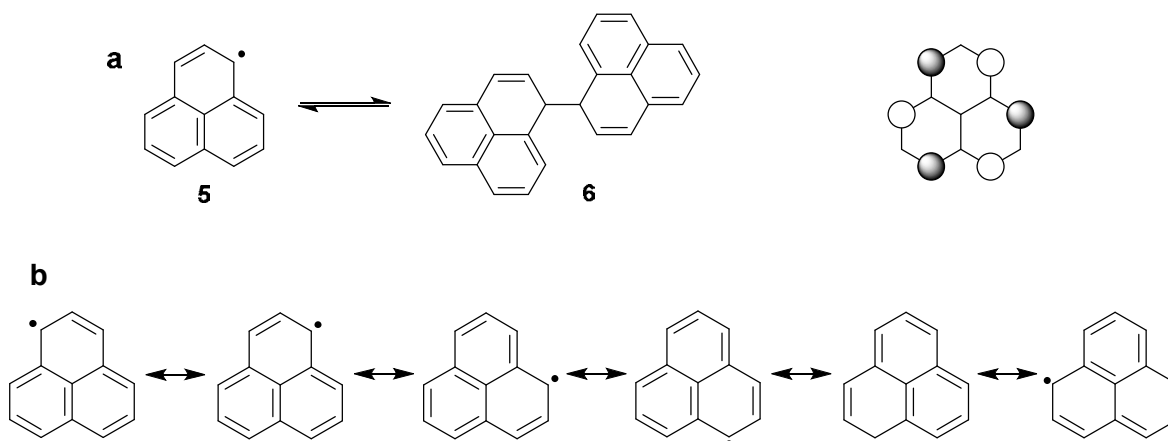


Figure 3. a) Dimerization of phenalenyl radical **5**^{21,22} to **6** (left) and the SOMO of **5** (right). b) The six most important resonance structures of phenalenyl radicals.

The majority of phenalenyl derivatives are prone to form dimers. Simple phenalenyls typically form σ -bonded dimers,^{23,25–27} while substituted phenalenyls often form π -bonded dimers that display antiparallel conformation²⁸ in order to minimise interactions between substituents (Figure 4).



Figure 4. Modes of dimerization for phenalenyl radicals: σ -dimer^{23,25-27} (left) and antiparallel π -dimer²⁸ (right).

The nature of π -bonding in phenalenyl dimers has received considerable attention over the years. The intermolecular multi-centre two-electron bond in the dimer is formed between the delocalised π -type SOMOs of the two radicals. The antiparallel arrangement provides a pathway for direct interaction of the 2p-orbitals of the α -carbon atoms, which generates considerable orbital overlap. The spin pairing between the two radical moieties is quite strong, and at room temperature, the dimers are diamagnetic.²⁹ The continuous increase in computing power has enabled more and more rigorous theoretical modelling of the nature of bonding in phenalenyl dimers as evidenced by the number of papers published in recent years.³⁰⁻³⁵

In addition to altering the way phenalenyl radicals form dimers, substituents on the phenalenyl periphery can also prevent dimerization altogether. Well-known examples are radicals **7**³⁶ and **8**³⁷ (Figure 5) that have chlorine and sulphur substituents, respectively, and which both exist as monomers in solution. The radical **7** is monomeric also in the solid state and displays antiparallel stacking with an intermolecular distance of 3.78 Å. The relatively long stacking distance is a consequence of the bent structure of **7** caused by repulsive interactions between the chlorine substituents. Because the Cl \cdots Cl distances in a planar molecule would become unfeasibly short, individual molecules of **7** are ruffled into a propeller-like shape.

In the early 21st century, a major new contribution to the field of phenalenyl chemistry was published by Haddon and co-workers. They developed a range of radicals **9** that consist of a boron atom chelated by two bidentate phenalenyl moieties (Figure 5).³⁸⁻⁴⁰ The phenalenyls in these formally zwitterionic compounds are spiroconjugated; the spin and charge are delocalised throughout the compound. The solid-state structures of these extremely oxygen-sensitive radicals are quite varied with few of them being monomeric. Interestingly, many of these phenalenyl systems form π -dimers in which only one phenalene moiety interacts with an adjacent molecule.⁴¹⁻⁴³ The solid state electric and magnetic properties of **9** are highly unusual, with few of the derivatives showing extremely high conductivity.⁴⁴⁻⁴⁶

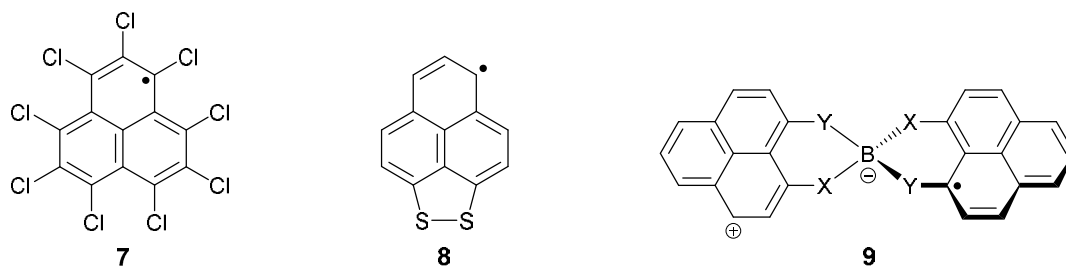


Figure 5. Fully chlorinated phenalenyl radical **7**³⁶, substituted phenalenyl radical **8**³⁷ and spiroconjugated radicals **9**³⁸⁻⁴⁰ (X, Y = O, O; NR, NR; O, NR).

Introducing heteroatoms into the phenalenyl structure has significant effects on the spin distribution and, therefore, the chemical behaviour of the radicals. Morita *et al.* synthesised a phenalenyl derivative **10**⁴⁷ that has two nitrogen atoms at the α -positions while Zheng and co-workers reported a derivative **11** with a nitrogen atom at the β -position (Figure 6).⁴⁸ In compound **10**, the nitrogen atoms have considerably less spin density than the four carbon atoms at α -positions. Interestingly, while **10** does form an antiparallel dimer in solution, it differs from the typical geometry of phenalenyl dimers by having the two rings tilted with respect to one another. An intriguing feature of compound **11** is that it lacks any tendency to form a dimer in solution.

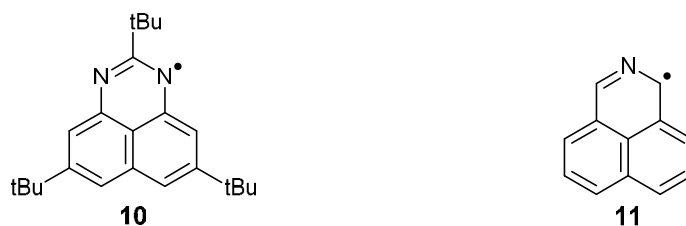


Figure 6. Phenalenyl derivatives **10**⁴⁷ and **11**⁴⁸ that incorporate nitrogen atom(s) in the molecular backbone.

Recently, Ueda *et al.* synthesised the first chiral phenalenyl-based neutral π -radical **12** (Figure 7).⁴⁹ This helicene-based radical is relatively stable; the solid material survives for a few weeks under air at -30 °C. It is stable in a degassed solution but decomposes within a few days when the solution is exposed to air. The most intriguing feature of **12** is its chirality which, in conjunction with its extensive spin delocalisation, may find use in materials chemistry.

Adding appropriate substituents increases the stability of phenalenyls. However, it is possible to stabilise phenalenyls without bulky substituents as demonstrated by Bucher and co-workers who prepared radicals **13** and **14**.⁵⁰ Both of these compounds can be stored under air for weeks without noticeable degradation. Compound **14** is the first non-planar phenalenyl-based radical that does not rely on bulky substituents to provide stability. Instead, radical **14** is stabilised by the incorporation of a heteroatom. EPR spectroscopy measurements showed significantly lower spin densities in the α -positions of the phenalenyl skeletons of **13** and **14** when compared to radical **8**, which is stabi-

lised via a disulphide bridge. The unpaired electron is still mostly confined to the phenalenyl moiety in both **13** and **14**, but the reduced spin densities on the α -positions do, nonetheless, result in reduced tendency to form σ -dimers.

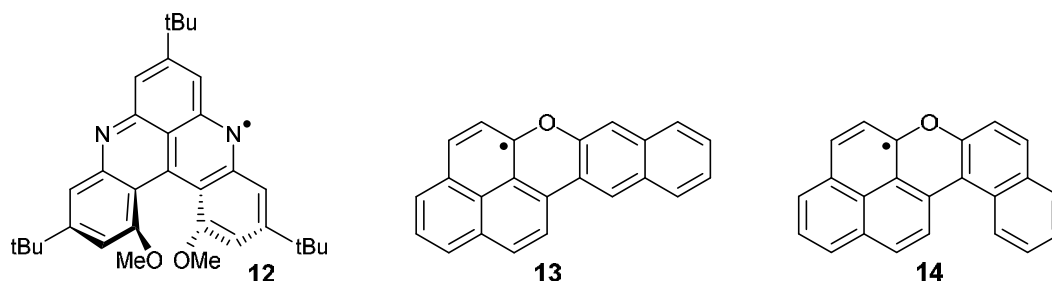


Figure 7. Chiral phenalenyl radical derivative **12**⁴⁹ and two electronically stabilised phenalenyl derivatives **13** and **14**.⁵⁰

Phenalenyl-type radicals have attracted the attention of synthetic chemists for several decades. However, the electronic spectroscopy of phenalenyl radicals had not been rigorously scrutinised until very recently by O'Connor *et al.*²⁴ Likewise, the decomposition mechanism of phenalenyl radicals has only recently been characterised in detail. The decomposition pathway begins with the dehydrogenation of the σ -dimer to biphenalenylidene, which then forms an isomer that goes through ring-closure and dehydrogenation to form peropyrene.⁵¹

Phenoxy radicals are another family of carbon-based radicals that have been studied for decades. They were exhaustively reviewed by Altwicker and more recently by Hicks.^{4,52} An intriguing example of phenoxy radicals is the galvinoxyl radical **15** (Figure 8).⁵³ It is extremely stable and possesses unusual solid state magnetic properties.⁵⁴ Theoretical modelling has shown there to be considerable spin density on the para carbon atoms of **15**.⁵⁵ Thus, galvinoxyl radicals can also be represented as delocalised allyl-type radicals **16** (Figure 8).⁵⁶

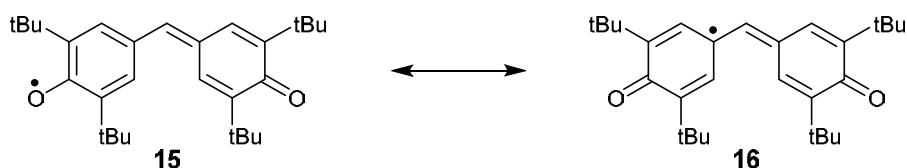


Figure 8. Galvinoxyl radical **15**⁵³ and its representation as an allyl-type radical **16**.⁵⁶

2.1.3 Hydrazyl radicals

Hydrazyls with the general form R_2NNR^\bullet do not usually form stable radicals. The striking exception is the well-known, commercially available radical **17** (*N,N'*-diphenyl-*N'*-picrylhydrazyl, commonly known as DPPH) shown in Figure 9. Resonance-delocalised hydrazyls such as verdazyls, on the other hand, form extensive families of stable radicals. Verdazyls have been known for decades,⁵⁷ and the closely related 6-oxoverdazyls were prepared soon after in the 1980s.⁵⁸

Verdazyls are air and water stable and thus are among the most stable of organic radicals. The general structures of verdazyls **18** and oxo-verdazyls **19** are shown in Figure 9. The π -type SOMO of verdazyls (Figure 9) has a nodal plane that prevents spin delocalisation onto the substituents attached to the carbon atoms on the molecular backbone. Though verdazyls do not require bulky substituents for stability, Paré *et al.* have demonstrated that *N*-isopropyl-substituted verdazyls are more stable than the corresponding *N*-methyl variants.⁵⁹

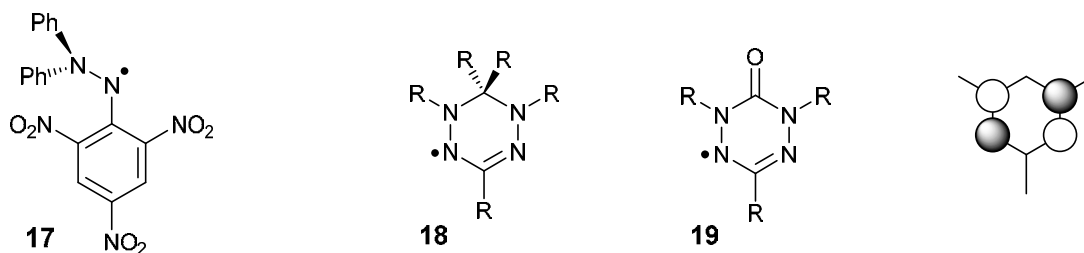
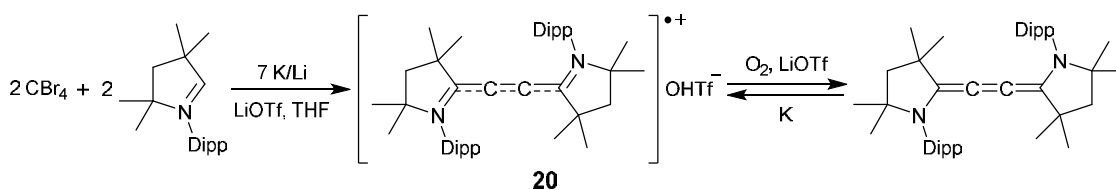


Figure 9. Hydrazyl radical **17** (left), the general structure of verdazyls **18** and oxo-verdazyls **19** (middle). The π -type SOMO of verdazyls (right).

Recently, Roesky *et al.* prepared an air-stable radical cation **20** based on a cyclic alkyl(amino) carbene (Scheme 1).⁶⁰ The authors first synthesised the corresponding neutral species, representing the first cumulene to employ a carbene, when they noticed that part of the insoluble material obtained after filtration slowly oxidised under exposure to air, giving radical **20**. An alternative high-yield route to the radical **20** was later developed (Scheme 1). Interestingly, **20** can be reduced to the cumulene or oxidised to give a corresponding dication. EPR spectroscopy and theoretical calculations indicate that the unpaired electron in radical **20** is mainly delocalised on the C₄ backbone with the two nitrogen centres having significantly less spin density.



Scheme 1. Synthesis of radical cation **20** and its oxidation to the corresponding cumulene.⁶⁰

2.1.4 Nitroxides and nitronyl nitroxides

Nitroxides are perhaps the most well-known class of stable radicals. The first organic nitroxide, porphyrexide **21** (Figure 10), was synthesised in 1901 by Piloty and Schwerin.⁶¹ Five decades later, using EPR spectroscopy, Holden *et al.* corroborated the radical character of **21**.⁶² Arguably, the most renowned and widely used nitroxide is the commercially available TEMPO **22** (Figure 10), which was prepared by Lebedev and Kazarnowskii in 1960.⁶³ There are numer-

ous nitroxide derivatives that are air and water stable and are not susceptible to dimerization or other radical-based reactions. Neiman *et al.* showed as early as the 1960s how nitroxides can be used in various organic reactions without the direct involvement of the aminoxyl group.⁶⁴ Nitroxide chemistry has been reviewed multiple times over the years, most recently in a book edited by Hicks.⁶

The aminoxyl group in nitroxides features a three-electron π -bond between the nitrogen and oxygen atoms, which ensues from the overlap of the $2p_z$ -orbitals of N and O. The contributions to the electronic structure from the two main resonance structures (Figure 10) has to be taken into account. The formal bond order between the three-electron bond of N–O is 1.5. This notion is substantiated by the bond energy (~ 419 kJ mol⁻¹) and the bond length ($1.25 \text{ \AA} < d_{\text{N-O}} < 1.30 \text{ \AA}$) that are approximately halfway between corresponding values for a N–OH single bond (222 kJ mol⁻¹, $\sim 1.43 \text{ \AA}$) and a N=O double bond (607 kJ mol⁻¹, $\sim 1.20 \text{ \AA}$).^{65,66}

The majority of spin density in nitroxides is localised on the nitrogen and oxygen atoms with the latter having a slightly higher proportion. When considering the O–H bond dissociation of hydroxylamines, the gain in energy from the delocalisation of the unpaired electron between N and O is roughly 126 kJ mol⁻¹.^{65,67} In comparison, the energy gain from the formation of a O–O bond is approximately 147 kJ mol⁻¹. Thus, the energy gain from the formation of one O–O bond does not compensate the delocalisation energy associated with two aminoxyl groups, which makes O–O dimerization of nitroxides thermodynamically unfavourable.

Essentially, the stability of nitroxides depends on the nitrogen substituents as the radical framework itself is inherently stable. The substituents may provide a pathway for decomposition, as is the case with alkyl nitroxides, for example. These compounds have a hydrogen atom α to the nitrogen and they easily undergo disproportionation. Stable nitroxides, such as **22**, typically have two substituents based on quaternary carbons at the α -position.

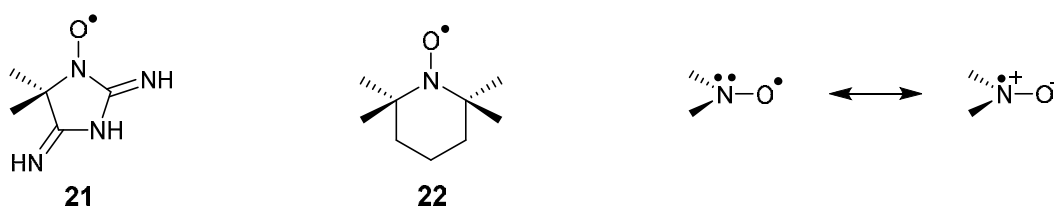


Figure 10. Porphyraxide radical **21**⁶¹ and TEMPO **22**⁶³ (left). Two main resonance structures of nitroxides (right).

Nitronyl nitroxides (NNO) **23** (Figure 11) are radicals that have interacting nitronyl and aminoxyl groups. The first nitronyl nitroxide was prepared in the early 1970s by Ullman *et al.*,⁶⁸ and the radicals have received considerable attention ever since, especially as building blocks for magnetic materials. The general properties of NNOs were determined early on, and the main features of their electronic structures were excellently reviewed a quarter of a century ago in a book.⁶⁹ NNOs equal nitroxides in stability since they contain all the required

features for stability, such as the lack of α -hydrogen atoms. The π -type SOMO (Figure 11) of a nitronyl nitroxide extends over both NO groups. There is a nodal plane at the central carbon atom. As a consequence, the spin density in NNOs is distributed equally between the two NO groups and is unaffected by the R group. This also means that a wide variety of R groups can be used without affecting the stability of the radical. The EPR spectra of NNOs is typically characterised by a five-line pattern with an intensity ratio of 1 : 2 : 3 : 2 : 1 that results from the coupling of the single unpaired electron to two equivalent nitrogen atoms. The nitrogen coupling constant in NNOs is roughly half of the typical values observed for nitroxides.



Figure 11. The general structure of nitronyl nitroxides **23** (left) and their π -type SOMO (right).^{68,69}

2.1.5 Sulphur-nitrogen radicals

Significant numbers of stable and persistent radicals contain only second-row elements, particularly carbon, nitrogen and oxygen. In many cases, the stability of these radicals is based on the anomalous behaviour of second-row p-block elements compared to their heavier congeners. For example, the tendency of lighter p-block elements to form π -bonds allows the unpaired electron to delocalise across the π -framework, increasing stability. Another factor affecting the stability is the lone-pair-rich nature of nitrogen and oxygen atoms, which increases the reactivity of nitrogen and oxygen-based nucleophiles when they are catenated to another heteroatom containing lone pairs.⁷⁰ This effect also decreases the bond strength of N-N, O-O and N-O σ -bonds, and when the bond in question would form between fragments that already contain bonds between N and/or O atoms, the resulting catenated system would become thermodynamically unstable.⁶

When moving beyond the second row in the p-block, the lone pairs become more diffuse, and their effect on the stability of the compounds becomes less of a factor. Many of the heavier p-block elements also have a tendency to form strong σ -bonds and significantly weaker π -bonds.⁷¹ The overall result of these changes in atomic properties is that many of the heavier p-block elements require considerable steric protection in order to form persistent and stable radicals. The striking exception is sulphur, especially in conjunction with nitrogen. However, an NS \cdot moiety is not, in general, as stable as the analogous NO \cdot . An illustrative example of the above is that while nitroxides R₂NO \cdot are numerous,

the corresponding thionitroxides R_2NS^\bullet typically exist at room temperature as their disulphide dimers.

The field of sulphur-nitrogen radical chemistry is broad and ever-growing. Multiple reviews have been written over the years, both on general chemistry and on certain aspects of the field.^{4,6,72} Of particular interest have been thiazyls that contain an unsaturated $S=N$ unit in which both S and N are two-coordinate. The π -bond in thiazyls is remarkably strong: it is an electron-rich, three-electron π -bond with the third unpaired electron lying in a π^* -orbital.⁷³ The radical coordination chemistry of thiazyls has recently been reviewed by Preuss,⁷⁴ while authors such as Kaszynski have conducted theoretical analyses of the properties of thiazyl radicals.^{75,76}

One of the simplest types of thiazyl radicals are thioaminyls **24**, and just like thionitroxides, thioaminyls tend to have a low level of persistence. Bulky substituents on the nitrogen centres are required in order to make the radicals stable enough to be isolable. The nature of the organic substituent on sulphur atoms is less important from a stability point of view; typically, substituted heteroaromatics are used. Oakley *et al.* have reported a stable radical **25** (Figure 12) that is essentially an annulated thioaminyl.⁷⁷ Crystallographic measurements reveal **25** to be monomeric in the solid state, while EPR analysis and computational data show the spin density to be localised equally on the four outer nitrogen atoms.

1,2,3,5-Dithiadiazolyl radicals (DTDA) **26** (Figure 12) were first discovered in the 1970s and have received considerable attention ever since. DTDA radicals can be considered as resonance delocalised thioaminyls, and they are typically indefinitely stable in the solid state. Interestingly, DTDA radicals are also thermally remarkably stable, allowing them to be purified by high-temperature sublimation. The π -type SOMO of DTDA radicals (Figure 12) is distributed symmetrically in a similar fashion to those in verdazyls, for example, and just like in verdazyls, there is a nodal plane passing through the single carbon atom, which prevents direct electronic conjugation of the substituent R with this orbital. DTDA radicals typically exist in equilibrium with the corresponding dimers in solution. Many of the initially reported samples were dimers also in the solid state, a prime example being the 4-phenyl-1,2,3,5-DTDA that was actually the first π -dimer of any radical to be structurally characterised.⁷⁸ The dimerization of DTDA radicals can be precluded by using suitable substituents.

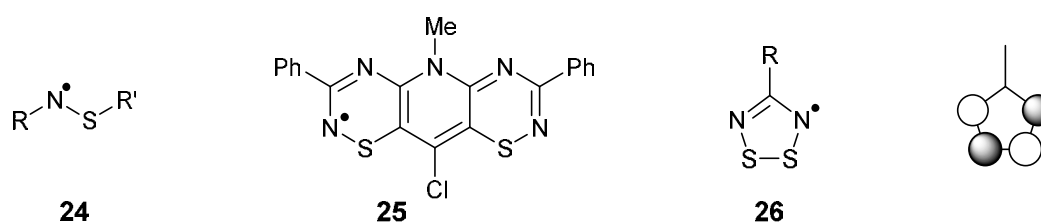


Figure 12. Thioaminyl radical **24**, annulated thioaminyl radical **25**⁷⁷ and the general structure of 1,2,3,5-dithiazolyl radicals **26** (left, middle). The π -type SOMO of DTDA (right).

Dithiazolyl radicals are closely related to DTDA's. There are numerous examples of dithiazolyls, the majority of which are indefinitely stable in the solid state and also generally air stable. The solid-state structure of 1,3,2-dithiazolyl **27** (Figure 13) is temperature dependent: at room temperature, **27** is monomeric and the structure consists of slipped π -stacks while at 150 K the structure is comprised of π -dimers.⁷⁹ Intriguingly, this structural transition from monomer to dimer is hysteretic: when increasing the temperature, the transition from dimer to monomer occurs at 190 K. Upon cooling, the transition back to dimer occurs at 120 K. Similar behaviour is observed for several other dithiazolyls, and Oakley *et al.* have determined the mechanistic aspects of this phenomenon in detail.^{80,81}

Oakley and co-workers have developed a number of sulphur-nitrogen radicals, among them the resonance-delocalised bisdithiazolyl radical **28** (Figure 13) with R being an alkyl substituent (propyl, butyl, pentyl or hexyl).⁸² The authors were studying the design of radical spin ladders in which intermolecular F \cdots S' contacts form the rungs of the ladder while the π -stacking of the radicals form the legs. This type of spin ladder could have huge potential in materials chemistry as the ladder structure allows the unpaired electron to act as a carrier of spin and charge throughout the structure. Oakley *et al.* showed that when R is a three-carbon chain (or shorter), the radical π -stacks are locked into pinwheel clusters. With longer alkyl chains, the adjacent columns of π -stacked radicals have short intermolecular F \cdots S' contacts due to the strong interaction between the electronegative fluorine atom and the electropositive sulphur. This gives rise to S = $\frac{1}{2}$ spin ladder arrays. When using a propyl substituent, the radical displayed an ideal spin ladder behaviour in the solid state as the interactions along the rungs and the legs were approximately equal.

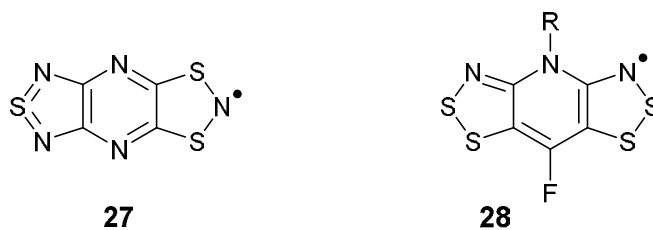


Figure 13. 1,3,2-Dithiazolyl radical **27**⁷⁹ and bisdithiazolyl radical **28**.⁸²

2.1.6 Sulphur radicals

The first thermally stable sulphuranyl radicals, stabilised by tridentate ligands, were already prepared in 1986, but these were merely persistent in solution and could not be isolated.^{83,84} Only very recently, the first stable, structurally characterised sulphuranyl radicals and their selenium analogues **29** (E = S or Se, Figure 14) were reported.⁸⁵ The authors used tridentate C₂F₅ ligands that provide considerable steric protection, thus allowing the radicals to be isolated as stable monomers. The radicals display reversible redox chemistry, and the authors were able to utilise this in building radical batteries where the chalcogen radi-

cals act as the cathode and silyl radicals as the anode. These batteries exhibit a practical discharge potential of ~ 1.8 V and stable cycle performance, proving the potential of using all-radical batteries as an alternative to traditional metal-based ones.

An interesting addition to sulphur radical chemistry was reported recently in the form of a radical cation **30a** (Figure 14) that has a three-electron σ -bond⁸⁶ between two sulphur atoms.⁸⁷ In the same paper, the authors also report a variant where one of the sulphur atoms is replaced by selenium **30b**. Both compounds form deep-coloured solutions in dichloromethane, but upon concentration, **30a** forms a stable monomeric solid while **30b** crystallises out as a dimer. Redissolving the dimer produces a deeply coloured solution that produces an identical EPR spectrum to the original sample. Both **30a** and dimeric **30b-30b** are stable at room temperature under an inert atmosphere. The existence of three-electron σ -bonds between two chalcogen atoms in both radical cations were confirmed by EPR spectroscopy, UV-Vis absorption and theoretical calculations. It should be noted, however, that in these examples, the three-electron bond has been weakened to an extent by partial delocalisation of spin density onto the adjacent phenyl rings.

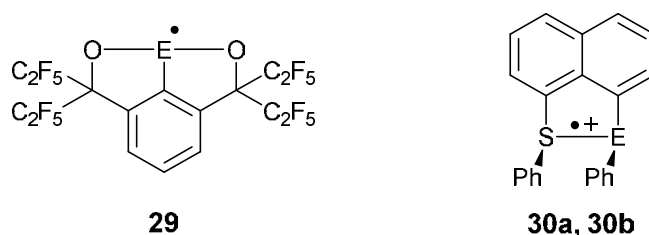


Figure 14. Chalcogen radicals **29** ($E = S$ or Se)⁸⁵ and radical cations **30a** ($E = S$) and **30b** ($E = Se$).⁸⁷

2.1.7 Inorganic main group radicals

Stable and persistent main group radicals with an unpaired electron located mainly on atoms other than C, N, O and S have not been studied to the same extent as radicals with spin density on the aforementioned elements. The methods to induce stability to “inorganic” main group element radicals are essentially the same as with the lighter “organic” elements. Extremely bulky substituents provide steric protection and a kinetic barrier to oligomerisation processes. Cyclic systems typically benefit from the delocalisation of the unpaired electron over the ring system, while heterocyclic radicals may also be stabilised by electronegative atoms.

The first persistent radicals of the heavier p-block elements were prepared and characterised in the 1970s and the results from the early forays into the chemistry of inorganic main group radicals were reviewed by Lappert and Lednor in 1976.⁸⁸ The early examples of inorganic radicals were fairly persistent – their half-lives ranged from several days to more than a year – and they were mostly stabilised by steric effects. The tin radical $R_3Sn\cdot$ ($R = (Me_3Si)_2CH$)

reported by Davidson *et al.* in 1973 was prepared by photolysis with visible light using R_2Sn as the starting material.⁸⁹ The radical displayed couplings to the methine protons and ^{119}Sn and ^{117}Sn nuclei in the EPR spectrum, and showed no signs of decomposition after being kept in a degassed benzene solution in the dark for weeks at room temperature. Using similar methods to those employed by Davidson and co-workers, Gynane *et al.* prepared phosphorus- and arsenic-centred radicals $[(Me_3Si)_2CH]_2E\cdot$ and $[(Me_3Si)_2N]_2E\cdot$ ($E = P$ or As).⁹⁰ These radicals were persistent in toluene solutions for at least over a month, and they were characterised by EPR spectroscopy showing strong couplings to phosphorus and arsenic nuclei, respectively.

The field of heavier main group radicals has since expanded, and nowadays a multitude of odd-electron species containing heavier p-block elements are known even though the number of reported examples pales in comparison to stable organic radicals. A comprehensive review by Power was published in 2003,³ and a chapter dedicated to the chemistry of the heavy p-block element radicals was included in a book published in 2010.⁶

There is only one electron difference between the electron configurations of boron and carbon. As a consequence, the history of boron radical chemistry harks back to the early 20th century. However, it wasn't until 1986 when a paper describing the crystallographic structural characterisation of a boron-based radical, a triarylboron anion, first appeared.⁹¹ The structure was determined from an ion-separated salt, $[Li(12\text{-crown-}4)_2][BMes_3]$, which exhibits surprising thermal stability as it decomposes only at ~ 240 °C. In the crystal structure, the anion is planar with only slight deviation in the C-B-C angles from 120°. An earlier paper demonstrated by EPR spectroscopy how the unpaired electron is mainly located at the boron centre ($a(^{11}B) = 7.84$ G).⁹²

In a similar fashion to the triarylboron radical anion, the structure of a diborane radical anion $[R_2BBR_2]^{*-}$, obtained by a one-electron reduction from a diboron compound R_2BBR_2 , was first characterised as the contact ion pair, $[Li(OEt_2)_2][MeO(Mes)BB(Mes)OMe]$.⁹³ The following year, an EPR spectrum was measured from a solvent-separated ion pair, $[K(18\text{-crown-}6)(THF)_2][Mes_2BB(Ph)Mes]$, which consists of a seven-line pattern with $a(^{11}B) = 13$ G.⁹⁴ This indicates a coupling between the two boron centres and is consistent with the formation of a π -radical.

Triarylboranes typically undergo a single reversible reduction and a subsequent irreversible one.⁹⁵ However, a paper published in 2007 reports the synthesis and characterisation of a 9-borylated acridinyl radical **31** (Figure 15) that undergoes two reversible reductions.⁹⁶ EPR spectroscopic analysis suggests that the spin density is delocalised over the acridinyl moiety with only a minimal contribution from the boron atom ($a(^{11}B) = 2.55$ G). At the same time, theoretical calculations indicate a considerable localisation of the unpaired electron in a B-C π -bonding orbital with significant polarisation towards the carbon atom. This led the authors to conclude that **31** possesses a weak boron-carbon π -bond.

In 2012, Aramaki *et al.* reported the first isolation and full characterisation of a stable, neutral biazaboracyclic radical **32** (Figure 15).⁹⁷ The radical contains

a planar boron centre connected to one fluorine and two nitrogen atoms. The relatively short B–F bond in the radical, 1.342(4) Å, is shorter than the sum of the covalent radii of the respective elements, 1.46 Å. In fact, the bond length is close to that observed in fluoroboraethene H₂C=BF (1.356 Å),⁹⁸ which suggests an electrostatic interaction between boron and fluorine in **32**. EPR spectroscopy and theoretical calculations indicate that the spin density is delocalised on the heterocyclic ring with a minimal contribution on the boron atom. Nonetheless, the radical reacts as a base-stabilised boryl radical when treated with benzoquinone or benzoyl peroxide.

Radical-cation radical-anion pairs play an integral role in single-electron transfer (SET) reactions. This inspired Braunschweig and co-workers to develop a boron-based stable radical-anion radical-cation pair **33**.⁹⁹ The authors chose to use a diborene for the radical-cation because diborenes have well-defined redox chemistry and the exceptional electron rich B=B double bond can be easily oxidised. Also, the oxidation of diborenes selectively affords stable radical-cations. It is worth noting that the reduction potential of diborenes with a B=B π-system is directly dependent on the energy of the HOMO, which in turn strongly depends on the nature and donor strength of the stabilizing Lewis base.¹⁰⁰

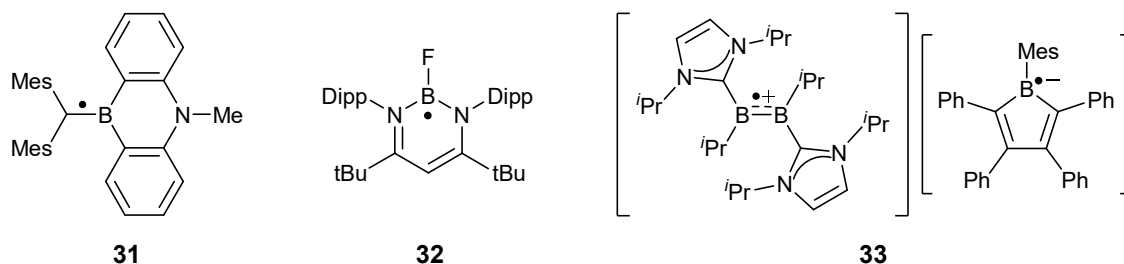


Figure 15. 9-Borylated acridinyl radical **31**,⁹⁶ biazaboracyclic radical **32**⁹⁷ and boron-centred radical-cation radical-anion pair **33**.⁹⁹

EPR spectroscopy confirmed that **33** is a radical-cation radical-anion pair. Removal of an electron from the π-bonding orbital between the two boron atoms causes the formal bond order to decrease from 2.0 to 1.5. This is evident also from the crystal structure; when compared to the precursor diborene, the boron-boron bond length of **33** is increased by 0.062 Å to 1.640 Å.

Stephan and co-workers recently reported the synthesis of neutral borocyclic radicals **34** and **35** (Figure 16) using frustrated Lewis pair (FLP) hydrogenation reactions.¹⁰¹ H₂ activation with polyaromatic diones and B(C₆F₅)₃ produced remarkably stable radicals in a high yield. The authors were able to use column chromatography to separate the radicals from side products and the radicals proved to be stable on silica. As isolated solids, the radicals are indefinitely stable under N₂, while they survive for several days in solution under 1 atm of O₂. EPR spectra and theoretical calculations indicate the delocalisation of the spin density over the aromatic backbone in both radicals with moderate contribution on the boron atoms ($a(^{11}\text{B}) = 2.58$ G and $a(^{11}\text{B}) = 2.80$ G for **34** and **35**, respectively).

The first stable radicals with an unpaired electron located mainly on a heavier group 13 element were synthesised in the early 1990s.^{102,103} Radicals containing aluminium, gallium or indium had been reported earlier, but they all exhibited significant delocalisation of the spin over organic substituent(s).

Cyclic heavier group 13 radicals and the corresponding acyclic variants can provide insight into the influence of the metal centre (M) to the stability of the radical species. These effects originate from the covalent radii and/or from the M–M bond strength. Persistent acyclic aluminium radical **36a** is an intermediate on the path to forming the stable cyclic radical **37a** (Figure 16).¹⁰⁴ The structure of **37a** consists of a triangle with two of the three aluminium atoms being three-coordinate while the third aluminium atom is four-coordinate. The bond length between the three-coordinate aluminium atoms is slightly shorter than the bond between the three- and four-coordinate aluminium atoms (2.703 Å and 2.756 Å, respectively). In the heavier gallium congener **37b** (Figure 16) the situation is the opposite: the bond length between the three-coordinate gallium atoms is 2.879 Å, while the bond involving the four-coordinate gallium is 2.527 Å.¹⁰⁵ This indicates an onset of a bond cleavage between the three-coordinate gallium atoms. While **37b** forms a stable radical in the solid state, it will eventually decompose in solution to form the acyclic radical **36b**.¹⁰⁶

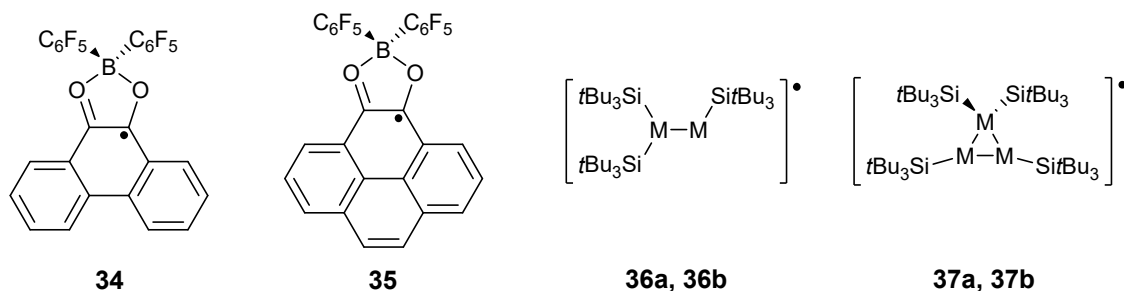


Figure 16. Borocyclic radicals **34**¹⁰¹ and **35**¹⁰¹ (left) and heavier group 13 radicals **36a** (M = Al),¹⁰⁴ **36b** (M = Ga),¹⁰⁵ **37a** (M = Al)¹⁰⁴ and **37b** (M = Ga)¹⁰⁶ (right).

Radicals of the heavier group 14 elements have garnered considerable attention over the years. A major contributor to the field has been the research group of Sekiguchi.¹⁰⁷ The first homocyclic, neutral group 14 radical **38** (Figure 17) was prepared in 1997.¹⁰⁸ This stable species was obtained by reducing (2,6-Mes₂C₆H₃)GeCl with KC₈. At the centre of the radical is a triangle formed by three germanium atoms, where one of the bonds exhibits a double-bond character. EPR spectroscopic measurements led the authors to conclude that the unpaired electron is localised on only one germanium atom. In a similar vein, the bicyclic, neutral germylene radical **39** (Figure 17) can be obtained by oxidation of the parent anion.¹⁰⁹ The EPR spectrum of **39** consists of two separate multiplets. The relatively small hyperfine coupling constants (HFCCs) suggest a π -radical character with the unpaired electron localised on a single germanium centre.

An intriguing example of a heavier group 14 radical by Sekiguchi *et al.* is the stable silyl radical **40** (Figure 17).¹¹⁰ This radical represents the first isolable

silyl radical, and it is an all-silicon congener of a cyclobutenyl radical. Two Si-Si bond lengths in the Si₄ ring are intermediate between single and double bonds, whereas the other two bonds are close single bonds, which altogether suggests an allylic structure. Likewise, the EPR spectrum indicates greater spin density on the terminal silicon atoms of the allylic structure ($a(^{29}\text{Si}) = 40.70 \text{ G}$ and $a(^{29}\text{Si}) = 37.40 \text{ G}$) when compared to the value of the central silicon ($a(^{29}\text{Si}) = 15.50 \text{ G}$).

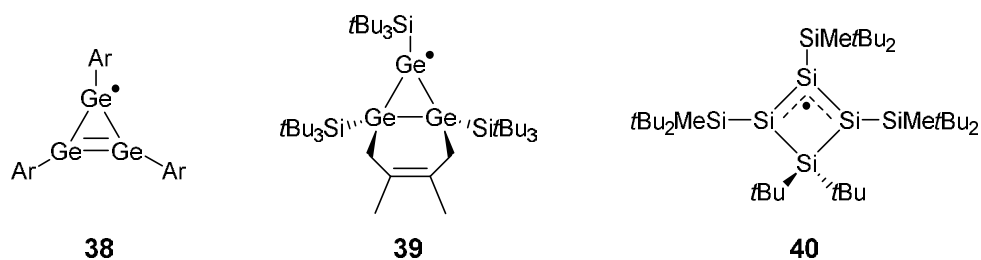


Figure 17. Germenyl radicals **38**¹⁰⁸ and **39**¹⁰⁹ and silyl radical **40**.¹¹⁰

As well as cyclic radicals, heavier group 14 elements can also form neutral, stable acyclic radicals. Illustrative examples of these types of radicals are the germenyl and silyl radicals **41** and **42**, respectively,¹¹¹ while an example of a superheavy group 14 element radical is the plumbyl radical **43** (Figure 18).^{112,113} The stability of these acyclic radicals is achieved by using bulky, electropositive silyl substituents, while the delocalisation of the unpaired electron via hyperconjugation between the p_z-orbital of the central heteroatom and the σ*-orbital of the Si-C(tBu) (in **41** and **42**) or Si-Si(Me) (in **43**) bonds stabilises the radicals further. Crystallographic measurements show the radicals **41** and **42** to have a trigonal planar geometry, while **43** is slightly distorted towards a pyramidal structure.

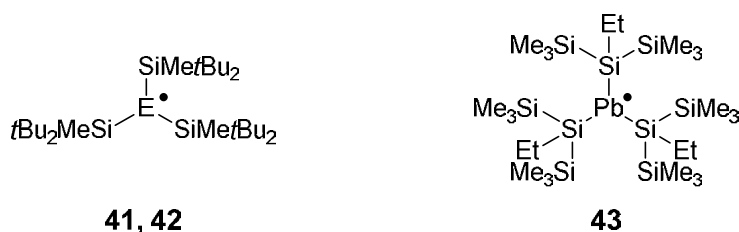


Figure 18. Stable acyclic group 14 radicals **41** (E = Ge),¹¹¹ **42** (E = Si)¹¹¹ and **43**.^{112,113}

The vast majority of stable radicals based on the heavier group 15 elements are phosphorus-containing species; relatively few stable radicals based on arsenic, antimony or bismuth have been reported. The two-coordinate phosphinyl radical $\cdot\text{PPh}_2$ and its arsenic analogue were reported in 1966, and this can be considered the starting point of phosphorus radical chemistry.¹¹⁴ Radicals of this type are typically produced by photolysis from chlorophosphine and electron-rich alkenes. The monomeric radicals thus obtained have a tendency to dimerise to form diamagnetic diphosphines. Appropriate choice of substituents can induce stability, however, as evidenced by the phosphinyl radical **44** and its

arsenic analogue **45** (Figure 19); these radicals are indefinitely stable in solution as well as in the gas phase.^{115,116} Vapor electron diffraction measurements reveal that both of these radicals are V-shaped with C-P-C and C-As-C angles of 104.0° and 101.2°, respectively. The radicals dimerise in the solid state via P-P and As-As bonding. While the bonds are 0.1 Å longer than typically observed for these types of compounds, the slight elongation does not induce their effortless dissociation in solution or in gas phase.

A viable method to increase the stability of phosphinyl radicals is the addition of amino groups. Bertrand and co-workers reported the synthesis of a stable diphosphaallyl radical **46** (Figure 19); the radical can be formed from the corresponding cyclic cation either by electrolysis or by reduction with metallic lithium.¹¹⁷ The EPR spectrum of **46** consists of a five-line pattern ($g = 2.0048$, intensity ratio 1 : 3 : 4 : 3 : 1) resulting from hyperfine coupling to two equivalent phosphorus nuclei ($a(^{31}\text{P}) = 9.4$ G), two equivalent nitrogen atoms ($a(^{14}\text{N}) = 1.5$ G) and a unique nitrogen centre ($a(^{14}\text{N}) = 9.9$ G). The delocalisation of the unpaired electron, as indicated by the EPR measurements, is a significant contributor to the stability of **46**.

Sulphur-containing compounds make up the vast majority of heavier group 16 element radicals, the likes of which include dithiadiazolylys and related heterocyclic systems. Similarly, for selenium- and tellurium-centred radicals, there is no great overabundance of odd-electron species containing group 17 elements. Perhaps one of the most significant of tellurium radicals is the first stable tellurium(III) radical cation **47** (Figure 19), obtained by one-electron oxidation of the neutral precursor with $\text{Ag}[\text{AsF}_6]$.¹¹⁸ The EPR spectrum of **47** consists of a single, broad signal, indicating small spin density on the nitrogen atoms. In other words, the unpaired electron is localised in a p-orbital at the tellurium centre. The stability of **47** arises from steric protection provided by the substituents and from electrostatic repulsion between the positively charged chalcogen centres.

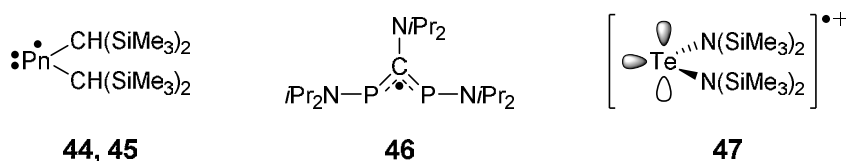


Figure 19. Stable pnictogen radicals **44** (Pn = P),^{115,116} **45** (Pn = As),^{115,116} **46**¹¹⁷ and tellurium-centred radical **47**.¹¹⁸

2.1.8 Biradicals and biradicaloids

Biradicals can essentially be described as molecules consisting of two unpaired electrons in two degenerate or nearly degenerate non-bonding molecular orbitals. They have a critical role in many bond breaking and bond formation processes. There are several papers discussing biradicals, including two excellent reviews by Grützmacher and Breher.^{119,120}

There are various types of biradicals. Trimethylenemethane (TMM)¹²¹ and tetramethyleneethane (TME)^{122,123} (Figure 20) represent quintessential delocalised biradicals (non-Kekulé molecules), while cyclopentane-1,3-diyl (CP(1,3))¹²⁴ and cyclobutanediyl (CB)¹²⁵ (Figure 20) are typical examples of localised biradicals with two well-defined radical substructures that are not conjugated in a way exhibited by classical π -systems. In essence, anti-aromatic molecules such as cyclobutadiene can be considered biradicals at their highest state of symmetry due to their degenerate pair of molecular orbitals occupied by π -electrons. Typically, organic biradicals are short-lived species under standard laboratory conditions, making them challenging to study experimentally. The two unpaired electrons readily go through a recombination to form a C-C single bond, which, for the most part, accounts for their high reactivity. Replacement of one or more of the carbon atoms in typical organic biradicals by main group elements generally stabilises the molecule, enabling its isolation and characterisation. The increased stability comes at a price, however, as the biradical character is reduced. Therefore, the term biradicaloid is more appropriate to describe these interesting main group species.

The radical centres in biradicals can interact with one another. As an example, in CB there is a through-space interaction between the two radical p-orbitals. This causes a relatively large HOMO-LUMO gap. The filled orbitals of π -symmetry of the bridging methylene units interact via bond interaction with the symmetric combination leading to a nearly degenerate orbital set. The strength of the exchange interaction between the two electrons, along with the overall electron correlation within the system, determines whether the electrons couple to give a singlet or a triplet state. For organic radicals, such as CB, the singlet and triplet states are very close in energy, with the triplet state being energetically slightly more favourable. For many main group biradicaloids, this situation is reversed. Theoretical considerations of biradicals and biradicaloids have shown that the singlet-triplet energy gap is one of the best experimental indicators of biradical character.^{126,127}

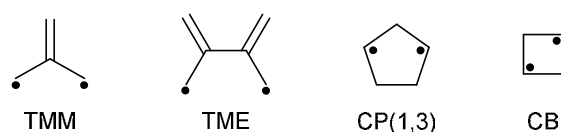


Figure 20. Archetypal organic biradicals: trimethylenemethane (TMM),¹²¹ tetramethyleneethane (TME),^{122,123} cyclopentane-1,3-diyl (CP(1,3))¹²⁴ and cyclobutanediyl (CB).¹²⁵

Even though research on biradicals extends back to the 1960s, it wasn't until 1995 when the first gram scale synthesis of singlet biradicaloids was reported by Niecke *et al.*¹²⁸⁻¹³² Specifically, 1,3-diphosphacyclobutane-2,4-diyls **48** (Figure 21) were formed in a 1 : 1 reaction between C-dichlorophosphaalkenes and *n*BuLi. The central ring in these P₂C₂ compounds is planar, while the carbon and phosphorus centres exhibit pyramidal coordination spheres. A relatively high inversion barrier prohibits the formation of a planar 6 π -conjugated heterocycle, resulting in a rather high biradical character. There is a remarkable differ-

ence in the stability of these two biradicaloids bearing different substituents, however. While the 2,2,6,6-tetramethylpiperidyl substituted species is unstable at room temperature and isomerises both in solution and in the solid state, the 1,3,5-tri-tert-butylbenzyl derivative is stable up to 150 °C.

A significant contribution to the field of biradical chemistry came in 2002 from Bertrand and co-workers when they prepared the localised, boron-centred singlet biradicaloid **49** (Figure 21).¹³³ Reaction between dichlorodiborane and 2 equivalents of lithium diisopropylphosphide produced **49** in a 68% yield. While the product is extremely air-sensitive, it is thermally remarkably stable with a melting point of 212 °C. Single-crystal X-ray measurements revealed the central ring to be perfectly planar. The P–B bond lengths were found to be 1.89 Å, which is slightly less than expected for single bonds, while the B–B distance is remarkably long at 2.57 Å, indicating that the B–B bond has been cleaved. Calculated geometrical parameters closely matched the experimental values obtained by X-ray diffraction measurements. The authors concluded that the use of sterically demanding substituents enabled the isolation and crystallisation of an iso(valence)electronic and isostructural transition state analogue of bicyclo[1.1.0]cyclobutane inversion.

More recently, Hinz *et al.* synthesised a mixed dipnictadiazanediyl **50** (Figure 21), representing the first heteroatomic biradicaloid, where P and As bear the radical character.¹³⁴ Compound **50** can be synthesised in a relatively large-scale reaction, and it is thermally stable up to and above 200 °C before decomposing without melting at 210 °C. A striking difference of **50** in comparison to homoatomic biradicaloids results from the symmetry breaking of the heteroatomic system: in **50**, the HOMO has a larger coefficient on the arsenic than on the phosphorus atom while the opposite is true for the LUMO. Because of the non-equivalence of the coefficients on the radical centres, biradicaloid **50** displays remarkable regioselectivity. This was demonstrated by treating **50** with CS₂ and phosphalkyne *t*Bu–C≡P. The reaction with CS₂ strongly favoured the formation of P–C and As–S bonds over P–S and As–C bonds. With *t*Bu–C≡P, the reaction yielded exclusively P–C and As–P bridged addition products.

A pioneering discovery was recently made by Sekiguchi and co-workers when they reported the first direct spectroscopic observation of a triplet diradical formed in a thermally induced rotation around a main-group π -bond.¹³⁵ The authors heated a solid sample of tetrakis(di-tert-butylmethylsilyl)disilene to obtain the triplet silyl diradical **51** (Figure 21). The sample produced a wide signal in the EPR spectrum at temperature range 350 – 410 K. The area of the half-field transition signal grew larger as the temperature was increased, which indicates that the triplet diradical is not the ground state; thus, the concentration of the diradical increases along with the temperature. The signal intensity also proved to be temperature reversible. Based on the experimental findings, the authors calculated the singlet-triplet energy gap to be roughly 30.6 kJ mol⁻¹. Theoretical calculations resulted in a singlet-triplet gap of the same order of magnitude. The calculations also demonstrated a highly twisted Si=Si bond for **51** with an average Si–Si–Si–Si dihedral angle of 75.2°. The spin density is locat-

ed almost completely in the two nearly orthogonal 3p-orbitals of the two central silicon atoms. The spins in **51** are nearly perpendicular to one another, which results in a greatly attenuated spin-spin interaction.

The examples presented above are just a few of the most significant results in the field of biradical chemistry, and much still remains to be discovered. As an example, organosulphur species form a group of compounds that have the potential to yield significant results and are definitely worthy of a closer look.¹³⁶⁻¹³⁸ Recently, Sekiguchi and co-workers carried out an extensive computational analysis on the properties of different types of biradicaloids.¹³⁹ Their main goal was to evaluate the potential of using biradicaloid compounds as building blocks of highly efficient open-shell, nonlinear optical materials.

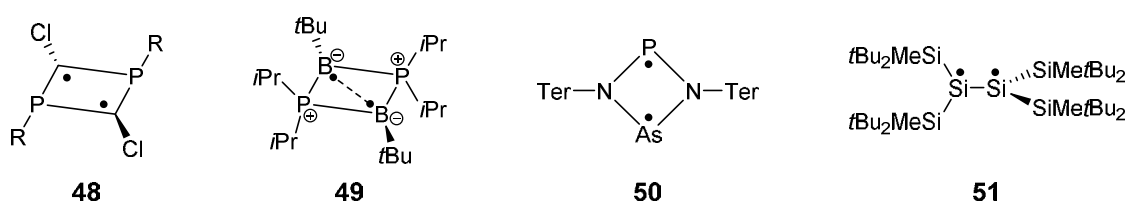


Figure 21. 1,3-Diphosphacyclobutane-2,4-diyl **48** (R = 2,2,6,6-tetramethylpiperidyl, 1,3,5-tri-tert-butylbenzyl),¹²⁸⁻¹³² boron-centred biradicaloid **49**,¹³³ heteroatomic biradicaloid **50**¹³⁴ (Ter = 2,6-bis(2,4,6-trimethylphenyl)phenyl) and triplet diradical **51**.¹³⁵

2.2 Transient radicals in organic synthesis

Stable radicals show promising potential as building blocks for new types of materials with technologically relevant properties; a good example is the possibility of using stable radicals in magnetic and conducting molecular materials.¹⁴⁰⁻¹⁴⁴ While new stable and persistent radicals are reported continuously, the vast majority of radicals are nevertheless transient, and many of these species are involved in chemical reactions. In the past, radical reactions were often considered to be too uncontrollable to be used productively in preparative synthesis.^{145,146} These days, however, radical reactions have emerged as a powerful tool in the development of novel synthetic routes, and they are frequently utilised in the synthesis of complex natural products. The majority of classical methods for generating C-C bonds rely on harsh reaction conditions achieved with strongly basic or acidic reagents and high temperatures. Such conditions are unsuited for many functional groups, which is a nuisance as this forces chemists to design synthetic routes that are long and circuitous rather than direct. On many occasions, radical reactions are more selective and predictable than their ionic counterparts. The functional group tolerance of radicals generally exceeds that exhibited by ionic reactions or other types of organic reactants. Typically, radical reactions can be carried out under pH-neutral conditions, and radicals can also be incorporated into elaborate cascade reactions that quickly and dramatically increase molecular complexity. Moreover, radical chemistry is

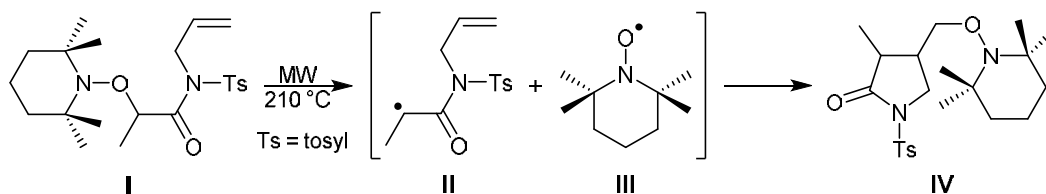
generally amenable to green chemistry. Numerous radical reactions can be carried out in water using environmentally benign reagents. The tolerance of water is a crucial benefit in itself: many traditional C-C bond-forming reactions need to be performed under rigorous exclusion of both water and oxygen.

The chemistry of radical reactions is vast and ever expanding. Therefore, this chapter shall act as a mere introduction to the use of radicals in synthetic chemistry. There is an abundance of literature covering the topic, from research papers to comprehensive reviews. Organic radical synthesis has been reviewed by Rowlands,^{146,147} while the use of inorganic radicals has been covered by Wille.¹⁴⁸ There are also reviews covering more specific topics, such as the persistent radical effect,¹⁴⁹ the catalysis of radical reactions¹⁵⁰ and radical reactions based on photogenerated intermediates.¹⁵¹

Organotin reagents have played a crucial role in the development of free-radical chemistry. These reagents have one major drawback, however, as they are highly toxic. Therefore, the urge to develop more benign methods has been a top priority for synthetic radical chemists. At the moment, there is an abundance of less harmful alternatives that can be used to replace toxic and often difficult-to-remove organotin reagents. Such alternatives include germanium and indium hydrides, thiols, and various transition metal-based, single-electron transfer reagents. There are also a number of organic reagents that have found use in radical reactions. An apt example of such organic species is the use of alkoxyamines in cross-coupling reactions.

An integral concept when discussing alkoxyamine reactions is the so-called persistent radical effect (PRE).^{149,152,153} PRE covers a large group of reactions in which two radicals are present, one being relatively long-lived or persistent while the other is transient in nature. These radicals react in a specific manner to yield the desired cross-coupling product. Due to the inefficiency of the persistent radical to undergo a homocoupling reaction, the non-selective reactions between the two radicals are subdued. Certain alkoxyamines yield, under thermal homolysis, persistent nitroxide radicals and short-lived carbon-centred radicals. The transient radicals will then undergo either cyclisation or intermolecular addition, after which they will react with the nitroxide radical to give the product. A majority of the radical precursors used in these reactions are based on TEMPO (**22**, Figure 10), and they are used in radical cyclizations and polymerisations.

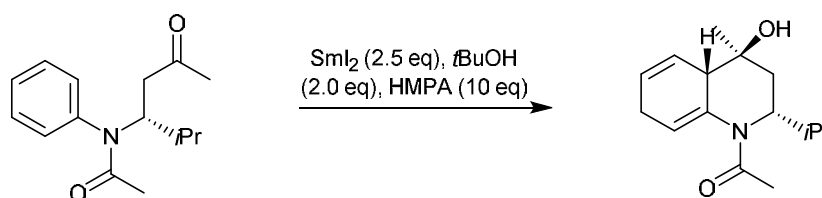
An example of utilisation of the PRE method is the cyclization of alkoxyamine **I** to lactam **IV** where **I** undergoes a reversible thermal homolysis to produce the stabilised radical **II** and TEMPO **III**. This is then followed by cyclization and irreversible trapping of the resulting primary radical to give **IV** as the product (Scheme 2).¹⁵⁴



Scheme 2. Cyclization of alkoxyamine **I** to lactame **IV** via radical intermediates.¹⁵⁴

Xanthates (*i.e.*, dithiocarbonates) are extremely useful in both inter- and intramolecular radical additions and, thus, offer a powerful alternative for organotin reagents. The key strength of xanthates is the broad applicability of the intermolecular addition to unactivated alkenes. This enables rapid assembly of complex structures as various functional groups can be brought together under mild reaction conditions. The presence of the xanthate group in the product also gives easy access to further modifications by both radical and non-radical pathways. Among the many papers covering the radical chemistry of xanthates are reviews written by Zard, who is one of the most prolific authors in the field.^{155,156}

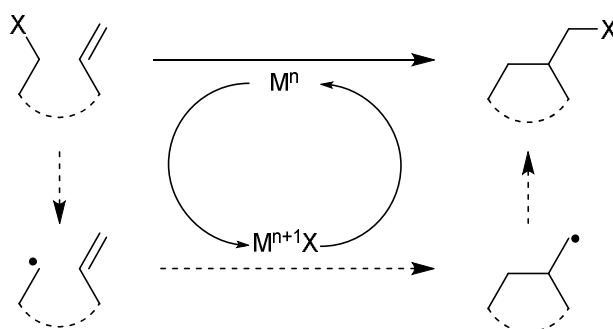
While there is an abundance of reagents that have found use in radical reactions, when focusing on the reactions themselves, radical cyclizations stand out as the most profuse class of radical transformations. This is mostly due to the high degree of regio-, chemo- and stereoselectivity taking place in the aforementioned reactions. Several radical additions to aryl rings result in the loss of aromaticity, which allows easy access to highly functionalised cyclic systems. An example of this type of reaction is the synthesis of hexahydroquinoline derivatives by regioselective protonation (Scheme 3).¹⁵⁷



Scheme 3. Synthesis of hexahydroquinoline derivatives (HMPA = hexamethylphosphoramide).¹⁵⁷

One of the most important categories among radical C–C bond-forming reactions are atom- and group-transfer reactions. The major advantage of these reactions is that they are isomerizations; therefore, no functionality is lost from the molecule, unlike what occurs in many other radical reactions. There are three basic categories of atom-transfer (and group-transfer) reactions: intermolecular atom-transfer radical addition (ATRA), atom-transfer radical cyclisation (ATRC) and atom-transfer radical polymerisation (ATRP). There are comprehensive reviews covering these specific topics.^{158,159} A vast array of transition metals are able to catalyse atom-transfer reactions. The basic mechanism of ATRA is presented in Scheme 4; while this is an oversimplification, it does provide

the general idea of how these reactions work. Essentially, ATRA is a redox reaction involving M^n and $M^{n+1}X$ complexes and an organic radical. The first step is halide abstraction that yields a stabilised radical and a metal complex $M^{n+1}X$ (the metal centre must be coordinatively unsaturated in order to enable atom abstraction). The next step is radical addition or cyclization that results in the formation of a carbon-carbon bond. In the final step, the newly formed, less stable radical reacts with $M^{n+1}X$ to give the product and the regenerated catalyst M^n . For the initial atom abstraction to take place, the C-X bond requires activation, which in turn requires the presence of electron-withdrawing groups to weaken the bond.

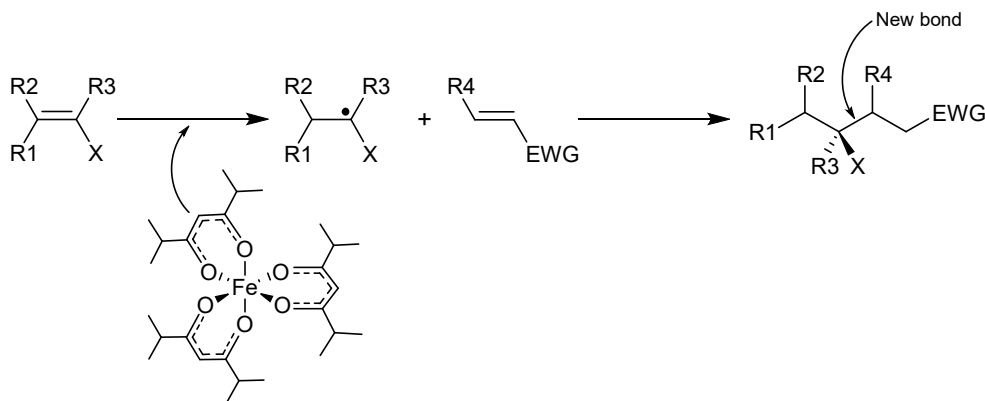


Scheme 4. General reaction mechanism of an atom-transfer radical addition.¹⁴⁷

Just like radical-addition reactions, radical rearrangements and fragmentations provide powerful tools for synthetic chemists. This includes the ability to sequence various transformations in elegant cascade reactions and tandem processes, which allows rapid increase in molecular complexity. As a result, remarkably elaborate compounds can be synthesised from simple and inexpensive starting materials. Among such compounds are various natural products, the synthesis of which would otherwise be challenging, if not impossible, using traditional synthetic procedures.

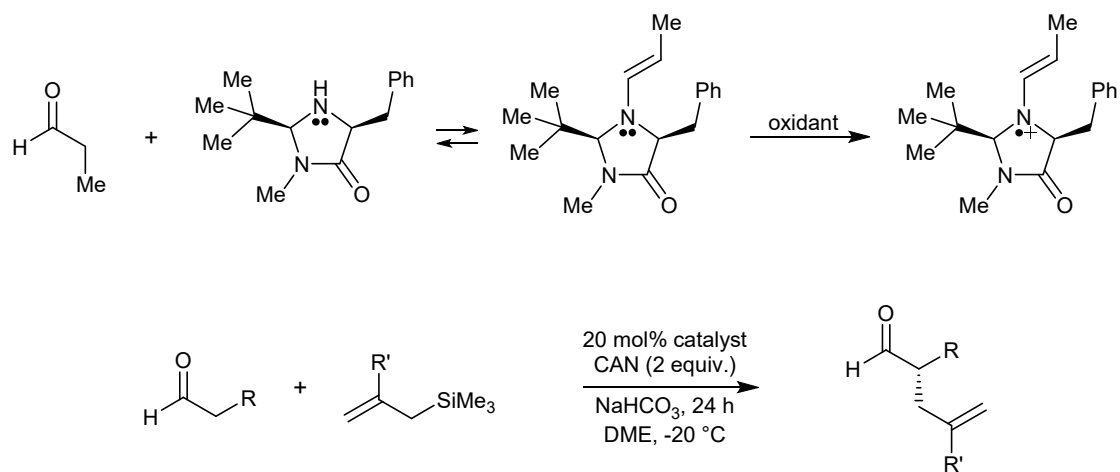
Radical reactions have proved to be highly useful in organic synthesis. However, they can be further improved by transition metal catalysis.¹⁶⁰ Using catalytic amounts of transition metal complexes in the generation and transformation of radicals provides explicit advantages over standard methods in radical chemistry. One such benefit is the improvement of reactions taking place under polar conditions. Many traditional transition metal catalysts have been palladium-based complexes. Recently, Lo *et al.* reported a C-C bond-forming reaction that utilises a relatively inexpensive iron complex (Scheme 5).¹⁶¹ While the ability of iron catalysts to generate free-radical intermediates from alkenes has been known for years,¹⁶² the method by Lo and co-workers was shown to be remarkably efficient. The authors used an iron catalyst that bears three, bulky diisobutyrylmethane ligands. It was shown that the optimal conditions for the catalyst to mediate C-C bond-forming reactions are when there is a reducing agent and a weakly basic additive (disodium phosphate) present. All organic reactions have limitations, and the issue with the alkene coupling reported by

Lo *et al.* is that bulky acceptor alkenes are not viable coupling partners. The substrate scope for the alkene used as a radical precursor is exceptionally broad, however.



Scheme 5. Alkene coupling reaction catalysed by an iron complex ($X = O, N, S, B, Si, F, Cl, Br, I$; EWG = electron-withdrawing group).¹⁶¹

Various transition metal complexes are common catalysts in organic synthesis. In recent years, organocatalysis has drawn the attention of many synthetic chemists. Organocatalysis is an area of research that relies on small organic molecules to act as catalysts for enantioselective transformations. The research group of MacMillan has made significant contributions to the field. In a paper published in 2007, they reported a method in which a single-electron oxidant is used to create a transient radical species from an aldehyde-based enamine.¹⁶³ This activates the parent aldehydes toward electrophilic addition and thus enables various heteroarylation and cyclization cascades. The synthetic procedure of MacMillan *et al.* is based on the formation of an imidazolidinone catalyst, which is a three π -electron radical cation. The radical cation is activated toward a variety of enantioselective catalytic transformations that were not conceivable with established catalysis concepts. The authors tested their method with a selection of allylation reactions using ceric ammonium nitrate as the stoichiometric oxidant and allyltrimethylsilane as the nucleophile. The formation of the catalyst and the general procedure of the test-reactions are shown in Scheme 6. The syntheses proved to work remarkably well: the yields varied from 70% to 88% with high enantiomeric excess. The results demonstrate the substantial scope of radical activation in organic synthesis, and this method will undoubtedly find use in preparation of natural products and pharmaceutical compounds.



Scheme 6. The allylation reactions reported by MacMillan *et al.* where an imidazolidinone radical cation is used as catalyst. The formation of the radical cation is shown on top and the general procedure of the allylation reactions at the bottom (CAN = ceric ammonium nitrate and DME = dimethoxyethane).¹⁶³

3 REACTIVE INTERMEDIATES

The formation of products in chemical reactions is often preceded by the formation of intermediates. Such intermediates are typically highly reactive, which shortens their lifetime and prevents their isolation. And yet these fleeting chemical entities are the key to understanding how chemical processes occur, making their characterisation and perhaps even isolation crucial in the quest to enhance our knowledge of chemistry. Typically, the characterisation of reactive intermediates is limited to fast, time-resolved spectroscopic measurements. However, in some specific cases, it is possible to isolate the intermediate in question, which enables its characterisation by conventional techniques. In recent years, as a result of the ever-increasing computing power of modern computers, quantum mechanical calculations have become more and more important in the identification of intermediates and the modelling of reaction pathways.

3.1 Characterisation of reactive species

3.1.1 Mass spectrometric studies of chemical intermediates

A majority of chemical reactions that are of interest to synthetic chemists take place in liquids, making various spectroscopic methods (for example, MS, IR, NMR and UV/Vis) integral in the characterisation of the reaction intermediates. Mass spectrometry is the most widely used of the aforementioned methods, as it allows direct tracking of reaction progress, detection of reactive compounds and the interrogation of mechanisms via appropriately designed experiments.¹⁶⁴ In recent years, there has been a burst both in the number and in the variety of available ionisation techniques. These advancements have enabled chemists to access chemistry at unprecedented timescales and to detect intermediates virtually under any set of conditions.

The most commonly used ionisation method is electrospray ionisation (ESI). It was initially developed in the late 1960s and adapted to practical use two decades later.^{165,166} In an ESI experiment, a plume of charged droplets from

the analyte solution is sprayed at atmospheric pressure. The droplets are then drawn into the heated inlet of the mass spectrometer where they evaporate and the ionised compounds are released for detection. There are a few key characteristics that have made ESI the principal method for solution state MS reaction monitoring, providing that the solvent is conductive.¹⁶⁴ First of all, mixtures of compounds dissolved in homogenous solutions are easily ionised by ESI, although the results thus obtained are typically qualitative. Electrospray also provides a constant source of ions, which makes this technique applicable to time-resolved studies of reactivity, ranging from seconds to minutes. Another virtue of ESI is that it is a soft ionisation technique, which means that the detected analytes are not generally fragmented. Finally, ESI is a ubiquitous technology, which means that the majority of researchers have access to the required instrumentation.

As a result of the above-mentioned characteristics, essentially all reactions occurring in solution can be studied by ESI-MS, including complex multicomponent reactions,¹⁶⁷ organometallic transformations,¹⁶⁸ polymerisation processes as well as inorganic reactions. ESI-MS is also suited for analysis of reactions involving air- and moisture-sensitive compounds as the reaction mixtures can be analysed *in situ* without affecting the chemical process taking place.¹⁶⁹ A number of reviews covering general reaction monitoring with ESI have been published in recent years. The reader is encouraged to look up some key reviews for a comprehensive understanding of the ESI-MS technique.^{168,170,171} Only a few essential examples of ESI-MS will be described here along with some key examples of direct MS reaction monitoring that use ionisation methods other than ESI.¹⁶⁴

Traditionally, time-dependent composition of an ongoing reaction is analysed by offline ESI-MS methods. Such techniques fail to give highly accurate data since the evaluation of exact reaction time is approximate at best. Furthermore, both the sampling of the reaction mixture and the subsequent sample manipulation require time. This prevents the analysis from starting at the beginning of the reaction when the all the reactants are initially mixed. More accurate results can be achieved by using microreactors coupled directly with the electrospray source^{170,172,173} or by using other, similar setups.¹⁷⁴

A ground-breaking technique for measuring high-quality, time-dependent MS spectra was developed by McIndoe *et al.*¹⁷⁵ The authors introduced the concept of pressurised sample infusion (PSI), which allows straightforward and continuous monitoring of reaction mixtures. In PSI, a small additional pressure is applied to a conventional Schlenk flask. This causes the reaction mixture to be continuously pumped to the ESI instrument through a short polyetheretherketone (PEEK) capillary, the tip of which is submerged in the solution. The pressure is provided by an inert gas, making this method applicable to air- and moisture-sensitive chemistry. Another advantage of PSI is that it allows monitoring of a reaction at any temperature below the boiling point of the solvent. This technique has been successfully applied to organometallic chemistry. PSI enables fast and accurate kinetic data by monitoring real-time growth and de-

cay of intermediates in catalytic reactions.¹⁷⁶ PSI has also provided extremely good results in real-time monitoring of three important reaction types. Short-lived intermediates (~5 s) were detected in Pd/C-catalyzed hydrogenolysis and several intermediates were observed in reductive amination as well as in Negishi cross-coupling reactions.¹⁷⁷

ESI-MS is widely used in the monitoring of both multicomponent reactions (MCR) and organocatalyzed reactions. The suitability of ESI-MS for studying these types of reactions results from two key features. First, the typically used reagents – carboxylic acids, amines, phenols and carbonyls – are polar and, therefore, susceptible to ionisation by ESI. Likewise, the intermediates are generally ionic and, consequently, demonstrate high ionisation efficiency.¹⁶⁷ The unique selectivity and the possibility of exploring wide concentration arrays makes ESI-MS ideal for mechanistic studies of complex, multistep reactions.

ESI-MS was successfully applied in the investigation of the Morita-Baylis-Hillman (MBH) reaction by Eberlin *et al.*¹⁷⁸ MBH is a multistep reaction that is catalysed by a nucleophilic catalyst, and it features a relatively complex catalytic cycle. The authors were able to intercept and characterise intermediates of the MBH reaction for the first time. A number of other unresolved factors regarding the mechanism of the MBH reaction have also been studied by ESI-MS measurements. Recently, Neto *et al.* studied the use of an imidazolium-based charged acrylate derivative as a reactant.¹⁷⁹ The aim of the study was to improve ESI-MS detection of the intermediates, and the authors managed to successfully characterise transient zwitterionic species and noncovalent adducts from the reaction path.

Research on the reaction mechanism of homogenous metal-catalysed reactions has progressed considerably in recent years. ESI-MS is an ideal method to study these reactions as it allows tracking of multiple metal complexes present in trace amounts in intricate solutions without perturbing their coordination sphere.¹⁶⁸ ESI-MS analysis of metal complexes is not affected by the requirement of the analysed species to be charged because metal complexes are either already charged or they are ionised by protonation during the spray generation. As an example, ESI-MS studies recently provided outstanding results in the investigation of nickel-mediated transformations. The mechanism of enantioselective nickel-catalysed Negishi arylation of propargylic bromides was studied by the combination of ESI-MS, heteronuclear NMR, EPR and crystallographic measurements.¹⁸⁰ The authors described a radical-chain mechanism where nickel goes through nickel(I), nickel(II) and nickel(III) oxidation states. They used ESI-MS to characterise the predominant aryl/nickel resting state of the catalyst, thus proving that the oxidative addition of the C-Br bond occurs through a bimetallic mechanism.

While electrospray ionisation has experienced considerable success in the analysis of chemical processes, it does have few significant limitations. First, reaction times of less than a few seconds require specific, sophisticated instrumentation. Second, ESI is not generally applicable to ionisation from nonpolar,

nonconductive solvents. Finally, compounds must be charged, or they must contain acidic or basic functionalities in order to be easily ionised. This has encouraged chemists to develop other methods to monitor reactions and characterise intermediates.

Desorption electrospray ionisation (DESI) is a surface ionisation variant of ESI.¹⁸¹ DESI was developed in 2004, and it has since been used in a variety of fields, including reaction monitoring and identification of reactive intermediates. The basic operational principle of DESI is similar to ESI. Just like ESI, the DESI source consists of coaxial inner and outer capillaries. The inner capillary carries either a pure solvent or a reagent solution while the outer capillary carries a high-pressure nebulising gas that generates a plume of droplets. An ionising potential can be applied at the source or to the solution prior to entering the source. Charged solvent droplets hit a surface containing the analyte, and as the droplets come into contact with the surface, the embedded analytes are extracted into a nascent liquid film. The impact of the primary droplets generates secondary microdroplets that contain the extracted analyte. These secondary droplets are then intercepted by the mass analyser.

After its invention, DESI was quickly developed to a technique capable of initiating and studying reactions at short timescales. One of the earliest modifications was to add derivatising reagents to the spray. It was shown that addition of hydrochloric acid into the spray solvent leads to increased formation of Cl^- adducts in negative ion mode.¹⁸² This concept was developed further to include derivatisation of analytes on the surface by adding analyte-specific reagents to the sprays.¹⁸³ The authors were able to selectively identify *cis*-diol functionalities in carbohydrates via cyclisation with phenylboronate ions contained in the electrospray. Following these early developments, DESI was also adapted for analysis of liquid-state reactions.^{184,185}

The reaction and analysis times in DESI-MS are on the order of milliseconds or less. This makes DESI an extremely suitable method for the detection of short-lived intermediates. A good example is the characterisation of intermediates formed in a rhodium-catalysed oxidative C-H amination reaction.¹⁸⁶ Computational results indicated that a rhodium nitrene with a lifespan of a microsecond forms during the reaction, which acts as the key N-transfer intermediate. An experimental setup was then created where a surface containing the Rh catalyst and the substrate was sprayed with a nitrene-containing solution. The predicted rhodium nitrene intermediate was detected as a Na^+ adduct using DESI-MS. By a clever use of deuterated dichloromethane, the authors discovered that the nitrene will abstract a hydrogen atom from the solvent if there is an insufficient concentration of the substrate present in the reaction vessel. This will lead to the formation of a mixed valent Rh(II/III) dimer that appears to be inactive. In a similar fashion, a short-lived diiron (III/IV) imido intermediate was characterised by DESI-MS.¹⁸⁷ This intermediate was found to be active for nitrene transfer and amine synthesis. Likewise, the abstraction of a hydrogen atom from the surrounding solvent competes with the nitrene transfer.

DESI can also be adapted to electrochemical mass spectrometry. Brown *et al.* recently applied DESI to detect electrochemically generated intermediates directly from an electrode surface.¹⁸⁸ The fast sampling times of DESI enabled the authors to identify highly reactive, previously undetected intermediates of uric acid and xanthene oxidations. Later on, the same authors managed to detect a highly unstable singly oxidised radical cation formed in an oxidative dimerization of *N,N*-dimethylaniline.¹⁸⁹

The examples described above demonstrate the suitability of DESI-MS for the detection of highly reactive intermediates. When compared to traditional ESI experiments, DESI allows much more rapid screening of reagents and reaction conditions in the pursuit of specific intermediates as changing from one reagent to another doesn't require the disassembly and rigorous cleaning often associated with ESI. One notable disadvantage of DESI is its generally poor applicability for the examination of air-sensitive chemistry, though there are examples where atmospheric deterioration has been reduced or avoided altogether.^{184,190}

3.1.2 Diffusion-ordered NMR in the characterisation of reaction intermediates

NMR spectroscopy with isotopically labelled compounds has an established role in the characterisation of compounds in solution. To some extent this can be a viable method in the identification of reactive intermediates as well. In recent years, diffusion-ordered NMR (DOSY)¹⁹¹ has become increasingly important for identifying compounds in solution. The diffusion coefficient D – the physical observable that can be derived from the diffusion NMR experiment – is sensitive to the size and shape of the compound.¹⁹² This allows the DOSY experiment to separate NMR signals of species according to their diffusion coefficients. There is no simple relationship between the diffusion coefficient and the molecular weight (MW), however, and while a number of empirical methods for relating diffusion coefficients to the MW have been proposed, they are restricted to a specific class of compounds.^{193–195} Recently, Neufeld and Stalke introduced a method that brings the accuracy of MW determination by DOSY to a new level.¹⁹⁶ This method is based on external calibration curves (ECC) that facilitate the determination of MWs for compounds with different geometries, regardless of NMR-specific properties or differences in temperature or solvent viscosity.

Prior to Neufeld and Stalke, the research group of Williard had developed a method for determining MWs by using internal calibration curves (ICC).¹⁹⁷ This method has some distinct disadvantages, however. For example, the internal references are limited to a set of specific prerequisites: the references need to be inert to the analyte in solution, their NMR signals must not overlap with other components, and the references should not be able to coordinate to the analyte. And these are just a few of the requirements. The ECC method overcomes most, if not all, of these limitations. In the ECC technique, the calibration curves are generated by measuring model compounds in independent NMR

samples as opposed to measuring them in the NMR sample that is being analysed; hence, the name external calibration curve.

One of the key features of ECC is that it is possible to simulate a large set of internal references by adding just one of them to the NMR sample. This interrelation has the significant advantage that it is not necessary to include all of the references in the same NMR sample. This, in turn, overcomes problems that stem from signal overlapping and analyte-reference interaction issues. Likewise, wasting chemicals and deuterated solvents can be avoided.

The ECC technique is a very robust method. The authors tested various sample concentrations (from 15 mM to 120 mM) and measurement temperatures (from room temperature to $-75\text{ }^{\circ}\text{C}$) and found these to have a minor effect on the accuracy of the MW predictions. For most of the studied compounds, the average deviation was within $\pm 9\%$ range. Remarkably, MW-determination is possible at temperatures near the boiling point of the solvent, which enables the detection of species that form during reactions at elevated temperatures.

While ECC isn't sensitive to changes in concentration or temperature, it does have one distinct disadvantage. The diffusion coefficient depends on the shape and on the hydrodynamic radius of the compound.¹⁹⁵ The latter results from the volume of the surrounding solvent molecules, the electron cloud and the volume of the atoms. And herein lies the problem: the volume of an atom is not proportional to its atomic weight. Halides are an embodiment of this issue; they have very high atomic masses in comparison to their atomic radii, which results in high mass density. This means that the MWs of compounds that contain heavy halides are underestimated. Therefore, a new calibration curve with references to comparable molar densities and geometries is required in order to obtain accurate molecular weights for compounds with high densities.

The use of external calibration curves has numerous advantages when compared to internal standards, but that is not to say that ICCs are futile. Recently, internal calibration curves were successfully used to characterise reactive intermediates in catalytic asymmetric reactions.¹⁹⁸ The authors' aim was to apply DOSY to complexes between basic substrates and Brønsted acids as this would provide insight into ion pairing and aggregation. The initial attempts using ^1H DOSY were hampered by signal overlapping, however, but subsequent experiments using ^{19}F DOSY provided excellent results: the agreement between DOSY-calculated and actual formula weights was extremely good. ^{19}F is well suited to DOSY experiments due to its well-resolved signals and high sensitivity.

Pedersen *et al.* applied ^1H - and ^{19}F - DOSY to carbohydrate chemistry by analysing reactive intermediates in glycosylation reactions at low temperature.¹⁹⁹ The authors studied the interaction of three different catalysts with glucosyl trichloroacetimidate and found that reaction paths and intermediates are different in each case. Two common catalysts, $\text{BF}_3 \cdot \text{OEt}_2$ and TMSOTf , yielded glucosyl-fluorides and triflates as intermediates whereas Tf_2NTMS was found to activate the trichloroacetimidate catalytically without cleaving the glycosidic bond.

3.1.3 Isolated and characterised intermediates

Various spectroscopic methods provide invaluable help in identifying and characterising reactive species and reaction intermediates. Nonetheless, being able to obtain a single crystal structure of the studied compound can be considered as the ultimate goal. There are numerous reports where chemists have successfully isolated and structurally characterised a reactive intermediate. In this section, a few essential examples from the field of main group chemistry will be presented.

The oxidation of organic compounds is an important reaction in synthetic chemistry. Traditionally, such reactions require transition metal catalysts or other environmentally harmful reagents. Therefore, developing environmentally benign processes is highly desirable. Maier *et al.* recently reported an acceptorless dehydrogenation of heterocycles that is catalysed by FLPs.²⁰⁰ In their study, molecular hydrogen is released during an oxidation of *N*-protected indolines and four other substrate classes by using boron-derived FLPs – namely, tris(pentafluorophenyl)borane $B(C_6F_5)_3$ – as the activating agent. The authors carried out a comprehensive investigation, including the characterisation of the intermediates by NMR and X-ray crystallography, and their study represents the first reported catalytic oxidation of organic substrates with simultaneous release of molecular hydrogen by FLPs.

Maier *et al.* reacted *N*-methyl hexahydrocarbazole with $B(C_6F_5)_3$ in a 1 : 2 scale at room temperature. The second equivalent of $B(C_6F_5)_3$ is needed in order to scavenge the proton from the transiently generated indolium intermediate. The authors were able to characterise the intermediate by 1D and 2D NMR spectroscopy. From an analogous reaction with 6-chloro-1-methylindoline in toluene, they were able to crystallise the intermediate **52** (Figure 22). The structure features a short intermolecular $NH \cdots HB$ distance of 1.73 Å between the indoline and the borane, indicating a dihydrogen bond.²⁰¹ After the initial reactions, a catalytic dehydrogenation using 5 mol-% of $B(C_6F_5)_3$ was tested. The authors used a variety of indolines as well as other substrates (isoindolines, 1,4-dihydropyridines, thiazoles and 1,2-dihydroquinolines) and achieved largely high-to-excellent yields. The catalytic reactions do require heating to 120 °C and, depending on the substrate, the reaction time can be up to 24 h.

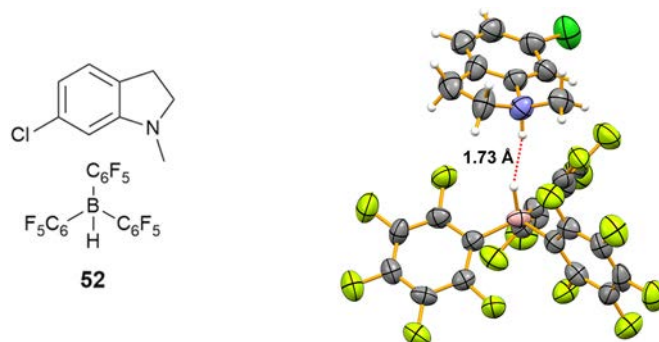
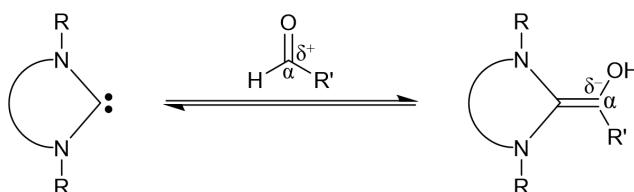


Figure 22. Structure of reactive intermediate **52** (left) and its corresponding single-crystal structure (right, CCDC: 1489310, thermal ellipsoids set at 50% probability).²⁰⁰

Interestingly, tris(2,4,6-trifluorophenyl)borane was found to be inactive in the dehydrogenative oxidation, but it can act as a hydride shuttle as boranes can undergo hydride exchange.²⁰² Therefore, using catalytic amounts of tris(2,4,6-trifluorophenyl)borane in combination with $B(C_6F_5)_3$ enhances the rate of the dehydrogenation reactions.

NHC-catalyzed formation of so-called Breslow intermediates (*i.e.*, (di)aminoenols) is an integral part of enzymatic and organocatalytic umpolung reactions.^{203,204} An example of such an intermediate is an aldehyde substrate where the innate polarity is inverted from electrophilic to nucleophilic (Scheme 7).^{205–207}



Scheme 7. Carbene-catalysed formation of a Breslow intermediate from an aldehyde.^{205–207}

Berkessel *et al.* reported the first unambiguous generation and characterisation of a number of Breslow intermediates (2,2-diamino enols).²⁰⁸ The authors discovered that simply combining a saturated carbene with an equimolar amount of aldehyde readily forms diaminoenols which, under rigorous exclusion of oxygen, persist for several hours. Instantaneous decomposition of the intermediates takes place upon exposure to air. The formation and longevity of the intermediates was monitored by NMR spectroscopy.

The effortless formation of 2,2-diamino enols proved the accessibility of the Breslow intermediates from aldehydes and NHCs. The authors then used Ph-C²H₂O and ¹H/²H NMR spectroscopy to show that the hydroxylic proton/deuteron in the 2,2-diamino enol product does indeed come from the aldehyde. This was followed by a synthesis of the 2,2-diamino enol ethers by alkylation and subsequent deprotonation of NHCs. Again, the authors prepared a series of Breslow intermediates, two of which they managed to crystallise from n-pentane (compounds **53** and **54**, Figure 23). These methylated Breslow intermediates were reported to be almost indefinitely stable under oxygen-free atmosphere but rapidly oxidise to afford the corresponding heterocyclic ureas under exposure to air.

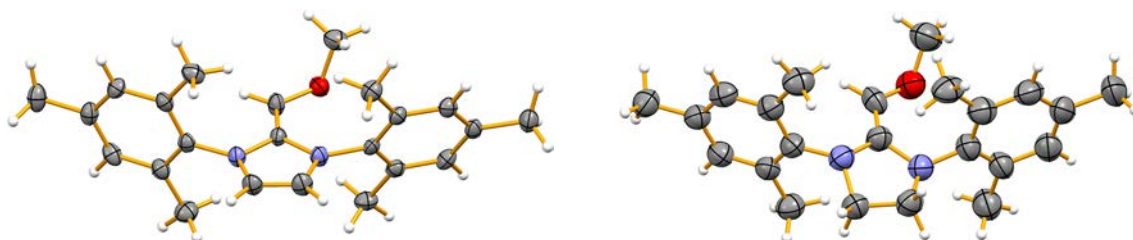


Figure 23. X-ray crystal structures of methylated Breslow intermediates **53** and **54** (CCDC: 892934 and 892935, respectively; thermal ellipsoids set at 50% probability).²⁰⁸

In their original study, Berkessel *et al.* were able to crystallographically characterise the O-methylated amino enols. In the following year, they published another study in which they managed to successfully crystallise three 2,2-diamino enols, two diamino enols and two azolium enolates.²⁰⁹ This enabled the authors to investigate the effects of electron density modulation on the structural parameters of the intermediates, especially around the reactive enol C=C bond.

In their previous paper, Berkessel *et al.* had shown how saturated imidazolidinylidene SIPr reacted smoothly with a variety of aldehydes at room temperature, which results in the formation of 2,2-diamino enols. Initial attempts to crystallise these compounds from THF were unsuccessful, but changing the solvent to benzene and rigorous exclusion of oxygen resulted in the crystallisation of three Breslow intermediates **55**, **56** and **57** (Figure 24). The OH hydrogen atom could be located in the Fourier map in each structure, and somewhat surprisingly, there is no inter- or intramolecular hydrogen bonding to or from the enol OH group. The crystal packing seems to be based on dispersive hydrocarbon interactions. The authors also carried out extensive reactivity studies, including high-level theoretical calculations, to model the reactivity and reaction paths of these NHC-catalysed umpolung reactions.

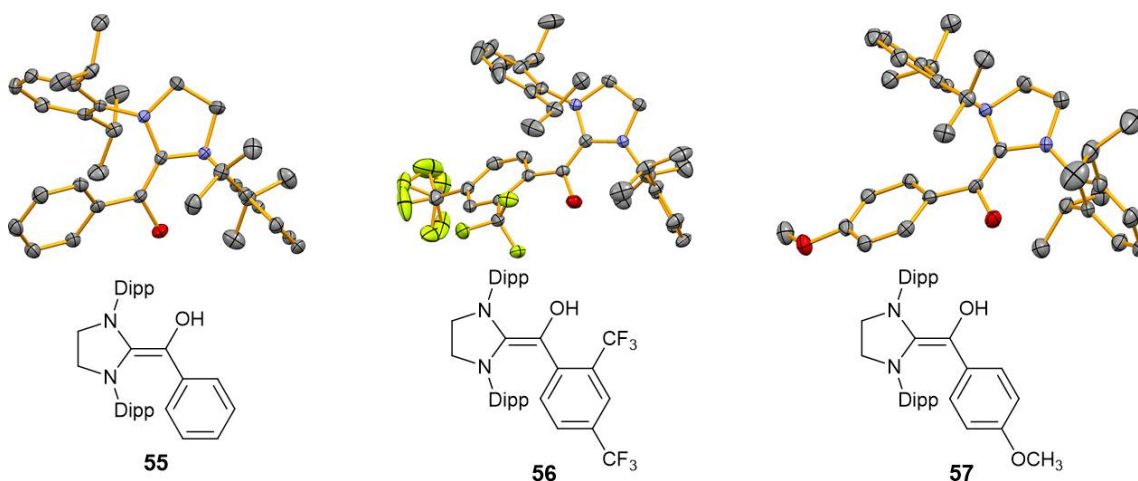


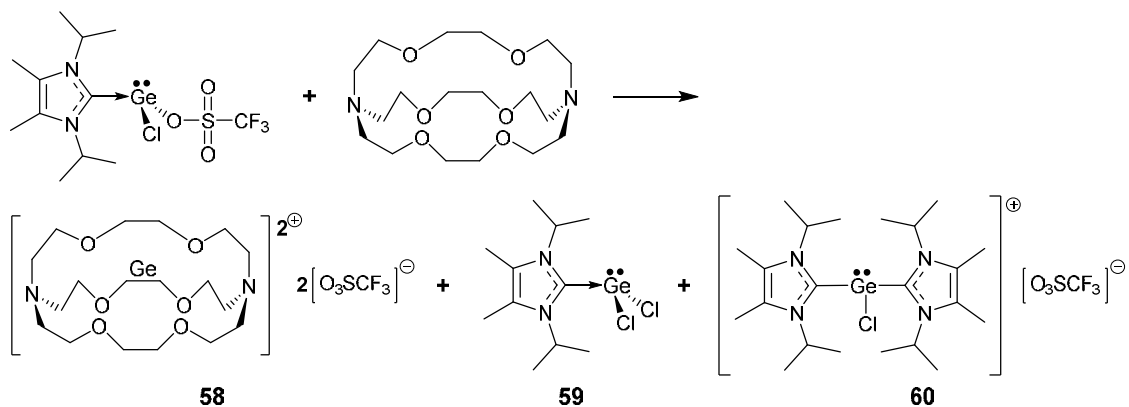
Figure 24. Crystal structures of 2,2-diamino enols (*i.e.*, Breslow intermediates) **55** – **57** (CCDC: 911917, 911918 and 911919, respectively; thermal ellipsoids set at 50 % probability, hydrogen atoms have been omitted for clarity).²⁰⁹

Research of reactive intermediates in organic chemistry has primarily been focused on carbenium ions (R_3C^+), carbanions (R_3C^-) and carbenes ($R_2C:$).²¹⁰ Open-shell variants include neutral ($R_3C\cdot$) and charged radicals. The reactivity of these intermediates stem mainly from their charge and open-shell character. Higher charge and further loss of electrons would only increase the reactivity of these species, thus making their isolation even more challenging. A series of six-electron carbon intermediates would be formed if one were to successively remove a ligand without its electron pair from the carbenium ion. A similar series of increasingly electron-deficient intermediates would be formed by successive removal of ligands with their electron pair. An extremely reactive species from

the aforementioned series is a carbon with a +2 charge and only two valence electrons (*i.e.*, C:²⁺).

Rupar *et al.* managed to isolate the germanium(II) dication, Ge:²⁺, which is analogous to C:²⁺.²¹¹ This was the first time a free, doubly charged non-metal (metalloid) ion was reported. Non-metallic cations differ in many respects from the metal cations that are often encountered in chemistry, such as Na⁺ and Ca²⁺. Instead of having four valence electron lone pairs, Ge:²⁺ possesses only one lone pair and three empty orbitals in its valence shell. The metallic cations are solvated in an aqueous solution, while Ge:²⁺ would react instantly with a nucleophile such as water due to its empty orbitals.

Isolating group 14 ions with vacant coordination sites can be achieved by using bulky ligands and/or using noncoordinating counterions.²¹² Using these methods will prevent the coordination of a fourth ligand that would complete the octet at the group 14 element.¹⁰⁷ Following these principles, Rupar *et al.* used cryptand [2.2.2] and an NHC complex of GeCl(O₃SCF₃)^[213] as starting materials in an attempt to isolate the germanium(II) dication. The authors added one equivalent of cryptand [2.2.2] to a solution containing three equivalents of GeCl(O₃SCF₃) and stirred the reaction mixture for 24 h (Scheme 8). They obtained the (Ge · cryptand [2.2.2])²⁺ complex **58** as a white powder. In addition to **58**, the authors obtained complex **59** and cationic dicarbene complex **60** from the mother liquor. They postulated that the precipitation of **58** caused the displaced chloride and carbene to react rapidly with two equivalents of GeCl(O₃SCF₃), which results in a displacement of the labile triflate and formation of **59** and **60**. The yields for **58**, **59** and **60** were 88, 81 and 96%, respectively.



Scheme 8. The synthesis of germanium complexes **58** – **60**.²¹¹

Rupar *et al.* carried out a thorough characterisation of compound **58**. ¹H NMR showed three distinct signals that result from the cryptand moiety, while there was no sign of signals attributable to a carbene moiety. ¹⁹F NMR showed one single resonance that results from the triflate anion. The crystal structure of **58** (Figure 25) shows the dicationic germanium to be located inside a cryptand cavity. The (Ge · cryptand [2.2.2])²⁺ complex has D₃ symmetry with the Ge atom located directly at the centre of the cage. The triflate anions do not interact with the germanium with the closest triflate-oxygen-germanium approach being 5.32

Å. The Ge-N and Ge-O distances in the crystal structure are 2.524(3) Å and 2.4856(16) Å, respectively. These are significantly longer than the typical lengths of Ge-N and Ge-O single bonds (1.85 Å and 1.80 Å, respectively).²¹⁴⁻²¹⁶ The elongation clearly indicates that the Ge atom has no significant bonding interactions with any of the cryptand atoms.

Finally, Rugar *et al.* carried out a comprehensive computational analysis on **58** in order to get a deeper understanding of its electronic structure. The natural bond orbital (NBO) analysis indicates no strong covalent bonding interaction for the Ge atom; the valence NBO on the germanium centre is a 4s non-bonding, lone electron pair. The Ge²⁺ cation is a strong Lewis acid, capable of accepting electron density from the cryptand heteroatoms, and the NBO analysis does indeed predict fairly significant interactions between the nitrogen and oxygen lone electron pairs and the virtual orbitals at the germanium centre. Natural population analysis of **58** exhibits a relatively high residual charge (+1.38) on the germanium centre, which indicates that a majority of the cationic charge remains on the Ge atom, regardless of the donor/acceptor interactions with the cryptand.

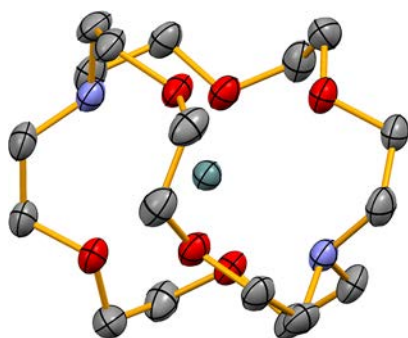
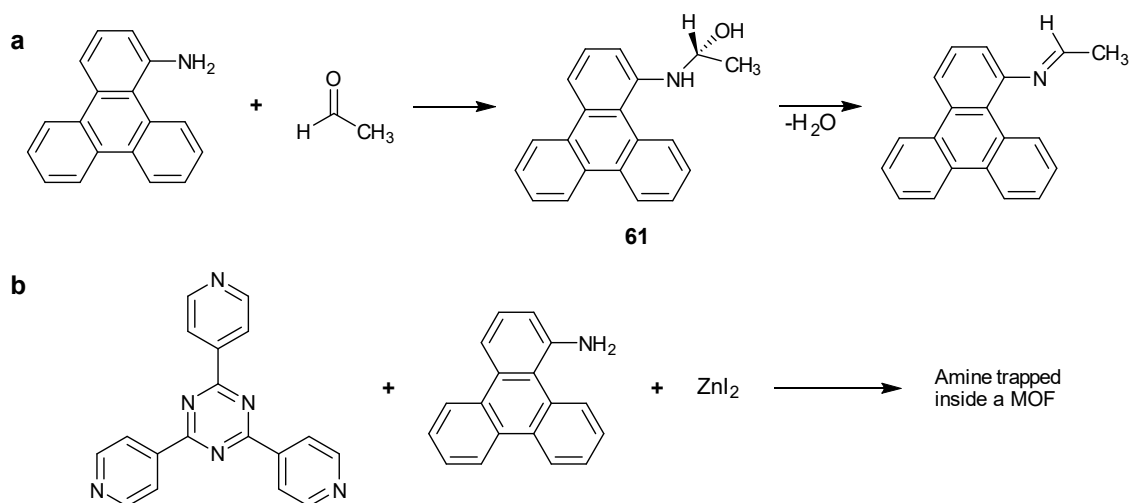


Figure 25. The crystal structure of **58** (CCDC: 704541).²¹¹ Triflate anions and hydrogen atoms have been omitted for clarity and thermal ellipsoids set at 50% probability.

Rugar *et al.* designed a system specifically for isolating the reactive Ge²⁺ cation. In a similar fashion, the approach reported by Kawamichi *et al.* utilised a porous crystalline framework to trap and crystallographically characterise an unstable hemiaminal intermediate **61**.²¹⁷ Kawamichi *et al.* studied a common organic reaction: the combination of an amine and an aldehyde to form a Schiff base (Scheme 9). The mechanism of this reaction has been studied extensively over the years, but direct observations of the elusive hemiaminal intermediate are rare. The crystal structure was obtained by trapping the hemiaminal in the reactive site of an enzyme, but structure determination in protein crystals is not a viable method for general characterisation of reactive intermediates.^{218,219}



Scheme 9. a) The synthesis of Schiff base via the hemiaminal intermediate **61**. b) The general procedure to prepare the metal-organic framework with the amine reactant trapped inside its porous cavity.²¹⁷

Kawamichi *et al.* used a porous coordination network of organic ligand molecules and metal ions – better known as metal-organic framework (MOF) – to trap the amine starting material. For this study, they used a MOF prepared by slowly diffusing layers of ZnI_2 , 2,4,6-tris(4-pyridyl)-1,3,5-triazine and 1-aminotriphenylene in nitrobenzene (Scheme 9).²²⁰ In order to allow rapid diffusion of reactants and thus enable chemical reactions to take place in the pores of the framework, Kawamichi *et al.* replaced nitrobenzene with a non-aromatic solvent by immersing the crystals in ethyl acetate for 24 hours. They then took a crystal and mounted it on a diffractometer, covered it with a capillary and cooled it to 215 K. The authors then introduced a continuous flow of an ethyl acetate solution of an acetaldehyde through the capillary for 10 min. The reaction was stopped by cooling the crystal to 90 K, after which crystal data were collected. The data revealed the transient hemiaminal intermediate **61** (Figure 26). After the data collection, the crystal was warmed to 270 K for 30 min to complete the condensation reaction. This was followed by cooling the crystal again to 90 K and collection of another set of diffraction data, which showed a complete conversion of the hemiaminal to the final imine product.

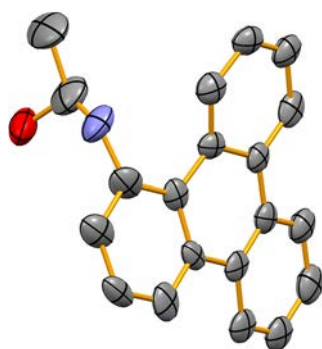


Figure 26. Thermal ellipsoid plot of hemiaminal intermediate **61** (CCDC: 725639, ellipsoids set at 30% probability, hydrogen atoms have been omitted for clarity).²¹⁷

The strategy reported by Kawamichi *et al.* can be extended to other intermediates, but it is not universally applicable.²¹⁹ For example, only reactions that occur under conditions that do not damage the coordination network can be studied by the method. Likewise, it is crucial that the reactions themselves do not degrade the relatively fragile network. Nevertheless, the method of Kawamichi *et al.* proves how postsynthetic modification of coordination networks is a widely applicable tool for isolation and characterisation of intermediates formed during chemical reactions.

4 RESULTS AND DISCUSSION

The methods used in the synthesis, characterisation and computational modelling of the studied systems are described briefly in the beginning of this chapter. A more detailed account can be found in Papers I – V.

4.1 Experimental methods

The experimental work was carried out under anaerobic and anhydrous conditions by applying Schlenk line techniques under an inert atmosphere or by using a drybox. X-ray crystal structure measurements were performed either with (1) an Agilent SuperNova dual wavelength diffractometer equipped with an Atlas CCD area-detector using Cu K α radiation, or (2) a Bruker APEX II diffractometer equipped with a CCD area-detector using Mo K α radiation. With the Agilent instrument, the data acquisition, reduction and analytical face-index based absorption correction was performed using CrysAlisPro²²¹ software. With the Bruker instrument, the cell refinement and data reduction were performed using the Bruker SAINT²²² software with semi-empirical SADABS absorption correction.²²³ The structures were solved by direct methods using SHELXT,²²⁴ Superflip²²⁵ or EDMA²²⁶ programs and refined on F^2 by full-matrix least-squares method using SHELXL²²⁴ program. The figures were drawn with the program Mercury.²²⁷

NMR spectroscopy was carried out using Bruker Avance NMR spectrometers (300 MHz, 400 MHz and 500 MHz instruments). The EPR spectra were recorded with a Magnettech GmbH MiniScope 200 X-band EPR spectrometer with the samples placed in a Teflon screw cap EPR tube. The EPR spectra were simulated using EasySpin²²⁸ software. Cyclic voltammetry measurements were performed either with a BASi epsilon potentiostat or with a Gamry Reference 600 potentiostat. Elementar Analysensysteme GmbH Vario EL III element analyser was used for the elemental analyses.

4.2 Computational methods

Theoretical calculations were primarily carried out by using density functional theory (DFT) and employing Gaussian 09 program package.²²⁹ The calculations were performed with the PBE1PBE exchange correlation functional^{230–233} using Ahlrichs' TZVP^{234,235} and def2-TZVP^{236,237} basis sets. Vibrational analyses were performed for all studied systems to ensure that the stationary points correspond to true minima or first order transition state on the potential energy surface. Where required, Grimme's empirical dispersion correction was used.²³⁸

4.3 Stable main group radicals

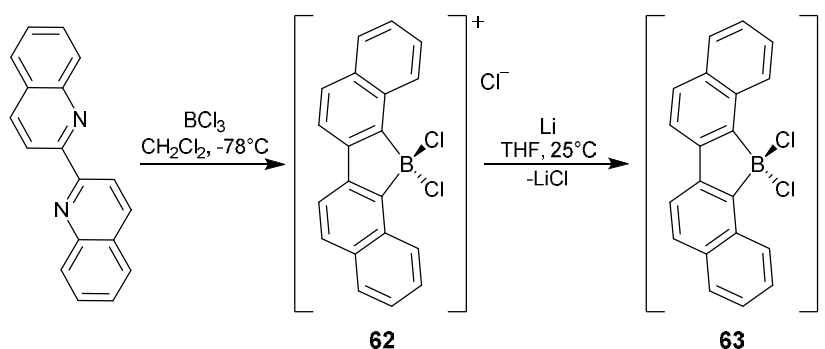
The past few decades have seen a wealth of new stable radicals being reported, including entire families of odd-electron species. However, the majority of known radicals are transient in nature, so there is still a considerable demand to develop new stable and persistent radical frameworks. Also, many of the known stable species require long and arduous synthetic procedures, so a call for simple and efficient synthesis is strong.

4.3.1 p-Block complexes of 2,2'-biquinoline^I

Coordination compounds of non-innocent ligands have promising potential in various areas of chemistry, particularly in bioinorganic chemistry.²³⁹ Under appropriate conditions, virtually any ligand can display non-innocent behaviour,²⁴⁰ but determining the charge on the ligand may sometimes be challenging.²⁴¹ Typically, adding or removing an electron affects intraligand bond lengths.²⁴² These changes can be detected by X-ray crystallography, but sometimes additional analyses, such as spectroscopy, voltammetry or magnetic measurements, are required to correctly define the charge state of the ligand.

In order to study the ligand behaviour of 2,2'-biquinoline (biq), the salt [(biq)BCl₂]Cl **62** and the corresponding radical [(biq)BCl₂][•] **63** were synthesised and characterised. The coordination of biq to boron prevents back-bonding and constrains all redox processes to the ligand framework, which enables univocal structural characterisation of a coordinated anionic biq radical.

2,2'-Biquinoline was dissolved in CH₂Cl₂ and cooled to -78 °C, followed by a dropwise addition of 1 equivalent of BCl₃ (Scheme 10). The reaction mixture turned yellow, and a bright yellow precipitate started to form. The reaction mixture was gradually warmed to room-temperature and, after an appropriate reaction time, the product was separated from the solution and dried under vacuum to afford **62** as a bright yellow solid in a quantitative yield. Single crystals of **62** were grown from a saturated CH₃CN solution at -20 °C.



Scheme 10. Synthesis of chloride salt **62** and a one-electron reduction of the cation to produce radical **63**.¹

The reduction of **62** was studied by cyclic voltammetry, which showed the cation to undergo a one-electron reduction at -0.82 V (*vs.* SCE). The reduction of **62** was performed at room temperature by dissolving a small amount of the compound in THF, followed by the addition of a stoichiometric amount of lithium (Scheme 10). After an appropriate reaction time, the solvent was removed *in vacuo* to give a black solid. The solid was redissolved in CH_2Cl_2 and filtered to afford **63** as a black powder. Single crystals of **63** were grown by dissolving a small amount of the black solid in CH_2Cl_2 and carefully layering *n*-hexane on top of the solution. This mixture was kept at -20 °C for a few days to afford dark yellow crystals.

An EPR spectrum of **63** was measured to study its paramagnetic properties (Figure 26). A very small amount of the black powdery solid was dissolved in CH_2Cl_2 to give a brownish-yellow solution. **63** is persistent in solution for hours without any signs of decomposition as long as it is stored under an inert atmosphere. The EPR spectrum consists of a symmetric 16-line pattern that is *ca.* 60 G wide ($g = 2.0006$). The spectrum was simulated by employing a fitting algorithm with calculated (PBE1PBE/TZVP) HFCCs used as the initial estimates of the true couplings.

The calculations show the SOMO to be almost completely confined to the ligand backbone with significant contributions from nitrogen and carbon atoms while the p-type orbitals on the two chlorine atoms exhibit notably smaller contributions (Figure 27). The calculated α -spin density of **63** (Figure 27) closely resembles the topology of the SOMO with spin polarisation effects, resulting in a concentration of β -spin density on boron and hydrogen atoms. The calculated HFCCs indicate a coupling of the unpaired electron mainly to one $^{10,11}\text{B}$ and two equivalent ^{14}N and $^{35,37}\text{Cl}$ nuclei with smaller couplings indicated for four unique pairs of ^1H nuclei (Table 1).

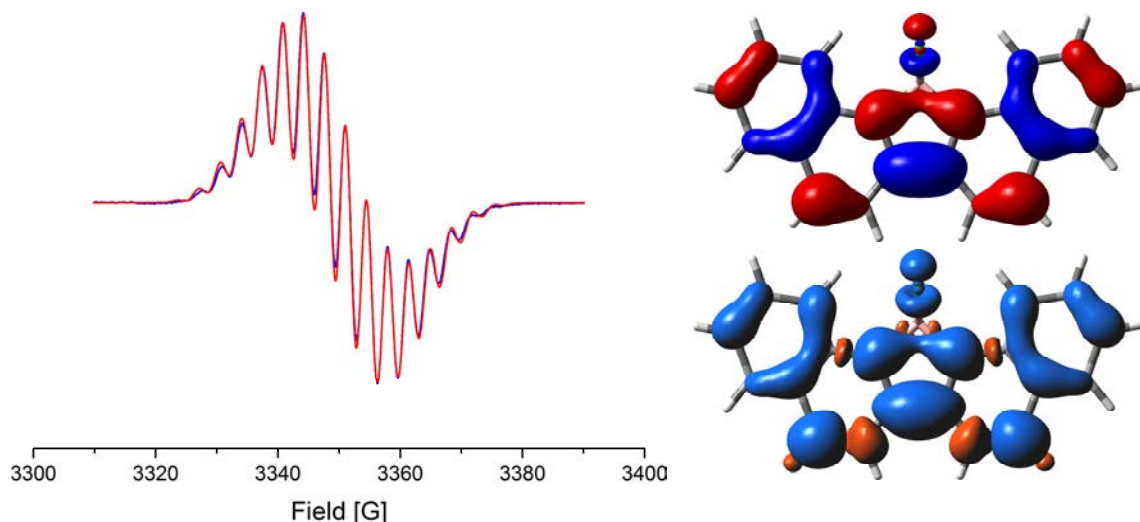


Figure 27. X-band EPR spectrum of a CH_2Cl_2 solution of **63** at room-temperature (left); experimental spectrum shown in blue and simulation in red. Isosurface plots of the SOMO (± 0.03 , top right) and spin density (± 0.0008 , bottom right) of **63**.¹

The HFCCs shown in Table 1 were used to simulate the EPR spectrum of **63** and the fit thus obtained was very good. The calculated HFCCs correspond well with the ones obtained from spectral fitting. The small HFCCs (less than 1.0 G) to ^1H nuclei remain ambiguous because of the broad spectral line width, which allows multiple and equally acceptable fits to the experimental data. The smaller ^1H couplings can be taken into account by increasing the line width, which shows that the other HFCCs change only little from one fit to another, collectively giving rise to the dominant 16-line pattern observed in the experimental spectrum. Crucially, all attempts to simulate the spectra with fewer HFCCs than those shown in Table 1 were unsuccessful. This shows that the data corresponds to the $[(\text{biq})\text{BCl}_2]^{\bullet}$ radical **63**, which in turn demonstrates that the ligand has undergone a one-electron reduction.

Table 1. Experimental and calculated hyperfine coupling constants (G) of **63**.^{1(a)}

Nucleus	Equivalent nuclei	Experimental	Calculated
$^{10}\text{B} / ^{11}\text{B}$	1	1.13 / 3.37	-1.54 / -4.59
^{14}N	2	2.75	2.41
$^{35}\text{Cl} / ^{37}\text{Cl}$	2	3.77 / 3.14	2.46 / 2.05
^1H	2	4.00	-3.83
^1H	2	0.91	-1.04
^1H	2	0.50	1.00
^1H	2	0.44	-0.85

^(a) Experimental parameters were obtained from a simulation optimised to match the recorded spectrum. The simulation used a Voigtian line shape with Gaussian and Lorentzian peak-to-peak line widths of 0.90 G and 0.15 G, respectively.

A comprehensive crystallographic analysis was performed for both **62** and **63**, allowing for important comparison between the structure of biq and its one-electron reduced anionic radical. The crystal structures of **62** and **63** are shown in Figure 28.

The crystal structure of **62** consists of $[(\text{biq})\text{BCl}_2]^+$ cations and Cl^- anions. The backbone of the biq ligand is slightly bent out of planarity, preventing perfect C_{2v} symmetry. Ion \cdots dipole interactions between the Cl^- anions and the C-H bonds dictate the solid state packing of **62**, causing the $[(\text{biq})\text{BCl}_2]^+$ cations to form layers along the crystallographic b -axis. The layer-like packing is affected by B-Cl \cdots H-C intermolecular interactions, which cause disruptions to the individual layers. The layers display π -stacking interactions with stack spacing of *ca.* 3.36 Å that is slightly less than the sum of van der Waals radii of two carbon atoms.

In the crystal structure of **63**, the C_{2v} symmetric radicals form well-arranged layers along the crystallographic c -axis with the BCl_2 moieties facing in alternate directions in neighbouring layers (Figure 29). The packing is dictated by B-Cl \cdots H-C hydrogen bonding and π -stacking interactions. The layers in **63** are uniformly spaced with a stack-spacing of *ca.* 3.40 Å. This is somewhat surprising as typically planar organic radicals interact antiferromagnetically to form π -dimers (see Section 2.1). The even spacing of layers in the crystal structure can be explained by the topology of the SOMO that leads to accidental orthogonality of adjacent magnetic orbitals in the solid-state structure. As a result, radical \cdots radical dimerization is not energetically favourable, causing molecules of **63** to remain essentially isolated in the solid state. This finding is supported by computational results that show the singlet and triplet states of a pair of adjacent radicals in the crystal structure to be separated by 0.5 kJ mol $^{-1}$.

The unpaired electron in **63** leads to lengthening on the N-C bonds from 1.342(4) Å and 1.346(4) Å to 1.373(5) Å and 1.380(5) Å, respectively. Conversely, the C-C bonds connecting the two quinoline moieties are shortened from 1.456(5) Å to 1.411(5) Å. This is consistent with the topology of the SOMO as well as with the results reported for the analogous 2,2'-bipyridine complexes $[(\text{bpy})\text{BCl}_2]\text{Cl}$ and $[(\text{bpy})\text{BCl}_2]^\bullet$.²⁴³

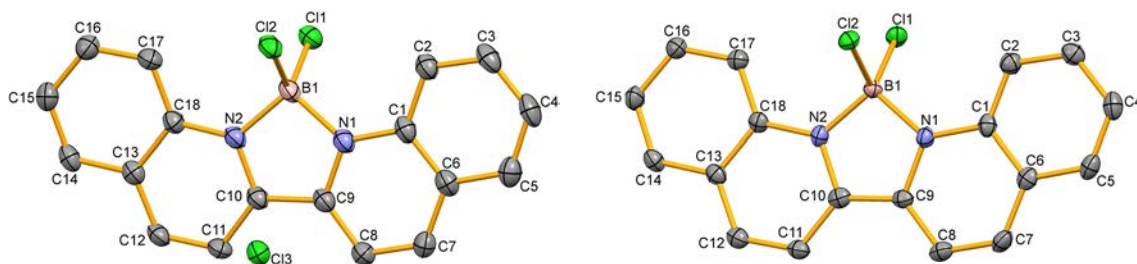


Figure 28. Crystal structures (50% probability, hydrogen atoms omitted for clarity) of **62** (left, CCDC: 1518783) and **63** (right, CCDC: 1518784).¹ Selected bond lengths (Å) and angles (°): (**62**) B1-N1 1.566(5), B1-N2 1.565(4), N1-C9 1.342(4), N2-C10 1.346(4), C9-C10 1.456(5), B1-Cl1 1.846(4), B1-Cl2 1.820(4), N1-B1-N2 98.7(3), Cl1-B1-Cl2 112.8(2); (**63**) B1-N1 1.536(5), B1-N2 1.541(5), N1-C9 1.380(5), N2-C10 1.373(5), C9-C10 1.411(5), B1-Cl1 1.863(4), B1-Cl2 1.874(4), N1-B1-N2 99.9(3), Cl1-B1-Cl2 109.9(2).

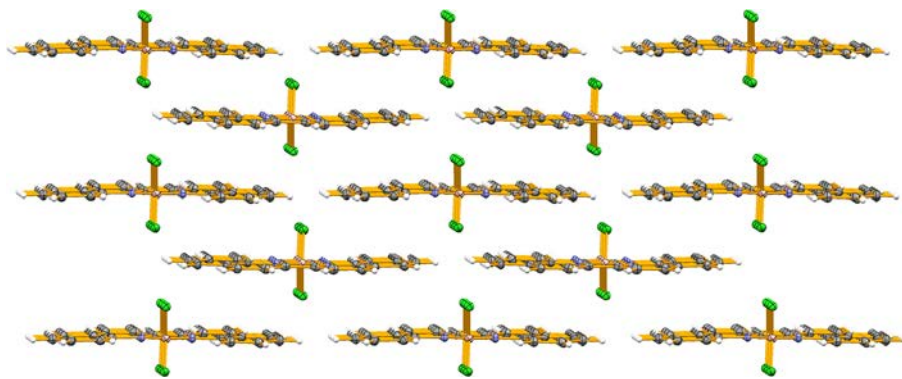


Figure 29. The packing of radicals **63** in the solid state shows well-arranged layers with a stack-spacing of *ca.* 3.40 Å.¹

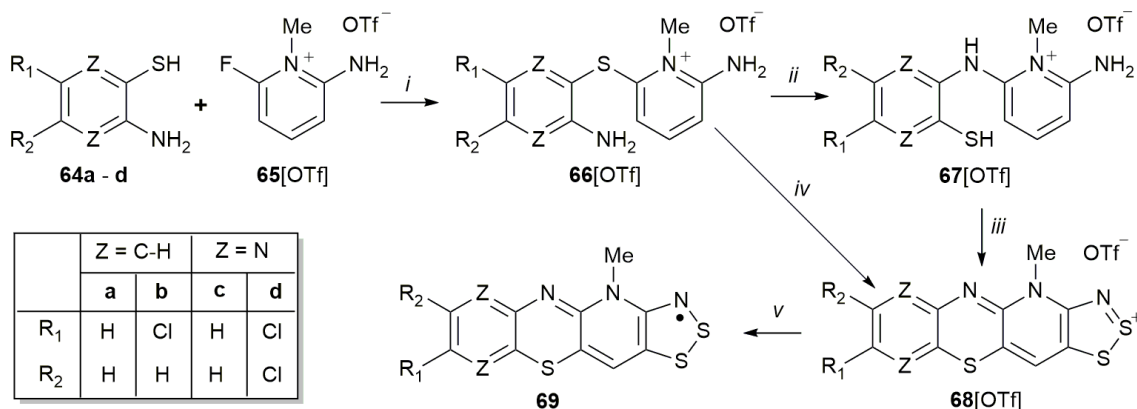
The metrical parameters of **62** and **63** provide the opportunity to investigate crystallographic data of transition metal complexes of biq to resolve possible ambiguities in their characterisation. Scarborough and Wieghardt have computationally studied a variety of bpy and biq complexes.²⁴⁴ They report the complex (biq)Ti(Cp)₂ to contain a Ti(III) centre and biq anion radical, although it is not certain whether the two unpaired electrons are ferromagnetically or antiferromagnetically coupled. While the structural trends observed for **62** and **63** corroborate the findings of Scarborough and Wieghardt, they also suggest that the complex Co(biq)₂, originally described as Co(0) species,²⁴⁵ should actually be considered as a Co(II) complex incorporating two anionic radicals. Strong structural evidence to support this view is the length of the intraligand C–C bond that connects the two quinoline moieties. The two ligands in the Co(biq)₂ complex are slightly inequivalent with short C–C distances of 1.427(6) Å and 1.431(5) Å.

A comprehensive theoretical study was performed on the electronic structure of Co(biq)₂ using multireference electron correlation methods (DKH-NEVPT2/DKH-SA-CASSCF(13,9)/def2-TZVP) to correctly identify the ligand charge state. The results show that the ground state of Co(biq)₂ is a spin-doublet that is separated from the first excited state by 1437 cm⁻¹. Decomposition of the ground state wave function into contributions from various electronic configurations reveal that *ca.* 60% of them contain a high-spin Co(II) ion and two anionic radical ligands. The remaining 40% consist of different ligand-to-metal and metal-to-ligand charge transfer configurations. These results demonstrate that the ground state of Co(biq)₂ should be viewed as an antiferromagnetically coupled high-spin Co(II) centre and two biq radicals that are stabilised by significant kinetic exchange.

4.3.2 Hybrid 1,4-thiazine-1,2,3-dithiazolyl radicals^{II}

The heterocyclic benzo-1,4-thiazine, commonly known as phenothiazine, was first synthesised in the late 19th century.²⁴⁶ Phenothiazine and its derivatives, like many other sulphur-nitrogen heterocycles, are viable candidates when designing stable radicals as they can readily undergo a one-electron oxidation to

form persistent radical cations. While the radical cations are relatively well established, comparatively little is known about neutral phenothiazinyls. One viable method to synthesise phenothiazine-based compounds is the Smiles rearrangement (SR),²⁴⁷ an intramolecular nucleophilic *ipso*-substitution reaction, which in this work was used to prepare new stable radicals **69** that fuse 1,4-thiazinyl and 1,2,3-dithiazolyl species into one single framework (Scheme 11).



Scheme 11. Synthesis of neutral radicals **69**.^{II} General synthetic procedures: (i) Na₂CO₃, CH₃CN, 5h; (ii) CH₃CN, sealed reaction vessel at 110 °C; (iii) excess S₂Cl₂, CH₃CN, reflux for 16 h; (iv) excess S₂Cl₂, CH₃CN, reflux for 16 h; (v) excess (CH₃)₈Fc, CH₃CN.

The condensation reaction of 2-aminobenzenethiols (**64a,b**) and 3-aminopyrazinethiols (**64c,d**) with 2-amino-6-fluoro-*N*-methylpyridinium triflate (**65[OTf]**) in the presence of excess anhydrous Na₂CO₃ (Scheme 11, step i) in acetonitrile produced the *N*-methylpyridinium thioether salts **66[OTf]** (Figure 30). The following step would be the S→N Smiles rearrangement at the thioether bond of the *N*-methylpyridinium to afford *N*-substituted derivatives **67[OTf]**. However, initial experiments raised concerns about the functionality and scope of the rearrangement, as instead of **67c[OTf]**, a test reaction produced the tautomeric pyrazinethione derivative **67c'**[OTf] (Figure 30).

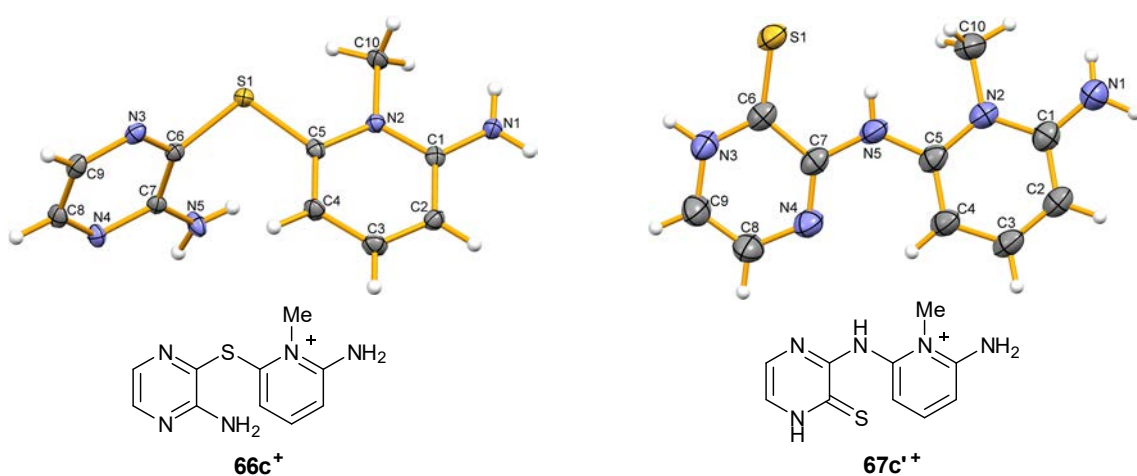


Figure 30. Thermal ellipsoid plots (50% probability) and line drawings of the cations in **66c[OTf]**·CH₃CN (CCDC: 1519804) and **67c'[OTf]** (CCDC: 1519805).^{II}

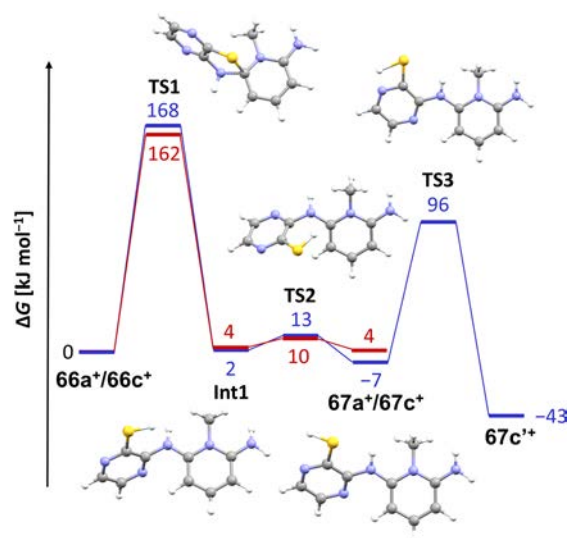


Figure 31. Reaction coordinate diagram showing the Smiles rearrangement reaction of **66a⁺** (red) and **66c⁺** (blue).¹¹ For clarity, only the structures of intermediates and transition states for the pathway from **66c⁺** to **67c^{''}** are shown.

In order to investigate the reactivity of the various thioether salts, a computational investigation of the reaction mechanism was performed at the DFT level (PBE1PBE-IEFPCM/def2-TZVP). Two representative systems, **66a⁺** and **66c⁺**, were studied, and the results are summarised as a reaction coordinate diagram in Figure 31. It was presumed that the reaction begins with an intramolecular nucleophilic attack of the benzo/pyrazine -NH₂ group, resulting in the formation of a cationic Meisenheimer complex. The data show that the initial reaction pathway is analogous for both **66a⁺** and **66c⁺**. The first transition state (TS), that is, the formation of the Meisenheimer complex, has a very high activation barrier. This is congruent with experimental observations. Furthermore, the formation of **67a⁺** and **67c⁺** is in both cases virtually an energy-neutral process. In the case of **66c⁺**, the driving force behind the SR reaction is the possibility of **67c⁺** to tautomerize to **67c^{''}**, which makes the overall transformation from **66c⁺** to **67c^{''}** exergonic by 43 kJ mol⁻¹. **66a⁺** is unable to undergo a similar tautomerization. Thus, the formation of **67a** is endergonic, albeit by a mere 4 kJ mol⁻¹.

Following computational studies, the cyclocondensation of **67c^{''}** was performed by refluxing it in acetonitrile with excess S₂Cl₂ for 16 h (Scheme 11, step *iii*). The main products were the salts **68c**[OTf] and **68d**[OTf]. Repeating the reaction multiple times showed that the ratio of **68c**[OTf] to **68d**[OTf] was variable, and its dependency on the reaction conditions was inconsistent.

The salt **66d**[OTf] failed to undergo the desired SR reaction to yield **67d**[OTf]. Nonetheless, it contained the appropriate substitution of chlorine on the pyrazine ring, which could potentially enable the formation of **68d**[OTf]. Therefore, a direct reaction was attempted where **66d**[OTf] was heated under reflux in acetonitrile for 16 h with S₂Cl₂ (Scheme 11, step *iv*). This resulted in the formation of **68d**[OTf] in a 40% yield, proving that Smiles rearrangement can occur concomitantly with cyclocondensation.

Additional experiments showed that a reaction of **66b**[OTf] with S_2Cl_2 produces **68b**[OTf] in moderate yields. Single crystals of **68b**[OTf] were grown from a propionitrile solution (Figure 32). Interestingly, the structure of **68b**[OTf] closely resembles **68d**[OTf] (Figure 32), indicating that the heterocyclic aromatic substituents have a minor effect on the structure of the 1,4-thiazine-1,2,3-dithiazolylum framework.

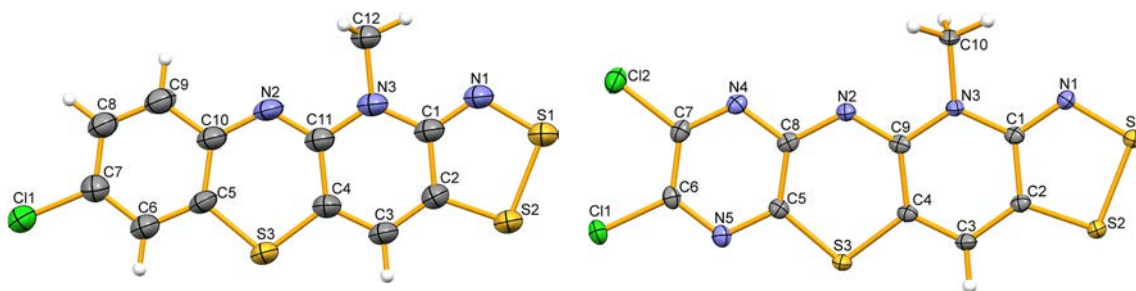


Figure 32. Thermal ellipsoid plots (50% probability) of the cations in **68b**[OTf] (left, CCDC: 1519806) and **68d**[OTf] (right, CCDC: 1519808).ⁱⁱ

Cyclic voltammetry measurements of **68b**[OTf] and **68d**[OTf] in CH_3CN showed a reversible +1/0 redox couple with $E_{1/2} = 0.031$ V and 0.220 V (*vs.* SCE), respectively. These results indicate octamethylferrocene ($(CH_3)_8Fc$) to be a suitable reducing agent for both cations. Furthermore, the cathodic shift in $E_{1/2}$ demonstrates that the heterocyclic aromatic substituents affect the electrochemical behaviour of the cations by altering the energy of their LUMO.

Reduction of **68b**[OTf] and **68d**[OTf] was performed in a degassed CH_3CN solution in an H-cell with an excess of $(CH_3)_8Fc$ (Scheme 11, step *v*). Radicals **69b** and **69d** were obtained as analytically pure crystalline solids. The crystal structure of **69b** belongs to the monoclinic space group $P2_1/c$ and the asymmetric unit consists of two effectively coplanar radicals in trans-cofacial arrangement (Figure 33). The shortest intermolecular $C \cdots C$ distances are close to the sum of van der Waals radii, indicating negligible solid state interactions between adjacent radicals.^{248,249} In the solid state, the radical moieties are arranged in a herringbone pattern (Figure 33), which is often observed for the related bisdithiazolylum radicals.

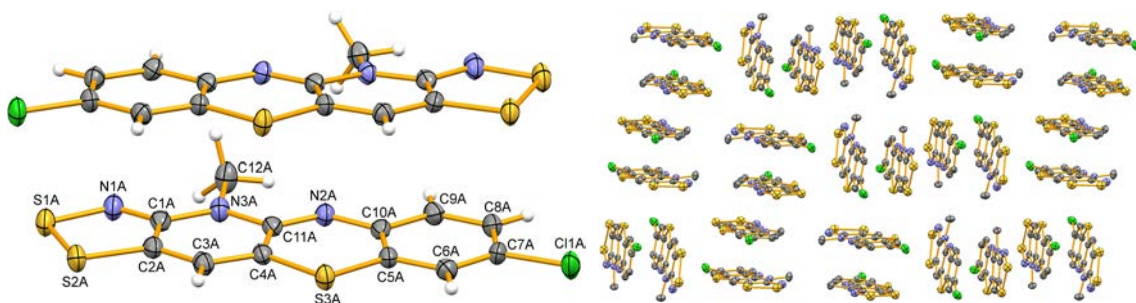


Figure 33. The asymmetric unit of **69b** (left, CCDC: 1519807) and the solid-state packing with hydrogen atoms omitted for clarity (right).ⁱⁱ Thermal ellipsoids set at 50% probability.

The paramagnetic nature of the radicals **69b** and **69d** was studied by X-band EPR spectroscopy and theoretical calculations. The room temperature EPR spectrum of **69b** in CH₂Cl₂ (Figure 34) consists of an eight-line pattern with no fine structure ($g = 2.0071$). A good simulation of the spectrum was obtained by using only three HFCCs: $a_{N1} = 3.83$ G to the nitrogen centre in the dithiazolyl ring, $a_{N2} = 2.24$ G to the nitrogen centre in the thiazyl ring and $a_{H3} = 2.13$ G to the hydrogen at the basal position. The calculations indicated smaller couplings (under 1.0 G) to hydrogen nuclei and the nitrogen on the *N*-methylpyridinium ring. These couplings were treated indirectly by adjusting the line shape as the broad spectral width did not allow their explicit consideration.

The EPR spectrum of **69d** (Figure 34) resembles that of **69b**. It consists of a ten-line pattern ($g = 2.0059$), and it was simulated with a reasonable fit by using three HFCCs: $a_{N1} = 4.84$ G to the nitrogen centre in the dithiazolyl ring, $a_{N2} = 1.69$ G to the nitrogen centre in the thiazyl ring and $a_{H3} = 1.97$ G to the hydrogen atom at the basal position. These values correspond well with the calculations, although the calculations do suggest minor couplings to the pyrazine nitrogen atoms and the two chlorine nuclei. These couplings are masked by the broad line width in the experimental spectrum.

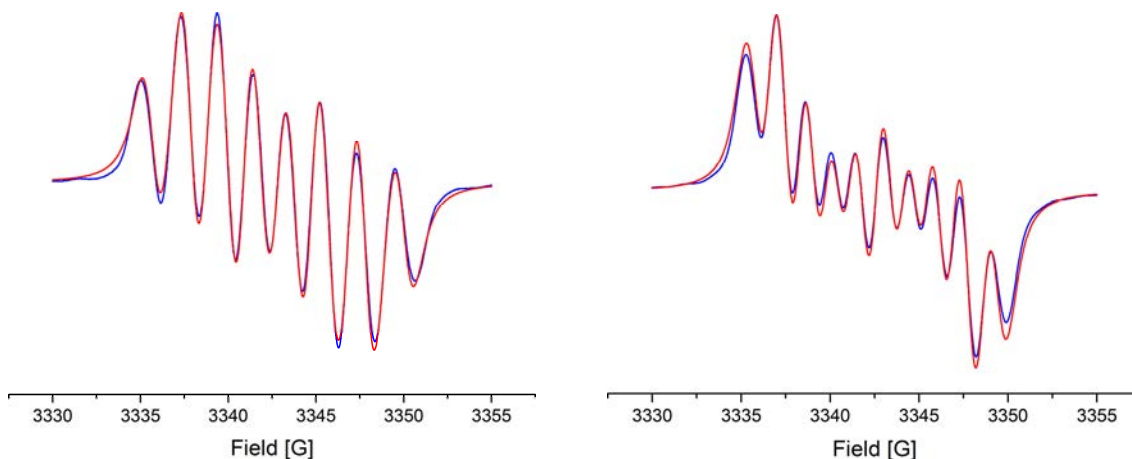


Figure 34. X-band EPR spectra of CH₂Cl₂ solutions of **69b** (left) and **69d** (right) at room temperature.^{II} Experimental spectra in blue and simulated spectra in red. The simulations used a Voigtian line shape with Gaussian/Lorentzian peak-to-peak line widths (G) of 0.67/0.92 and 0.90/0.87 for **69b** and **69d**, respectively.

The DFT calculations are consistent with the EPR spectroscopic measurements. Furthermore, the calculations show the SOMO and the spin density of the radicals to be delocalised over the molecular framework (Figure 35). Natural population analysis of **69b** assigned 40 and 50% of the α -spin density on the 1,4-thiazinyl and 1,2,3-dithiazolyl moieties, respectively. This holds true for **69d** as well, albeit the spin distribution is somewhat more localised on the 1,2,3-dithiazolyl moiety. Hence, the spectroscopic and computational studies demonstrate that radicals **69b** and **69d** can be considered hybrids of 1,4-thiazinyls and 1,2,3-dithiazolyls.

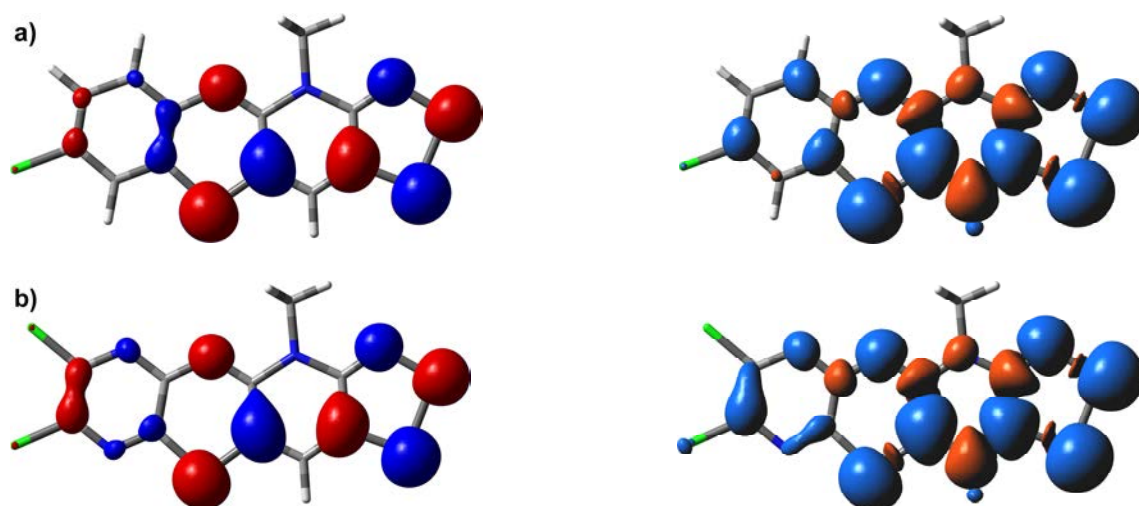


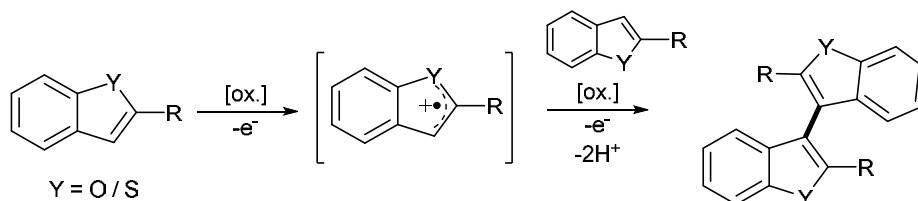
Figure 35. Isosurface plots of the SOMOs (± 0.04 , left) and spin densities (± 0.0009 , right) of a) **69b** and b) **69d**.^{II}

4.4 Reactive intermediates

4.4.1 DDQ-generated radical intermediate^{III}

Quinones are widely used oxidisers in synthetic chemistry. A well-known example is 2,3-dichloro-5,6-cyano-1,4-quinone (DDQ); it is frequently used in organic synthesis and other chemical conversions due to its high oxidative power. It has also been shown that strong acids further increase the oxidative power of quinones. In essence, there are three types of pathways typically associated with oxidation: hydride abstraction, hydrogen atom transfer and single-electron transfer (SET).²⁵⁰

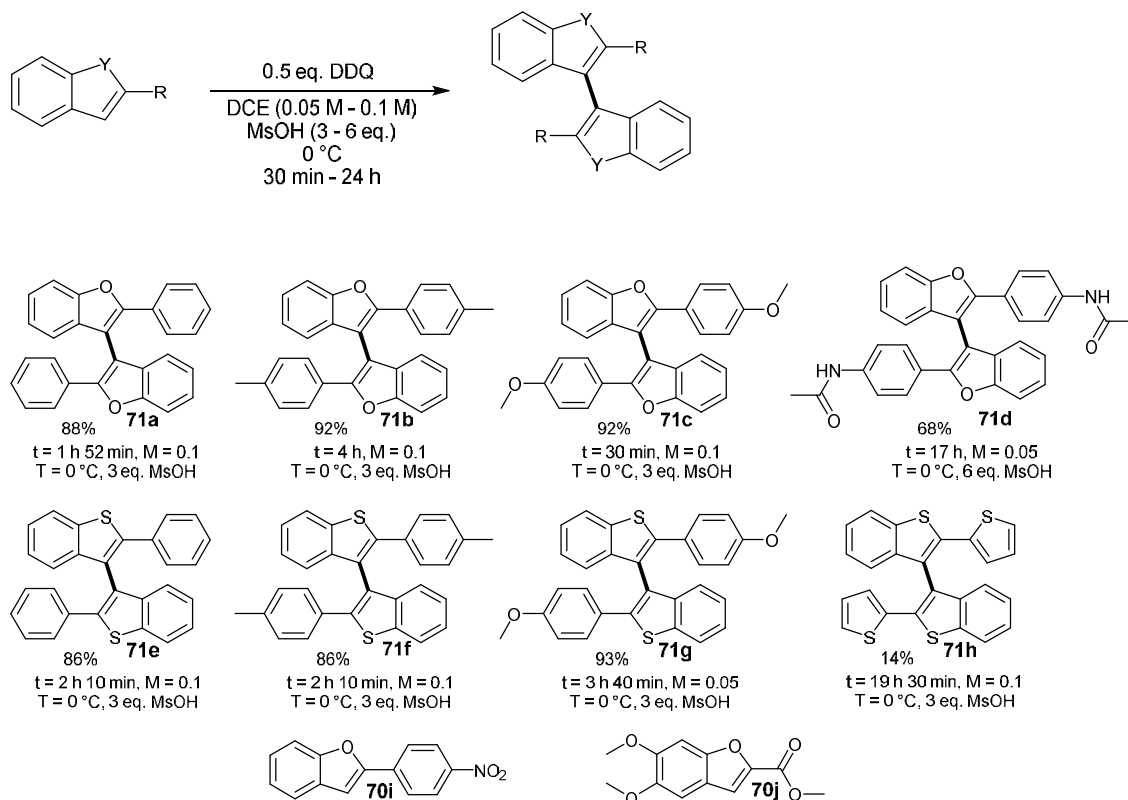
3,3'-bibenzo[*b*]furan and 3,3'-bibenzo[*b*]thiophene motifs are commonly found in natural products, and they are employed in a number of chemical applications such as catalysis and organic electrode materials. Many of the traditional coupling methods used to produce bibenzo derivatives require the use of prefunctionalised starting materials, transition metal catalysts, or air-sensitive synthetic procedures. Therefore, there is a demand for a straightforward synthetic procedure to prepare 3,3'-bibenzo[*b*]furan and 3,3'-bibenzo[*b*]thiophene skeletons. The general synthetic route that was used to obtain the bibenzo derivatives in this work is shown in Scheme 12.



Scheme 12. DDQ-mediated coupling that progresses through one-electron oxidation, C-C bond formation and another one-electron oxidation.^{III}

The coupling of 2-phenylbenzofuran was chosen as the test reaction. Preliminary studies on the synthesis showed that an acid additive was required for the reaction to progress. Various acids were tested, but only methanesulphonic acid (MsOH) was found to work in a satisfactory fashion. Trifluoroacetic acid (TFA) worked to some extent, but the results were both concentration and substrate dependent. Screening of solvents revealed dichloroethane (DCE) to give the best yields. When optimizing the reaction conditions, three factors were set as variables: temperature, amount of DDQ and molarity, with the latter having the most significant effect. It quickly transpired that the best yield (99% by NMR, 88% isolated yield) was obtained with 0.1 M of reactant and 0.5 equivalents of DDQ at 0 °C.

Once the reaction conditions were optimised, the scope of the reaction was determined. The products obtained in the experiments are shown in Scheme 13. With 2-arylbenzo-*[b]*furans, the corresponding 2,2'-bis(aryl)-3,3'-bibenzo-*[b]*furans were obtained in yields ranging from 86% to 92%. When the 2-aryl substituent was functionalised at the *para*-position with an amide group, the yield was slightly lower (68%). Somewhat disappointingly, the electron-poor 2-(4-nitrophenyl)benzo-*[b]*furan **70i** could not be coupled by this synthetic procedure. Stronger acids and different oxidants were tried to no avail. However, the corresponding 2,2'-bis(aryl)-3,3'-bibenzo-*[b]*thiophenes were obtained in comparably high yields to the related benzo-*[b]*furans. Regrettably, the 3,3'-homocoupling product 2,2'-bis(2-thienyl)-3,3'-bibenzo-*[b]*thiophene **71h** was only obtained in a 14% yield. This is most likely caused by the structure of the reactant enabling reactivity at two sites, benzo-*[b]*thiophene 3- and thiophene 5-positions, which leads to oligomerization. The oxidative 3,3'-homocoupling of the electron-rich substrate **70j** did not take place under the reaction conditions employed.



Scheme 13. Reaction conditions and isolated yields for DDQ/ H^+ -mediated homocoupling of benzofurans and benzothiofurans.^{III} Substrates **70i** and **70j** did not yield any products.

The assumption was that the examined coupling reactions are initiated by a SET between the substrate and the DDQ/ H^+ . Therefore, the oxidation potential of the substrate would determine its reactivity. In order to investigate this relationship, the relative oxidation potentials of the substrates were measured (*vs.* Fc/ Fc^+ couple), and the results were compared with the values obtained from theoretical calculations (Table 2). The experimental and calculated oxidation potentials have a strong systematic correlation, albeit the computational values underestimate the potential by $\sim 0.31\text{ V}$ (Figure 36). This could be expected as the systematic underestimation of oxidation potentials by pure DFT functionals is well-known.²⁵¹ Both the experimental and calculated oxidation potentials were normalised to **70c** in order to compare the relative potentials. At this point it became evident that the oxidation potentials correlate well with the observed reactivity and also provide an explanation of why the homocoupling of **70i** failed as DDQ is not a strong enough oxidiser to induce reactivity.

Table 2. Experimental and calculated oxidation potentials of substrates **70a** – **70j** (*vs.* Fc/Fc⁺).^{III} Values in parenthesis have been normalised to **70c** to compare relative potentials.

Substrate	Exp. (Exp.n.) / V	Calc. (Calc.n.) / V	Exp. - Calc. (Exp.n. - Calc.n.) / V
70a	1.070 (0.280)	0.749 (0.305)	0.321 (-0.03)
70b	0.925 (0.135)	0.627 (0.183)	0.298 (-0.05)
70c	0.790 (0.000)	0.444 (0.000)	0.346 (0.00)
70d	0.810 (0.020)	0.557 (0.113)	0.253 (-0.09)
70e	1.055 (0.265)	0.782 (0.338)	0.273 (-0.07)
70f	1.000 (0.210)	0.689 (0.245)	0.311 (-0.04)
70g	0.845 (0.055)	0.527 (0.083)	0.318 (-0.03)
70h	0.910 (0.120)	0.595 (0.151)	0.315 (-0.03)
70i	1.310 (0.520)	1.060 (0.616)	0.250 (-0.10)
70j	1.100 (0.310)	0.685 (0.241)	0.415 (0.07)

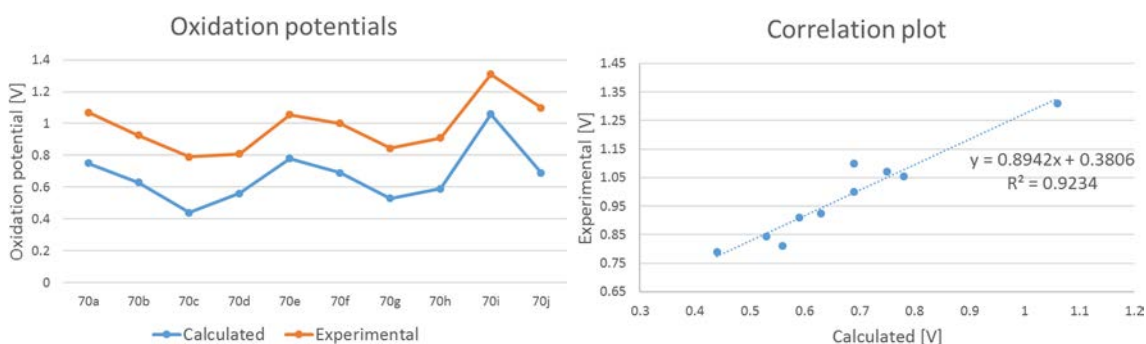
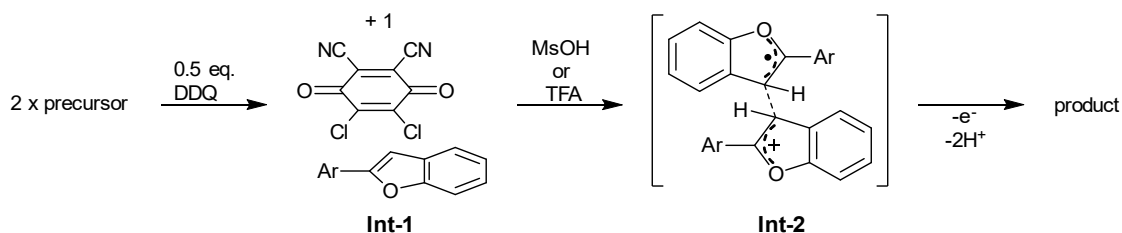


Figure 36. Experimental and calculated oxidation potentials of substrates **70a** – **70j** (left) and the correlation between them (right).^{III}

Based on both experimental and computational findings, a mechanism was proposed for the 3,3'-coupling reaction (Scheme 14). The reaction begins with DDQ forming a charge-transfer complex with the substrate (**Int-1**). The formation of the complex induces a colour change that can be observed both visually and by UV-Vis spectroscopy. The structure of the 2 : 1 intermediate complex of DDQ and **70c** was also determined by single crystal X-ray diffraction.



Scheme 14. Proposed reaction mechanism for the intermolecular 3,3'-coupling of 2-arylbenzo[*b*]furans and 2-arylbenzo[*b*]thiophenes.^{III}

The coupling reaction is initiated by SET from the substrate to DDQ, which in turn is set in motion by the addition of an acid that increases the oxidative power of the quinone. This causes the formation of an electrophilic radical cation which reacts with a nucleophilic neutral substrate to form a radical cation intermediate **Int-2**. The product is obtained from this second intermediate after elimination of two protons and a second SET. An alternative reaction pathway could result from the deprotonation of the substrate, followed by its coupling with a neutral substrate, to form a radical intermediate. This would then yield the product via elimination of one proton and a second SET. The radical cation mechanism is more likely, however, as it is consistent with the one reported for MoCl₅-mediated coupling of arenes.²⁵²

The reaction was monitored using both NMR and EPR spectroscopy. The disappearance of NMR signals coincides with the appearance of a strong EPR signal (Figure 37) upon adding the acid, indicating the presence of a radical species. The EPR signal consists of a singlet peak with a *g* value of 2.0023. The lack of any fine structure in the signal is most likely the result of a predominant dynamic equilibrium occurring during the reaction. This prevents the observation of fine structure in the time scale of an EPR measurement. Interestingly, the radical intermediate is not particularly air or moisture sensitive as the reaction could be carried out under ambient atmosphere using non-dried solvents. Likewise, the EPR spectrum could be measured in an open-top sample tube.

This DDQ/H⁺-mediated 3,3'-homocoupling reaction of 2-arylbenzo[b]furans and 2-arylbenzo[b]thiophenes is a prime example of a metal-free synthetic procedure that produces high yields while foregoing the requirement of harsh reaction conditions or air- and moisture-sensitive techniques. It is applicable to a variety of organic starting materials, and the reactivity can be predicted based on the oxidation potentials of the starting materials. It showcases the synthetic power of radical reactions.

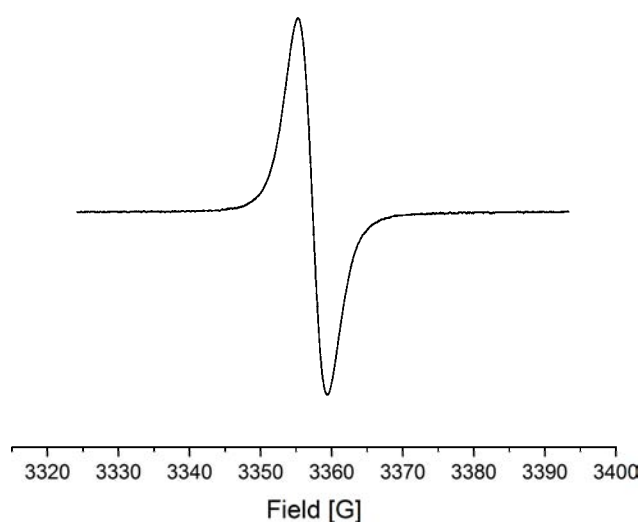
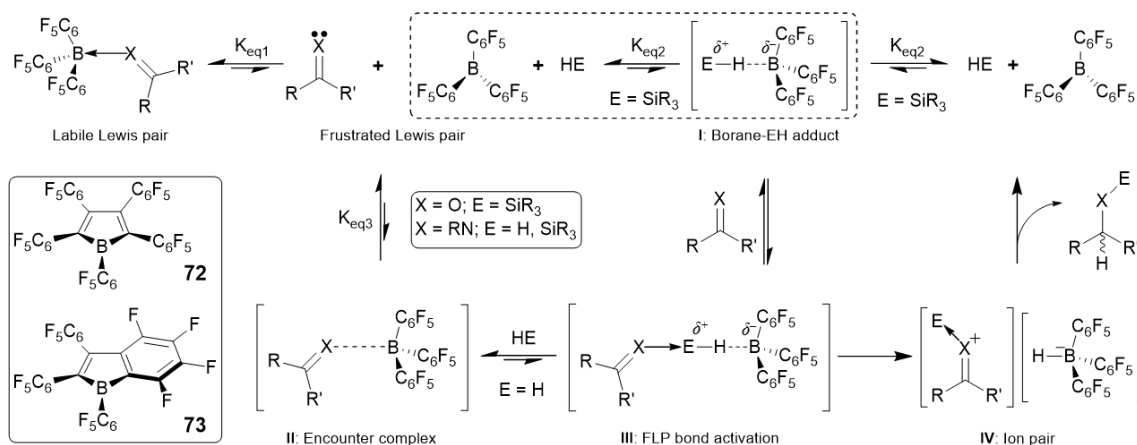


Figure 37. X-band EPR spectrum ($g = 2.0023$) measured from a sample taken from a mixture containing 1 eq. of **70a**, 0.5 eq. DDQ and 3 eq. MsOH in DCE (0.1 M solution) at 0 °C.^{III}

4.4.2 Borane-silane complex involved in metal-free hydrosilylations^{IV}

Transition metal catalysts are typically used in homogenous processes that require a bond-activation step. A number of d-block metals are known to conduct the hydrosilylation and/or hydrogenation of unsaturated organic functions, for example, C=O, C=N and C=C bonds. The key first step in the catalytic cycle in these systems is the Si-H or H-H bond activation at the transition metal centre. The disadvantages of such catalysts are the high cost and toxicity of the most commonly used metals. Main group elements could provide a cheaper and less harmful alternative to d-block elements, but it is challenging to coax the main group elements to mediate the bond-activation step required for catalytic turnover.

Strongly Lewis acidic organoborane compounds, such as tris(pentafluorophenyl)borane $B(C_6F_5)_3$, are known to catalyse the hydrosilylation of carbonyl and imine functions.^{253,254} This was initially thought to occur via classical Lewis acid-Lewis base interactions, but eventually it transpired that the true role of the borane was to activate the silane.²⁵⁵ This leads to the formation of a borane-silane adduct **I** (Scheme 15), which is then susceptible to attack at the silicon centre by the Lewis basic substrate, resulting in the formation of the bond-activation intermediate **III**. This type of bond cleavage is known as FLP bond activation. It has been postulated that a weak encounter complex **II**, stabilised by secondary C-H \cdots F interactions, might form prior to FLP activation of H₂ via **III**.^{256,257} Regardless of whether the path to **III** progresses via **I** or **II**, the bond activation transition state leads to an ion pair **IV**, which then proceeds to the product by hydride transfer from the $[HB(C_6F_5)_3]^-$ to the substrate carbon while the borane catalyst is regenerated.

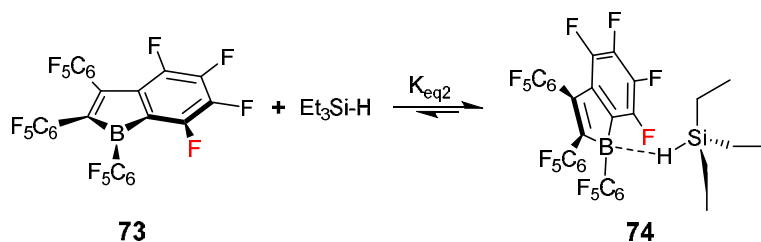


Scheme 15. The mechanism of FLP activation of Si-H and H-H bonds.^{IV} This scheme illustrates the reaction paths and equilibria involved in the activation and cleavage of Si-H and H-H bonds by Lewis acid/base pairs. The formation of borane/E-H adduct **I** is the key intermediate in the FLP activation of these bonds. Inset (bottom left): antiaromatic borole **72** and boraindene **73**.

The aforementioned mechanism was generally accepted, but the specific nature of the adducts **I** or the encounter complexes **II** remained opaque. While $B(C_6F_5)_3$ is known to react with Et_3SiH to produce bispentafluorophenyl borane $HB(C_6F_5)_2$ and $Et_3SiC_6F_5$ in a process where the borane-silane adduct is implicated,²⁵⁸ attempts to experimentally verify the existence of the adduct had not been successful. Therefore, it seems that K_{eq2} in Scheme 15 is highly unfavourable towards the formation of adduct **I** for the Lewis acid $B(C_6F_5)_3$.

In order to alter the equilibrium K_{eq2} to be more favourable towards the formation of the borane-silane adduct **I**, more Lewis basic silane or more Lewis acidic borane should be used. Perfluoropentaphenyl borole **72**²⁵⁹ (Scheme 15) is an extremely Lewis acidic compound, but its poor solubility prevents its use in hydrosilylation reactions. 1,2,3-Tris(pentafluorophenyl)-4,5,6,7-tetrafluoro-1-boraindene **73**²⁶⁰ (Scheme 15) is as equally Lewis acidic as **72** but more soluble in common inert solvents. **73** is red both in the solid state and in toluene solution. The red colour results from a weak absorption that is caused by a forbidden transition involving the empty p-orbital on the boron centre. Upon complexation of a Lewis base, this absorption is disrupted and the formed adducts are pale yellow.

1 – 2 Equivalents of Et_3SiH were added to a red solution of **73** in deuterated toluene (Scheme 16). At room temperature, the colour of the solution remained red, while 1H and ^{19}F NMR showed the components to remain largely unchanged. In other words, while adduct formation was not favourable in these conditions, **73** is stable towards reactions with the silane. Upon cooling the solution to 195 K, a reversible red-to-yellow colour change was observed, which is a strong implication of the silane coordinating to the boraindene to form adduct **74**.



Scheme 16. The formation of the borane-silane adduct **74**.^{IV}

The initial qualitative observation was confirmed by variable-temperature (VT) ^{19}F NMR spectroscopy. When the temperature was lowered, the majority of the resonances in the ^{19}F NMR spectrum remained largely in place, shifting only slightly upfield. However, the chemical shift for the fluorine *ortho* to boron on the boraindenyl moiety (Scheme 16, red F) was significantly perturbed, caused by the strongly favoured adduct formation at lower temperatures (Figure 38). Interestingly, this shift was perfectly reversible when lowering and raising the temperature. Similarly, when ^{19}F NMR measurements were performed at room temperature with varying amounts of excess Et_3SiH added, a significant shift of the *ortho*-fluorine resonance was observed.

It was assumed that the adduct is bonded via a Si-H \cdots B bridge. This was supported by ^1H NMR and IR measurements. The resonance of the silane hydrogen in the ^1H NMR spectrum shifted over 1 ppm upfield upon cooling the solution from 298 to 213 K. This affected the ^{29}Si satellites and, as the temperature was lowered and the equilibrium shifted towards **74**, the $J_{\text{Si-H}}$ coupling constant dropped from 177 Hz in free $\text{Et}_3\text{Si-H}$ to 107(2) Hz at 213 K. This lowering of the coupling constant is caused by the interaction of the silane with the boron centre, which weakens the Si-H bond. Likewise, the stretching frequency of the Si-H bond is affected by the adduct formation. The $\nu_{\text{Si-H}}$ stretch in free Et_3SiH is a sharp band at 2103 cm^{-1} , whereas in a solid sample of **74**, the corresponding signal was found to be a broad band at 1918 cm^{-1} .

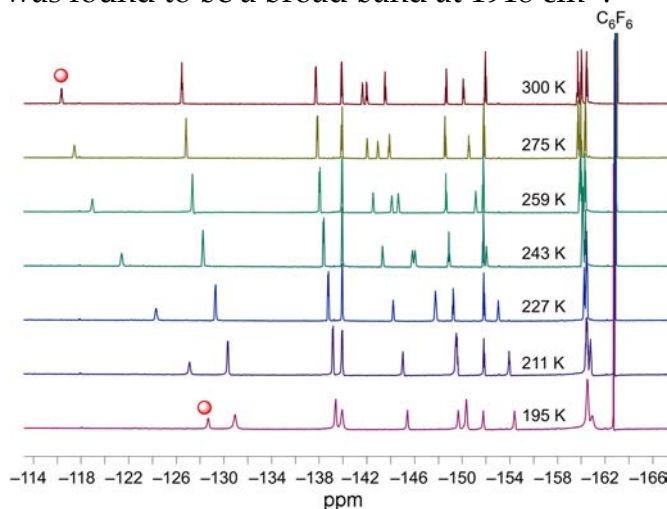


Figure 38. Variable-temperature ^{19}F NMR spectra demonstrating the significant shift of the fluorine atom *ortho* to the boraindene boron (red dot) observed upon the formation of **74**.^{IV}

Single crystals of **74** were grown by layering neat Et_3SiH onto a toluene solution of **73** at $-35\text{ }^\circ\text{C}$ and allowing the silane to slowly diffuse with the boraindene solution. The crystal structure of **74** (Figure 39) confirms the spectroscopic findings of the silane binding the borane via the Si-H bond. The bridging hydrogen H1 was found in the Fourier map and refined isotropically. The Si1-H1 and B1-H1 distances were 1.51(2) and 1.46(2) Å, respectively, which indicates that the hydrogen remained associated mainly with the silicon atom (typical Si-H distances are *ca.* 1.48 Å while typical B-H distances in perfluoroaryl hydridoborate anions are *ca.* 1.14 Å). Thus, **74** should be viewed as a Lewis acid/base adduct rather than an ion pair. The structure also indicates C-H \cdots F van der Waals interactions between F9 and C27 and F4 and C29 with close contacts of 3.138(3) and 3.262(2) Å, respectively. These interactions are likely to stabilise the adduct further.

Comprehensive DFT-level calculations were performed on adduct **74**. The optimised geometry of **74** is mostly consistent with the structural parameters obtained by crystallography. The calculated Si1-H1 bond length and the non-bonded distances between the fluorine and carbon atoms are longer in the optimised geometry, however. These differences can be explained by the uncer-

tainty of the bridging hydrogen atom's location in the Fourier map and crystal-packing effects that are not taken into account in gas-phase calculations.

Atoms-in-molecules analysis of the Si1–H1 bond in adduct **74** reveals its properties to be comparable to Si–H bond in the free silane, which points to locally similar electronic structures. This is in stark contrast with the data for the B1–H1 bond critical point in **74**, which is notably divergent from the results obtained for the $[\text{HB}(\text{C}_6\text{F}_5)_3]^-$ anion. These results lend more credence to the view of **74** being a Lewis acid/base adduct. The calculations predict an enthalpy of $\Delta H^\circ_{\text{calc}} = -21 \text{ kJ mol}^{-1}$ for silane binding. This is congruent with the experimental value of $-29.7(3) \text{ kJ mol}^{-1}$ obtained by van't Hoff analysis.

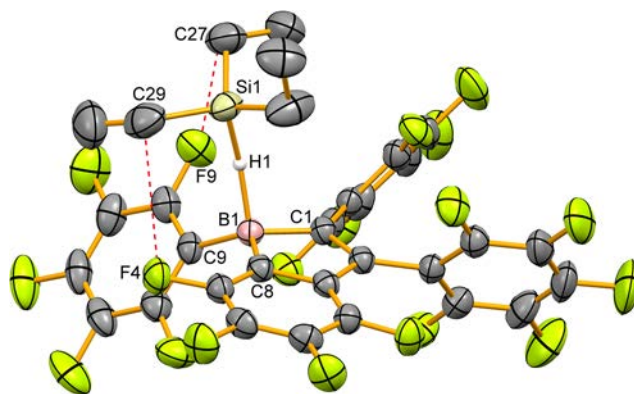


Figure 39. Crystal structure of boraindene-silane adduct **74** (thermal ellipsoids set at 50% probability, CCDC: 1010911).^{iv} Only the bridging hydrogen H1 is shown. Red dashed lines indicate close contacts. Selected bond lengths (Å), non-bonded distances (Å) and bond angles (°) [calculated values in brackets]: B1–C1: 1.616(3) [1.607], B1–C8: 1.608(3) [1.594], B1–C9: 1.605(3) [1.597], B1–H1: 1.46(2) [1.402], Si1–H1: 1.51(2) [1.608], F4–C29: 3.262(2) [4.717], F9–C27: 3.138(3) [3.171], C1–B1–C8: 100.58(15) [100.91], C1–B1–C9: 122.89(16) [121.06], C8–B1–C9: 120.84(17) [122.57], B1–H1–Si1: 157(2) [154.45].

Further calculations were carried out to study the stability of **74**. The bonding of the silane in adduct **74** was compared to two model systems, namely, the Et_3SiH adduct with $\text{B}(\text{C}_6\text{F}_5)_3$ (*i.e.*, **I**) and the hypothetical Et_3SiH adduct with perfluoroarylborole **72** (denoted as **V**). The calculated enthalpies and Gibbs energies are shown in Table 3. It was found that **I** is the weakest adduct of the three studied systems, while the bond strength in **V** is comparable to that in **74**. Furthermore, a detailed analysis of the borane-silane bonding interaction allows the quantification of the energy components that originate from distortion of fragment geometries (ΔE_{dist}) and electronic effects that stabilise the adducts (ΔE_{inst}). The distortion energy is smallest in adduct **I**, but it also has the weakest bonding interaction, making it the least bound system. The distortion energies in both **V** and **74** are greater than in **I**, but the considerably stronger bonding interactions between the borole/boraindene and silane easily overcome the distortion energies. The calculated hydride affinities for **72**, **73** and $\text{B}(\text{C}_6\text{F}_5)_3$ are -593 , -564 and -538 kJ mol^{-1} , respectively, which is a result that is in line with their Lewis acidities (*i.e.*, **72** is the strongest Lewis acid). It can therefore be concluded that a high Lewis acidity of **73** does not explain the stability of adduct **74**; rather, it is the fine balance between the steric and electronic effects in the adduct.

Table 3. Calculated bonding parameters of adducts **74**, **I** and **V**.^{IV}

Adduct	ΔH°_{calc} (kJ mol ⁻¹)	ΔG°_{calc} (kJ mol ⁻¹)	ΔE_{dist} (kJ mol ⁻¹)	ΔE_{inst} (kJ mol ⁻¹) ^a
74	-21	32	75	-102
I	-6	56	68	-79
V	-20	42	103	-129

^a The sum of ΔE_{dist} and ΔE_{inst} equals ΔH_{calc} at 0 K.

4.4.3 Structure elucidation of a purported reactive intermediate^V

Crystallographic characterisation of an intermediate formed in the synthesis of tetra-*n*-butylammonium bicarbonate, [(*n*-C₄H₉)₄N]HCO₃, was recently reported by Ackermann *et al.*²⁶¹ The isolation and characterisation of the intermediate could be considered remarkable, as there are only a few structurally characterised simple adducts of CO₂. Moreover, the reported intermediate displayed an exceptionally long C–OH bond of 1.563(6) Å.

The reported synthetic procedure can be recapitulated as follows. CO₂ was bubbled through an aqueous solution of tetra-*n*-butylammonium hydroxide, [*n*Bu₄N]OH. After neutral pH was achieved, the reaction mixture was dehydrated azeotropically by using successive portions of diethyl ether, resulting in the formation of a colourless powder. This powder was spectroscopically identified as tetra-*n*-butylammonium bicarbonate, [*n*Bu₄N]HCO₃. The saturated diethyl ether solution of the product was allowed to slowly evaporate, which resulted in the formation of colourless crystals.

The structure obtained by single crystal X-ray diffraction studies was reported as that of an arrested anionic intermediate [O₂C⋯OH]⁻. The authors described the anion to be encapsulated within a hydrophobic pocket formed by the tetra-*n*-butylammonium, [*n*Bu₄N]⁺, cations. The pocket contains two symmetry-related anions in a head-to-tail orientation, with a 4.71 Å O⋯O distance between the oxygen atoms of the hydroxy groups. Rather intriguingly, as there are no hydrogen-bond acceptors on the cation and due to the orientation of the anions, the hydroxy groups appear to be devoid of any secondary bonding interactions. Nevertheless, the crystal structure does show multiple C–H moieties on the cation that are in range to form weak C–O⋯H interactions with the anion. The authors suggest these interactions to aid the structural stability of the intermediate.

The results published for [*n*Bu₄N][O₂C⋯OH] can be compared with the cyanofornate anion, a simple adduct of cyanide and CO₂.²⁶² In the cyanofornate, the anion features an sp–sp² C–C bond with a bond length of 1.480(9) Å. It would seem plausible that a bicarbonate trapped inside a hydrophobic host scaffold would display a regular C–OH bond when no strong inter-ionic interactions are present. The hydrophobic pocket in the work of Ackermann *et al.* does not offer any apparent reason that would explain the stabilisation of the putative long C⋯O bond. The C⋯O bond length in [*n*Bu₄N][O₂C⋯OH] is

actually comparable to the C–C distance of 1.544 Å calculated for an isolated cyanofornate anion in vacuum. Thus, it could be possible for the reported salt to contain the common acetate anion, $[\text{O}_2\text{CCH}_3]^-$, with a normal C–C bond length.

In order to uncover the true identity of the salt reported by Ackermann *et al.*, a fresh sample of tetra-*n*-butylammonium acetate, $[\text{nBu}_4\text{N}][\text{O}_2\text{CCH}_3]$ **75**, was purchased. The container was opened under an inert atmosphere, a single crystal was removed directly from the bottle and a complete X-ray crystallographic study was performed on the crystal at 125 K. After collecting the low-temperature data, another data set for the same crystal was collected at room temperature. Additionally, colourless plate-like crystals were grown from a meticulously dried, saturated diethyl ether solution of $[\text{nBu}_4\text{N}][\text{O}_2\text{CCH}_3]$. The structure of the crystal thus obtained was found to be identical to the one determined for the fresh sample.

The unit cell parameters for **75** and for the structure obtained by Ackermann *et al.* are shown in Table 4. The actual data collection temperature for $[\text{nBu}_4\text{N}][\text{O}_2\text{C}\cdots\text{OH}]$ is not known as there is conflicting information between the original publication and the CIF file obtained from the CCDC repository. The space group for **75** is $P2_1/n$, that is, the same as reported for $[\text{nBu}_4\text{N}][\text{O}_2\text{C}\cdots\text{OH}]$. It is also evident from the parameters shown in Table 4 that the data are for identical species, or at the very least the compounds are extremely closely related.

Table 4. Unit-cell parameters for the structure reported in ref. 261 (CCDC: 1008313) and for $[\text{nBu}_4\text{N}][\text{O}_2\text{CCH}_3]$ **75** (CCDC: 1036823).^v

	T[K]	<i>a</i>	<i>b</i>	<i>c</i>	β	V[Å ³]
ref. 261	n.a.	10.755(2)	13.497(2)	13.948(2)	101.876(2)	1981.4(5)
75	125	10.7273(12)	13.3080(15)	13.9495(15)	101.9615(13)	1948.2(6)
75	297	10.8277(16)	13.799(2)	13.968(2)	101.1851(19)	2047.3(9)

The geometrical data of **75** were compared to the data reported for $[\text{nBu}_4\text{N}][\text{O}_2\text{C}\cdots\text{OH}]$. Geometrical parameters were considered to be significantly different if the difference between the two was larger than three times the standard uncertainty. The data used for this comparison were taken from the original publication of Ackermann *et al.* When analysing the data, it became evident that the two models are equivalent and represent the same structure. Crucially, comparison between the C17 \cdots C18/O3 bond in the two structures shows no significant difference in the bond length. Moreover, the CH₃ substituent in the acetate anion accurately replicates the large thermal motion reported for the O3 atom of bicarbonate. A comparison between the C18 refinement and the original model with O3 shows no significant differences in the structural parameters. This is illustrated in Figure 40, which displays an overlay of the thermal ellipsoid plots for **75** and $[\text{nBu}_4\text{N}][\text{O}_2\text{C}\cdots\text{OH}]$. The two structures are perfectly superimposable on one another, indicating a common origin.

As can be expected from the essentially identical unit-cells of **75** and the structure reported for $[n\text{Bu}_4\text{N}][\text{O}_2\text{C}\cdots\text{OH}]$, the packing and inter-ionic interactions in the two structures are also consistent with one another. Particularly, the arrangement of anions in the hydrophobic pocket is remarkably similar. The average difference in the $\text{H}\cdots\text{A}$ distances is a mere 0.06 \AA , and the average difference in the DHA angles is 4° . In both structures, the anions exhibit a head-to-tail orientation. The $\text{O}\cdots\text{O}$ distance between the two hydroxy groups in the $[\text{O}_2\text{C}\cdots\text{OH}]^-$ anions is 4.71 \AA as reported by Ackermann *et al.* In the refinement of **75**, the shortest $\text{C18}\cdots\text{C18}$ was found to be $4.665(4)\text{ \AA}$ (Figure 41). The difference between the two values is a mere 0.04 \AA , which can be considered negligible over the relatively long distance.

Based on the crystallographic analysis of **75**, it seems evident that the structure reported for $[n\text{Bu}_4\text{N}][\text{O}_2\text{C}\cdots\text{OH}]$ is actually that of $[n\text{Bu}_4\text{N}][\text{O}_2\text{CCH}_3]$. Without access to the original crystallographic data, however, the possibility remains that the two compounds are in fact different but simply isostructural. To rule out this possibility, geometry optimisations for the bicarbonate and the acetate anions were performed, both in the gas-phase and within the hydrophobic pocket formed by six $[n\text{Bu}_4\text{N}]^+$ cations.

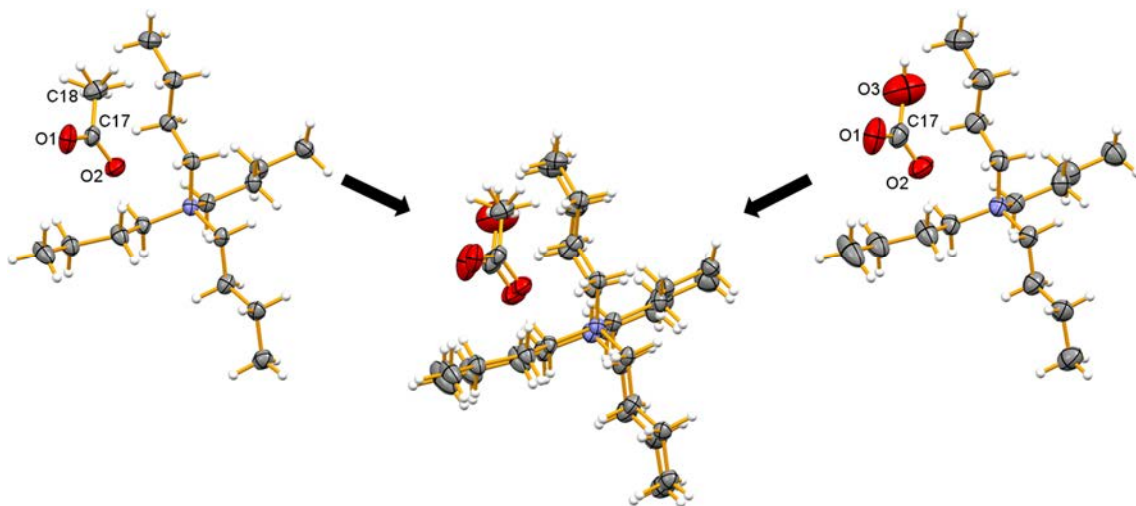


Figure 40. Thermal ellipsoid plots (50% probability) for **75** at 125 K (left, CCDC: 1036823) and for the proposed $[n\text{Bu}_4\text{N}][\text{O}_2\text{C}\cdots\text{OH}]$ salt (right, CCDC: 1008313), along with an overlay of the two structures (centre).^v The overlay is intentionally left slightly offset to better highlight the similarities of the two structures.

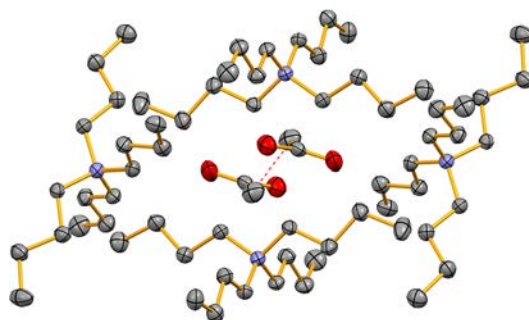


Figure 41. Thermal ellipsoid plot (50% probability, hydrogen atoms omitted for clarity) of the pocket formed by $[n\text{Bu}_4\text{N}]^+$ cations, enclosing a pair of acetate anions.^v The red dashed line indicates the shortest $\text{C18}\cdots\text{C18}$ contact (4.665(4) Å) in the structure.

The geometry of a free bicarbonate anion was optimised in the gas-phase at the CCSD(T)-F12b/VTZ-F12 level of theory. The results were found to parallel those reported for $[n\text{Bu}_4\text{N}][\text{O}_2\text{C}\cdots\text{OH}]$. The optimised C–OH bond length was 1.433 Å, and the OCO angle was 132.3°. Nearly the same set of values were obtained with dispersion-corrected density functional theory (PBE1PBE-D3BJ/def-TZVP): the C–OH distance was 1.437 Å, and the OCO angle was 132.4°. Similarly, the CCSD(T)-F12b/VTZ-F12 optimised geometry of an acetate anion was reproduced well at the computationally significantly less expensive PBE1PBE-D3BJ/def-TZVP level ($d(\text{C}-\text{C}) = 1.552$ Å, $(\text{OCO}) = 128.8^\circ$ *vs.* $d(\text{C}-\text{C}) = 1.557$ Å and $(\text{OCO}) = 129.1^\circ$, respectively). Thus, the PBE1PBE-D3BJ/def-TZVP method was used in all calculations.

The structure of the hydrophobic pocket (six $[n\text{Bu}_4\text{N}]^+$ cations and two anions) was extracted from the crystallographic data. The cations were frozen in place and a full structural optimisation of the anions was then performed within the environment provided by the cations. The optimisation performed on the acetate shows the metrical parameters of the anion to be consistent with its gas-phase geometry: $d(\text{C}-\text{C}) = 1.531$ Å and $(\text{OCO}) = 126.2^\circ$. The corresponding values for the optimised bicarbonate anion are $d(\text{C}-\text{OH}) = 1.393$ Å and $(\text{OCO}) = 129.7^\circ$. These results demonstrate that the weak $\text{C}-\text{H}\cdots\text{O}$ interactions are not strong enough to support a long $\text{C}\cdots\text{O}$ bond in $[n\text{Bu}_4\text{N}][\text{O}_2\text{C}\cdots\text{OH}]$. Furthermore, even if $[n\text{Bu}_4\text{N}][\text{O}_2\text{C}\cdots\text{OH}]$ would be isostructural with **75**, the bicarbonate would be expected to have a conventional C–O bond length.

The crystallographic and computational data indicate that the crystal structure reported for $[n\text{Bu}_4\text{N}][\text{O}_2\text{C}\cdots\text{OH}]$ is in fact that of $[n\text{Bu}_4\text{N}][\text{O}_2\text{CCH}_3]$. There were a number of other factors in the original publication that can be considered as major flaws. As an example, there is no information that would link the crystal structure to the bulk powder, and no elemental analysis was performed on the crystalline material. Also, the synthetic reference provided by the authors describes the preparation of $[n\text{Bu}_4\text{N}] \cdot \text{ASM} \cdot \text{HCO}_3$ salts (where ASM is an amine-based structural motif ligand),²⁶³ not the synthesis of $[n\text{Bu}_4\text{N}]\text{HCO}_3$.

An important question that remains is the origin of the acetate anion in the work published by Ackermann *et al.* A possible source could be the $[n\text{Bu}_4\text{N}]\text{OH}$

reagent that was used, which does contain trace amounts of other cations and anions. Another explanation is the cleavage of diethyl ether during distillation, which could produce some ethanol that, in turn, could form acetate in the presence of adventitious oxygen. It is possible that the diethyl ether was contaminated to begin with since ethanol is the precursor to most commercial sources of diethyl ether. Regardless of the source, a small amount of acetate could have been present in the bulk powder, which then crystallises out from the ether solution.

5 CONCLUSIONS

The main focus of this dissertation was in the synthesis of new stable main group radicals and the characterisation of reactive intermediates formed in chemical reactions. Three new stable radicals were synthesised and comprehensively characterised, while studies of reactive intermediates provided new knowledge of coupling reactions and hydrosilylations. X-ray crystallography, EPR spectroscopy and theoretical calculations played a crucial role in all of the studies performed.

The 2,2'-biquinoline-based coordination compounds $[(\text{biq})\text{BCl}_2]\text{Cl}$ and $[(\text{biq})\text{BCl}_2]^\bullet$ represent the first structurally characterised p-block complexes of biquinoline. The redox processes in the compounds are exclusively confined to the ligand framework, which allows unambiguous determination of the structural effects resulting from ligand reduction. The data thus obtained enabled the reinterpretation of the electronic structure of $\text{Co}(\text{biq})_2$, a complex that was initially reported to contain Co^0 but actually has the metal in the +II oxidation state. The ligand charge state can be determined by its metrical parameters, and the data provided by this study allow this method to be used for metal complexes incorporating the redox non-innocent 2,2'-biquinoline.

The Smiles rearrangement reaction, with concurrent or subsequent cyclocondensation with sulphur monochloride, was shown to provide a convenient and modifiable route to a new class of hybrid 1,4-thiazine-1,2,3-dithiazolylum salts. The cations can then be easily reduced to the corresponding stable neutral radicals that have the unpaired electron delocalised over both 1,4-thiazinyl and 1,2,3-dithiazolyl moieties. The customisable framework of the synthesised hybrid radical species offers ample new opportunities for the design of molecular materials that may feature novel physical properties.

DDQ was shown to promote metal-free intermolecular oxidative dehydrogenative 3,3'-coupling of 2-aryl-benzo[*b*]furans and 2-aryl-benzo[*b*]thiophenes in the presence of a strong acid. The DDQ/substrate charge transfer complex was found to initiate the reaction, which then proceeds via oxidation of the substrate into an electrophilic radical cation that reacts with

another neutral substrate molecule. The reactivity was found to correlate strongly with the oxidation potential of the substrate.

Perfluoroarylborane Lewis acids are known to catalyse the addition of silicon-hydrogen bonds across C=C, C=N and C=O double bonds. While the hydrosilylation had been postulated to occur via borane activation of the silane Si-H bond, the key borane-silane adduct had not been observed experimentally. It was now shown that the strongly Lewis acidic, antiaromatic 1,2,3-tris(pentafluorophenyl)-4,5,6,7-tetrafluoroboraindene forms an isolable adduct with triethylsilane. The isolation and characterisation of the borane-silane adduct allows the investigation of the detailed reaction mechanism between such adducts and nucleophilic substrates.

The crystallographic characterisation of an intermediate in the formation of tetra-*n*-butylammonium bicarbonate had been reported. The intermediate was claimed to exhibit an unusually long C-OH bond. A detailed crystallographic and computational analysis showed the reported crystal structure to be that of tetra-*n*-butylammonium acetate, an unwanted side product formed in the original reaction.

In summary, synthetic procedures to new, stable main group radicals were presented along with detailed studies on the mechanisms and intermediates of quintessential chemical reactions. An emphasis was on thorough and detailed characterisation of both products and intermediates alike.

REFERENCES

- 1 Gomberg, M. *J. Am. Chem. Soc.* **1900**, *22*, 757–771.
- 2 Griller, D.; Ingold, K. U. *Acc. Chem. Res.* **1976**, *9*, 13–19.
- 3 Power, P. P. *Chem. Rev.* **2003**, *103*, 789–810.
- 4 Hicks, R. G. *Org. Biomol. Chem.* **2007**, *5*, 1321–1338.
- 5 Martin, C. D.; Soleilhavoup, M.; Bertrand, G. *Chem. Sci.* **2013**, *4*, 3020–3030.
- 6 Hicks, R. G. *Stable Radicals: Fundamentals and Applied Aspects of Odd-Electron Compounds*, John Wiley & Sons, Ltd: Chichester, UK, **2010**.
- 7 Schlenk, W.; Weickel, T.; Herzenstein, A. *Justus Liebig's Ann. der Chemie* **1910**, *372*, 1–20.
- 8 Lankamp, H.; Nauta, W. T.; MacLean, C. *Tetrahedron Lett.* **1968**, *9*, 249–254.
- 9 Neumann, W. P.; Uzick, W.; Zarkadis, A. K. *J. Am. Chem. Soc.* **1986**, *108*, 3762–3770.
- 10 Andersen, P.; Klewe, B. *Acta Chem. Scand.* **1967**, *21*, 2599–2607.
- 11 Kahr, B.; Engen, D. Van; Gopalan, P. *J. Am. Chem. Soc.* **1993**, *5*, 729–732.
- 12 Neumann, W. P.; Penenory, A.; Stewen, U.; Lehnig, M. *J. Am. Chem. Soc.* **1989**, *111*, 5845–5851.
- 13 Maki, A. H.; Allendoerfer, R. D.; Danner, J. C.; Keys, R. T. *J. Am. Chem. Soc.* **1968**, *90*, 4225–4231.
- 14 Ballester, M.; Riera-Figueras, J.; Castaner, J.; Badfa, C.; Monso, J. M. *J. Am. Chem. Soc.* **1971**, *93*, 2215–2225.
- 15 Veciana, J.; Carilla, J.; Miravittles, C.; Molins, E. *J. Chem. Soc., Chem. Commun.* **1987**, 812–814.
- 16 Falle, H. R.; Luckhurst, G. R.; Horsfield, A.; Ballester, M. *J. Chem. Phys.* **1969**, *50*, 258.
- 17 Ballester, M. *Acc. Chem. Res.* **1985**, *18*, 380–387.
- 18 Armet, O.; Veciana, J.; Rovira, C.; Riera, J.; Castaner, J.; Molins, E.; Rius, J.; Miravittles, C.; Olivella, S.; Brichfeus, J. *J. Phys. Chem.* **1987**, *91*, 5608–5616.
- 19 Carilla, J.; Fajarí, L.; Juliá, L.; Riera, J.; Viadel, L. *Tetrahedron Lett.* **1994**, *35*, 6529–6532.
- 20 Carilla, J.; Fajarí, L.; Juliá, L.; Sañé, J.; Rius, J. *Tetrahedron* **1996**, *52*, 7013–7024.
- 21 Reid, D. H. *Tetrahedron* **1958**, *3*, 339–352.
- 22 Sogo, P. B.; Nakazaki, M.; Calvin, M. *J. Chem. Phys.* **1957**, *26*, 1343–1345.
- 23 Reid, D. H. *Q. Rev. Chem. Soc.* **1965**, *19*, 274–302.
- 24 O'Connor, G. D.; Troy, T. P.; Roberts, D. A.; Chalyavi, N.; Fückel, B.; Crossley, M. J.; Nauta, K.; Stanton, J. F.; Schmidt, T. W. *J. Am. Chem. Soc.* **2011**, *133*, 14554–14557.
- 25 Broser, W.; Kurreck, H.; Oestreich-Janzen, S.; Schlömp, G.; Fey, H.-J.; Kirste, B. *Tetrahedron* **1979**, *35*, 1159–1166.
- 26 Zaitsev, V.; Rosokha, S. V.; Head-Gordon, M.; Kochi, J. K. *J. Org. Chem.* **2006**, *71*, 520–526.
- 27 Liao, P.; Itkis, M. E.; Oakley, R. T.; Tham, F. S.; Haddon, R. C. *J. Am. Chem. Soc.* **2004**, *126*, 14297–14302.

- 28 Goto, K.; Kubo, T.; Yamamoto, K.; Nakasuji, K.; Sato, K.; Shiomi, D.; Takui, T.; Kubota, M.; Kobayashi, T.; Yakusi, K.; Ouyang, J. *J. Am. Chem. Soc.* **1999**, *121*, 1619–1620.
- 29 Takano, Y.; Taniguchi, T.; Isobe, H.; Kubo, T.; Morita, Y.; Yamamoto, K.; Nakasuji, K.; Takui, T.; Yamaguchi, K. *J. Am. Chem. Soc.* **2002**, *124*, 11122–11130.
- 30 Tian, Y.-H.; Kertesz, M. *J. Am. Chem. Soc.* **2010**, *132*, 10648–10649.
- 31 Kolb, B.; Kertesz, M.; Thonhauser, T. *J. Phys. Chem.* **2013**, *117*, 3642–3649.
- 32 Mou, Z.; Uchida, K.; Kubo, T.; Kertesz, M. *J. Am. Chem. Soc.* **2014**, *136*, 18009–18022.
- 33 Mou, Z.; Uchida, K.; Kubo, T.; Kertesz, M. *J. Am. Chem. Soc.* **2015**, *137*, 13989–13989.
- 34 Mou, Z.; Kubo, T.; Kertesz, M. *Chem. Eur. J.* **2015**, *21*, 18230–18236.
- 35 Tian, Y.-H.; Sumpter, B. G.; Du, S.; Huang, J. *J. Phys. Chem. Lett.* **2015**, *6*, 2318–2325.
- 36 Koutentis, P. A.; Chen, Y.; Cao, Y.; Best, T. P.; Itkis, M. E.; Beer, L.; Oakley, R. T.; Cordes, A. W.; Brock, C. P.; Haddon, R. C. *J. Am. Chem. Soc.* **2001**, *123*, 3864–3871.
- 37 Haddon, R. C.; Wudl, F.; Kaplan, M. L.; Marshall, J. H.; Cais, R. E.; Bramwell, F. B. *J. Am. Chem. Soc.* **1978**, *100*, 7629–7633.
- 38 Chi, X.; Itkis, M. E.; Patrick, B. O.; Barclay, T. M.; Reed, R. W.; Oakley, R. T.; Cordes, A. W.; Haddon, R. C. *J. Am. Chem. Soc.* **1999**, *121*, 10395–10402.
- 39 Mandal, S. K.; Itkis, M. E.; Chi, X.; Samanta, S.; Lidsky, D.; Reed, R. W.; Oakley, R. T.; Tham, F. S.; Haddon, R. C. *J. Am. Chem. Soc.* **2005**, *127*, 8185–8196.
- 40 Pal, S. K.; Itkis, M. E.; Reed, R. W.; Oakley, R. T.; Cordes, A. W.; Tham, F. S.; Siegrist, T.; Haddon, R. C. *J. Am. Chem. Soc.* **2004**, *126*, 1478–1484.
- 41 Chi, X.; Itkis, M. E.; Kirschbaum, K.; Pinkerton, A. A.; Oakley, R. T.; Cordes, A. W.; Haddon, R. C. *J. Am. Chem. Soc.* **2001**, *123*, 4041–4048.
- 42 Chi, X.; Itkis, M. E.; Reed, R. W.; Oakley, R. T.; Cordes, A. W.; Haddon, R. C. *J. Phys. Chem. B* **2002**, *106*, 8278–8287.
- 43 Itkis, M. E.; Chi, X.; Cordes, A. W.; Haddon, R. C.; Wolf, S. A.; Sarma, S. Das; Haddon, R. C.; Sitzmann, H.; Koutentis, P. A.; Chi, X.; Ballester, M.; Goto, K.; Chi, X.; Krober, J.; Codjovi, E.; Kahn, O.; Groliere, F.; Jay, C.; Kahn, O.; Martinez, C. J.; Fujita, W.; Awaga, K.; Nakatani, K.; Yu, P. *Science* **2002**, *296*, 1443–1445.
- 44 Pal, S. K.; Itkis, M. E.; Tham, F. S.; Reed, R. W.; Oakley, R. T.; Haddon, R. C. *Science* **2005**, *309*, 281–284.
- 45 Mandal, S. K.; Samanta, S.; Itkis, M. E.; Jensen, D. W.; Reed, R. W.; Oakley, R. T.; Tham, F. S.; Donnadiou, B.; Haddon, R. C. *J. Am. Chem. Soc.* **2006**, *128*, 1982–1994.
- 46 Bag, P.; Itkis, M. E.; Pal, S. K.; Donnadiou, B.; Tham, F. S.; Park, H.; Schlueter, J. A.; Siegrist, T.; Haddon, R. C. *J. Am. Chem. Soc.* **2010**, *132*, 2684–2694.

- 47 Morita, Y.; Aoki, T.; Fukui, K.; Nakazawa, S.; Tamaki, K.; Suzuki, S.; Fuyuhiko, A.; Yamamoto, K.; Sato, K.; Shiomi, D.; Naito, A.; Takui, T.; Nakasuji, K. *Angew. Chem. Int. Ed.* **2002**, *41*, 1793–1796.
- 48 Zheng, S.; Lan, J.; Khan, S. I.; Rubin, Y. *J. Am. Chem. Soc.* **2003**, *125*, 5786–5791.
- 49 Ueda, A.; Wasa, H.; Suzuki, S.; Okada, K.; Sato, K.; Takui, T.; Morita, Y. *Angew. Chem. Int. Ed.* **2012**, *51*, 6691–6695.
- 50 Anamimoghadam, O.; Symes, M. D.; Long, D.-L.; Sproules, S.; Cronin, L.; Bucher, G. *J. Am. Chem. Soc.* **2015**, *137*, 14944–14951.
- 51 Uchida, K.; Ito, S.; Nakano, M.; Abe, M.; Kubo, T. *J. Am. Chem. Soc.* **2016**, *138*, 2399–2410.
- 52 Altwicker, E. R. *Chem. Rev.* **1967**, *67*, 475–531.
- 53 Coppinger, G. M. *J. Am. Chem. Soc.* **1957**, *79*, 501–502.
- 54 Dietz, F.; Tyutyulkov, N.; Baumgarten, M. *J. Phys. Chem. B* **1998**, *102*, 3912–3916.
- 55 Novak, I.; Kovač, B. *Chem. Phys. Lett.* **2005**, *413*, 351–355.
- 56 Kirste, B.; Harrer, W.; Kurreck, H. *J. Am. Chem. Soc.* **1985**, *107*, 20–28.
- 57 Kuhn, R.; Trischmann, H. *Angew. Chem. Int. Ed.* **1963**, *2*, 155–155.
- 58 Neugebauer, F. A.; Fischer, H.; Siegel, R. *Chem. Ber.* **1988**, *121*, 815–822.
- 59 Paré, E. C.; Brook, D. J. R.; Brieger, A.; Badik, M.; Schinke, M. *Org. Biomol. Chem.* **2005**, *3*, 4258–4261.
- 60 Li, Y.; Mondal, K. C.; Samuel, P. P.; Zhu, H.; Orben, C. M.; Panneerselvam, S.; Dittrich, B.; Schwederski, B.; Kaim, W.; Mondal, T.; Koley, D.; Roesky, H. W. *Angew. Chem. Int. Ed.* **2014**, *53*, 4168–4172.
- 61 Piloty, O.; Schwerin, B. G. *Berichte der Dtsch. Chem. Gesellschaft* **1901**, *34*, 1870–1887.
- 62 Holden, A. N.; Yager, W. A.; Merritt, F. R. *J. Chem. Phys.* **1951**, *19*, 1319.
- 63 Lebedev, O. L.; Kazarnovskii, S. N. *Zhurnal Obs. Khimii* **1960**, *30*, 1631–1635.
- 64 Neiman, M. B.; Rozantzev, E. G.; Mamedova, Y. G. *Nature* **1962**, *196*, 472–474.
- 65 Breuer, E.; Aurich, H. G.; Nielsen, A. In *Nitrones, Nitronates and Nitroxides*; 313–370, John Wiley & Sons, Inc.: Chichester, UK, **1989**.
- 66 Hass, H. B.; Riley, E. F. *Chem. Rev.* **1943**, *32*, 373–430.
- 67 Mahoney, L. R.; Mendenhall, G. D.; Ingold, K. U. *J. Am. Chem. Soc.* **1973**, *95*, 8610–8614.
- 68 Ullman, E. F.; Osiecki, J. H.; Boocock, D. G. B.; Darcy, R. *J. Am. Chem. Soc.* **1972**, *94*, 7049–7059.
- 69 Caneschi, A.; Gatteschi, D.; Rey, P. *Progress in Inorganic Chemistry*, Wiley, **1991**.
- 70 Smith, M. B.; March, J. *March's Advanced Organic Chemistry*, Wiley, New York, **2001**.
- 71 Norman, N. C. *Polyhedron* **1993**, *12*, 2431–2446.
- 72 Chivers, T. *Chem. Rev.* **1985**, *85*, 341–365.
- 73 Chivers, T. *A guide to chalcogen-nitrogen chemistry*, World Scientific, **2005**.

- 74 Preuss, K. E. *Dalton Trans.* **2007**, 21, 2357–2369.
- 75 Kaszynski, P. J. *Phys. Chem. A* **2001**, 105, 7615–7625.
- 76 Kaszynski, P. J. *Phys. Chem. A* **2001**, 105, 7626–7633.
- 77 Beer, L.; Haddon, R. C.; Itkis, M. E.; Leitch, A. A.; Oakley, R. T.; Reed, R. W.; Richardson, J. F.; VanderVeer, D. G. *Chem. Commun.* **2005**, 124, 1218–1220.
- 78 Vegas, A.; Pérez-Salazar, A.; Banister, A. J.; Hey, R. G. *J. Chem. Soc., Dalton Trans.* **1980**, 1812–1815.
- 79 Barclay, T. M.; Cordes, A. W.; George, N. A.; Haddon, R. C.; Itkis, M. E.; Mashuta, M. S.; Oakley, R. T.; Patenaude, G. W.; Reed, R. W.; Richardson, J. F.; Zhang, H. *J. Am. Chem. Soc.* **1998**, 120, 352–360.
- 80 Brusso, J. L.; Clements, O. P.; Haddon, R. C.; Itkis, M. E.; Leitch, A. A.; Oakley, R. T.; Reed, R. W.; Richardson, J. F. *J. Am. Chem. Soc.* **2004**, 126, 8256–8265.
- 81 Brusso, J. L.; Clements, O. P.; Haddon, R. C.; Itkis, M. E.; Leitch, A. A.; Oakley, R. T.; Reed, R. W.; Richardson, J. F. *J. Am. Chem. Soc.* **2004**, 126, 14692–14693.
- 82 Legin, K.; Wong, J. W. L.; Winter, S. M.; Mailman, A.; Dube, P. A.; Oakley, R. T. *Inorg. Chem.* **2013**, 52, 2188–2198.
- 83 Perkins, C. W.; Clarkson, R. B.; Martin, J. C. *J. Am. Chem. Soc.* **1986**, 108, 3206–3210.
- 84 Perkins, C. W.; Martin, J. C. *J. Am. Chem. Soc.* **1986**, 108, 3211–3214.
- 85 Imada, Y.; Nakano, H.; Furukawa, K.; Kishi, R.; Nakano, M.; Maruyama, H.; Nakamoto, M.; Sekiguchi, A.; Ogawa, M.; Ohta, T.; Yamamoto, Y. *J. Am. Chem. Soc.* **2016**, 138, 479–482.
- 86 Pauling, L. *J. Am. Chem. Soc.* **1931**, 53, 3225–3237.
- 87 Zhang, S.; Wang, X.; Sui, Y.; Wang, X. *J. Am. Chem. Soc.* **2014**, 136, 14666–14669.
- 88 Lappert, M. F.; Lednor, P. W. *Adv. Organomet. Chem.* **1976**, 14, 345–399.
- 89 Davidson, P. J.; Hudson, A.; Lappert, M. F.; Lednor, P. W. *J. Chem. Soc., Chem. Commun.* **1973**, 829–830.
- 90 Gynane, M. J. S.; Hudson, A.; Lappert, M. F.; Power, P. P. *J. Chem. Soc., Chem. Commun.* **1976**, 623–624.
- 91 Olmstead, M. M.; Power, P. P. *J. Am. Chem. Soc.* **1986**, 108, 4235–4236.
- 92 Leffler, J. E.; Watts, G. B.; Tanigaki, T.; Dolan, E.; Miller, D. S. *J. Am. Chem. Soc.* **1970**, 92, 6825–6830.
- 93 Grigsby, W. J.; Power, P. P. *Chem. Commun.* **1996**, 92, 2235–2236.
- 94 Grigsby, W. J.; Power, P. *Chem. Eur. J.* **1997**, 3, 368–375.
- 95 Cummings, S. A.; Iimura, M.; Harlan, C. J.; Kwaan, R. J.; Trieu, I. V.; Norton, J. R.; Bridgewater, B. M.; Jäkle, F.; Sundararaman, A.; Tilset, M. *Organometallics* **2006**, 25, 1565–1568.
- 96 Chiu, C.-W.; Gabbai, F. P. *Angew. Chem. Int. Ed.* **2007**, 46, 1723–1725.
- 97 Aramaki, Y.; Omiya, H.; Yamashita, M.; Nakabayashi, K.; Ohkoshi, S.; Nozaki, K. *J. Am. Chem. Soc.* **2012**, 134, 19989–19992.

- 98 Deakyne, C. A.; Thomas, H. M.; Liebman, J. F. *J. Fluor. Chem.* **2009**, *130*, 836–845.
- 99 Bissinger, P.; Braunschweig, H.; Damme, A.; Hörl, C.; Krummenacher, I.; Kupfer, T. *Angew. Chem. Int. Ed.* **2015**, *54*, 359–362.
- 100 Bissinger, P.; Braunschweig, H.; Damme, A.; Kupfer, T.; Krummenacher, I.; Vargas, A. *Angew. Chemie Int. Ed.* **2014**, *53*, 5689–5693.
- 101 Longobardi, L. E.; Liu, L.; Grimme, S.; Stephan, D. W. *J. Am. Chem. Soc.*, **2016**, *138*, 2500–2503.
- 102 Pluta, C.; Pörschke, K.-R.; Krüger, C.; Hildenbrand, K. *Angew. Chem. Int. Ed.* **1993**, *32*, 388–390.
- 103 He, X.; Bartlett, R. A.; Olmstead, M. M.; Ruhlandt-Senge, K.; Sturgeon, B. E.; Power, P. P. *Angew. Chem. Int. Ed.* **1993**, *32*, 717–719.
- 104 Wiberg, N.; Blank, T.; Kaim, W.; Schwederski, B.; Linti, G. *Eur. J. Inorg. Chem.* **2000**, *2000*, 1475–1481.
- 105 Wiberg, N.; Amelunxen, K.; Nöth, H.; Schwenk, H.; Kaim, W.; Klein, A.; Scheiring, T. *Angew. Chem. Int. Ed.* **1997**, *36*, 1213–1215.
- 106 Wiberg, N.; Blank, T.; Amelunxen, K.; Nöth, H.; Knizek, J.; Habereeder, T.; Kaim, W.; Wanner, M. *Eur. J. Inorg. Chem.* **2001**, *2001*, 1719–1727.
- 107 Lee, V. Y.; Sekiguchi, A. *Acc. Chem. Res.* **2007**, *40*, 410–419.
- 108 Olmstead, M. M.; Pu, L.; Simons, R. S.; Power, P. P. *Chem. Commun.* **1997**, 1595–1596.
- 109 Ishida, Y.; Sekiguchi, A.; Kobayashi, K.; Nagase, S. *Organometallics* **2004**, *23*, 4891–4896.
- 110 Sekiguchi, A.; Matsuno, T.; Ichinohe, M. *J. Am. Chem. Soc.* **2001**, *123*, 12436–12437.
- 111 Sekiguchi, A.; Fukawa, T.; Nakamoto, M.; Lee, V. Y.; Ichinohe, M. *J. Am. Chem. Soc.* **2002**, *124*, 9865–9869.
- 112 Förster, C.; Klinkhammer, K. W.; Tumanskii, B.; Krüger, H.-J.; Kelm, H. *Angew. Chem. Int. Ed.* **2007**, *46*, 1156–1159.
- 113 Becker, M.; Förster, C.; Franzen, C.; Hartrath, J.; Kirsten, E.; Knuth, J.; Klinkhammer, K. W.; Sharma, A.; Hinderberger, D. *Inorg. Chem.* **2008**, *47*, 9965–9978.
- 114 Schmidt, U.; Kabitzke, K.; Markau, K.; Müller, A. *Chem. Ber.* **1966**, *99*, 1497–1501.
- 115 Hinchley, S. L.; Morrison, C. A.; Rankin, D. W. H.; Macdonald, C. L. B.; Wiacek, R. J.; Cowley, A. H.; Lappert, M. F.; Gundersen, G.; Clyburne, J. A. C.; Power, P. P. *Chem. Commun.* **2000**, 2045–2046.
- 116 Hinchley, S. L.; Morrison, C. A.; Rankin, D. W. H.; Macdonald, C. L. B.; Wiacek, R. J.; Voigt, A.; Cowley, A. H.; Lappert, M. F.; Gundersen, G.; Clyburne, J. A. C.; Power, P. P. *J. Am. Chem. Soc.* **2001**, *123*, 9045–9053.
- 117 Canac, Y.; Baceiredo, A.; Schoeller, W. W.; Gigmes, D.; Bertrand, G. *J. Am. Chem. Soc.* **1997**, *119*, 7579–7580.
- 118 Björgvinsson, M.; Heinze, T.; Roesky, H. W.; Pauer, F.; Stalke, D.; Sheldrick, G. M. *Angew. Chem. Int. Ed.* **1991**, *30*, 1677–1678.
- 119 Grützmacher, H.; Breher, F. *Angew. Chem. Int. Ed.* **2002**, *41*, 4006–4011.

- 120 Breher, F. *Coord. Chem. Rev.* **2007**, *251*, 1007–1043.
- 121 Dowd, P. *J. Am. Chem. Soc.* **1966**, *88*, 2587–2589.
- 122 Dowd, P. *J. Am. Chem. Soc.* **1970**, *92*, 1066–1068.
- 123 Dowd, P.; Chang, W.; Paik, Y. H. *J. Am. Chem. Soc.* **1986**, *108*, 7416–7417.
- 124 Abe, M.; Adam, W.; Heidenfelder, T.; Nau, W. M.; Zhang, X. *J. Am. Chem. Soc.* **2000**, *122*, 2019–2026.
- 125 Jain, R.; Sponsler, M. B.; Coms, F. D.; Dougherty, D. A. *J. Am. Chem. Soc.* **1988**, *110*, 1356–1366.
- 126 Rajca, A. *Chem. Rev.* **1994**, *94*, 871–893.
- 127 Dougherty, D. A. *Acc. Chem. Res.* **1991**, *24*, 88–94.
- 128 Niecke, E.; Fuchs, A.; Baumeister, F.; Nieger, M.; Schoeller, W. W. *Angew. Chem. Int. Ed.* **1995**, *34*, 555–557.
- 129 Schmidt, O.; Fuchs, A.; Gudat, D.; Nieger, M.; Hoffbauer, W.; Niecke, E.; Schoeller, W. W. *Angew. Chem. Int. Ed.* **1998**, *37*, 949–952.
- 130 Niecke, E.; Fuchs, A.; Nieger, M. *Angew. Chem. Int. Ed.* **1999**, *38*, 3028–3031.
- 131 Niecke, E.; Fuchs, A.; Nieger, M.; Schmidt, O.; Schoeller, W. W. *Angew. Chem. Int. Ed.* **1999**, *38*, 3031–3034.
- 132 Schoeller, W. W.; Begemann, C.; Niecke, E.; Gudat, D. *J. Phys. Chem. A* **2001**, *105*, 10731–10738.
- 133 Scheschkewitz, D.; Amii, H.; Gornitzka, H.; Schoeller, W. W.; Bourissou, D.; Bertrand, G. *Science* **2002**, *295*, 1880–1881.
- 134 Hinz, A.; Schulz, A.; Villinger, A. *Angew. Chem. Int. Ed.* **2015**, *54*, 668–672.
- 135 Kostenko, A.; Tumanskii, B.; Karni, M.; Inoue, S.; Ichinohe, M.; Sekiguchi, A.; Apeloig, Y. *Angew. Chem. Int. Ed.* **2015**, *54*, 12144–12148.
- 136 Barclay, T. M.; Cordes, A. W.; de Laat, R. H.; Goddard, J. D.; Haddon, R. C.; Jeter, D. Y.; Mawhinney, R. C.; Oakley, R. T.; Palstra, T. T. M.; Patenaude, G. W.; Reed, R. W.; Westwood, N. P. C. *J. Am. Chem. Soc.* **1997**, *119*, 2633–2641.
- 137 Decken, A.; Cameron, T. S.; Passmore, J.; Rautiainen, J. M.; Reed, R. W.; Shuvaev, K. V.; Thompson, L. K. *Inorg. Chem.* **2007**, *46*, 7436–7457.
- 138 Cameron, T. S.; Decken, A.; Grein, F.; Knapp, C.; Passmore, J.; Rautiainen, J. M.; Shuvaev, K. V.; Thompson, R. C.; Wood, D. J. *Inorg. Chem.* **2010**, *49*, 7861–7879.
- 139 Matsui, H.; Fukuda, K.; Takamuku, S.; Sekiguchi, A.; Nakano, M. *Chem. Eur. J.* **2015**, *21*, 2157–2164.
- 140 Ratera, I.; Veciana, J. *Chem. Soc. Rev.* **2012**, *41*, 303–349.
- 141 Mas-Torrent, M.; Crivillers, N.; Rovira, C.; Veciana, J. *Chem. Rev.* **2012**, *112*, 2506–2527.
- 142 Sugawara, T.; Komatsu, H.; Suzuki, K. *Chem. Soc. Rev.* **2011**, *40*, 3105–3118.
- 143 Tomlinson, E. P.; Hay, M. E.; Boudouris, B. W. *Macromolecules* **2014**, *47*, 6145–6158.
- 144 Oyaizu, K.; Nishide, H. *Adv. Mater.* **2009**, *21*, 2339–2344.
- 145 Chatgililoglu, C. *Acc. Chem. Res.* **1992**, *25*, 188–194.
- 146 Rowlands, G. J. *Tetrahedron* **2009**, *65*, 8603–8655.
- 147 Rowlands, G. J. *Tetrahedron* **2010**, *66*, 1593–1636.

- 148 Wille, U. *Chem. Eur. J.* **2002**, *8*, 340–347.
- 149 Fischer, H. *Chem. Rev.* **2001**, *101*, 3581–3610.
- 150 Studer, A.; Curran, D. P. *Angew. Chem. Int. Ed.* **2016**, *55*, 58–102.
- 151 Ravelli, D.; Protti, S.; Fagnoni, M. *Chem. Rev.* **2016**, *116*, 9850–9913.
- 152 Studer, A. *Chem. Soc. Rev.* **2004**, *033*, 267–273.
- 153 Studer, A.; Schulte, T. *Chem. Rec.* **2005**, *5*, 27–35.
- 154 Wetter, C.; Studer, A. *Chem. Commun.* **2004**, *5*, 174–175.
- 155 Zard, S. Z. *Angew. Chem. Int. Ed.* **1997**, *36*, 672–685.
- 156 Quiclet-Sire, B.; Zard, S. Z. *Chem. Eur. J.* **2006**, *12*, 6002–6016.
- 157 Gross, S.; Reissig, H.-U. *Synlett* **2002**, *2002*, 2027–2030.
- 158 Clark, A. J. *Chem. Soc. Rev.* **2002**, *31*, 1–11.
- 159 Pintauer, T.; Matyjaszewski, K. *Chem. Soc. Rev.* **2008**, *37*, 1087–1097.
- 160 Ford, L.; Jahn, U. *Angew. Chem. Int. Ed.* **2009**, *48*, 6386–6389.
- 161 Lo, J. C.; Gui, J.; Yabe, Y.; Pan, C.-M.; Baran, P. S. *Nature* **2014**, *516*, 343–348.
- 162 Kato, K.; Mukaiyama, T. *Chem. Lett.* **1992**, *21*, 1137–1140.
- 163 Beeson, T. D.; Mastracchio, A.; Hong, J.-B.; Ashton, K.; Macmillan, D. W. C. *Science* **2007**, *316*, 582–585.
- 164 Ingram, A. J.; Boeser, C. L.; Zare, R. N. *Chem. Sci.* **2016**, *7*, 39–55.
- 165 Dole, M.; Mack, L. L.; Hines, R. L.; Mobley, R. C.; Ferguson, L. D.; Alice, M. B. *J. Chem. Phys.* **1968**, *49*, 2240.
- 166 Fenn, J. B.; Mann, M.; Meng, C. K.; Wong, S. F.; Whitehouse, C. M. *Science* **1989**, *246*, 64–71.
- 167 Alvim, H. G. O.; da Silva Júnior, E. N.; Neto, B. A. D. *RSC Adv.* **2014**, *4*, 54282–54299.
- 168 Vikse, K. L.; Ahmadi, Z.; McIndoe, J. S. *Coord. Chem. Rev.* **2014**, *279*, 96–114.
- 169 Yunker, L. P. E.; Stoddard, R. L.; McIndoe, J. S. *J. Mass Spectrom.* **2014**, *49*, 1–8.
- 170 Zhu, W.; Yuan, Y.; Zhou, P.; Zeng, L.; Wang, H.; Tang, L.; Guo, B.; Chen, B. *Molecules* **2012**, *17*, 11507–11537.
- 171 Schröder, D. *Acc. Chem. Res.* **2012**, *45*, 1521–1532.
- 172 Santos, L. S. *Eur. J. Org. Chem.* **2008**, *2008*, 235–253.
- 173 Santos, L. S.; Knaack, L.; Metzger, J. O. *Int. J. Mass Spectrom.* **2005**, *246*, 84–104.
- 174 Tremel, P.; Iacobucci, C.; Massi, L.; Olivero, S.; Gal, J.-F.; Duñach, E. *New J. Chem.* **2015**, *39*, 7453–7458.
- 175 Vikse, K. L.; Woods, M. P.; McIndoe, J. S. *Organometallics* **2010**, *29*, 6615–6618.
- 176 Luo, J.; Theron, R.; Sewell, L. J.; Hooper, T. N.; Weller, A. S.; Oliver, A. G.; McIndoe, J. S. *Organometallics* **2015**, *34*, 3021–3028.
- 177 Yan, X.; Sokol, E.; Li, X.; Li, G.; Xu, S.; Cooks, R. G. *Angew. Chem. Int. Ed.* **2014**, *53*, 5931–5935.
- 178 Santos, L. S.; Pavam, C. H.; Almeida, W. P.; Coelho, F.; Eberlin, M. N. *Angew. Chem. Int. Ed.* **2004**, *43*, 4330–4333.

- 179 Rodrigues, T. S.; Silva, V. H. C.; Lalli, P. M.; de Oliveira, H. C. B.; da Silva, W. A.; Coelho, F.; Eberlin, M. N.; Neto, B. A. D. *J. Org. Chem.* **2014**, *79*, 5239–5248.
- 180 Schley, N. D.; Fu, G. C. *J. Am. Chem. Soc.* **2014**, *136*, 16588–16593.
- 181 Takáts, Z.; Wiseman, J. M.; Gologan, B.; Cooks, R. G. *Science* **2004**, *306*, 471–473.
- 182 Cotte-Rodríguez, I.; Takáts, Z.; Talaty, N.; Chen, H.; Cooks, R. G. *Anal. Chem.* **2005**, *77*, 6755–6764.
- 183 Chen, H.; Cotte-Rodríguez, I.; Cooks, R. G. *Chem. Commun.* **2006**, *306*, 597–599.
- 184 Perry, R. H.; Brownell, K. R.; Chingin, K.; Cahill, T. J.; Waymouth, R. M.; Zare, R. N. *PNAS* **2012**, *109*, 2246–2250.
- 185 Chung, K.; Banik, S. M.; De Crisci, A. G.; Pearson, D. M.; Blake, T. R.; Olsson, J. V.; Ingram, A. J.; Zare, R. N.; Waymouth, R. M. *J. Am. Chem. Soc.* **2013**, *135*, 7593–7602.
- 186 Perry, R. H.; Cahill, T. J.; Roizen, J. L.; Du Bois, J.; Zare, R. N. *PNAS* **2012**, *109*, 18295–18299.
- 187 Gouré, E.; Avenier, F.; Dubourdeaux, P.; Sénèque, O.; Albrieux, F.; Lebrun, C.; Clémancey, M.; Maldivi, P.; Latour, J.-M. *Angew. Chem. Int. Ed.* **2014**, *53*, 1580–1584.
- 188 Brown, T. A.; Chen, H.; Zare, R. N. *J. Am. Chem. Soc.* **2015**, *137*, 7274–7277.
- 189 Brown, T. A.; Chen, H.; Zare, R. N. *Angew. Chem. Int. Ed.* **2015**, *54*, 11183–11185.
- 190 Ingram, A. J.; Wolk, A. B.; Flender, C.; Zhang, J.; Johnson, C. J.; Hintermair, U.; Crabtree, R. H.; Johnson, M. A.; Zare, R. N. *Inorg. Chem.* **2014**, *53*, 423–433.
- 191 Johnson, C. S. *Prog. Nucl. Magn. Reson. Spectrosc.* **1999**, *34*, 203–256.
- 192 Pregosin, P. S.; Anil Kumar, P. G.; Fernández, I. *Chem. Rev.* **2005**, *105*, 2977–2998.
- 193 Chen, H. C.; Chen, S. H. *J. Phys. Chem.* **1984**, *88*, 5118–5121.
- 194 Macchioni, A.; Ciancaleoni, G.; Zuccaccia, C.; Zuccaccia, D. *Chem. Soc. Rev.* **2008**, *37*, 479–489.
- 195 Evans, R.; Deng, Z.; Rogerson, A. K.; McLachlan, A. S.; Richards, J. J.; Nilsson, M.; Morris, G. A. *Angew. Chem. Int. Ed.* **2013**, *52*, 3199–3202.
- 196 Neufeld, R.; Stalke, D. *Chem. Sci.* **2015**, *6*, 3354–3364.
- 197 Li, D.; Keresztes, I.; Hopson, R.; Williard, P. G. *Acc. Chem. Res.* **2009**, *42*, 270–280.
- 198 Subramanian, H.; Jasperse, C. P.; Sibi, M. P. *Org. Lett.* **2015**, *17*, 1429–1432.
- 199 Qiao, Y.; Ge, W.; Jia, L.; Hou, X.; Wang, Y.; Pedersen, C. M. *Chem. Commun.* **2016**, *52*, 11418–11421.
- 200 Maier, A. F. G.; Tussing, S.; Schneider, T.; Flörke, U.; Qu, Z.-W.; Grimme, S.; Paradies, J. *Angew. Chem. Int. Ed.* **2016**, *55*, 12219–12223.
- 201 Custelcean, R.; Jackson, J. E. *Chem. Rev.* **2001**, *101*, 1963–1980.
- 202 Heiden, Z. M.; Lathem, A. P. *Organometallics* **2015**, *34*, 1818–1827.
- 203 Breslow, R. *J. Am. Chem. Soc.* **1957**, *79*, 1762–1763.

- 204 Breslow, R. *J. Am. Chem. Soc.* **1958**, *80*, 3719–3726.
- 205 Grossmann, A.; Enders, D. *Angew. Chem. Int. Ed.* **2012**, *51*, 314–325.
- 206 Enders, D.; Niemeier, O.; Henseler, A. *Chem. Rev.* **2007**, *107*, 5606–5655.
- 207 Bugaut, X.; Glorius, F. *Chem. Soc. Rev.* **2012**, *41*, 3511–3522.
- 208 Berkessel, A.; Elfert, S.; Yatham, V. R.; Neudörfl, J.-M.; Schlörer, N. E.; Teles, J. H. *Angew. Chem. Int. Ed.* **2012**, *51*, 12370–12374.
- 209 Berkessel, A.; Yatham, V. R.; Elfert, S.; Neudörfl, J.-M. *Angew. Chem. Int. Ed.* **2013**, *52*, 11158–11162.
- 210 Lambert, J. B. *Science* **2008**, *322*, 1333–1334.
- 211 Rupar, P. A.; Staroverov, V. N.; Baines, K. M. *Science* **2008**, *322*, 1360–1363.
- 212 Krossing, I.; Raabe, I. *Angew. Chem. Int. Ed.* **2004**, *43*, 2066–2090.
- 213 Rupar, P. A.; Jennings, M. C.; Baines, K. M. *Organometallics* **2008**, *27*, 5043–5051.
- 214 Baines, K. M.; Stibbs, W. G. *Coord. Chem. Rev.* **1995**, *145*, 157–200.
- 215 Stender, M.; Phillips, A. D.; Power, P. P. *Inorg. Chem.* **2001**, *40*, 5314–5315.
- 216 Rasika Dias, H. V.; Wang, Z. *J. Am. Chem. Soc.* **1997**, *119*, 4650–4655.
- 217 Kawamichi, T.; Haneda, T.; Kawano, M.; Fujita, M. *Nature* **2009**, *461*, 633–635.
- 218 Heine, A.; DeSantis, G.; Luz, J. G.; Mitchell, M.; Wong, C.-H.; Wilson, I. A. *Science* **2001**, *294*, 369–374.
- 219 Cohen, S. M. *Nature* **2009**, *461*, 602–603.
- 220 Kawano, M.; Kawamichi, T.; Haneda, T.; Kojima, T.; Fujita, M. *J. Am. Chem. Soc.* **2007**, *129*, 15418–15419.
- 221 Agilent Technologies, Oxford, UK 2012.
- 222 Bruker Inc., Madison, Wisconsin, USA 2008.
- 223 Bruker Inc., Madison, Wisconsin, USA 2009.
- 224 Sheldrick, G. M. *Acta Cryst. A* **2008**, *64*, 112–122.
- 225 Palatinus, L.; Chapuis, G. *J. Appl. Crystallogr.* **2007**, *40*, 786–790.
- 226 Palatinus, L.; Prathapa, S. J.; van Smaalen, S. *J. Appl. Crystallogr.* **2012**, *45*, 575–580.
- 227 Macrae, C. F.; Edgington, P. R.; McCabe, P.; Pidcock, E.; Shields, G. P.; Taylor, R.; Towler, M.; van de Streek, J. *J. Appl. Crystallogr.* **2006**, *39*, 453–457.
- 228 Stoll, S.; Schweiger, A. *J. Magn. Reson.* **2006**, *178*, 42–55.
- 229 Frisch, M. J.; Trucks, G. W.; Schlegel, H. B.; Scuseria, G. E.; Robb, M. A.; Cheeseman, J. R.; Scalmani, G.; Barone, V.; Mennucci, B.; Petersson, G. A.; Nakatsuji, H.; Caricato, M.; Li, X.; Hratchian, H. P.; Izmaylov, A. F.; Bloino, J.; Zheng, G.; Sonnenberg, J. L.; Hada, M.; Ehara, M.; Toyota, K.; Fukuda, R.; Hasegawa, J.; Ishida, M.; Nakajima, T.; Honda, Y.; Kitao, O.; Nakai, H.; Vreven, T.; Montgomery Jr., J. A.; Peralta, J. E.; Ogliaro, F.; Bearpark, M.; Heyd, J. J.; Brothers, E.; Kudin, K. N.; Staroverov, V. N.; Kobayashi, R.; Normand, J.; Raghavachari, K.; Rendell, A.; Burant, J. C.; Iyengar, S. S.; Tomasi, J.; Cossi, M.; Rega, N.; Millam, J. M.; Klene, M.; Knox, J. E.; Cross, J. B.; Bakken, V.; Adamo, C.; Jaramillo, J.; Gomperts, R.; Stratmann, R. E.; Yazyev, O.; Austin, A. J.; Cammi, R.; Pomelli, C.;

- Ochterski, J. W.; Martin, R. L.; Morokuma, K.; Zakrzewski, V. G.; Voth, G. A.; Salvador, P.; Dannenberg, J. J.; Dapprich, S.; Daniels, A. D.; Farkas, Ö.; Foresman, J. B.; Ortiz, J. V.; Cioslowski, J.; Fox, D. J.; Gaussian, Inc., Wallingford CT, 2009.
- 230 Perdew, J. P.; Burke, K.; Ernzerhof, M. *Phys. Rev. Lett.* **1996**, *77*, 3865–3868.
- 231 Perdew, J. P.; Ernzerhof, M.; Burke, K. *J. Chem. Phys.* **1996**, *105*, 9982–9985.
- 232 Perdew, J. P.; Burke, K.; Ernzerhof, M. *Phys. Rev. Lett.* **1997**, *78*, 1396–1396.
- 233 Adamo, C.; Barone, V. *J. Chem. Phys.* **1999**, *110*, 6158–6170.
- 234 Schäfer, A.; Horn, H.; Ahlrichs, R. *J. Chem. Phys.* **1992**, *97*, 2571–2577.
- 235 Schäfer, A.; Huber, C.; Ahlrichs, R. *J. Chem. Phys.* **1994**, *100*, 5829–5835.
- 236 Weigend, F.; Ahlrichs, R. *Phys. Chem. Chem. Phys.* **2005**, *7*, 3297–3305.
- 237 Weigend, F. *Phys. Chem. Chem. Phys.* **2006**, *8*, 1057–1065.
- 238 Grimme, S.; Antony, J.; Ehrlich, S.; Krieg, H. *J. Chem. Phys.* **2010**, *132*, 154104–154119.
- 239 Kaim, W.; Schwederski, B. *Coord. Chem. Rev.* **2010**, *254*, 1580–1588.
- 240 Kaim, W. *Eur. J. Inorg. Chem.* **2012**, *2012*, 343–348.
- 241 Butschke, B.; Fillman, K. L.; Bendikov, T.; Shimon, L. J. W.; Diskin-Posner, Y.; Leitus, G.; Gorelsky, S. I.; Neidig, M. L.; Milstein, D. *Inorg. Chem.* **2015**, *54*, 4909–4926.
- 242 Brown, S. N. *Inorg. Chem.* **2012**, *51*, 1251–1260.
- 243 Mansell, S. M.; Adams, C. J.; Bramham, G.; Haddow, M. F.; Kaim, W.; Norman, N. C.; McGrady, J. E.; Russell, C. A.; Udeen, S. J. *Chem. Commun.* **2010**, *46*, 5070–5072.
- 244 Scarborough, C. C.; Wieghardt, K. *Inorg. Chem.* **2011**, *50*, 9773–9793.
- 245 Reagen, W. K.; Radonovich, L. J. *J. Am. Chem. Soc.* **1989**, *111*, 3881–3886.
- 246 Bernthsen, A. *Berichte der Dtsch. Chem. Gesellschaft* **1883**, *16*, 2896–2904.
- 247 Truce, W. E.; Kreider, E. M.; Brand, W. W. *Org. React.* **1970**, *18*, 99–215.
- 248 Dance, I. *New J. Chem.* **2003**, *27*, 22–27.
- 249 Bondi, A. *J. Phys. Chem.* **1964**, *68*, 441–451.
- 250 Wurche, F.; Sicking, W.; Sustmann, R.; Klärner, F.-G.; Rüdhardt, C. *Chem. Eur. J.* **2004**, *10*, 2707–2721.
- 251 Baik, M.-H.; Friesner, R. A. *J. Phys. Chem. A* **2002**, *106*, 7407–7412.
- 252 Leppin, J.; Schubert, M.; Waldvogel, S. R.; Heinze, K. *Chem. Eur. J.* **2015**, *21*, 4229–4232.
- 253 Parks, D. J.; Piers, W. E. *J. Am. Chem. Soc.* **1996**, *118*, 9440–9441.
- 254 Blackwell, J. M.; Sonmor, E. R.; Scoccitti, T.; Piers, W. E. *Org. Lett.* **2000**, *2*, 3921–3923.
- 255 Parks, D. J.; Blackwell, J. M.; Piers, W. E. *J. Org. Chem.* **2000**, *65*, 3090–3098.
- 256 Grimme, S.; Kruse, H.; Goerigk, L.; Erker, G. *Angew. Chem. Int. Ed.* **2010**, *49*, 1402–1405.
- 257 Rokob, T. A.; Bakó, I.; Stirling, A.; Hamza, A.; Pápai, I. *J. Am. Chem. Soc.* **2013**, *135*, 4425–4437.
- 258 Parks, D. J.; von H. Spence, R. E.; Piers, W. E. *Angew. Chem. Int. Ed.* **1995**, *34*, 809–811.
- 259 Fan, C.; Piers, W. E.; Parvez, M. *Angew. Chem. Int. Ed.* **2009**, *48*, 2955–2958.

- 260 Houghton, A. Y.; Karttunen, V. A.; Piers, W. E.; Tuononen, H. M. *Chem. Commun.* **2014**, 50, 1295–1298.
- 261 Ackermann, S. L.; Wolstenholme, D. J.; Frazee, C.; Deslongchamps, G.; Riley, S. H. M.; Decken, A.; McGrady, G. S. *Angew. Chem. Int. Ed.* **2015**, 54, 164–168.
- 262 Murphy, L. J.; Robertson, K. N.; Harroun, S. G.; Brosseau, C. L.; Werner-Zwanziger, U.; Moilanen, J.; Tuononen, H. M.; Clyburne, J. A. C. *Science* **2014**, 344, 75–78.
- 263 Dalapati, S.; Jana, S.; Saha, R.; Alam, M. A.; Guchhait, N. *Org. Lett.* **2012**, 14, 3244–3247.

ORIGINAL PAPERS

I

SYNTHESIS AND CHARACTERISATION OF P-BLOCK COMPLEXES OF BIQUINOLINE AT DIFFERENT LIGAND CHARGE STATES

Reproduced with kind permission by
Juha Hurmalainen, Akseli Mansikkamäki, Ian S. Morgan, Anssi Peuronen and
Heikki M. Tuononen.

Dalton Transactions **2017**, 46, 1377-1381.
Copyright © 2017 The Royal Society of Chemistry



Cite this: *Dalton Trans.*, 2017, **46**, 1377

Received 28th November 2016,
Accepted 6th January 2017

DOI: 10.1039/c6dt04504a

rsc.li/dalton

Synthesis and characterisation of p-block complexes of biquinoline at different ligand charge states†

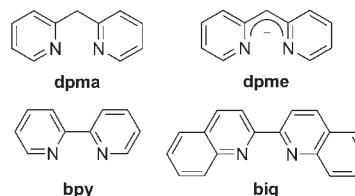
Juha Hurmalainen, Akseli Mansikkamäki, Ian S. Morgan, Anssi Peuronen and Heikki M. Tuononen*

The first examples of p-block coordination complexes of biquinoline, namely [(biq)BCl₂]Cl and [(biq)BCl₂]^{•-}, were synthesized and structurally characterized. The acquired data allowed the estimation of the ligand charge state based on its metrical parameters. The subsequent use of this protocol, augmented with theoretical calculations, revealed ambiguities in the published data for transition metal complexes of biquinoline.

Coordination compounds of redox-active, that is, (redox) non-innocent ligands¹ have received increasing attention in the past decades due to their potential application in many areas such as bond activation and catalysis,² and their importance in bioinorganic chemistry and enzymatic transformations in particular.³ Whilst various classes of redox-active ligands have already been identified and developed, any ligand can, in principle, display non-innocent behaviour under the right conditions.⁴ However, correctly identifying the charge on the ligand can sometimes be problematic.⁵ In a typical scenario, an addition or a removal of an electron causes changes in intraligand bond lengths that can be detected by high-resolution X-ray structure analysis.⁶ In some cases, crystallography needs to be augmented with other techniques such as voltammetry, spectroscopy, magnetic measurements, and theoretical calculations to unambiguously determine the ligand charge.

In our previous contribution, we examined the coordination chemistry of 2,2'-dipyridylmethane (dpma) and the possibility of it to display non-innocent behaviour akin to that known for 2,2'-bipyridine (bpy), an omnipresent redox-active bidentate ligand.⁷ The results revealed that, due to its methylene bridge, dpma is not only an inferior electron acceptor but also more reactive than bpy. We have already shown that both of these

problems can be alleviated by deprotonating dpma to 2,2'-dipyridylmethene (dpme).⁸ In a similar fashion, the redox properties of bpy can be affected *via* structural modifications that alter its HOMO–LUMO gap, the simplest being the extension of the conjugated ring system. In this context, it is interesting that, to the best of our knowledge, (biq)Ti(Cp)₂ (Cp = cyclopentadienyl) is the only structurally characterized coordination compound of 2,2'-biquinoline (biq) that supposedly contains the ligand as a radical anion.⁹ However, the complex was originally described as a Ti(II) species, not Ti(III). Even though the electronic structure of (biq)Ti(Cp)₂ has recently been examined theoretically,¹⁰ there is a clear need for structural data on coordination compounds of 2,2'-biquinoline (biq) in which the ligand charge can be unequivocally determined.

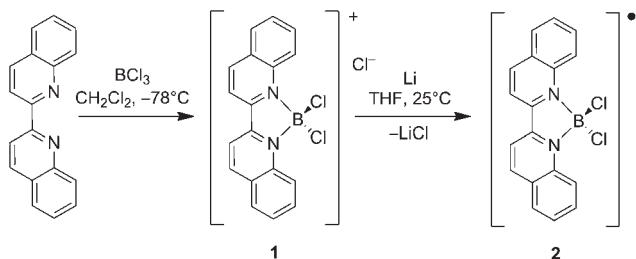


Herein, we report the synthesis and characterization of the salt [(biq)BCl₂]Cl (**1**) and the one-electron reduction of its cation to give the paramagnetic complex [(biq)BCl₂]^{•-} (**2**). The coordination of biq to boron completely eliminates the possibility for back-bonding and confines all redox processes to the ligand framework, allowing an unambiguous structural characterization of a coordinated anionic biq radical. The acquired results lend further credence to the idea that redox non-innocence is a more common phenomenon in the chemistry of biq than heretofore recognized. A notion we emphasize by theory-aided reinterpretation of the electronic structure of the complex Co(biq)₂.

A stoichiometric 1 : 1 reaction between BCl₃ and biq was carried out in CH₂Cl₂ at –78 °C, resulting in slow formation of a yellow precipitate (Scheme 1). The reaction mixture was allowed to warm to room temperature and, after an appropriate reaction time, the product was separated from the solution and dried under reduced pressure to afford **1** as a yellow solid in fully

University of Jyväskylä, Department of Chemistry, Nanoscience Centre, P.O. Box 35, FI-40014, University of Jyväskylä, Finland. E-mail: heikki.m.tuononen@jyu.fi; Tel: +358-40-805-3713

† Electronic supplementary information (ESI) available: Complete experimental details for the synthesis and characterization of **1** and **2**, and a full account of the conducted theoretical calculations. CCDC 1518783 and 1518784 for **1** and **2**, respectively. For ESI and crystallographic data in CIF or other electronic format see DOI: 10.1039/c6dt04504a



Scheme 1 Synthesis of the salt **1** and its reduction to the neutral radical **2**.

quantitative yield. The purity of **1** was confirmed by multi-nuclear NMR spectroscopy and elemental analysis (see ESI†). Once precipitated, **1** has very different solubility properties and it only sparingly redissolves in coordinating solvents such as THF and CH_3CN . Thus, light yellow single crystals of **1** could be grown from a saturated CH_3CN solution kept at -20°C for a few days.

The crystal structure of **1** shows the presence of discrete $[(\text{biq})\text{BCl}_2]^+$ cations and Cl^- anions. The BCl_2 moiety is symmetrically chelated by the biq ligand, resulting in a tetrahedral geometry around the boron centre (Fig. 1). The structure of the cation is close to, but not quite, C_{2v} symmetry with the backbone of the biq ligand slightly twisted away from planarity. The packing of **1** in the solid state is largely dictated by ion...dipole interactions between the Cl^- anions and the C–H bonds in the biq ligand that collectively organize the

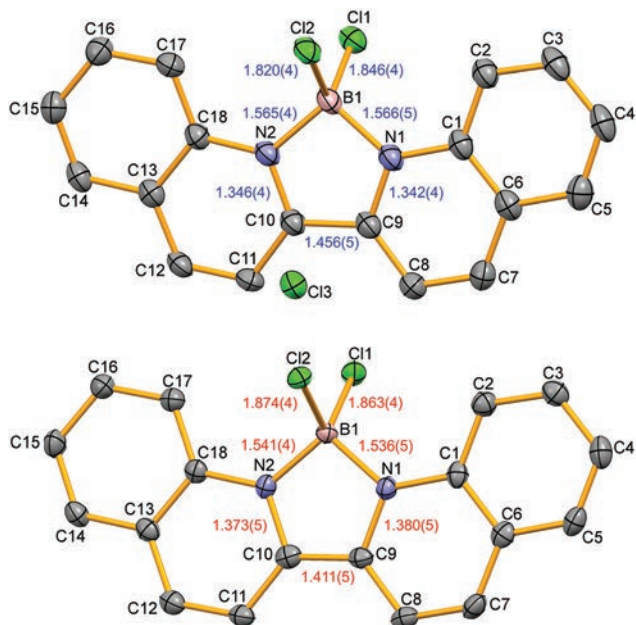


Fig. 1 Thermal ellipsoid plots (50% probability, hydrogen atoms omitted for clarity) of **1** (top) and **2** (bottom). Selected bond lengths (Å) are shown in the figure. Selected bond angles ($^\circ$): (1) N1–B1–N2 98.7(3), B1–N1–C9 110.9(3), N1–C9–C10 109.6(3), B1–N2–C10 110.3(3), N2–C10–C9 110.4(3), Cl1–B1–Cl2 112.8(2); (2) N1–B1–N2 99.9(3), B1–N1–C9 109.9(3), N1–C9–C10 110.0(3), B1–N2–C10 110.0(3), N2–C10–C9 110.1(3), Cl1–B1–Cl2 109.9(2).

$[(\text{biq})\text{BCl}_2]^+$ cations to layers along the crystallographic b -axis (see ESI†). The layer-like packing of **1** is, however, far from perfect as the arrangement of the cations in the solid state is also affected by B–Cl...H–C intermolecular interactions. The individual layers are also connected *via* π -stacking interactions with a stack spacing of *ca.* 3.36 Å, *i.e.* slightly less than the sum of van der Waals radii of two carbon atoms.

Even though the favourable electron accepting properties of biq have been known since the late 1980s,¹¹ the reduction of **1** was examined by cyclic voltammetry (see ESI†) to determine how the coordination of the ligand tunes its redox potential. The results showed that the $[(\text{biq})\text{BCl}_2]^+$ cation undergoes a one electron reduction at -0.82 V (*vs.* SCE) that can be compared with the reduction potential of the free biq ligand, -2.07 V (*vs.* Ag/Ag⁺).¹¹ Although weaker reducing agents would certainly have sufficed, alkali metals were chosen because the expected side products, the salts MCl (M = Li, Na), can easily be separated from the product. Thus, the reduction of **1** was performed by using metallic lithium as the reducing agent.

The reduction was carried out at 25°C by dissolving a small amount of **1** in THF, after which a stoichiometric amount of the metal was added (Scheme 1). The initially yellow-greenish solution slowly turned dark. After an appropriate reaction time, the solvent was removed under reduced pressure to afford a black solid that was redissolved in CH_2Cl_2 and filtered. Removal of the solvent *in vacuo* yielded **2** as a very dark, almost black, powder in good yield. Dark yellow single crystals of **2** were grown by redissolving the powder in CH_2Cl_2 and carefully layering *n*-hexane on top of the solution before letting it sit at -20°C for a few days. Compound **2** is extremely air sensitive and crystals of it decompose rapidly if removed from the protecting Fomblin® oil and exposed to atmospheric oxygen.

The paramagnetic nature of **2** was confirmed by dissolving a very small amount of the powdery product in CH_2Cl_2 and measuring the EPR spectrum of the resulting orange-yellow solution (Fig. 2). Once in solution, **2** is persistent for hours,

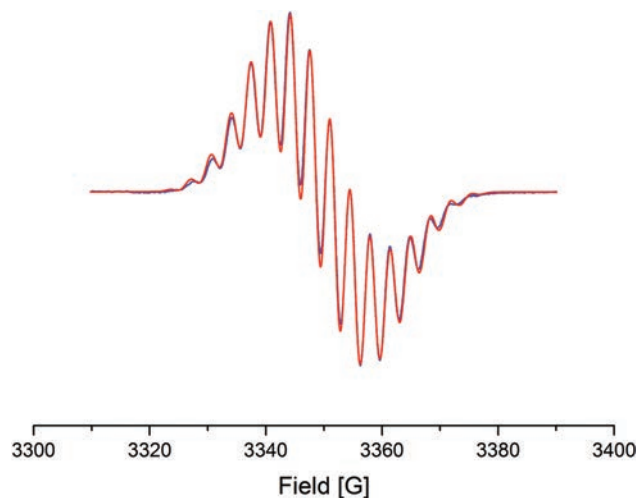


Fig. 2 Experimental (blue) and simulated (red) X-band EPR spectra of a CH_2Cl_2 solution of **2** at room temperature.

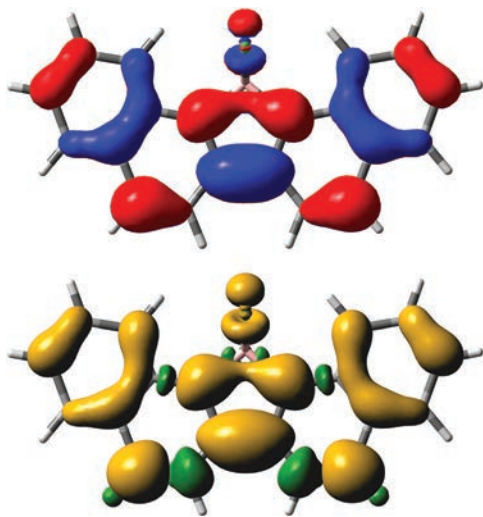


Fig. 3 Isosurface plots of the SOMO (± 0.03 , top) and spin density (± 0.0008 , bottom) of **2**.

showing no signs of decomposition under an inert atmosphere at room temperature. The EPR spectrum consists of a symmetric 60 G wide 16-line pattern at $g = 2.0006$ with no visible fine structure. Consequently, the simulation of the spectrum was performed using a fitting algorithm and calculated (PBE1PBE/TZVP) hyperfine coupling constants (hfccs) as initial estimates of the true couplings (see ESI†).

The calculations showed that the singly occupied molecular orbital (SOMO) of **2** (Fig. 3) is, as anticipated, almost exclusively confined to the ligand framework with major contributions from nitrogen and carbon along with significantly smaller contributions from the p-type orbitals on the two chlorine atoms. The calculated α -spin density of **2** mirrors the topology of the SOMO, while spin polarization effects lead to concentration of β -spin density on boron and hydrogen atoms (Fig. 3). Consequently, the calculated hfccs indicate coupling of the unpaired electron primarily to one $^{10,11}\text{B}$ and two equivalent ^{14}N and $^{35,37}\text{Cl}$ nuclei as well as to four unique pairs of ^1H centres (Table 1). The hfccs calculated for the other ^1H nuclei in **2** are significantly smaller (absolute values less than

0.50 G) and were, therefore, excluded from the simulation and treated indirectly by adjusting line shape.

Excellent simulation of the EPR spectrum of **2** (Fig. 2) was obtained by using the hfccs given in Table 1. In general, there is a good agreement between the hfccs obtained by spectral fitting and those given by theory, especially for the heavier nuclei. It needs to be emphasized that the small hfccs (less than 1.00 G) to ^1H nuclei remain ambiguous as the broad spectral line width allows for multiple equally acceptable fits to the experimental data. The smaller ^1H couplings can also be treated indirectly by increasing the line width, which shows that the other hfccs change very little from one fit to the other and collectively give rise to the dominant 16-line pattern in the experimental spectrum. Furthermore, all attempts to simulate the experimental EPR spectrum with fewer hfccs than those to one $^{10,11}\text{B}$ and two equivalent ^{14}N , $^{35,37}\text{Cl}$, and ^1H nuclei were unsuccessful. Thus, we are confident that the data corresponds to the $[(\text{biq})\text{BCl}_2]^\cdot$ radical, which indicates that the ligand has undergone a one electron reduction.

The identity of **2** was subsequently confirmed *via* full crystallographic analysis. The molecular structure of the radical has C_{2v} symmetry with a fully planar ligand backbone (Fig. 1). The crystallographic data for **2** (and $[(\text{biq})\text{BCl}_2]^\cdot$) allow for interesting relationships to be drawn between the electronic structure of the biq ligand and its metrical parameters. Specifically, the unpaired electron leads to lengthening of the N–C bonds (from 1.342(4) and 1.346(4) Å to 1.373(5) and 1.380(5) Å) and shortening of the C–C bond connecting the two quinoline units (from 1.456(5) to 1.411(5) Å), which is fully consistent with the topology of the SOMO of **2** as well as trends established for the bpy ligand at different charge states.¹⁰ In the latter context, the metrical parameters of **1** and **2** can be compared to that of the analogous bpy complexes $[(\text{bpy})\text{BCl}_2]^\cdot$ and $[(\text{bpy})\text{BCl}_2]^\cdot$,¹² which shows that the annulation of the ligand has virtually no effect on key intraligand bond lengths and changes in them upon reduction. Furthermore, while $[(\text{bpy})\text{BCl}_2]^\cdot$ has been called a persistent radical, it is in fact isolable and essentially indefinitely stable in the solid state under anaerobic conditions.¹²

The metrical parameters of **1** and **2** can be compared with crystallographic data reported for transition metal complexes of biq for any apparent ambiguities in their characterization.¹³ It has already been discussed in the literature that, according to theoretical evidence, the complex $(\text{biq})\text{Ti}(\text{Cp})_2$ contains a $\text{Ti}(\text{III})$ centre and a biq anion radical though it is not certain if the two unpaired electrons couple ferromagnetically or antiferromagnetically.¹⁰ The structural trends established herein corroborate the above interpretation and also suggest that the complex $\text{Co}(\text{biq})_2$, originally described as a $\text{Co}(0)$ species,¹⁴ should instead be viewed as a $\text{Co}(\text{II})$ complex incorporating two anionic biq radicals. The strongest structural evidence supporting this view is the length of the intraligand C–C bond that connects the two quinoline units: the two biq ligands in $\text{Co}(\text{biq})_2$ are inequivalent with short C–C distances of 1.427(6) and 1.431(5) Å. Consequently, the electronic structure of $\text{Co}(\text{biq})_2$ was subjected to a comprehensive theoretical analysis

Table 1 Experimental and calculated hyperfine coupling constants [G] of **2**^a

Nucleus	Equivalent nuclei	Exptl.	Calc.
$^{10}\text{B}/^{11}\text{B}$	1	1.13/3.37	−1.54/−4.59
^{14}N	2	2.75	2.41
$^{35}\text{Cl}/^{37}\text{Cl}$	2	3.77/3.14	2.46/2.05
^1H	2	4.00	−3.83
^1H	2	0.91	−1.04
^1H	2	0.50	1.00
^1H	2	0.44	−0.85

^a Experimental parameters were determined from a simulation optimized to match the recorded spectrum. The simulation used a Voigtian line shape with Gaussian and Lorentzian peak-to-peak line widths of 0.90 and 0.15 G, respectively.

using multireference methods (NEVPT2/SA-CASSCF(13,9)) to correctly identify the ligand charge state (see ESI†).

The theoretical results show that the ground state of $\text{Co}(\text{biq})_2$ is a spin-doublet that is separated from the first excited state by 1437 cm^{-1} . Decomposition of the ground state wave function into contributions from various electronic configurations shows that roughly 60% of them contain a high-spin $\text{Co}(\text{II})$ ion and two anionic radical ligands; the remaining 40% includes different ligand-to-metal and metal-to-ligand charge transfer configurations. Thus, rather than invoking extensive metal-to-ligand backbonding to explain the observed structural features,¹⁴ the ground state of $\text{Co}(\text{biq})_2$ should instead be viewed in terms of an antiferromagnetically coupled high-spin $\text{Co}(\text{II})$ centre and two biq radicals, stabilized by strong kinetic exchange.

There are other examples of complexes incorporating the biq ligand that potentially deserve a second look. For example, the intraligand metrical parameters in $[(\text{biq})\text{Ru}(\text{[9]aneS}_3)\text{Cl}][\text{PF}_6]$ ($[\text{9]aneS}_3 = 1,4,7\text{-trithiacyclononane}$),¹⁵ and the short C–C bond connecting the two quinoline units in particular (1.39(2) Å), hint of the possibility of an anionic radical and $\text{Ru}(\text{III})$ but this interpretation has not been discussed. Further evidence supporting the presence of an anionic biq radical is seen in the solid state packing of $[(\text{biq})\text{Ru}(\text{[9]aneS}_3)\text{Cl}][\text{PF}_6]$ in which the cations form distinctive dimers *via* π -stacking interactions between the biq ligands (shortest C...C distance *ca.* 3.31 Å). Interestingly, the same kind of packing is not observed for analogous complexes employing related polypyridine ligands,¹⁵ which suggests that the dimeric arrangement in $[(\text{biq})\text{Ru}(\text{[9]aneS}_3)\text{Cl}][\text{PF}_6]$ might result from weak antiferromagnetic interactions between two biq anion radicals. Further experimental and theoretical data are clearly needed to test the validity of this hypothesis.

We conclude our work with a discussion of the packing of 2 in the solid state. In this instance, the radicals form well-arranged layers along the crystallographic *c*-axis with the BCl_2 moieties facing in alternate directions in neighbouring layers (see ESI†). The packing is again dictated by B–Cl...H–C hydrogen bonding along with π -stacking interactions that connect the individual layers. Interestingly, the layers in 2 are essentially uniformly spaced (stack spacing *ca.* 3.40 Å), which is surprising considering that planar organic radicals typically interact antiferromagnetically to form π -dimers,¹⁶ generally leading to something else than even spaced stacking in the solid state. A classic example is the solid state structure of the 2,5,8-tri-*tert*-butylphenalenyl radical in which the radicals form π -dimers (C...C distances *ca.* 3.29 Å) that are strongly antiferromagnetically coupled.¹⁷

The even spacing of layers in the crystal structure of 2 can be explained by considering the topology of the SOMO that leads to accidental orthogonality of adjacent magnetic orbitals in the observed structure (see ESI†). Consequently, radical...radical dimerization is not energetically preferred and the molecules of 2 remain essentially isolated in the solid state. This interpretation is supported by theoretical calculations (PBE1PBE/TZVP) that show the singlet and triplet

states of a pair of adjacent radicals in the crystal structure geometry of 2 to be separated by 0.5 kJ mol^{-1} .

In summary, we have synthesized two related coordination compounds of biquinoline, $[(\text{biq})\text{BCl}_2]\text{Cl}$ and $[(\text{biq})\text{BCl}_2]^+$, in which the ligand adopts different charge states. The compounds are the first structurally characterized p-block complexes of biquinoline and, by confining all redox processes to the ligand framework, allow the structural consequences of ligand reduction to be unambiguously determined. The acquired data were subsequently used to establish a reinterpretation of the electronic structure of $\text{Co}(\text{biq})_2$ which was shown to contain the metal in the +II (not 0) oxidation state by help of theoretical calculations. The estimation of ligand charge state by means of its metrical parameters is already a well-established practice for metal complexes of bipyridine and, with the data reported herein, this practice can, and in fact should, be extended to complexes incorporating the redox non-innocent biquinoline ligand.

Financial support from the University of Jyväskylä, the Academy of Finland (project numbers 136929, 253907, and 272900), the Technology Industries of Finland Centennial Foundation, and the Foundation for Research of Natural Resources in Finland is gratefully acknowledged. We thank Laboratory Technician Elina Hautakangas (University of Jyväskylä) and Dr Robert W. Reed (University of Guelph) for elemental analyses and cyclic voltammetry, respectively.

Notes and references

- (a) P. J. Chirik and K. Wieghardt, *Science*, 2010, **327**, 794; (b) C. K. Jørgensen, *Coord. Chem. Rev.*, 1966, **1**, 164.
- For some recent examples, see: (a) A. R. Corcos, O. Villanueva, R. C. Walroth, S. K. Sharma, J. Bacsá, K. M. Lancaster, C. E. MacBeth and J. F. Berry, *J. Am. Chem. Soc.*, 2016, **138**, 1796; (b) D. L. J. Broere, L. L. Metz, B. de Bruin, J. N. H. Reek, M. A. Siegler and J. I. van der Vlugt, *Angew. Chem., Int. Ed.*, 2015, **54**, 1516; (c) L. A. Berben, *Chem. – Eur. J.*, 2014, **21**, 2734; (d) T. W. Myers and L. A. Berben, *J. Am. Chem. Soc.*, 2013, **135**, 9988; (e) V. K. K. Praneeth, M. R. Ringenberg and T. R. Ward, *Angew. Chem., Int. Ed.*, 2012, **51**, 10228.
- W. Kaim and B. Schwederski, *Coord. Chem. Rev.*, 2010, **254**, 1580.
- W. Kaim, *Eur. J. Inorg. Chem.*, 2012, 343.
- B. Butschke, K. L. Fillman, T. Bendikov, L. J. W. Shimon, Y. Diskin-Posner, G. Leitus, S. I. Gorelsky, M. L. Neidig and D. Milstein, *Inorg. Chem.*, 2015, **54**, 4909.
- S. N. Brown, *Inorg. Chem.*, 2012, **51**, 1251.
- P. Vasko, V. Kinnunen, J. Moilanen, T. R. Roemmele, R. T. Boeré, J. Konu and H. M. Tuononen, *Dalton Trans.*, 2015, **44**, 18247.
- J. Moilanen, J. Borau-Garcia, R. Roesler and H. M. Tuononen, *Chem. Commun.*, 2012, **48**, 8949.
- (a) I. M. Piglosiewicz, R. Beckhaus, G. Wittstock, W. Saak and D. Haase, *Inorg. Chem.*, 2007, **46**, 7610; (b) I. M. Piglosiewicz,

- R. Beckhaus, W. Saak and D. Haase, *J. Am. Chem. Soc.*, 2005, **127**, 1419.
- 10 C. C. Scarborough and K. Wieghardt, *Inorg. Chem.*, 2011, **50**, 9773.
- 11 R. Abdel-Hamid, *Bull. Soc. Chim. Fr.*, 1986, 733.
- 12 S. M. Mansell, C. J. Adams, G. Bramham, M. F. Haddow, W. Kaim, N. C. Norman, J. E. McGrady, C. A. Russell and S. J. Udeen, *Chem. Commun.*, 2010, **46**, 5070.
- 13 The Cambridge Structural Database: C. R. Groom, I. J. Bruno, M. P. Lightfoot and S. C. Ward, *Acta Crystallogr., Sect. B: Struct. Sci.*, 2016, **72**, 171.
- 14 W. K. Reagen and L. J. Radonovich, *J. Am. Chem. Soc.*, 1989, **111**, 3881.
- 15 J. Madureira, T. M. Santos, B. J. Goodfellow, M. Lucena, J. P. de Jesus, M. G. Santana-Marques, M. G. B. Drew and V. Félix, *J. Chem. Soc., Dalton Trans.*, 2000, 4422.
- 16 *Stable Radicals: Fundamentals and Applied Aspects of Odd-Electron Compounds*, ed. R. G. Hicks, John Wiley & Sons Ltd, New York, 2010.
- 17 (a) K. Goto, T. Kubo, K. Yamamoto, K. Nakasuji, K. Sato, D. Shiomi, T. Takui, M. Kubota, T. Kobayashi, K. Yakusi and J. Ouyang, *J. Am. Chem. Soc.*, 1999, **121**, 161; (b) Y. Takano, T. Taniguchi, H. Isobe, T. Kubo, Y. Morita, K. Yamamoto, K. Nakasuji, T. Takui and K. Yamaguchi, *J. Am. Chem. Soc.*, 2002, **124**, 11122.

II

SYNTHESIS OF NEW HYBRID 1,4-THIAZINYL-1,2,3-DITHIAZOLYL RADICALS VIA SMILES REARRANGEMENT

Reproduced with kind permission by Petra Vasko, Juha Hurmalainen, Akseli
Mansikkamäki, Anssi Peuronen, Aaron Mailman and Heikki M. Tuononen.

Dalton Transactions **2017**, *in press*, DOI: 10.1039/c7dt03243a

Copyright © 2017 The Royal Society of Chemistry

COMMUNICATION

Synthesis of new hybrid 1,4-thiazinyl-1,2,3-dithiazolyl radicals *via* Smiles rearrangement†

Cite this: DOI: 10.1039/c7dt03243a

Received 1st September 2017,
Accepted 4th October 2017

DOI: 10.1039/c7dt03243a

rsc.li/dalton

Petra Vasko,  Juha Hurmalainen, Akseli Mansikkamäki, Anssi Peuronen,
Aaron Mailman* and Heikki M. Tuononen *

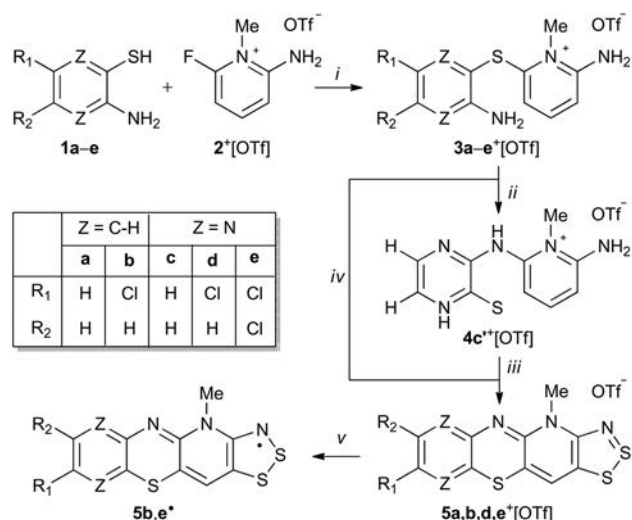
The condensation reaction of 2-aminobenzenethiols and 3-amino-pyrazinethiols with 2-amino-6-fluoro-*N*-methylpyridinium triflate afforded thioether derivatives that were found to undergo Smiles rearrangement and cyclocondensation with sulphur monochloride to yield new hybrid 1,4-thiazine-1,2,3-dithiazolium cations. The synthesized cations were readily reduced to the corresponding stable neutral radicals with spin densities delocalized over both 1,4-thiazinyl and 1,2,3-dithiazolyl moieties.

The heterocyclic benzo-1,4-thiazine, or simply phenothiazine, was first synthesized more than a century ago.¹ Over the years, phenothiazine and its numerous derivatives have been broadly examined, largely due to their biological activity and use as antipsychotic drugs.² The widespread interest in the medicinal chemistry of phenothiazine has also spurred the development of a variety of synthetic protocols for the preparation of new compounds. Of topical interest is the Smiles rearrangement,³ an intramolecular nucleophilic *ipso*-substitution reaction, which has found extensive use in the preparation of a number of phenothiazine-based heterocycles.⁴

The application potential of phenothiazines extends beyond pharmaceuticals and they can also be used as building blocks for functional materials. This stems from the ability of phenothiazine and its derivatives to undergo facile one-electron oxidation to persistent radical cations,⁵ which have been characterized by both EPR spectroscopy and X-ray crystallography.^{6,7} In recent years, the materials-oriented research has shifted the synthetic focus towards linked and fused oligomers of phenothiazine as well as phenothiazine-based polymers because of their applicability as switchable molecules, photosensitizers, cathode-active materials, and organic open-shell polymers to name a few.⁸

Regardless of the wealth of data on cation radicals of phenothiazine, little is known about neutral phenothiazinyls even though these radicals were reported in the early 1960s.⁹ The majority of data on phenothiazinyl radicals are limited to spectroscopic studies and, to the best of our knowledge, there are no reports of X-ray crystallographic investigations. This is surprising considering that the related heterocyclic 1,2-thiazinyl radicals have been thoroughly characterized despite their persistent nature.¹⁰ Consequently, in an effort to extend the chemistry of neutral phenothiazinyl derivatives, we report the use of the Smiles rearrangement reaction to prepare new stable radicals 5* that fuse the 1,4-thiazinyl and 1,2,3-dithiazolyl moieties into a single framework (Scheme 1).

The molecular scaffold in radicals 5* was chosen because of the wide range of physical and chemical properties of thiazyl-based radicals that make them useful building blocks for



Scheme 1 Synthesis of neutral radicals 5*. Reagents and general conditions: (i) Na₂CO₃, MeCN, 5 h; (ii) MeCN, sealed vessel, 110 °C; (iii) excess S₂Cl₂, MeCN, reflux, 16 h; (iv) excess S₂Cl₂, MeCN, reflux, 16 h; (v) excess Me₃Fc, MeCN. Highest yields obtained: 4c**[OTf] 79%, 5a*[OTf] 2%, 5b*[OTf] 43%, 5d*[OTf] 48%, 5e*[OTf] 78%, 5b· 81%, and 5e· 70%.

Department of Chemistry, Nanoscience Centre, University of Jyväskylä, P.O. Box 35,
FI-40014, Finland. E-mail: aaron.m.mailman@jyu.fi, heikki.m.tuononen@jyu.fi

† Electronic supplementary information (ESI) available: Full details of synthetic, spectroscopic, computational, and crystallographic work. CCDC 1519804–1519808, 1536800 and 1536801. For ESI and crystallographic data in CIF or other electronic format see DOI: 10.1039/c7dt03243a

molecular materials, both as free species and as coordinating ligands.¹¹ While the first examples of closely related hybrid 1,2,3-dithiazolo-1,2,4-thiadiazinyl radicals have only been reported in the last few years,¹² *N*-alkylpyridinium bridged bis-1,2,3-dithiazolyls and their selenium variants, with mirror plane symmetry, have been extensively explored.^{11b,13} Many of these radicals were initially pursued as possible single component molecular conductors. However, their diverse magnetic properties, including ferromagnetic ordering, are notable compared to related classes of light atom molecular radicals such as nitroxides, triazinyls, and verdazyls.^{11b} Thus, the pursuit of new molecular thiazyl radicals continues to attract considerable attention, which has now lead us to explore new extend aromatic systems based on the synthetically useful *N*-alkylpyridinium template.

The condensation reaction of 2-aminobenzenethiols (**1a,b**) and 3-aminopyrazinethiols (**1c,d,e**) with 2-amino-6-fluoro-*N*-methylpyridinium triflate ($2^+[\text{OTf}]$)¹² in the presence of excess anhydrous Na_2CO_3 in acetonitrile (MeCN) afforded *N*-methylpyridinium thioether salts **3a-e**⁺[OTf] (Scheme 1, step i).

Recrystallization of $3^+[\text{OTf}]$ from appropriate solvents gave analytically pure crystalline solids, which were characterized by IR and NMR (^1H , ^{13}C) spectroscopy as well as by single crystal X-ray diffraction analysis (for **3c**⁺[OTf], Fig. 1a).

It was anticipated that the salts $3^+[\text{OTf}]$ would undergo *S* → *N* Smiles rearrangement (SR) reaction by intramolecular nucleophilic *ipso*-substitution at the thioether bond of the *N*-methylpyridinium, affording *N*-substituted derivatives **4**⁺[OTf] (Scheme 1, step ii). After screening different reaction conditions on NMR scale, an essentially quantitative reaction was realised for **3c**⁺[OTf] but only after heating for 8 days at 80 °C. The purported SR reaction was performed on preparative scale in a sealed pressure vessel at 110 °C in MeCN, which gave an isolated product in high yield (80%) only after 40 h.

Single crystal X-ray diffraction analysis confirmed the heavy atom (non-hydrogen) connectivity of **4c**⁺[OTf], but instead of the expected thiol, the product was found to be the tautomeric pyrazinethione derivative **4c**⁺[OTf] (Fig. 1b). The ^1H -NMR

spectrum of the product (in anhydrous CD_3CN) revealed that the signals for the pyridinium $-\text{NH}_2$ and pyrazine C–H protons are distinctively downfield shifted compared to **3c**⁺[OTf] and the appearance of a broad singlet at δ 9.60 ppm is tentatively assigned to the pyrazino $-\text{NH}$ proton (N3 in Fig. 1b). It is notable that the ^1H -NMR spectrum of **4c**⁺[OTf] does not show an observable signal for the bridging $-\text{NH}$ group (N5 in Fig. 1b).

The lack of similar reactivity for the other thioether salts **3**⁺[OTf] even under more forceful conditions led us to perform a density functional study of the reaction mechanism at the PBE1PBE-IEFPCM/def2-TZVP level of theory. The results of computational investigations are summarized in Fig. 2 for two representative systems, **3a**⁺ and **3c**⁺.

It is evident from the computed data (Fig. 2) that the initial reaction pathway is similar for both **3a**⁺ and **3c**⁺. It was assumed that the SR reaction begins with an intramolecular nucleophilic attack of the benzo/pyrazine $-\text{NH}_2$ group to form a cationic Meisenheimer complex **Int1**.³ This step has a very high activation barrier, **TS1**, in agreement with experimental observations. Furthermore, the formation of **4a**⁺ and **4c**⁺ is in both cases an essentially energy neutral process. However, what drives the SR reaction forward in the case of **3c**⁺ is the possibility for **4c**⁺ to tautomerize to the experimentally characterized form **4c**⁺, which renders the overall reaction exergonic by 43 kJ mol^{-1} . In this respect, it is surprising that no SR reaction was realized for **3d**⁺ and **3e**⁺ even though these derivatives are also able to tautomerize to the corresponding pyrazinethiones. A computational analysis of their reaction pathways showed that the formation of both **4d**⁺ and **4e**⁺ is exergonic, though only by 20 and 11 kJ mol^{-1} , respectively. Hence, the SR

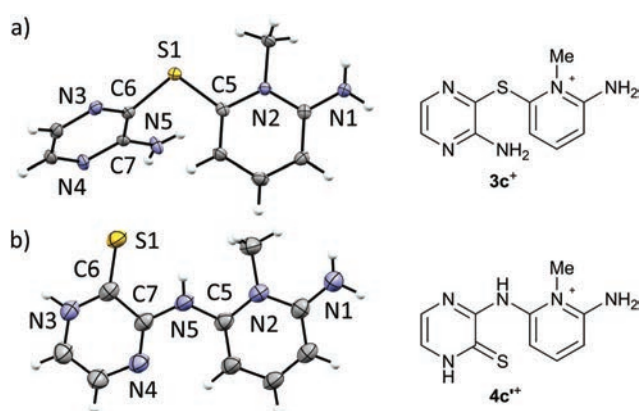


Fig. 1 ORTEP plots (left, thermal ellipsoids at 50% probability) and line drawings (right) of the cations in (a) **3c**⁺[OTf]·MeCN and (b) **4c**⁺[OTf].

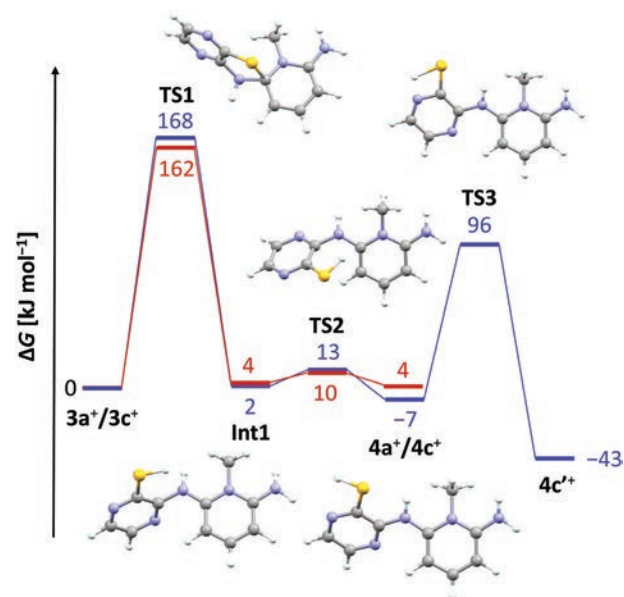


Fig. 2 Reaction coordinate diagram (PBE1PBE-IEFPCM/def2-TZVP) for the Smiles rearrangement reaction of **3a**⁺ (red) and **3c**⁺ (blue). For clarity, the structures of intermediates and transition states are only shown for the pathway from **3c**⁺ to **4c**⁺.

reaction becomes less-favoured for each chlorine substituent added, making $4c^{+}$ the most favourable product of the different derivatives **a–e** considered. Consequently, $4c^{+}$ is the only species able to form at experimental reaction conditions.

Having confirmed the identity of $4c^{+}$ [OTf], its cyclocondensation with excess S_2Cl_2 was performed by refluxing the reactants in MeCN for 16 h (Scheme 1, step iii). Low-resolution positive ion electrospray ionization mass spectrometry (+ESI-MS) showed that the main products from the reaction were the salt $5c^{+}$ [OTf] and the doubly chlorinated analogue $5e^{+}$ [OTf]. Repeated syntheses confirmed that the $5c^{+}$ [OTf]: $5e^{+}$ [OTf] ratio is variable and does not depend on the reaction conditions in any obvious manner. However, the chlorinated product $5e^{+}$ [OTf] could be crystallised from the reaction mixture using MeCN, affording a small amount of purple blocks. Unsatisfied with the low yield of $5e^{+}$ [OTf], we attempted the direct reaction of S_2Cl_2 with thioether $3e^{+}$ [OTf] that already contains an appropriate substitution of chlorine on the pyrazine ring to potentially afford another route to $5e^{+}$ [OTf] (Scheme 1, step iv). To our delight, $5e^{+}$ [OTf] was obtained in good isolated yield (78%) as confirmed by IR spectroscopy and +ESI-MS.

To explore the scope of this alternative pathway to 5^{+} [OTf], the reactivity of $3a^{+}$ [OTf], $3b^{+}$ [OTf], and $3d^{+}$ [OTf] with S_2Cl_2 was also investigated. In the case of $3a^{+}$ [OTf], +ESI-MS suggested that the product is a mixture of the non-chlorinated salt $5a^{+}$ [OTf] with its chlorinated analogues containing one or more chlorine atoms. Hence, $5a^{+}$ [OTf] was obtained in very low isolated yield (2%). Condensation reactions of S_2Cl_2 with aromatic amines containing an unsubstituted *para*-position (or those containing a good leaving group) are well-known to undergo simultaneous chlorination. Consequently, the reaction of S_2Cl_2 with the chlorinated species $3b^{+}$ [OTf] and $3d^{+}$ [OTf] was found to offer a practical route to derivatives $5b^{+}$ [OTf] and $5d^{+}$ [OTf] without further chlorination, albeit in moderate yield (43 and 48%, respectively). This further demonstrates that SR and cyclocondensation can take place concomitantly rather than sequentially, providing another route to different derivatives of 5^{+} [OTf].

Cyclic voltammetry performed on solutions of 5^{+} [OTf] in MeCN (with 0.1 M $n-Bu_4NPF_6$ as the supporting electrolyte) displayed a reversible +1/0 redox couple with $E_{1/2} = 0.031$ V and 0.220 V (vs. SCE) for $5b^{+}$ [OTf] and $5e^{+}$ [OTf], respectively. The cathodic shift in $E_{1/2}$ indicates that the heterocyclic aromatic substituent affects the electrochemical behaviour of the cations by altering the energy of their lowest unoccupied molecular orbital. This provides opportunities to fine-tune the electronic properties of the cations 5^{+} through careful choice of substituents. Furthermore, the $E_{1/2}$ values for $5b^{+}$ [OTf] and $5d^{+}$ [OTf] clearly demonstrate that octamethylferrocene (Me_8Fc) is a suitable reducing agent for both cations. The cyclic voltammetry measurements also revealed that the 0/–1 redox couple is irreversible for $5e^{+}$ [OTf], while $5b^{+}$ [OTf] appears to undergo significant decomposition under the same conditions. The estimated E_{cell} of $5e^{+}$ [OTf] is 0.720 V, which is smaller than those of related bisdithiazolyl radicals

($E_{cell} = 0.851$ V) but comparable to analogous bisthiaselenazolyls ($E_{cell} = 0.745$ V).¹⁴ Reduction of $5b^{+}$ [OTf] and $5e^{+}$ [OTf] was performed by slow diffusion of a degassed MeCN solution of the salt through a medium porosity sintered glass frit into a similar degassed MeCN solution of excess of Me_8Fc . This afforded the radicals $5b^{\bullet}$ and $5e^{\bullet}$ as analytically pure crystalline solids (Scheme 1, step v). In the case of $5b^{\bullet}$, crystals suitable for single crystal X-ray diffraction were obtained as small lustrous bronze blocks. The crystal structure of $5b^{\bullet}$ belongs to the centrosymmetric monoclinic space group $P2_1/c$. The asymmetric unit consists of two essentially coplanar radicals in *trans*-cofacial arrangement (Fig. 3) with the shortest intermolecular C...C interactions very close to the sum of van der Waals radii.¹⁵ This suggests that the radicals are not strongly interacting in the solid state. The radicals in the asymmetric unit of $5b^{\bullet}$ and those related to them by an inversion centre form π -stacked motifs that are arranged in a herringbone pattern similar to those typically observed for related bisdithiazolyl radicals.^{14,16}

The electronic structures of $5b^{\bullet}$ and $5e^{\bullet}$ were investigated by a combination of computational (PBE1PBE/def2-TZVP) methods and EPR spectroscopy. The calculations showed that the singly occupied molecular orbital and the spin density of 5^{\bullet} are delocalized over the molecular backbone (Fig. 4). Specifically, natural population analysis assigned 40 and 55% of the α -spin density of $5b^{\bullet}$ on the 1,4-thiazinyl and 1,2,3-dithiazolyl moieties, respectively; the spin distribution of $5e^{\bullet}$ is slightly more localised on the 1,2,3-dithiazolyl moiety. Consequently, the radicals **5** can be considered hybrids of 1,4-thiazinyls and 1,2,3-dithiazolyls, which underlines the fact that the line drawing in Scheme 1 is an oversimplified picture of their electronic structure. In this respect, population analyses of $5b^{+}$ and $5d^{+}$ showed that the sulphur atom on the 1,4-thiazine ring is the single most positively charged nucleus in the structures. However, the shortest anion...cation contacts in crystal structures of $5b^{+}$ [OTf] and $5d^{+}$ [OTf] involve the two sulphur atoms on the 1,2,3-dithiazolyl moiety.

The room-temperature EPR spectrum of $5b^{\bullet}$ in CH_2Cl_2 (Fig. 5a) consists of an eight line pattern with $g = 2.0071$ and no fine-structure. A good simulation of the spectrum was obtained by using hyperfine couplings (hfc) to the nitrogen nuclei in the dithiazolyl ($a_{N1} = 0.383$ mT) and thiazyl

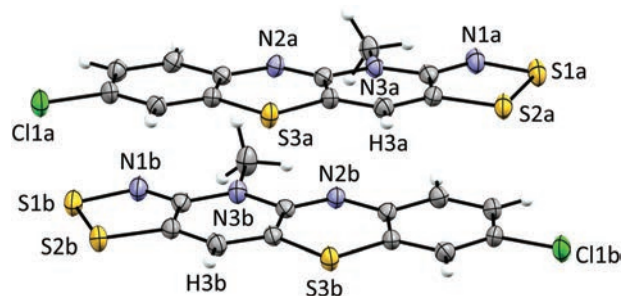


Fig. 3 ORTEP plot of the asymmetric unit of $5b^{\bullet}$ (thermal ellipsoids at 50% probability).

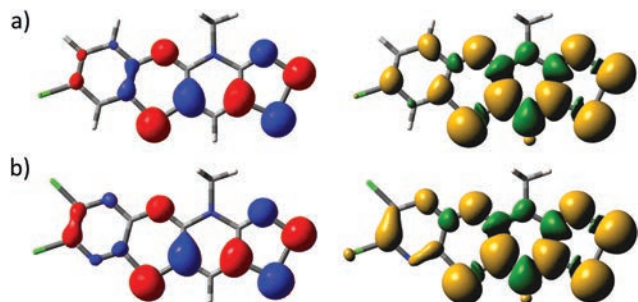


Fig. 4 Isosurface plots of the SOMOs (± 0.04 , left) and spin densities (± 0.001 , right) of (a) $5b^{\bullet}$ and (b) $5e^{\bullet}$.

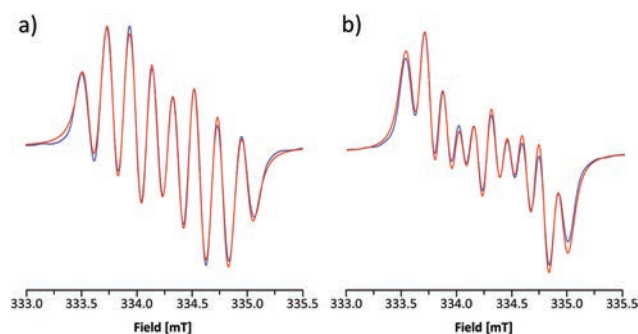


Fig. 5 Experimental (blue) and simulated (red) X-band EPR spectra of CH_2Cl_2 solutions of (a) $5b^{\bullet}$ and (b) $5e^{\bullet}$ at room temperature. The simulations used Voigtian functions with Gaussian/Lorentzian peak-to-peak line widths (mT) of 0.067/0.092 and 0.090/0.087 for $5b^{\bullet}$ and $5d^{\bullet}$, respectively.

($a_{\text{N}2} = 0.224$ mT) rings as well as to one hydrogen atom at the basal position ($a_{\text{H}3} = 0.213$ mT). The assignment of hfc's was based on a computational analysis of $5b^{\bullet}$ ($a_{\text{N}1} = 0.304$, $a_{\text{N}2} = 0.206$, and $a_{\text{H}3} = 0.375$ mT), which also suggested the presence of smaller couplings to hydrogen nuclei ($a_{\text{H}} \approx -0.070$ mT) and the nitrogen atom on the *N*-methylpyridinium ring ($a_{\text{N}3} = -0.052$ mT). However, the broad spectral line width did not allow the explicit consideration of these hfc's in simulations for which reason they were treated indirectly by adjusting the line shape. The EPR spectrum of $5e^{\bullet}$ is similar to that of $5b^{\bullet}$ with $g = 2.0059$. The spectrum consists of ten broad lines and a good simulation of it was obtained by using hfc's to the nitrogen nuclei in the dithiazolyl ($a_{\text{N}1} = 0.484$ mT) and thiazyl ($a_{\text{N}2} = 0.169$ mT) rings as well as to the hydrogen atom at the basal position ($a_{\text{H}3} = 0.197$ mT). This view is well supported by calculations ($a_{\text{N}1} = 0.356$, $a_{\text{N}2} = 0.153$, and $a_{\text{H}3} = 0.332$ mT), which also revealed minute coupling of the unpaired electron to the pyrazine nitrogen atoms.

Having shown that the SR reaction offers a viable route to 5^{\bullet} , the scope of the two established pathways was examined further. Considering the utilization of 5^{\bullet} in practical applications, the stability of the radicals is of particular importance. In this context, delocalization of the spin density on the 1,4-thiazinyl moiety is desired. Thus, we chose the quinoxaline

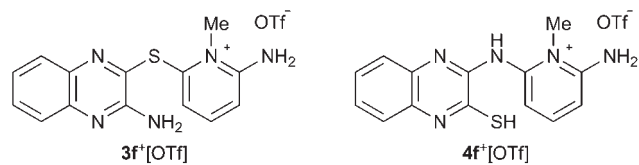


Chart 1

derivative $4f^{\bullet}[\text{OTf}]$ as our primary target. The synthesis of $3f^{\bullet}[\text{OTf}]$ from 3-aminoquinoxalinethiol and 2-amino-6-fluoro-*N*-methylpyridinium trifluoromethanesulfonate was performed as described in Scheme 1 (step i). To our delight, $3f^{\bullet}[\text{OTf}]$ undergoes the SR reaction (step ii) extremely easily as some $4f^{\bullet}[\text{OTf}]$ was formed even during recrystallization of $3f^{\bullet}[\text{OTf}]$. Complete conversion required refluxing $3f^{\bullet}[\text{OTf}]$ in MeCN for 6 h, giving $4f^{\bullet}[\text{OTf}]$ in high isolated yield (80%). The identity of $3f^{\bullet}[\text{OTf}]$ and $4f^{\bullet}[\text{OTf}]$ was confirmed by both NMR spectroscopy and single-crystal X-ray crystallography. This demonstrates that, when using appropriate 3-aminoquinoxalinethiols, the SR reaction is an extremely viable pathway for the synthesis of salts $4^{\bullet}[\text{OTf}]$, which yield the corresponding stable neutral radicals 5^{\bullet} after ring closure and reduction (Chart 1).

Conclusions

In this communication, we have shown that the Smiles rearrangement reaction, either followed by cyclocondensation or performed concurrently with it, offers a viable and modifiable route to a new class of hybrid 1,4-thiazine-1,2,3-dithiazolylum salts $5^{\bullet}[\text{OTf}]$, which can be readily reduced to yield the corresponding neutral radicals 5^{\bullet} with spin densities delocalized over both 1,4-thiazinyl and 1,2,3-dithiazolyl moieties. Future work will focus on the characterisation of transport properties of 5^{\bullet} and related radicals, along with the exploration of their coordination chemistry. This will provide opportunities for the design of molecular materials that may exhibit novel physical properties.

Conflicts of interest

There are no conflicts to declare.

Acknowledgements

This work was financially supported by the University of Jyväskylä, the Academy of Finland (projects 253907 and 289172) and the European Union's H2020 programme (under the Marie Skłodowska-Curie grant agreement 659123). We thank Laboratory Technicians Johanna Lind and Elina Hautakangas for running the +ESI-MS and EA measurements, respectively.

Notes and references

- 1 A. Bernthsen, *Ber. Dtsch. Chem. Ges.*, 1883, **16**, 2896.
- 2 See, for example: (a) A. Jaszczyszyn, K. Gasiorowski, P. Swiatek, W. Malinka, K. Cieslik-Boczula, J. Petrus and B. Czarnik-Matusiewicz, *Pharmacol. Rep.*, 2012, **64**, 16; (b) M. J. Ohlow and B. Moosmann, *Drug Discovery Today*, 2011, **16**, 119; (c) G. Sudeshna and K. Parimal, *Eur. J. Pharmacol.*, 2010, **648**, 6; (d) M. Wainwright and L. Amaral, *Trop. Med. Int. Health*, 2007, **10**, 501; (e) *Phenothiazines and 1,4-Benzothiazines. Chemical and Biomedical Aspects (Bioactive Molecules, Vol. 4)*, ed. R. R. Gupta, Elsevier, Amsterdam, 1988.
- 3 W. E. Truce, E. M. Kreider and W. W. Brand, *Org. React.*, 1970, **18**, 99.
- 4 See, for example: (a) B. Morak-Młodawska, K. Pluta, M. Latocha and M. Jeleń, *Med. Chem. Res.*, 2016, **25**, 2425; (b) M. Jeleń, K. Pluta, K. Suwińska, B. Morak-Młodawska, M. Latocha and A. Shkurenko, *J. Mol. Struct.*, 2015, **1099**, 10; (c) N. Gautam, A. Guleria, M. K. Sharma, S. K. Gupta, A. Goyal and D. C. Gautam, *Curr. Bioact. Compd.*, 2014, **10**, 189; (d) Y. Zhao, Y. Bai, Q. Zhang, Z. Chen, Q. Dai and C. Ma, *Tetrahedron Lett.*, 2013, **54**, 3253; (e) M. Jeleń, K. Suwińska, C. Besnard, K. Pluta and B. Morak-Młodawska, *Heterocycles*, 2012, **85**, 2281; (f) B. Morak-Młodawska, K. Suwińska, K. Pluta and M. Jeleń, *J. Mol. Struct.*, 2012, **1015**, 94; (g) N. Gautam, K. Goyal, O. Saini, A. Kumar and D. C. Gautam, *J. Fluorine Chem.*, 2011, **132**, 420.
- 5 (a) F. Kehrman and L. Diserens, *Ber.*, 1915, **48**, 318; (b) R. Pummerer and S. Gassner, *Ber.*, 1913, **46**, 2310.
- 6 (a) S. C. Blackstock and T. D. Selby, in *Magnetic Properties of Organic Materials*, ed. P. M. Lahti, Marcel Dekker Inc., New York, 1999, p. 165.
- 7 (a) K. Kozawa and T. Uchida, *Acta Crystallogr., Sect. C: Cryst. Struct. Commun.*, 1993, **49**, 267; (b) K. Kozawa, T. Hoshizaki and T. Uchida, *Bull. Chem. Soc. Jpn.*, 1991, **64**, 2039; (c) K. Kozawa and T. Uchida, *Acta Crystallogr., Sect. C: Cryst. Struct. Commun.*, 1990, **46**, 1006; (d) ; (e) ; (f) A. Singhabhandhu, P. D. Robinson, J. H. Fang and W. E. Geiger Jr., *Inorg. Chem.*, 1975, **14**, 318.
- 8 For recent examples, see: (a) Z.-S. Huang, H. Meier and D. Cao, *J. Mater. Chem. C*, 2016, **4**, 2404; (b) X. Wang, Z. Zhang, Y. Song, Y. Su and X. Wang, *Chem. Commun.*, 2015, **51**, 11822; (c) H. Oka, *Org. Lett.*, 2010, **12**, 448; A. W. Franz, L. N. Popa, F. Rominger and T. J. J. Müller, *Org. Biomol. Chem.*, 2009, **7**, 469; (d) H. Oka, *J. Mater. Chem.*, 2008, **18**, 1927; (e) A. A. Golriz, T. Suga, H. Nishide, R. Berger and J. S. Gutmann, *RSC Adv.*, 2005, **5**, 22947; (f) T. Okamoto, M. Kuratsu, M. Kozaki, K. Hirotsu, A. Ichimura, T. Matsushita and K. Okada, *Org. Lett.*, 2004, **6**, 3493; (g) Z. Gomurashvili and J. V. Crivello, *Macromolecules*, 2002, **35**, 2962.
- 9 (a) Y. Tsujino, *Tetrahedron Lett.*, 1968, **9**, 4111; (b) C. Jackson and N. K. D. Patel, *Tetrahedron Lett.*, 1967, **8**, 2255; (c) B. C. Gilbert, P. Hanson, R. O. C. Norman and B. T. Sutcliffe, *Chem. Commun.*, 1966, 161; (d) H. J. Shine and E. E. Mach, *J. Org. Chem.*, 1965, **30**, 2130; (e) C. Bodea and I. Silberg, *Nature*, 1963, **198**, 883.
- 10 (a) M. J. Sienkowska, J. M. Farrar and P. Kaszynski, *Liquid Cryst.*, 2007, **34**, 19; (b) P. Kaszynski, *Molecules*, 2004, **9**, 716; (c) V. Benin and P. Kaszynski, *J. Org. Chem.*, 2000, **65**, 8086.
- 11 (a) K. E. Preuss, *Coord. Chem. Rev.*, 2015, **289–290**, 49; (b) R. G. Hicks, in *Stable Radicals Fundamentals and Applied Aspects of Odd-Electron Compounds*, ed. R. G. Hicks, John Wiley & Sons Ltd., Wiltshire, 2010, p. 317.
- 12 S. M. Winter, A. R. Baló, R. J. Roberts, K. Lekin, A. Assoud, P. A. Dube and R. T. Oakley, *Chem. Commun.*, 2013, **49**, 1603.
- 13 See for example: (a) K. Lekin, K. Ogata, A. Maclean, A. Mailman, S. M. Winter, A. Assoud, M. Mito, J. S. Tse, S. Desgreniers, N. Hirao, P. A. Dube and R. T. Oakley, *Chem. Commun.*, 2016, **52**, 13877; (b) S. M. Winter, S. Hill and R. T. Oakley, *J. Am. Chem. Soc.*, 2015, **137**, 3720; (c) K. Lekin, J. W. L. Wong, S. M. Winter, A. Mailman, P. A. Dube and R. T. Oakley, *Inorg. Chem.*, 2013, **52**, 2188; (d) A. A. Leitch, K. Lekin, S. M. Winter, L. E. Downie, H. Tsuruda, J. S. Tse, M. Mito, S. Desgreniers, P. A. Dube, S. Zhang, Q. Liu, C. Jin, Y. Oshishi and R. T. Oakley, *J. Am. Chem. Soc.*, 2011, **133**, 6051.
- 14 (a) J. Brusso, S. Derakshan, M. E. Itkis, H. Kleinke, R. C. Haddon, R. T. Oakley, R. W. Reed, J. F. Richardson, C. M. Robertson and L. K. Thompson, *Inorg. Chem.*, 2006, **45**, 10958; (b) L. Beer, J. L. Brusso, R. C. Haddon, M. E. Itkis, R. T. Oakley, R. W. Reed, J. F. Richardson, R. A. Secco and X. Yu, *Chem. Commun.*, 2005, 5745.
- 15 (a) I. Dance, *New J. Chem.*, 2003, **27**, 22; (b) A. J. Bondi, *J. Phys. Chem.*, 1964, **68**, 441.
- 16 (a) L. Beer, J. F. Britten, O. P. Clements, R. C. Haddon, M. E. Itkis, K. M. Matkovich, R. T. Oakley and R. W. Reed, *Chem. Mater.*, 2004, **16**, 1564; (b) L. Beer, J. F. Britten, J. L. Brusso, A. W. Cordes, R. C. Haddon, M. E. Itkis, D. S. MacGregor, R. T. Oakley, R. W. Reed and C. M. Robertson, *J. Am. Chem. Soc.*, 2003, **125**, 14394.

III

**INTERMOLECULAR OXIDATIVE DEHYDROGENATIVE
3,3'-COUPLING OF BENZO[B]FURANS AND
BENZO[B]THIOPHENES PROMOTED BY DDQ/H⁺:
TOTAL SYNTHESIS OF SHANDOUGENINE B**

Reproduced with kind permission by Tom Wirtanen, Mikko Muuronen, Juha Hurmalainen, Heikki M. Tuononen, Martin Nieger and Juho Helaja.

Organic Chemistry Frontiers **2016**, 3, 1738–1745.

Copyright © 2016 The Royal Society of Chemistry



Cite this: *Org. Chem. Front.*, 2016, **3**, 1738

Intermolecular oxidative dehydrogenative 3,3'-coupling of benzo[*b*]furans and benzo[*b*]thiophenes promoted by DDQ/H⁺: total synthesis of shandougenine B†‡

T. Wirtanen,^{*a} M. Muuronen,^a J. Hurmalainen,^b H. M. Tuononen,^b M. Nieger^a and J. Helaja^{*a}

With an excess of a strong acid, 2,3-dichloro-5,6-dicyano-1,4-quinone (DDQ) is shown to promote metal-free intermolecular oxidative dehydrogenative (ODH) 3,3'-coupling of 2-aryl-benzo[*b*]furans and 2-aryl-benzo[*b*]thiophenes up to 92% yield as demonstrated with 9 substrates. Based on the analysis of oxidation potentials and molecular orbitals combined with EPR, NMR and UV-Vis observations, the studied reaction is initiated by a DDQ-substrate charge transfer complex and presumably proceeds *via* oxidation of the substrate into an electrophilic radical cation that further reacts with another molecule of a neutral substrate. The coupling reactivity can easily be predicted from the oxidation potential of the substrate and the morphology of its frontier molecular orbitals. The intermolecular ODH coupling reaction allowed a concise total synthesis of the natural product shandougenine B.

Received 5th July 2016,
Accepted 27th September 2016

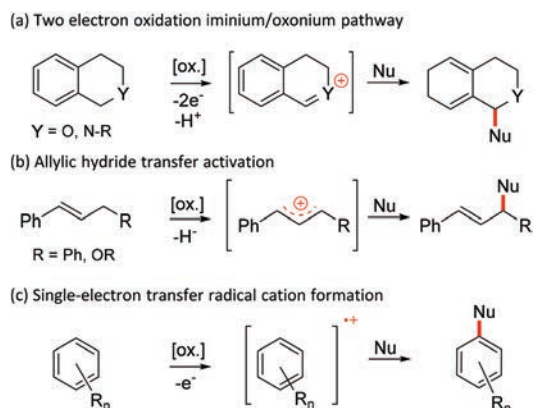
DOI: 10.1039/c6qo00331a

rs.c.li/frontiers-organic

Introduction

Quinones are important oxidizers in both biological and synthetic chemical conversions.¹ For example, the high oxidative power of 2,3-dichloro-5,6-dicyano-1,4-quinone (DDQ) makes it a frequently used oxidant in various chemical conversions. Broadly categorizing, there are three commonly accepted mechanistic pathways associated with oxidation: hydride abstraction, hydrogen atom transfer and single electron transfer (SET).²

It has previously been shown that quinone promoted heteroatomic oxidations associated with α -deprotonation (Scheme 1a) or direct hydride transfer (Scheme 1b) lead to the formation of good electrophiles (*e.g.* iminium, oxonium or allylic cations) that can be coupled with various nucleophiles (Nu).^{3,4} Similarly, an electrophile can be generated by one electron oxidation of a neutral substrate into a radical cation



Scheme 1 Quinone mediated metal-free approaches for intermolecular oxidative dehydrogenative (ODH) couplings.

that can subsequently react with different nucleophiles such as water or aryl (Scheme 1c).^{3,5,6a} The last mechanistic pathway operates in many quinone mediated intramolecular oxidative couplings of aryls, but reports on analogous intermolecular couplings are quite rare.^{3,6a-c} Common to these reactions is that quinones are used in the presence of a strong acid promotor (*e.g.* TFA, MsOH, H₂SO₄, TfOH, HClO₄ or HFSO₃), which has been shown to increase the oxidative power of the quinone considerably.⁶

^aDepartment of Chemistry, A.I. Virtasen aukio 1, University of Helsinki, 00014, Finland. E-mail: juho.helaja@helsinki.fi

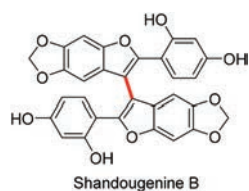
^bDepartment of Chemistry, Nanoscience Center, University of Jyväskylä, P.O. Box 35, FI-40014 Jyväskylä, Finland

† This paper is dedicated to Professor Ari M. P. Koskinen on the occasion of his 60th birthday.

‡ Electronic supplementary information (ESI) available: Crystallographic data, xyz-coordinates, cyclic voltammetry data and EPR, ¹H and ¹³C NMR spectra (PDF). And X-ray crystallographic data for DDQ: 1c (1:2) complex (CIF). CCDC 1477482 (1c_DDQ). For ESI and crystallographic data in CIF or other electronic format see DOI: 10.1039/c6qo00331a



Numerous synthetic methods have been used to construct the 3,3'-bibenzo[*b*]furan and 3,3'-bibenzo[*b*]thiophene skeletons intermolecularly.^{7–13} This structural motif is found in natural products,¹⁴ diphosphine metal ligands,^{7a,8a,b} diphosphine oxide organocatalysts¹⁵ and in organic chiral electrodes.¹⁶ Nevertheless, many of the modern high yielding coupling methods require the use of prefunctionalized starting materials, stoichiometric or substoichiometric amounts of transition metals or air sensitive or pyrophoric reagents (Scheme 2a). However, benzo[*b*]furans and benzo[*b*]thiophenes can be 3,3'-coupled from unfunctionalized monomers directly by the Brønsted acid mediated Friedel–Crafts reaction to dihydro-3,3'-benzofused intermediates in variable yields (Scheme 2b).^{10,17} The McMurry coupling of 3-oxobenzofurans has also been shown to offer a viable route to dihydrogenated intermediates (Scheme 2b).⁷ These intermediates can then be dehydrogenated either thermally (Friedel–Crafts) or with a stoichiometric amount of an oxidant such as DDQ (McMurry).



In our previous studies, we have observed that carbonyl rich heterogeneous carbon materials can catalyze the oxidative coupling of various unfunctionalized benzo-fused heterocycles.¹⁸ In that paper, we also observed that DDQ is capable of mediating a similar 3,3'-homocoupling of 2-phenyl-benzo[*b*]furan in the presence of MsOH.^{18b} Herein we report the optimization of the synthetic procedure, the study of the reaction scope and an improved understanding of the reaction mechanism

via experimental and computational studies (Scheme 2c). We also demonstrate the usefulness of the devised method in the first total synthesis of the 3,3'-bibenzo[*b*]furan natural product, shandougenine B.^{14b}

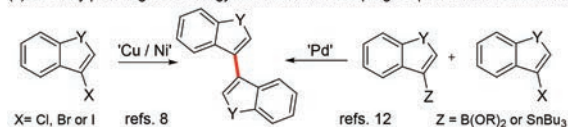
Results and discussion

We began the development of our method with non-optimized reaction conditions, 1 eq. of DDQ, 5 eq. of MsOH and 1 eq. of **1a** in DCM (0.05 M) at RT, which yielded 2,2'-bis(phenyl)-3,3'-bibenzo[*b*]furan **2a** in 61% yield in 1 h.^{18b} In preliminary studies, we found that an acid additive was necessary for the progress of the reaction. Therefore, we tested the effect of several acids on the reaction and found that, out of these, only MsOH worked satisfactorily (Table 1, entries 1–3, see the ESI† for kinetic data). Later we noticed that the behaviour of TFA was both concentration and substrate dependent. At higher concentrations TFA could promote the reaction of **1a** to **2a**, whereas in more dilute solutions it promoted the coupling of the more electron rich substrate **1c** to **2c**.¹⁹ Next, we screened solvents and found that DCE worked better than DCM or CHCl₃, and that MeNO₂ gave a low yield (Table 1, entries 3–6). We then employed a two level full factorial design for three factors to optimize the reaction conditions.²⁰ Entry 3 was chosen as the centre point and molarity, temperature and the amount of DDQ were set as variables (Table 1, entries 3 and 7–14). One corner of the screened reaction space (+1, –1, –1) gave a very high (99%) yield (entry 11) and no further optimization was deemed necessary.²¹

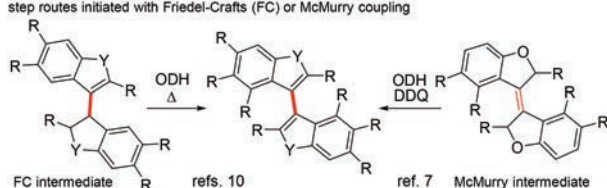
After determining the optimized reaction conditions, the scope of the reaction was studied next. In the case of 2-aryl-benzo[*b*]furans, we were able to obtain the corresponding 2,2'-bis(aryl)-3,3'-bibenzo[*b*]furans in good to excellent isolated yields (Scheme 3, **2a–c**). A slightly lower yield (68%) of the coupling product **2d** was obtained when the 2-aryl substituent was functionalized with an amide group at the *para*-position. However, the electron poor 2-(4-nitrophenyl)benzo[*b*]furan **1i** could not be coupled even in the presence of a stronger acid TfOH or with different oxidants such as *p*-tetrachloro-*o*-quinone or ammonium persulfate (see below). To our pleasure, we could, however, obtain the corresponding 2,2'-bis(aryl)-3,3'-bibenzo[*b*]thiophenes, **2e–g**, in equally high yields as the related bibenzo[*b*]furans **2a–c**. Undesirably, the 3,3'-homocoupling product **2h**, 2,2'-bis(2-thienyl)-3,3'-bibenzo[*b*]thiophene was obtained only in 14% yield. We believe that the reason for such a low yield is in the structure of **1h** that enables reactivity at two sites, benzo[*b*]thiophene 3- and thiophene 5-positions, leading to oligomerization. The oxidative 3,3'-homocoupling of the electron rich substrate **1j** would have given a direct route to the natural product kynapcin-24,^{14a} but we could not obtain any product under the reaction conditions employed (see below).

Based on previous studies,⁶ it seemed reasonable that the reactions are initiated by a SET between the substrate and the DDQ/H⁺ and the oxidation potential of a particular substrate

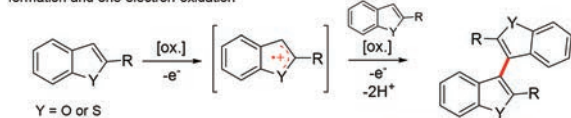
(a) Currently prevailing methodology: metal mediated couplings of prefunctionalized substrates



(b) Examples of oxidative dehydrocoupling of dihydro bibenzo[*b*](thio)furan intermediates: two step routes initiated with Friedel–Crafts (FC) or McMurry coupling



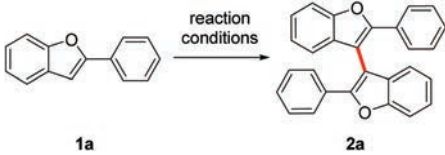
(c) This work: DDQ mediated coupling via consecutive one-electron oxidation, C–C bond formation and one-electron oxidation



Scheme 2 Various synthetic routes to 3,3'-bibenzo[*b*]furan and 3,3'-bibenzo[*b*]thiophene skeletons.

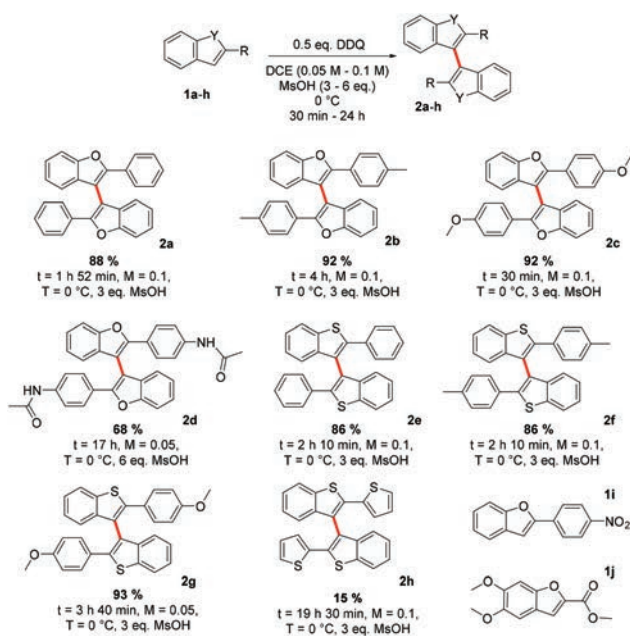


Table 1 Optimization of reaction conditions



Entry	Solvent (molarity)	T (°C)	Time (h)	Acid additive (3 eq.)	Amount of DDQ (eq.)	NMR yield ^a (%)
1	DCM (0.05)	RT	O/N	TFA	1	n.r.
2	DCM (0.05)	RT	O/N	Sc(OTf) ₃	1	n.r.
3	DCM (0.05)	RT	O/N	MsOH	1	75
4	CHCl ₃ (0.05)	RT	1.5	MsOH	1	56
5	DCE (0.05)	RT	1.5	MsOH	1	88
6	MeNO ₂ (0.05)	RT	1.5	MsOH	1	11
7	DCE (0.01)	0	1.5	MsOH	0.5	0
8	DCE (0.01)	0	1.5	MsOH	1.5	0
9	DCE (0.01)	40	1.5	MsOH	0.5	0
10	DCE (0.01)	40	1.5	MsOH	1.5	25
11	DCE (0.1)	0	1.5	MsOH	0.5	99 (88) ^b
12	DCE (0.1)	0	1.5	MsOH	1.5	61
13	DCE (0.1)	40	1.5	MsOH	0.5	84
14	DCE (0.1)	40	1.5	MsOH	1.5	8

^a Determined with ¹H NMR using 1,3,5-trimethoxybenzene as an internal standard. ^b Isolated yield. O/N = overnight.



Scheme 3 Reaction conditions and isolated yields for DDQ/H⁺ mediated homocoupling of benzofurans and benzothiofurans **1a–h** to **2a–h**. Substrates **1i** and **1j** failed to yield a product (see the text for details).

would be directly related to its reactivity. Consequently, we measured the relative oxidation potentials of compounds **1a–j** vs. FcH/FcH⁺ couple, and compared the results with data from theoretical calculations (Table 2). It is clearly evident that both oxidation potentials normalized to **1c** have strong systematic correlation (the absolute value is underestimated by ca. 0.31 V).²³ Furthermore, both the calculated and the experi-

Table 2 Experimental and calculated oxidation potentials (vs. FcH/FcH⁺)²²

Substrate	Exp. ^a (Exp.n.) ^b /V	Calc. (Calc.n.) ^b /V	Exp. – Calc. (Exp.n. – Calc.n.) ^b /V
1a	1.070 (0.280)	0.749 (0.305)	0.321 (–0.03)
1b	0.925 (0.135)	0.627 (0.183)	0.298 (–0.05)
1c	0.790 (0.000)	0.444 (0.000)	0.346 (0.00)
1d	0.810 (0.020)	0.557 (0.113)	0.253 (–0.09)
1e	1.055 (0.265)	0.782 (0.338)	0.273 (–0.07)
1f	1.000 (0.210)	0.689 (0.245)	0.311 (–0.04)
1g	0.845 (0.055)	0.527 (0.083)	0.318 (–0.03)
1h	0.910 (0.120)	0.595 (0.151)	0.315 (–0.03)
1i	1.310 (0.520)	1.060 (0.616)	0.250 (–0.10)
1j	1.100 (0.310)	0.685 (0.241)	0.415 (0.07)

^a Measurements were carried out in DCM with 0.05 M NBu₄PF₆ as the supporting electrolyte. ^b Values in parenthesis have been normalized to **1c** to see relative potentials.

mental oxidation potentials correlate well with the observed reactivity and provide a rationale as for why the homocoupling of **1i** was unsuccessful. With an oxidation potential of 1.310 V, **1i** is not oxidized by DDQ.

The oxidation potentials do not, however, explain why **1j** fails to homocouple even though it has an oxidation potential comparable to **1a** and **1f**. If we consider that dimerization involves the energetically closest MOs,²⁴ we can then pay our attention to the morphology of the SOMO of the radical cation and the HOMO of the neutral substrate. For a successful 3,3'-homocoupling, a high contribution from the C3-carbon to the nucleophile's HOMO and the electrophile's SOMO is imperative. As shown in Fig. 1, this is certainly true for **1a** but not for **1j**. Thus, it is clear that, in order to predict reactivity, both



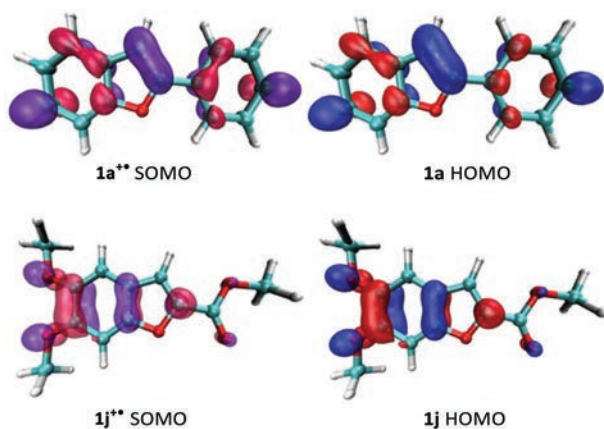
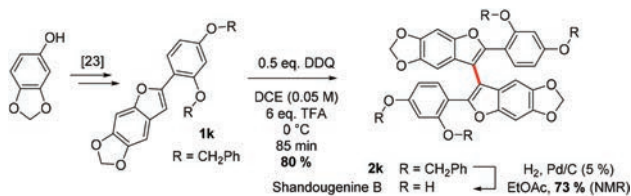


Fig. 1 Frontier molecular orbitals of **1a** and **1j** (HOMOs) and the respective cation radicals (SOMOs).

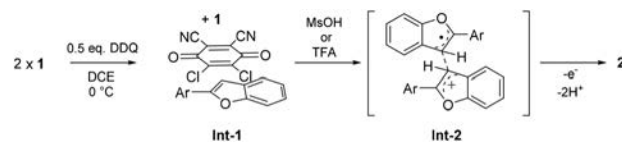
the oxidation potential of the substrate and the morphology of its frontier orbitals need to be considered.

Finally, to demonstrate the applicability of our approach, we endeavoured to synthesise shandougenine B. Prior to the synthesis, we predicted the oxidative homocoupling to be favourable based on its low oxidation potential and a high contribution from the C3-carbon to the frontier MOs (see the ESI†). Substrate **1k** was prepared with the reported literature procedure²⁵ and the homocoupling reaction promoted with 6 eq. of TFA and 0.5 eq. of DDQ (Scheme 4). To our delight, the dimerization of **1k** proceeded smoothly and the corresponding dimer could be isolated in 80% yield. After subsequent removal of the benzyl groups, the antioxidant shandougenine B was obtained in 73% yield (NMR) under standard conditions. Interestingly, the biological origin of shandougenine B has been hypothesised to be oxidative coupling of the monomer *Sophora* as it is also present in the roots of *Sophora tonkinensis*.^{14b} Our successful synthesis of shandougenine B *via* an oxidative route certainly supports this hypothesis.

In the proposed mechanism (Scheme 5), DDQ initially forms a charge transfer (CT) complex with the substrate (**Int-1**). The formation of a CT complex is seen visually by a colour change and confirmed by UV-vis spectroscopy for **1a–c** (Fig. 2 top). Furthermore, the structure of a 2 : 1 complex of **1c** and DDQ was determined by single crystal X-ray diffraction (Fig. 2 bottom, see the ESI† for details).²⁶ The layered structure



Scheme 4 Synthesis of shandougenine B with DDQ-mediated oxidative homocoupling as the key strategic step.



Scheme 5 Proposed reaction mechanism for the intermolecular oxidative dehydrogenative 3,3'-coupling of 2-aryl-benzo[*b*]furans and 2-aryl-benzo[*b*]thiophenes.

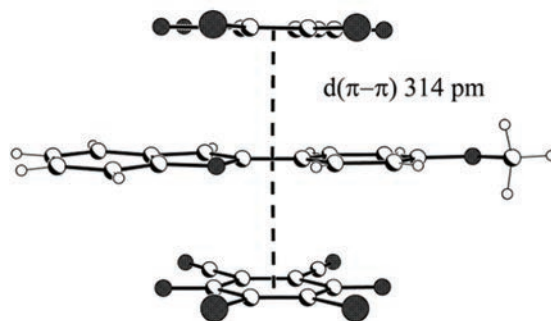
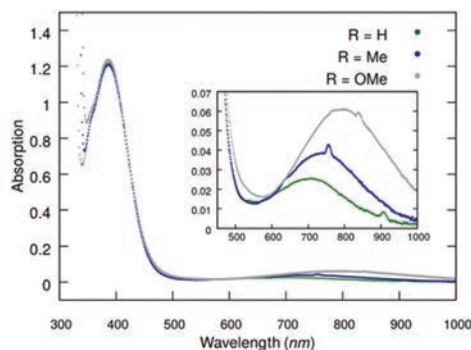


Fig. 2 (Top) UV-vis spectra of DCE solutions of **1a–c** and DDQ in a 2 : 1 ratio. (Bottom) Side view of the stacked packing of DDQ and **1c** in the crystal structure of a 1 : 2 adduct between DDQ and **1c**.

of the complex between **1c** and DDQ shows a short (3.14 Å) distance between the electron donor and the acceptor, which is a prerequisite for efficient electron transfer.²⁷

In our mechanistic scenario, the actual coupling reaction is initiated by a SET from **1** to DDQ, which is, in turn, triggered and promoted by addition of an acid that increases the oxidative power of DDQ.⁶ The formed electrophilic radical cation **1⁺** can then react with a nucleophilic neutral substrate **1** to form a radical cation intermediate **Int-2**, from which product **2** is obtained after elimination of two protons and a second SET. Alternatively, **1⁺** could deprotonate and couple with neutral **1** to form a neutral radical intermediate, leading to **2** *via* elimination of one proton and a second SET. At this point, the radical cation mechanism seems more likely as it is analogous to the one reported for MoCl₅-mediated dehydrogenative coupling of arenes.²⁸ Monitoring the reaction with NMR and EPR spectroscopy implies that the purported mechanism is conceivable as the disappearance of the NMR signals is accompanied by an appearance of an EPR signal upon



addition of the acid (see the ESI†). Moreover, our preliminary calculations show that the **Int-2** structure is a local minimum on the potential energy surface when **1**⁺ and **1** are coupled together *via* their C3-carbon atoms (see the ESI†). Detailed computational investigations of the reaction mechanism are currently underway.

Conclusions

We have developed a metal free DDQ/H⁺ mediated 3,3'-homocoupling reaction of 2-aryl-benzo[*b*]furans and 2-aryl-benzo[*b*]thiophenes. The feasibility of the reaction was found to correlate with the oxidation potential of the substrate and the morphology of its frontier molecular orbitals. The usefulness of this approach was demonstrated in *a priori* examination of the monomer Sophora that was successfully dimerized with the developed synthetic method, resulting in the first total synthesis of a natural product shandougénine B.

Experimental

Computational methods

All calculations were performed with the Turbomole 7.0 program package.²⁹ The solvent environment was taken into account with the COSMO approach with a dielectric constant of 10.125 for 1,2-dichloroethane.³⁰ The geometries were optimized using the TPSS functional³¹ augmented with D3 dispersion correction.³² Ahlrichs' def2-TZVP basis sets were used for all atoms as implemented in Turbomole.³³ A modified integration grid M4 was employed along with the MARI-J approximation augmented with a suitable auxiliary basis set.^{34,35} Vibrational frequencies were calculated numerically for all stationary points and were found to verify their correspondence to true minima (zero imaginary frequencies) and to obtain Gibbs free energies. Absolute oxidation potentials were calculated using a standard protocol ($E^{\circ} = \Delta G_{298.15\text{ K}}/nF$; where $n = 1$ and $F = 96.48\text{ kcal mol}^{-1}\text{ V}^{-1}$) and were further normalized to the FcH/FcH⁺ couple in DCE by subtracting 4.927 eV from all calculated values.²³ The use of FcH/FcH⁺ couple as a reference for data employing nonaqueous solvents is recommended by IUPAC.³⁶ Molecular orbitals were visualized with the program VMD.^{24b}

General remarks

Unless otherwise specified, all materials were purchased from commercial sources and used as received without further purification. Known benzo[*b*]thiophenes were prepared with CuI/TMEDA catalysed annulation of 2-bromo alkynylbenzenes.³⁷ Known benzo[*b*]furans were synthesized from 2-iodophenol in a cascade Sonogashira/5-*endo*-dig cyclisation reaction similar to that described in the literature.³⁸

¹H, and ¹³C{¹H} NMR spectra were recorded using a Varian Mercury 300 or Varian Inova 500 spectrometer at 27 °C. ¹H spectra were referenced to tetramethylsilane (TMS, 0.0 ppm) or

to residual solvent peaks (CDCl₃ 7.26 ppm; *d*₆-DMSO 2.50 ppm, CD₃OD 3.31 ppm and CD₂Cl₂ 5.32 ppm). ¹³C{¹H} NMR spectra were referenced to residual solvent peaks (CDCl₃ 77.16 ppm; *d*₆-DMSO 39.52 ppm and CD₃OD 49.00 ppm). HRMS data were acquired with a JEOL JMS-700 instrument using EI ionization mode. UV-vis spectra were recorded on a Varian Cary 50 spectrometer at 27 °C. Cyclic voltammetry was performed with a Gamry Reference 600 potentiostat using a scan rate of 150 mV s⁻¹. Solid samples of **1a-j** (1–2 mg) were dissolved into a DCM solution containing 0.05 M of NBu₄PF₆ as the supporting electrolyte. Potentials were scanned at RT in a single compartment cell fitted with Pt electrodes and referenced to FcH/FcH⁺ couple. Details of single crystal X-ray structure determinations are given in the ESI.†

General procedure for homocouplings

Starting material (1 eq.) and DDQ (0.5 eq.) were mixed and dissolved in DCE (0.05 or 0.1 M). The formation of a CT-complex was observed from a colour change and the mixture was cooled to 0 °C and MsOH or TFA (3 or 6 eq.) was added to the mixture. After a given amount of time, the reaction mixture was filtered through a pad of basic Al₂O₃ and washed with chloroform. Purification of the crude product after evaporation of solvents was performed by flash chromatography (SiO₂).

2,2'-Bis(phenyl)-3,3'-bibenzo[*b*]furan (2a). Following the general procedure with 51.2 mg (0.264 mmol, 1 eq.) of **1a**, 30 mg (0.132 mmol, 0.5 eq.) of DDQ, 2.6 mL of DCE and 76.1 mg (0.792 mmol, 3 eq., 51 μl) of MsOH. Purification of the crude product with 0 : 1 → 40 : 1 (hexanes : EtOAc) afforded **2a** in 88% yield (44.7 mg, 0.116 mmol). Spectral data is in accordance with published data.^{18b} ¹H NMR (500 MHz, CDCl₃) δ 7.76 (d, *J* = 7.9 Hz, 4H), 7.62 (d, *J* = 8.3 Hz, 2H), 7.33 (t, *J* = 7.6 Hz, 2H), 7.26–7.21 (m, 6H), 7.16–7.08 (m, 4H). ¹³C NMR (75 MHz, CDCl₃) δ 154.5, 152.1, 130.6, 129.6, 128.7, 128.7, 126.4, 125.1, 123.2, 120.9, 111.4, 107.8.

2,2'-Bis(4-methylphenyl)-3,3'-bibenzo[*b*]furan (2b). Following the general procedure with 41.3 mg (0.198 mmol, 1 eq.) of **1b**, 22.5 mg (0.0992 mmol, 0.5 eq.) of DDQ, 2.0 mL of DCE and 57.2 mg (0.595 mmol, 3 eq., 38.6 μl) of MsOH. Purification of the crude product with 0 : 1 → 40 : 1 (hexanes : EtOAc) afforded **2b** in 92% yield (37.9 mg, 0.0914 mmol). Spectral data is in accordance with published data.^{18b} ¹H NMR (500 MHz, CDCl₃) δ 7.69 (d, *J* = 8.2 Hz, 4H), 7.63 (d, *J* = 8.3 Hz, 2H), 7.35–7.30 (m, 2H), 7.16–7.09 (m, 4H), 7.07 (d, *J* = 8.2 Hz, 4H), 2.30 (s, 6H). ¹³C NMR (75 MHz, CDCl₃) δ 154.4, 152.4, 138.7, 129.8, 129.4, 127.9, 126.3, 124.8, 123.1, 120.7, 111.2, 107.2, 21.5.

2,2'-Bis(4-methoxyphenyl)-3,3'-bibenzo[*b*]furan (2c). Following the general procedure with 43.9 mg (0.196 mmol, 1 eq.) of **1c**, 22.2 mg (0.0979 mmol, 0.5 eq.) of DDQ, 2.0 mL of DCE and 56.5 mg (0.587 mmol, 3 eq., 38 μl) of MsOH. Purification of the crude product with 20 : 1 (hexanes : EtOAc) afforded **2c** in 92% yield (40.1 mg, 0.0898 mmol). Spectral data is in accordance with published data.^{18b} ¹H NMR (500 MHz, CDCl₃) 7.76–7.71 (m, 4H), 7.61 (d, *J* = 8.2 Hz, 2H), 7.34–7.29 (m, 2H), 7.16–7.09 (m, 4H), 6.82–6.77 (m, 4H), 3.75 (s, 6H). ¹³C NMR



(126 MHz, CDCl₃) δ 159.9, 154.3, 152.3, 129.9, 127.9, 124.5, 123.4, 123.0, 120.6, 114.2, 111.1, 106.2, 55.3.

***N,N'*-(3,3'-Bibenzo[*b*]furan)-2,2'-diylbis(1,4-phenylene)diacetamide (2d)**. Following the general procedure under dry conditions with 14.3 mg (0.0569 mmol, 1 eq.) of **1d**, 6.6 mg (0.0291 mmol, 0.5 eq.) of DDQ, 1.14 mL of DCE and 32.8 mg (0.34 mmol, 6 eq., 22.2 μ l) of MsOH. Purification of the crude product with 20:1 (DCM:MeOH) afforded **2d** in 68% yield (9.7 mg, 0.0194 mmol). ¹H NMR (500 MHz, DMSO) δ 10.03 (s, 2H), 7.74 (d, *J* = 8.3 Hz, 2H), 7.61 (d, *J* = 8.7 Hz, 4H), 7.53 (d, *J* = 8.7 Hz, 4H), 7.36 (t, *J* = 7.7 Hz, 2H), 7.14 (t, *J* = 7.5 Hz, 2H), 7.03 (d, *J* = 7.7 Hz, 2H), 2.01 (s, 6H). ¹³C NMR (126 MHz, DMSO) δ 168.5, 153.6, 151.5, 139.9, 128.8, 126.4, 125.0, 124.2, 123.3, 119.9, 118.9, 111.4, 105.9, 24.0. HRMS (EI⁺) calcd for [C₃₂H₂₄N₂O₄]⁺ *m/z*: 500.1736, found: 500.1731.

2,2'-Bis(phenyl)-3,3'-bibenzo[*b*]thiophene (2e). Following the general procedure with 30.4 mg (0.145 mmol, 1 eq.) of **1e**, 16.4 mg (0.0723 mmol, 0.5 eq.) of DDQ, 1.4 mL of DCE and 41.7 mg (0.434 mmol, 3 eq., 28.2 μ l) of MsOH. Purification of the crude product with 0:1 \rightarrow 40:1 (hexanes:EtOAc) afforded **2e** in 86% yield (26.1 mg, 0.0624 mmol). Spectral data is in accordance with published data.^{18b} ¹H NMR (500 MHz, CDCl₃) δ 7.89 (d, *J* = 8.0 Hz, 2H), 7.39–7.32 (m, 4H), 7.27–7.22 (m, 2H), 7.12–7.08 (m, 2H), 7.07–7.01 (m, 8H). ¹³C NMR (75 MHz, CDCl₃) δ 142.5, 140.8, 139.0, 134.2, 128.5, 128.4, 127.8, 126.6, 124.8, 124.7, 123.8, 122.3.

2,2'-Bis(4-methylphenyl)-3,3'-bibenzo[*b*]thiophene (2f). Following the general procedure with 40.6 mg (0.181 mmol, 1 eq.) of **1f**, 20.5 mg (0.0905 mmol, 0.5 eq.) of DDQ, 1.8 mL of DCE and 52.2 mg (0.543 mmol, 3 eq., 35.3 μ l) of MsOH. Purification of the crude product with 0:1 (hexanes) \rightarrow 40:1 (hexanes:DCM) \rightarrow 20:1 (hexanes:EtOAc) \rightarrow 10:1 (hexanes:EtOAc) \rightarrow 1:1 (hexanes:EtOAc) afforded **2f** in 86% yield (26.1 mg, 0.0624 mmol). Spectral data is in accordance with published data.^{18b} ¹H NMR (500 MHz, CDCl₃) δ 7.90–7.87 (m, 2H), 7.35–7.29 (m, 4H), 7.24–7.19 (m, 2H), 7.08 (d, *J* = 8.2 Hz, 4H), 6.93–6.89 (m, 4H), 2.24 (s, 6H). ¹³C NMR (75 MHz, CDCl₃) δ 142.4, 141.0, 138.7, 137.8, 131.4, 129.2, 128.2, 126.2, 124.6, 123.6, 122.2, 21.3.

2,2'-Bis(4-methoxyphenyl)-3,3'-bibenzo[*b*]thiophene (2g). Following the general procedure with 45.9 mg (0.191 mmol, 1 eq.) of **1g**, 21.7 mg (0.0955 mmol, 0.5 eq.) of DDQ, 3.8 mL of DCE and 55.1 mg (0.573 mmol, 3 eq., 37.2 μ l) of MsOH. Purification of the crude product with 20:1 (hexanes:EtOAc) \rightarrow 10:1 (hexanes:EtOAc) afforded **2g** in 93% yield (44.3 mg, 0.0884 mmol). Spectral data is in accordance with published data.^{18b} ¹H NMR (500 MHz, CDCl₃) δ 7.88 (d, *J* = 8.0 Hz, 2H), 7.36–7.28 (m, 4H), 7.22 (t, *J* = 7.5 Hz, 2H), 7.08 (d, *J* = 8.8 Hz, 4H), 6.64 (d, *J* = 8.8 Hz, 4H), 3.71 (s, 6H). ¹³C NMR (75 MHz, CDCl₃) δ 159.4, 142.2, 141.0, 138.6, 129.6, 126.8, 125.7, 124.6, 124.5, 123.5, 122.2, 113.9, 55.3.

2,2'-Bis(2-thienyl)-3,3'-bibenzo[*b*]thiophene (2h). Following the general procedure with 36.5 mg (0.169 mmol, 1 eq.) of **1h**, 19.1 mg (0.0844 mmol, 0.5 eq.) of DDQ, 1.7 mL of DCE and 48.7 mg (0.5061 mmol, 3 eq., 32.9 μ l) of MsOH. Purification of the crude product with 0:1 \rightarrow 40:1 afforded **2h** in 15% yield

(5.2 mg, 0.01237 mmol). ¹H NMR (500 MHz, CDCl₃) δ 7.87 (d, *J* = 8.1 Hz, 2H), 7.38–7.30 (m, 2H), 7.22–7.18 (m, 6H), 7.07 (d, *J* = 5.0 Hz, 2H), 6.86 (t, *J* = 4.1 Hz, 2H). ¹³C NMR (126 MHz, CDCl₃) δ 140.7, 138.3, 137.2, 135.9, 127.5, 127.1, 126.5, 125.3, 125.1, 123.2, 122.2, 77.2. HRMS (EI⁺) calcd for [C₂₄H₁₄S₄]⁺ *m/z*: 429.9978, found: 429.9984

Benzylated shandougenine B (2k)

Following the general procedure under dry conditions and under Ar with 16.1 mg (0.0357 mmol, 1 eq.) of **1k**, 4.1 mg (0.0179 mmol, 0.5 eq.) of DDQ, 0.72 mL of DCE and 24.4 mg (0.214 mmol, 6 eq., 16.5 μ l) of TFA. Purification of the crude product with 20:1 \rightarrow 5:1 \rightarrow 3:1 (hexanes:EtOAc) afforded **2k** in 80% yield (12.9 mg, 0.01435 mmol). ¹H NMR (300 MHz, CDCl₃) δ 7.42–7.31 (m, 10H), 7.23–7.16 (m, 6H), 7.09–7.03 (m, 4H), 7.01–7.00 (m, 2H), 6.96 (d, *J* = 8.5 Hz, 2H), 6.67–6.66 (m, 2H), 6.31 (d, *J* = 2.3 Hz, 2H), 6.26 (dd, *J* = 8.5, 2.3 Hz, 2H), 5.96 (dd, *J* = 5.1, 1.3 Hz, 4H), 4.91 (s, 4H), 4.61 (s, 4H). ¹³C NMR (75 MHz, CDCl₃) δ 160.2, 157.4, 150.3, 149.8, 145.9, 144.2, 136.9, 131.6, 128.8, 128.3, 128.2, 127.6, 126.9, 122.8, 113.9, 110.4, 105.9, 101.2, 100.9, 99.4, 93.3, 70.2, 69.9.

Shandougenine B

2k (6.5 mg, 0.00723 mmol) and 25 mg of 5% Pd/C (wetted ~50% H₂O) in 2.5 mL ethyl acetate were stirred vigorously for 10 h 30 min under a H₂-balloon. After filtration through diatomaceous earth, evaporation of volatiles and redissolution to CD₃OD, shandougenine B was obtained in 73% yield (NMR). The analytical sample was purified with column chromatography using 10:1 (DCM:MeOH) as the eluent. Spectral data is in accordance with published data.^{14b} ¹H NMR (500 MHz, CD₃OD) δ 7.40 (d, *J* = 8.5 Hz, 2H), 6.99 (s, 2H), 6.40 (dd, *J* = 8.5, 2.4 Hz, 2H), 6.27 (s, 2H), 6.19 (d, *J* = 2.3 Hz, 2H), 5.85 (d, *J* = 7.2 Hz, 4H). ¹³C NMR (75 MHz, CD₃OD) δ 160.8, 157.0, 151.5, 151.1, 147.2, 145.5, 131.8, 123.5, 111.6, 110.7, 108.8, 103.7, 102.4, 99.8, 93.9. HRMS (EI⁺) calcd for [C₃₀H₁₈O₁₀]⁺ *m/z* 538.0900 found: 538.0899.

Acknowledgements

TW is grateful to Finnish Cultural, Emil Aaltonen, Magnus Ehrnrooth and Otto Malm Foundations for funding. Financial support from the Academy of Finland [project no. 129062 (J. H.) and project no. 289172 (H. M. T.)] is acknowledged. The Finnish National Centre for Scientific Computing (CSC) is recognized for computational resources. M.Sc. Mikko Mäkelä and M.Sc. Otto Seppänen from University of Helsinki are acknowledged for their help in kinetic experiments.

Notes and references

- 1 S. Patai and Z. Rappoport, *The Chemistry of the quinonoid compounds*, Wiley, Chichester, 1988, vol. 2.



- 2 F. Wurche, W. Sicking, R. Sustmann, F.-G. Klärner and C. Rüchardt, *Chem. – Eur. J.*, 2004, **10**, 2707–2721.
- 3 Selected reviews: (a) M. Grzybowski, K. Skonieczny, H. Butenschön and D. T. Gryko, *Angew. Chem., Int. Ed.*, 2013, **52**, 9900–9930; (b) A. E. Wendlandt and S. S. Stahl, *Angew. Chem., Int. Ed.*, 2015, **54**, 14638–14658; (c) R. Narayan, K. Matcha and A. P. Antonchick, *Chem. – Eur. J.*, 2015, **21**, 14678–14693.
- 4 Oxidative C–H functionalization reviews: (a) C. S. Yeung and V. M. Dong, *Chem. Rev.*, 2011, **111**, 1215–1292; (b) C. Liu, J. Yuan, M. Gao, S. Tang, W. Li, R. Shi and A. Lei, *Chem. Rev.*, 2015, **115**, 12138–12204.
- 5 Triplet state DDQ benzene oxidation: K. Ohkubo, A. Fujimoto and S. Fukuzumi, *J. Am. Chem. Soc.*, 2014, **135**, 5368–5371.
- 6 DDQ E_{red} of 0.6 V (vs. SCE) is shifted up to ~1.7 V (vs. SCE) with an acid additive (a)–(c); (a) L. Zhai, R. Shukla, S. H. Wadumethrige and R. Rathore, *J. Org. Chem.*, 2010, **75**, 4748–4760; (b) L. Zhai, R. Shukla and R. Rathore, *Org. Lett.*, 2009, **11**, 3474–3477; (c) I. M. Matheson, O. C. Musgrave and C. J. Webster, *Chem. Commun.*, 1965, 278–279; (d) T. S. Navale, K. Thakur and R. Rathore, *Org. Lett.*, 2011, **13**, 1634–1637; (e) S. Fukuzumi, K. Ishikawa, K. Hironaka and T. Toshio, *J. Chem. Soc., Perkin Trans. 2*, 1987, 751–760; (f) R. Rathore and J. K. Kochi, *Acta Chem. Scand.*, 1998, **52**, 114–130; (g) K. L. Handoo and K. Gadru, *Curr. Sci.*, 1986, **55**, 920–922; (h) O. Hammerich and D. V. Parker, *Acta Chem. Scand. Ser. B*, 1982, **36**, 63–64; (i) H. Y. Cho and L. T. Scott, *Tetrahedron Lett.*, 2015, **56**, 3458–3462.
- 7 McMurry coupling of ketones followed by an oxidation with DDQ: (a) N. G. Andersen, M. Parvez and B. A. Keay, *Org. Lett.*, 2000, **2**, 2817–2820; (b) N. G. Andersen, M. Parvez, R. McDonald and B. A. Keay, *Can. J. Chem.*, 2004, **82**, 145–161.
- 8 Transition metal mediated homocoupling of 3-halogenbenzo[*b*](thio)furans: (a) T. Benincori, E. Brenna, F. Sannicolò, L. Trimarco, P. Antognazza, E. Cesarotti, F. Demartin and T. Pilati, *J. Org. Chem.*, 1996, **61**, 6244–6251; (b) T. Benincori, E. Brenna, F. Sannicolò, L. Trimarco, P. Antognazza and E. Cesarotti, *J. Chem. Soc., Chem. Commun.*, 1995, 685–686; (c) M. Wynberg and M. Cabell, *J. Org. Chem.*, 1973, **38**, 2814–2816; (d) T. Qi, Y. Guo, Y. Liu, H. Xi, H. Zhang, X. Gao, Y. Liu, K. Lu, C. Du, G. Yu and D. Zhu, *Chem. Commun.*, 2008, 6227–6229; (e) Y. Fort, S. Becker and P. Caubère, *Tetrahedron*, 1994, **50**, 11893–11902; (f) Z. Wang, C. Zhao, D. Zhao, C. Li, J. Zhang and H. Wang, *Tetrahedron*, 2010, **66**, 2168–2174; (g) M. Mězlova, H. Petříčková, P. Maloň, V. Kozmík and J. Svoboda, *Collect. Czech. Chem. Commun.*, 2003, **68**, 1020–1038.
- 9 Gold-catalyzed oxidative coupling of 2-arylbenzo[*b*]furans: M. G. Auzias, M. Neuburger and H. A. Wegner, *Synlett*, 2010, 2443–2448.
- 10 Acid mediated Friedel–Crafts type coupling to form a dihydrogenated benzofused dimer followed by ODH: (a) benzo[*b*]thiofurans in 10% H_3PO_4 : A. R. Katritzky and M. Balasubramanian, *Energy Fuels*, 1992, **6**, 431–438; (b) PPA-SiO₂ mediated coupling of furanocoumarins: S. Koul, T. K. Razdan, C. S. Andotra, A. K. Kalla, S. Koul and S. C. Taneja, *Synth. Commun.*, 2002, **32**, 1529–1534.
- 11 BuLi/S₈ mediated coupling of benzo[*b*]furans: T. Janosik, B. Stensland and J. Bergman, *J. Org. Chem.*, 2002, **67**, 6220–6223.
- 12 Palladium catalyzed coupling of 3-halogen and 3-stannate/boronic acid derivatives: (a) L.-Y. Yang, C.-F. Chang, Y.-C. Huang, Y.-J. Lee, C. C. Hu and T.-H. Tseng, *Synthesis*, 2009, 1175–1179; (b) O. Galangau, T. Nakashima, F. Maurel and T. Kawai, *Chem. – Eur. J.*, 2015, **21**, 8471–8482; (c) K. Tanaka, H. Suzuki and H. Osuga, *Tetrahedron Lett.*, 1997, **38**, 457–460.
- 13 Homocoupling of boronic acids: S. A. R. Mulla, S. S. Chavan, M. Y. Pathan, S. M. Inamdar and T. M. Y. Shaihk, *RSC Adv.*, 2015, **5**, 24675–24680.
- 14 (a) K.-S. Song and I. Raskin, *J. Nat. Prod.*, 2002, **65**, 76–78; (b) G. Luo, Y. Yang, M. Zhou, Q. Ye, Y. Liu, J. Gu, G. Zhang and Y. Luo, *Fitoterapia*, 2014, **99**, 21–27.
- 15 V. Simonini, M. Benaglia and T. Benincori, *Adv. Synth. Catal.*, 2008, **350**, 561–564.
- 16 S. Arnaboldi, T. Benincori, R. Cirilli, W. Kutner, M. Magni, P. R. Mussini, K. Noworyta and F. Sannicolò, *Chem. Sci.*, 2015, **6**, 1706–1711.
- 17 Originally, the idea of acid catalyzed dimerization of benzo-fused heterocycles is presented in skatole 2,2'-dimerization in HCl diethylether: F. Smith and A. E. Walter, *J. Chem. Soc.*, 1961, 940–943.
- 18 (a) J. E. Perea-Buceta, T. Wirtanen, O.-V. Laukkanen, M. K. Mäkelä, M. Nieger, M. Melchionna, N. Huittinen, J. A. Lopez-Sanchez and J. Helaja, *Angew. Chem., Int. Ed.*, 2013, **52**, 11835–11839; (b) T. Wirtanen, M. K. Mäkelä, J. Sarfraz, P. Ihalainen, S. Hietala, M. Melchionna and J. Helaja, *Adv. Synth. Catal.*, 2015, **357**, 3718–3726.
- 19 In DCM, TFA fails to promote the catalysis of **1a** to **2a** at 0.15 M, while the coupling proceeds effectively in 0.3 M TFA in DCE. In the case of **1c**, the TFA concentration of 0.2 M in DCM is enough to promote the coupling to **2c**.
- 20 R. Carlson and J. E. Carlson, *Design and Optimization in Organic Synthesis*, Elsevier, 2005, ISBN: 0-444-51527-5.
- 21 It can be concluded that the molarity was the most important parameter among those tested.
- 22 M. Namazian, C. Y. Lin and M. L. Coote, *J. Chem. Theory Comput.*, 2010, **6**, 2721–2725.
- 23 The systematic underestimation of oxidation potentials with pure DFT functionals is well-known: M.-H. Baik and R. A. Friesner, *J. Phys. Chem. A*, 2002, **106**, 7407–7412.
- 24 (a) For example, the energy difference between the SOMO of radical **1a**[•] and the HOMO and LUMO of neutral **1a** is –1.41 and –4.49 eV, respectively; (b) Orbitals visualized using VMD software with 0.06 cutoff: W. Humphrey, A. Dalke and K. Schulten, *J. Mol. Graphics*, 1996, **14**, 33–38.
- 25 B. A. McKittrick, R. T. Scannell and R. Stevenson, *J. Chem. Soc., Perkin Trans. 1*, 1982, 3017–3020.



- 26 From the mixture of DDQ and **1c** in DCM–hexane, we were able to grow a 1:2 DDQ:**1c** crystal suitable for X-ray characterization.
- 27 Charge-transfer complex has been shown to be a real intermediate in hydride transfer from the Michler's hydride to DDQ: K. M. Zaman, S. Yamamoto, N. Nishimura, J. Maruta and S. Fukuzumi, *J. Am. Chem. Soc.*, 1994, **116**, 12099–12100.
- 28 The radical cation mechanism is analogous to the one found in mechanistic study of MoCl₅-mediated dehydrogenative coupling of arenes: J. Leppin, M. Schubert, S. R. Waldvogel and K. Heinze, *Chem. – Eur. J.*, 2015, **21**, 4229–4232.
- 29 TURBOMOLE V7.0 2015, a development of University of Karlsruhe and Forschungszentrum Karlsruhe GmbH, 1989–2007, TURBOMOLE GmbH, since 2007; available from <http://www.turbomole.com>.
- 30 A. Schafer, A. Klamt, D. Sattel, J. C. W. Lohrenz and F. Eckert, *Phys. Chem. Chem. Phys.*, 2000, **2**, 2187–2193.
- 31 J. Tao, J. P. Perdew, V. N. Staroverov and G. E. Scuseria, *Phys. Rev. Lett.*, 2003, **91**, 146401.
- 32 S. Grimme, J. Antony, S. Ehrlich and H. Krieg, *J. Chem. Phys.*, 2010, **132**, 154104.
- 33 F. Weigend and R. Ahlrichs, *Phys. Chem. Chem. Phys.*, 2005, **7**, 3297–3305.
- 34 M. Sierka, A. Hogekamp and R. Ahlrichs, *J. Chem. Phys.*, 2003, **118**, 9136–9148.
- 35 F. Weigend, *Phys. Chem. Chem. Phys.*, 2006, **8**, 1057–1065.
- 36 G. Gritzner and J. Kuta, *Pure Appl. Chem.*, 1984, **56**, 461–466.
- 37 L.-L. Sun, C.-L. Deng, R.-Y. Tang and X.-G. Zhang, *J. Org. Chem.*, 2011, **76**, 7546–7550.
- 38 N. G. Kundu, M. Pal, J. S. Mahanty and S. K. Dasgupta, *J. Chem. Soc., Chem. Commun.*, 1992, 41–42.



IV

DIRECT OBSERVATION OF A BORANE-SILANE COMPLEX INVOLVED IN FRUSTRATED LEWIS-PAIR-MEDIATED HYDROSILYLATIONS

Reproduced with kind permission by Adrian Y. Houghton, Juha Hurmalainen,
Akseli Mansikkamäki, Warren E. Piers and Heikki M. Tuononen.

Nature Chemistry **2014**, 6, 983–988.

Copyright © 2014 Nature Publishing Group

Direct observation of a borane–silane complex involved in frustrated Lewis-pair-mediated hydrosilylations

Adrian Y. Houghton¹, Juha Hurmalainen², Akseli Mansikkamäki², Warren E. Piers^{1*} and Heikki M. Tuononen^{2*}

Perfluorarylborane Lewis acids catalyse the addition of silicon–hydrogen bonds across C=C, C=N and C=O double bonds. This ‘metal-free’ hydrosilylation has been proposed to occur via borane activation of the silane Si–H bond, rather than through classical Lewis acid/base adducts with the substrate. However, the key borane/silane adduct had not been observed experimentally. Here it is shown that the strongly Lewis acidic, antiaromatic 1,2,3-tris(pentafluorophenyl)-4,5,6,7-tetrafluoro-1-boraindene forms an observable, isolable adduct with triethylsilane. The equilibrium for adduct formation was studied quantitatively through variable-temperature NMR spectroscopic investigations. The interaction of the silane with the borane occurs through the Si–H bond, as evidenced by trends in the Si–H coupling constant and the infrared stretching frequency of the Si–H bond, as well as by X-ray crystallography and theoretical calculations. The adduct’s reactivity with nucleophiles demonstrates conclusively the role of this species in metal-free ‘frustrated-Lewis-pair’ hydrosilylation reactions.

Homogeneous catalytic processes that necessitate a bond-activation step typically require catalysts based on transition metals to achieve turnover. Accordingly, many catalysts from metals across the transition period are known to conduct the hydrosilylation and/or hydrogenation of unsaturated organic functions, such as C=O, C=N and C=C bonds. In such systems, the Si–H or H–H bonds are activated via oxidative addition or σ -bond metathesis processes at the transition-metal centre as a key first step in the catalytic cycle¹.

Although such catalysts offer many advantages, two drawbacks are the high cost and toxicity of the metals most typically employed in such applications. There has therefore been significant interest in developing highly active, selective catalysts based on more economical and less harmful elements, such as the first-row transition metals² or main-group elements^{3,4}. With regard to the latter class of ‘metal-free’ catalysts, the primary challenge lies in coaxing compounds of the main-group element into mediating the critical bond-activation step necessary for catalytic turnover⁵.

In this context, our observation in the mid-1990s that the strongly Lewis acidic organoborane trispentafluorophenyl borane, B(C₆F₅)₃ (ref. 6), was a highly active catalyst for the hydrosilylation of carbonyl⁷ and imine⁸ functions has proved to be a key discovery in the development of metal-free catalyst systems for the addition of Si–H^{9–13} and subsequently H–H^{14–16} across a number of unsaturated bonds. Although we surmised initially that B(C₆F₅)₃ served to activate the carbonyl group via a classical Lewis acid–Lewis base interaction, kinetic and mechanistic studies strongly suggested that, even though such adducts are quite thermodynamically favoured^{17,18}, the true role of the borane was to activate the silane^{7,19}, as depicted in Fig. 1. The putative borane–silane adduct **I** is then susceptible to attack at the silicon by the Lewis basic substrate, which results in the bond-activation intermediate **III**. This type of bond cleavage has come to be termed ‘frustrated-Lewis-pair’ (FLP) bond

activation^{20,21}, particularly when $K_{\text{eq}1}$ favours the free Lewis acid/base pair. Even when this equilibrium favours classical adduct formation, the lability of the species can allow for ‘thermally induced frustration’²² whereby an Si–H/borane adduct **I** mediates bond cleavage via a FLP-type mechanism. In the hydrogenation chemistry, the role of an H₂·B(C₆F₅)₃ adduct (**I**, E = H) is still in question²³, and proposals that involve the formation of a weak ‘encounter complex’ **II**, stabilized by secondary C–H...F interactions, prior to FLP activation of H₂ via **III** have strong computational support^{24,25}. Whether the path to **III** involves an EH·B(C₆F₅)₃ adduct **I** or an encounter complex **II**, the bond-activation transition state leads to an ion pair **IV** that proceeds to product on the transfer of hydride from the [HB(C₆F₅)₃][–] to the substrate carbon, regenerating the B(C₆F₅)₃ catalyst. Much experimental and computational²⁶ support for this general mechanistic proposal has appeared in the years since our first disclosure of this chemistry. In addition to our own kinetic and labelling investigations^{7,19}, Oestreich has used stereo-pure silanes to demonstrate elegantly that, as the mechanism predicts, the Walden inversion at silicon via structure **I** for E = R₃Si is, indeed, operative^{27,28}. Furthermore, in some cases the ion-pair intermediate **IV** can be observed spectroscopically^{8,29}.

This cumulative body of evidence resulted in a high degree of acceptance for this mechanism in the literature, but the specific nature of the adducts **I**, or of encounter complexes of type **II**, remained experimentally opaque^{23,30}. It has been observed that B(C₆F₅)₃ reacts slowly with Et₃SiH^{31,32} to give bispentafluorophenyl borane, HB(C₆F₅)₂ (ref. 33) along with Et₃SiC₆F₅, a process in which a borane–silane adduct is implicated. However, extensive attempts to detect this adduct through low-temperature spectroscopic studies^{19,34} consistently failed to provide convincing evidence for its presence in solution. In other words, $K_{\text{eq}2}$ in Scheme 1 appears to strongly disfavour the formation of adduct **I** for the Lewis acid B(C₆F₅)₃. We were thus intrigued by a recent report

¹Department of Chemistry, University of Calgary, 2500 University Drive NW, Calgary, Alberta T2N 1N4, Canada, ²Department of Chemistry, Nanoscience Center, University of Jyväskylä, PO Box 35, FI-40014 Jyväskylä, Finland. *e-mail: wpiers@ucalgary.ca; heikki.m.tuononen@jyu.fi

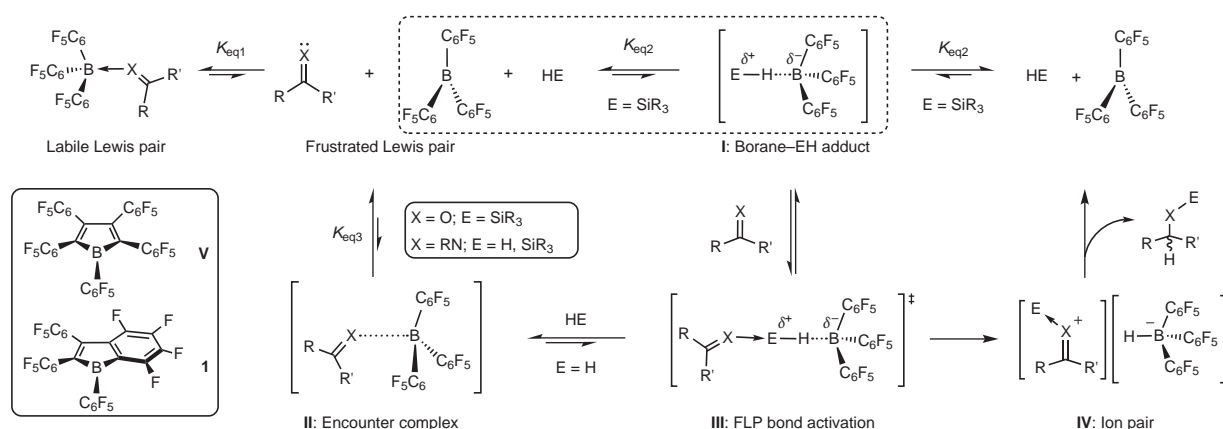


Figure 1 | The mechanism of FLP activation of Si-H and H-H bonds. The various important equilibria involved in the activation and cleavage of Si-H and H-H bonds by Lewis acid/base pairs are depicted. Although the formation of classical Lewis acid/base adducts ($K_{\text{eq}1}$) may be favoured, free Lewis acids may also interact with E-H to form a borane/E-H adduct, which is the key intermediate in the FLP activation of these bonds. This equilibrium, $K_{\text{eq}2}$, is highlighted by the box with dashed lines. Such adducts **I** have not been experimentally observed. Inset: structures of antiaromatic borole **V** and boraindene **1**.

from Berke and co-workers³⁵ in which they claimed to have observed substantial amounts of $\text{Et}_3\text{Si-H} \rightarrow \text{B}(\text{C}_6\text{F}_5)_3$ in solution via ^{29}Si NMR spectroscopy at 233 K. However, as their procedures did not appear to involve careful drying of the borane before use, it seemed probable that the peak assigned to this adduct was, in fact, caused by $\text{Et}_3\text{SiOSiEt}_3$, which forms rapidly when wet borane^{36,37} is treated with silane via rapid dehydrogenative silylation of water^{38,39}. We confirmed this postulate by recording the ^{29}Si NMR spectrum of an authentic sample of $\text{Et}_3\text{SiOSiEt}_3$. Thus, this report of the detection of the $\text{Et}_3\text{Si-H} \rightarrow \text{B}(\text{C}_6\text{F}_5)_3$ adduct³⁵ must be viewed as erroneous, and these species remain experimentally elusive.

To tilt the equilibrium $K_{\text{eq}2}$ in favour of a borane silane adduct **I**, the use of either a silane that is more Lewis basic or a borane that is more Lewis acidic might be contemplated. As the latitude for increasing the Lewis basicity of the silane is rather narrow⁴⁰, we explored the latter strategy. To this end, we utilized antiaromaticity in combination with perfluorination to prepare Lewis acidic boranes that were even stronger than $\text{B}(\text{C}_6\text{F}_5)_3$. For example, we have shown that perfluoropentaphenylborole⁴¹ (**V**, Fig. 1, inset) is an extremely Lewis acidic compound that binds CO ⁴² and activates dihydrogen towards H-H bond cleavage^{43,44}. In the latter reaction, an adduct of H_2 with **V** is clearly implicated. Borole **V** also undergoes less-well-defined reactions with silanes that involve cleavage of the Si-H bond⁴⁵ but, because of the compound's low solubility in non-donor solvents, we have been unable to conduct low-temperature spectroscopic studies aimed at detecting either an H_2 or a silane adduct of **V**. Accordingly, recently we reported the synthesis of 1,2,3-tris(pentafluorophenyl)-4,5,6,7-tetrafluoro-1-boraindene⁴⁶, **1** (Fig. 1), a borane of essentially equal Lewis acidic strength as **V**, but substantially more soluble than **V** in typical inert solvents. Here we describe its behaviour in the presence of triethylsilane, Et_3SiH , and fully demonstrate the viability of borane-silane adducts **I**.

Results and discussion

The synthesis and characterization of boraindene **1** has been described previously⁴⁶. It is a red solid that retains this colour in toluene solution; the colour is the result of a weak absorption in the visible region at 465 nm ($\epsilon = 900 \text{ M}^{-1} \text{ cm}^{-1}$, see Supplementary Fig. 1) caused by a forbidden transition that involves the empty *p* orbital on the Lewis acidic boron centre. On complexation of a Lewis base, this absorption is disrupted and the colour of the resulting adducts is pale yellow. Thus, the formation of a Lewis acid/base adduct that involves **1** is apparent with the naked eye by this red-to-yellow colour change.

To explore the potential for adduct formation between **1** and Et_3SiH ($K_{\text{eq}2}$, Fig. 2a), 1–2 equiv. silane were added to a red solution of **1** in *d*₈-toluene. No visible change in colour was observed at room temperature (Fig. 2b) and little change to the components of the solution occurred, as judged by ^{19}F and ^1H NMR spectroscopy. The 13 separate resonances in the ^{19}F NMR spectrum of **1** remained essentially unperturbed, whereas the signal for the Si-H moiety in Et_3SiH was a sharp septet at 3.79 ppm, essentially the same chemical shift as observed in pure samples of Et_3SiH . These observations show that, although adduct formation was not favoured under these conditions, boraindene **1** is stable towards reactions with silane that lead to ring-opening processes observed for **V** and related compounds⁴⁵. Therefore, when a reversible red-to-yellow colour change was evident on cooling this solution to 195 K (Fig. 2b), the coordination of silane to the boraindene to form adduct **2** was strongly implicated. We therefore followed up this encouraging qualitative evidence with a detailed spectroscopic, structural and computational study, aimed at establishing thermodynamic parameters for the equilibrium $K_{\text{eq}2}$ and characterizing borane/silane adduct **2**.

Variable-temperature ^{19}F NMR experiments were conducted on solutions of **1** with varying amounts of Et_3SiH in *d*₈-toluene. As the temperature was lowered, most of the resonances in the ^{19}F NMR spectrum shifted slightly upfield, but the chemical shift for the fluorine *ortho* to boron on the boraindenyl core (coloured red in Fig. 2a) was significantly perturbed as adduct formation was favoured at lower temperatures (Fig. 2c). The drifting of this resonance was completely reversible as the temperature was lowered and raised. A similar phenomenon was observed in a series of ^{19}F NMR spectra recorded at room temperature with varying amounts of excess silane added (Supplementary Fig. 2). Both experiments indicate that, as the equilibrium shifts towards adduct **2**, the chemical shift of the *ortho*-fluorine atom moves closer to its absolute value in **2**. As the position of the resonance for the *ortho*-fluorine is a weighted average of the chemical shift of this fluorine in the free boraindene **1** and adduct **2**, this series of spectra can be utilized to extract the mole fraction of each species and evaluate the equilibrium constant $K_{\text{eq}2}$. This was done by titrating 26 mM solutions of **1** with measured amounts of added silane at six different temperatures. Treatment of this data using the binding isotherm equation allowed for the determination of $K_{\text{eq}2}$ at these temperatures (see Supplementary Fig. 3 and Supplementary Table 1), which facilitated a van't Hoff analysis (Fig. 2d) that yielded thermodynamic parameters of $\Delta H^\circ = -29.7(3) \text{ kJ mol}^{-1}$ and $\Delta S^\circ = -100(1) \text{ J mol}^{-1} \text{ K}^{-1}$ for $K_{\text{eq}2}$. The enthalpy associated with silane binding is approximately double that calculated for the binding of Et_3SiH to $\text{B}(\text{C}_6\text{F}_5)_3$.

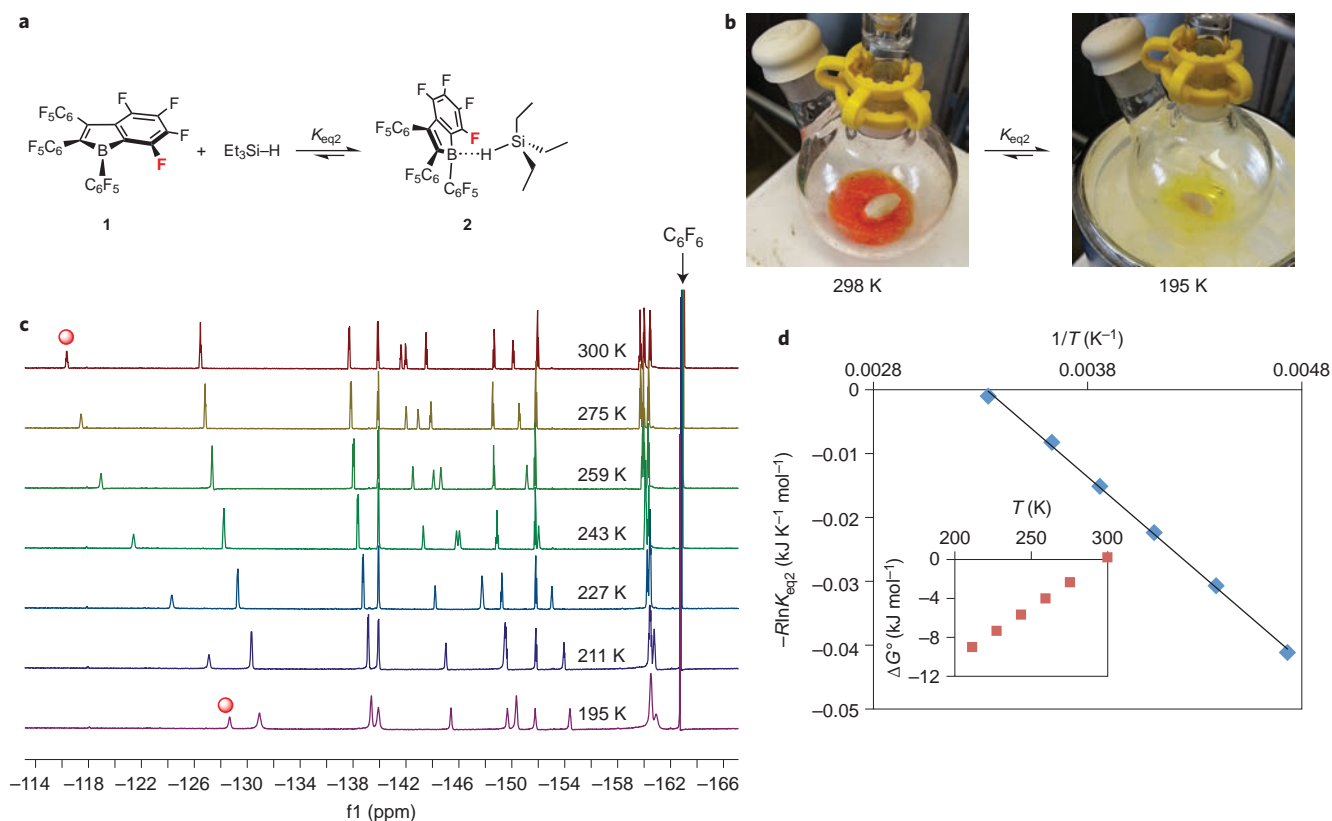


Figure 2 | Equilibrium formation of borane-silane adduct 2. **a**, Schematic representation of adduct formation between 1,2,3-tris(pentafluorophenyl)-4,5,6,7-tetrafluoro-1-borindene, **1**, and triethylsilane, an example of equilibrium $K_{\text{eq}2}$ as depicted in Fig. 1. **b**, The visible colour change observed on cooling solutions of **1** and Et_3SiH from room temperature to 195 K with dry ice/acetone; on warming, the red colour of **1** returns. **c**, Variable-temperature ^{19}F NMR spectra of this mixture, internally referenced to C_6F_6 , illustrate the significant perturbation in the chemical shift of the fluorine atom *ortho* to the boraindene boron atom (resonance marked by the red circle). **d**, Van't Hoff analysis of the equilibrium, which yields thermodynamic parameters $\Delta H^\circ = -29.7(3) \text{ kJ mol}^{-1}$ and $\Delta S^\circ = -100(1) \text{ J mol}^{-1} \text{ K}^{-1}$ for $K_{\text{eq}2}$; inset gives a plot of ΔG° versus temperature.

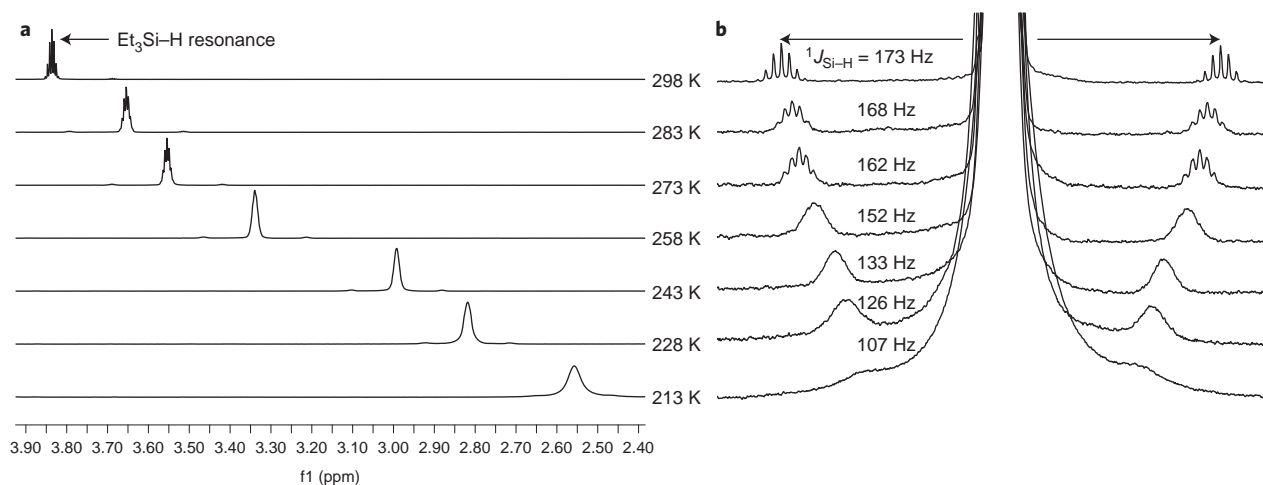


Figure 3 | Partial proton NMR spectrum of solutions of **1 and $\text{Et}_3\text{Si-H}$.** **a**, Region of the spectrum showing the upfield shift for the Si-H resonance as the temperature is lowered and the equilibrium $K_{\text{eq}2}$ favours adduct **2**. **b**, Overlaid and expanded resonance showing the steady contraction in the one-bond Si-H coupling constant as the equilibrium shifts towards adduct **2**.

(refs 26,34), but still rather weak, and the unfavourable entropic term renders the equilibrium approximately thermoneutral at room temperature (Fig. 2d, inset), completely consistent with our macroscopic and spectroscopic observations.

We depict the adduct as being bonded via a $\text{Si-H}\cdots\text{B}$ bridge; this is consistent with computed structures for adducts that involve

$\text{B}(\text{C}_6\text{F}_5)_3$ (refs 26,34). The variable-temperature ^1H NMR and infrared spectra for **2** provide experimental support for this assignment. As the temperature was lowered from 298 to 213 K, the signal for the silane hydrogen in the ^1H NMR spectrum moved more than 1 ppm upfield (Fig. 3a). An expansion of this signal to render the ^{29}Si satellites visible shows clearly that, as the temperature was lowered and

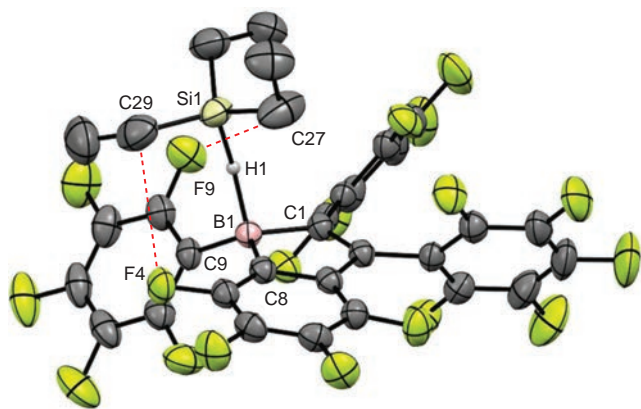


Figure 4 | Crystal structure of boraindene-silane adduct **2 (50% probability ellipsoids).** For hydrogen, only the bridging hydrogen atom H1 is shown. Boron, silicon, carbon, fluorine and hydrogen atoms are in pink, light green, charcoal grey, lime green and grey, respectively. Red dashes indicate the close non-bonded contacts. Selected bond lengths (Å), non-bonded distances (Å) and bond angles (°) [calculated values]: B1–C1 = 1.616(3) [1.607], B1–C8 = 1.608(3) [1.594], B1–C9 = 1.605(3) [1.597], B1–H1 = 1.46(2) [1.402], Si1–H1 = 1.51(2) [1.608], F4–C29 = 3.262(2) [4.717], F9–C27 = 3.138(3) [3.171], C1–B1–C8 = 100.58(15) [100.91], C1–B1–C9 = 122.89(16) [121.06], C8–B1–C9 = 120.84(17) [122.57], B1–H1–Si1 = 157 [154.45].

the equilibrium shifted towards **2**, the value for the $^1J_{\text{Si-H}}$ coupling constant dropped smoothly from 177 Hz in free $\text{Et}_3\text{Si-H}$ to a value of 107(2) Hz at 213 K (Fig. 3b). A lowering of this coupling constant was expected⁴⁷ as the Si–H bond weakens on interaction with the boron centre. It was also anticipated that the stretching frequency of the Si–H bond would be impacted on adduct formation and, indeed, a broad band at $1,918\text{ cm}^{-1}$ was observed in solid samples of **2** precipitated from solutions of **1** in neat Et_3SiH at 195 K (Supplementary Fig. 4). The $\nu_{\text{Si-H}}$ stretch for free silane is a sharp band at $2,103\text{ cm}^{-1}$; the broadness of the band in **2** is typical of such $\nu_{\text{asSi-H-E}}$ moieties⁴⁸. Furthermore, when samples of d_1 -**2** are prepared using $\text{Et}_3\text{Si-D}$, this band shifted from its position at $1,918\text{ cm}^{-1}$ to $\sim 1,400\text{ cm}^{-1}$ in the fingerprint region of the spectrum (Supplementary Fig. 4).

That we were able to perform infrared spectroscopy on solid samples of **2** encouraged us to pursue the compound's crystallization for the purpose of structural analysis by X-ray diffraction. When neat Et_3SiH was layered onto a toluene solution of boraindene **1** at -35°C in a 5 mm glass tube and allowed to diffuse slowly together, X-ray quality crystals were obtained and the structure determined; a thermal ellipsoid depiction of the molecular structure is given in Fig. 4 along with selected metric parameters. In **2**, the silane binds the borane via the Si–H bond, to form a somewhat bent Si1–H1–B1 bridge (157°). The bridging hydrogen H1 was found and refined on the difference map, which provided Si1–H1 and B1–H1 bond distances of 1.51(2) and 1.46(2) Å, respectively. Thus, the hydrogen remained mainly associated with silicon because typical Si–H distances are $\sim 1.48\text{ Å}$ (ref. 47), whereas B–H distances in perfluoroaryl hydridoborate anions are around 1.14 Å (ref. 49) and **2** can be viewed as a Lewis acid/base adduct rather than an ion pair of the form $[\text{Et}_3\text{Si}]^+[\text{HB}(\text{Ar}^{\text{F}})_3]^-$. Although the interaction is weak, the boron centre is significantly pyramidalized relative to the planar boron in **1**⁴⁶, with the sum of the C–B–C angles amounting to $344.3(2)^\circ$. The adduct also appears stabilized by secondary C–H...F van der Waals interactions as evidenced by close contacts between F9 and C27 (3.138(3) Å) and F4 and C29 (3.262(2) Å).

Adduct **2** was studied further by density functional theory (see the Supplementary Information). Most of the optimized structural

Table 1 | Calculated bonding parameters of the adducts **2, **I** and **VI**.**

Adduct	$\Delta H^\circ_{\text{calc}}$ (kJ mol ⁻¹)	$\Delta G^\circ_{\text{calc}}$ (kJ mol ⁻¹)	ΔE_{dist} (kJ mol ⁻¹)*	ΔE_{inst} (kJ mol ⁻¹)*
2	-21	32	75	-102
I	-6	56	68	-79
VI	-20	42	103	-129

*The sum of ΔE_{dist} and ΔE_{inst} equals ΔH_{calc} at 0 K.

parameters of **2** correspond well with those in the crystal structure (Fig. 4, caption), but the calculated Si1–H1 bond length and the non-bonded distances between the F and C atoms are longer than those in the X-ray structure. This can be explained by the uncertainty in the location of the bridging hydrogen in the difference-density map and crystal-packing effects that are not accounted for in gas-phase calculations. An atoms-in-molecules analysis⁵⁰ of the Si1–H1 bond critical point in **2** yields properties comparable to those for the Si–H bond in the free silane, which indicates locally similar electronic structures. In contrast, the data for the B1–H1 bond critical point in **2** differ considerably from results obtained for the anion $[\text{HB}(\text{C}_6\text{F}_5)_3]^-$, which supports the view of **2** as a Lewis acid/base adduct. The calculated enthalpy associated with silane binding, $\Delta H^\circ_{\text{calc}}$, is -21 kJ mol^{-1} , which is in agreement with the value obtained from the van't Hoff analysis; the corresponding $\Delta G^\circ_{\text{calc}}$ is 32 kJ mol^{-1} .

To probe the stability of **2** further, calculations were carried out to compare the bonding in **2** to that in the Et_3SiH adduct with $\text{B}(\text{C}_6\text{F}_5)_3$ (that is, **I** in Fig. 1) and in the hypothetical adduct with perfluoroarylborole **V** (denoted **VI**). The calculated enthalpies and Gibbs energies (Table 1) show that adduct **I** is clearly the weakest of the three, whereas adduct **VI** is predicted to be as strongly bound as **2**. A further decomposition of the energy components that arise from distortion of fragment geometries (ΔE_{dist}) and electronic (bonding) effects that stabilize the adducts (ΔE_{inst}). Adduct **I** has the smallest distortion energy, but is nevertheless the least bound because of it has the weakest bonding interaction. Although the distortion energies in **2** and, in particular, **VI** are greater than that in **I**, the difference is more than compensated by stronger bonding interactions between the boraindene/borole and silane. The data in Table 1 also suggest that the Lewis acidity of the investigated boranes decreases in the series $\text{V} > \text{I} > \text{B}(\text{C}_6\text{F}_5)_3$, a notion corroborated by calculated hydride affinities of -593 , -564 and -538 kJ mol^{-1} , respectively. Thus, a fine balance between steric and electronic effects, rather than the high Lewis acidity of **1** alone, explains the stability of adduct **2**.

The characterization of **2** in both solution and the solid state represents the first direct evidence for the long-proposed activation of silane by perfluoroarylboranes⁷. Although intramolecular Si–H...B interactions have been noted⁵¹, the intermolecular silane borane adduct **2** is explicitly relevant to metal-free, FLP²⁰-mediated hydrosilylations of unsaturated functions. To demonstrate that adduct **2** reacts in ways that are consistent with the mechanistic proposals in Fig. 1, we examined its reactivity towards a simple nucleophile (Fig. 5). Boraindene **1** and silane were dissolved in toluene and cooled to -78°C , and then 1 equiv. of dry bis(triphenylphosphine)iminium chloride, $[\text{PPN}]^+[\text{Cl}]^-$, added to form, immediately and quantitatively, the $[\text{PPN}]^+$ salt of the hydridoborate anion, **3**, and Et_3SiCl (Fig. 5a). The latter was identified by comparison with an authentic sample, whereas **3** exhibited ^{11}B NMR (-16.2 ppm) and ^1H NMR (1.6 ppm, $^1J_{\text{BH}} = 90\text{ Hz}$) data consistent with the formation of a hydridoborate⁴⁹. The chloroborate **4** that might be expected to form competitively (Fig. 5a) was not observed; this was confirmed by synthesizing it separately from **1** and

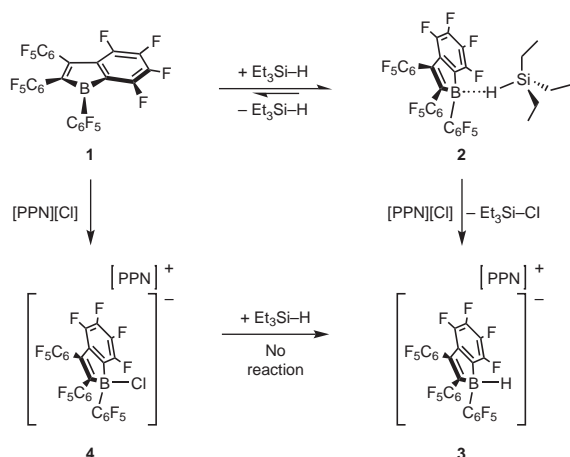


Figure 5 | Reactivity of boraindene silane adduct 2. Schematic representation of the reactivity of both **1** and **2** with PPN chloride.

[PPN]⁺[Cl]⁻. Furthermore, a control experiment in which **4** was treated with excess Et₃SiH showed that this is not a viable pathway to **3**. Indeed, when the boraindene **1**/Et₃SiH mixture was treated with [PPN]⁺[Cl]⁻ at room temperature, the hydridoborate **3** was the exclusive boron-containing product. From equilibrium thermodynamic data, under these conditions the speciation of **2** in solution is less than 5% relative to that of free boraindene **1**, which suggests that the borane–silane adduct reacts with chloride ion at least 20 times faster than the free boraindene. On the face of it, this seems quite surprising, but it is in line with the high rates hydrosilylation of imine and carbonyl functions by B(C₆F₅)₃; clearly, these borane silane adducts are highly reactive towards nucleophiles. The isolation and characterization of **2** allows us to explore the detailed mechanism by which this and related adducts react with various nucleophilic substrates.

Methods

1,2,3-tris(pentafluorophenyl)-4,5,6,7-tetrafluoro-1-boraindene **1** was prepared as described elsewhere⁴⁶; triethylsilane was purchased from Sigma-Aldrich and dried via distillation under vacuum from calcium hydride. Unless explicitly stated otherwise, all operations were carried out under a purified argon atmosphere using either inert-atmosphere-glovebox or vacuum-line techniques. Dichloromethane was dried over and distilled from CaH₂, then distilled from molecular sieves after at least three days. Toluene, hexanes and benzene were dried over and distilled from sodium/benzophenone. Argon was passed through a Matheson TriGas cartridge (model M641-02) prior to use to remove traces of water and oxygen. All NMR analyses (¹H, ¹³C{¹H} DEPT-Q, ¹¹B, ¹⁹F, ³¹P) were performed on either a Bruker 400 MHz or 600 MHz instrument. The X-ray crystallography analysis was performed on suitable crystals coated in Paratone oil and mounted on a Bruker Smart APEX II with a three-circle diffractometer. Full descriptions of the methods used for data accumulation and analysis, as well as representative NMR and infrared spectra and computational results, are given in the Supplementary Information.

Received 27 June 2014; accepted 18 August 2014;
published online 28 September 2014

References

- Hartwig, J. F. *Organotransition Metal Chemistry—From Bonding to Catalysis*. (Univ. Science Books, 2010).
- Bullock, R. M. Abundant metals give precious hydrogenation performance. *Science* **342**, 1054–1055 (2013).
- Frey, G. D., Lavallo, V., Donnadiou, B., Schoeller, W. W. & Bertrand, G. Facile splitting of hydrogen and ammonia by nucleophilic activation at a single carbon center. *Science* **316**, 439–441 (2007).
- Welch, G. C., Juan, R. R. S., Masuda, J. D. & Stephan, D. W. Reversible, metal-free hydrogen activation. *Science* **314**, 1124–1126 (2006).
- Spikes, G. H., Fettingner, J. C. & Power, P. P. Facile activation of dihydrogen by an unsaturated heavier main group compound. *J. Am. Chem. Soc.* **127**, 12232–12233 (2005).
- Massey, A. G., Park, A. J. & Stone, F. G. A. Tris(pentafluorophenyl)boron. *Proc. Chem. Soc.* 212 (1963).

- Parks, D. J. & Piers, W. E. Tris(pentafluorophenyl)borane-catalyzed hydrosilylation of aromatic aldehydes, ketones, and esters. *J. Am. Chem. Soc.* **118**, 9440–9441 (1996).
- Blackwell, J. M., Sonmor, E. R., Scocitti, T. & Piers, W. E. B(C₆F₅)₃-catalyzed hydrosilylation of imines via silyliminium intermediates. *Org. Lett.* **2**, 3921–3923 (2000).
- Rubin, M., Schwier, T. & Gevorgyan, V. Highly efficient B(C₆F₅)₃-catalyzed hydrosilylation of olefins. *J. Org. Chem.* **67**, 1936–1940 (2002).
- Blackwell, J. M., Morrison, D. J. & Piers, W. E. B(C₆F₅)₃-catalyzed hydrosilylation of enones and silyl enol ethers. *Tetrahedron* **58**, 8247–8254 (2002).
- Berkefeld, A., Piers, W. E. & Parvez, M. Tandem frustrated Lewis pair/tris(pentafluorophenyl)borane-catalyzed deoxygenative hydrosilylation of carbon dioxide. *J. Am. Chem. Soc.* **132**, 10660–10661 (2010).
- Müther, K., Mohr, J. & Oestreich, M. Silylium ion promoted reduction of imines with hydrosilanes. *Organometallics* **32**, 6643–6646 (2013).
- Chen, D., Leich, V., Pan, F. & Klankermayer, J. Enantioselective hydrosilylation with chiral frustrated Lewis pairs. *Chem. Eur. J.* **18**, 5184–5187 (2012).
- Chase, P. A., Welch, G. C., Jurca, T. & Stephan, D. W. Metal-free catalytic hydrogenation. *Angew. Chem. Int. Ed.* **46**, 8050–8053 (2007).
- Chase, P. A., Jurca, T. & Stephan, D. W. Lewis acid-catalyzed hydrogenation: B(C₆F₅)₃-mediated reduction of imines and nitriles with H₂. *Chem. Commun.* 1701–1703 (2008).
- Chernichenko, K. *et al.* A frustrated-Lewis-pair approach to catalytic reduction of alkenes to *cis*-alkenes. *Nature Chem.* **5**, 718–723 (2013).
- Parks, D. J., Piers, W. E., Parvez, M., Atencio, R. & Zaworotko, M. J. Synthesis and solution and solid-state structures of tris(pentafluorophenyl)borane adducts of PhC(O)X (X=H, Me, OEt, NPr₂). *Organometallics* **17**, 1369–1377 (1998).
- Blackwell, J. M., Piers, W. E., Parvez, M. & McDonald, R. Solution and solid-state characteristics of imine adducts with tris(pentafluorophenyl)borane. *Organometallics* **21**, 1400–1407 (2002).
- Parks, D. J., Blackwell, J. M. & Piers, W. E. Studies on the mechanism of B(C₆F₅)₃-catalyzed hydrosilylation of carbonyl functions. *J. Org. Chem.* **65**, 3090–3098 (2000).
- Stephan, D. W. ‘Frustrated Lewis pairs’: a concept for new reactivity and catalysis. *Org. Biomol. Chem.* **6**, 1535–1539 (2008).
- Stephan, D. W. & Erker, G. Frustrated Lewis pairs: metal-free hydrogen activation and more. *Angew. Chem. Int. Ed.* **49**, 46–76 (2010).
- Rokob, T. A., Hamza, A., Stirling, A. & Pápai, I. On the mechanism of B(C₆F₅)₃-catalyzed direct hydrogenation of imines: inherent and thermally induced frustration. *J. Am. Chem. Soc.* **131**, 2029–2036 (2009).
- Piers, W. E., Marwitz, A. J. V. & Mercier, L. G. Mechanistic aspects of bond activation with perfluoroarylboranes. *Inorg. Chem.* **50**, 12252–12262 (2011).
- Grimme, S., Kruse, H., Goerigk, L. & Erker, G. The mechanism of dihydrogen activation by frustrated Lewis pairs revisited. *Angew. Chem. Int. Ed.* **49**, 1402–1405 (2010).
- Rokob, T. A., Bakó, I., Stirling, A., Hamza, A. & Pápai, I. Reactivity models of hydrogen activation by frustrated Lewis pairs: synergistic electron transfers or polarization by electric field? *J. Am. Chem. Soc.* **135**, 4425–4437 (2013).
- Sakata, K. & Fujimoto, H. Quantum chemical study of B(C₆F₅)₃-catalyzed hydrosilylation of carbonyl group. *J. Org. Chem.* **78**, 12505–12512 (2013).
- Rendler, S. & Oestreich, M. Conclusive evidence for an S_N2–Si mechanism in the B(C₆F₅)₃-catalyzed hydrosilylation of carbonyl compounds: implications for the related hydrogenation. *Angew. Chem. Int. Ed.* **47**, 5997–6000 (2008).
- Hog, D. T. & Oestreich, M. B(C₆F₅)₃-catalyzed reduction of ketones and imines using silicon-stereogenic silanes: stereoinduction by single-point binding. *Eur. J. Org. Chem.* **2009**, 5047–5056 (2009).
- Hermeke, J., Mewald, M. & Oestreich, M. Experimental analysis of the catalytic cycle of the borane-promoted imine reduction with hydrosilanes: spectroscopic detection of unexpected intermediates and a refined mechanism. *J. Am. Chem. Soc.* **135**, 17537–17546 (2013).
- Marwitz, A. J. V., Dutton, J. L., Mercier, L. G. & Piers, W. E. Dihydrogen activation with ^tBu₃P/B(C₆F₅)₃: a chemically competent indirect mechanism via *in situ* generated *p*-^tBu₂P–C₆F₄–B(C₆F₅)₂. *J. Am. Chem. Soc.* **133**, 10026–10029 (2011).
- Parks, D. J., Piers, W. E. & Yap, G. P. A. Synthesis, properties, and hydroboration activity of the highly electrophilic borane bis(pentafluorophenyl)borane, HB(C₆F₅)₂. *Organometallics* **17**, 5492–5503 (1998).
- Nikonov, G. I., Vyboishchikov, S. F. & Shirobokov, O. G. Facile activation of H–H and Si–H bonds by boranes. *J. Am. Chem. Soc.* **134**, 5488–5491 (2012).
- Parks, D. J., von H. Spence, R. E. & Piers, W. E. Bis(pentafluorophenyl)borane: synthesis, properties, and hydroboration chemistry of a highly electrophilic borane reagent. *Angew. Chem. Int. Ed. Engl.* **34**, 809–811 (1995).
- Chojnowski, J. *et al.* Mechanism of the B(C₆F₅)₃-catalyzed reaction of silyl hydrides with alkoxysilanes. Kinetic and spectroscopic studies. *Organometallics* **24**, 6077–6084 (2005).
- Jiang, Y. *et al.* The ‘catalytic nitrosyl effect’: NO bending boosting the efficiency of rhodium based alkene hydrogenations. *J. Am. Chem. Soc.* **135**, 4088–4102 (2013).

36. Bergquist, C. *et al.* Aqua, alcohol, and acetonitrile adducts of tris(perfluorophenyl)borane: evaluation of Brønsted acidity and ligand lability with experimental and computational methods. *J. Am. Chem. Soc.* **122**, 10581–10590 (2000).
37. Beringhelli, T., Maggioni, D. & D'Alfonso, G. ^1H and ^{19}F NMR investigation of the reaction of $\text{B}(\text{C}_6\text{F}_5)_3$ with water in toluene solution. *Organometallics* **20**, 4927–4938 (2001).
38. Blackwell, J. M., Foster, K. L., Beck, V. H. & Piers, W. E. $\text{B}(\text{C}_6\text{F}_5)_3$ -catalyzed silylation of alcohols: a mild, general method for synthesis of silyl ethers. *J. Org. Chem.* **64**, 4887–4892 (1999).
39. Gevorgyan, V., Rubin, M., Benson, S., Liu, J.-X. & Yamamoto, Y. A novel $\text{B}(\text{C}_6\text{F}_5)_3$ -catalyzed reduction of alcohols and cleavage of aryl and alkyl ethers with hydrosilanes. *J. Org. Chem.* **65**, 6179–6186 (2000).
40. Richter, D., Tan, Y., Antipova, A., Zhu, X.-Q. & Mayr, H. Kinetics of hydride abstractions from 2-arylbenzimidazolines. *Chem. Asian J.* **4**, 1824–1829 (2009).
41. Fan, C., Piers, W. E. & Parvez, M. Perfluoropentaphenylborole. *Angew. Chem. Int. Ed.* **48**, 2955–2958 (2009).
42. Fukazawa, A. *et al.* Reaction of pentaarylboroles with carbon monoxide: an isolable organoboron carbonyl complex. *Chem. Sci.* **3**, 1814–1818 (2012).
43. Fan, C., Mercier, L. G., Piers, W. E., Tuononen, H. M. & Parvez, M. Dihydrogen activation by antiaromatic pentaarylboroles. *J. Am. Chem. Soc.* **132**, 9604–9606 (2010).
44. Houghton, A. Y., Karttunen, V. A., Fan, C., Piers, W. E. & Tuononen, H. M. Mechanistic studies on the metal-free activation of dihydrogen by antiaromatic pentaarylboroles. *J. Am. Chem. Soc.* **135**, 941–947 (2012).
45. Braunschweig, H., Damme, A., Hörl, C., Kupfer, T. & Wahler, J. Si–H bond activation at the boron center of pentaphenylborole. *Organometallics* **32**, 6800–6803 (2013).
46. Houghton, A. Y., Karttunen, V. A., Piers, W. E. & Tuononen, H. M. Hydrogen activation with perfluorinated organoboranes: 1,2,3-tris(pentafluorophenyl)-4,5,6,7-tetrafluoro-1-boradene. *Chem. Commun.* **50**, 1295–1298 (2014).
47. Corey, J. Y. & Braddock-Wilking, J. Reactions of hydrosilanes with transition-metal complexes: formation of stable transition-metal silyl compounds. *Chem. Rev.* **99**, 175–292 (1998).
48. Nava, M. & Reed, C. A. Triethylsilyl perfluoro-tetraphenylborate, $[\text{Et}_3\text{Si}^+][\text{F}_{20}\text{BPh}_4^-]$, a widely used nonexistent compound. *Organometallics* **30**, 4798–4800 (2011).
49. Berkefeld, A. *et al.* Carbon monoxide activation via O-bound CO using decamethylscandocinium–hydridoborate ion pairs. *J. Am. Chem. Soc.* **134**, 10843–10851 (2012).
50. Bader, R. F. W. *Atoms in Molecules: A Quantum Theory* (Oxford Univ. Press, 1990).
51. Wrackmeyer, B., Milius, W. & Tok, O. L. Reaction of alkyn-1-yl(diorganyl)silanes with 1-boraadamantane: Si–H–B bridges confirmed by the molecular structure in the solid state and in solution. *Chem. Eur. J.* **9**, 4732–4738 (2003).

Acknowledgements

Funding for the experimental work described was provided by the Natural Sciences and Engineering Research Council of Canada in the form of a Discovery Grant to W.E.P. Funding for the computational work described was provided by the Academy of Finland in the form of a Research Grant and Fellowship to H.M.T.

Author contributions

A.Y.H. and W.E.P. conceived and designed the experiments, A.Y.H. performed the experiments and determined the X-ray structure, H.M.T. and A.M. conceived and designed the computational work, J.H. and A.M. executed the calculations and performed data analyses. A.Y.H., W.E.P. and A.M. co-wrote the paper with input from J.H. and H.M.T.

Additional information

Supplementary information and chemical compound information are available in the online version of the paper. Reprints and permissions information is available online at www.nature.com/reprints. Correspondence and requests for materials should be addressed to W.E.P. and H.M.T.

Competing financial interests

The authors declare no competing financial interests.

V

COMMENT ON “CRYSTALLOGRAPHIC SNAPSHOT OF AN ARRESTED INTERMEDIATE IN THE BIOMIMETIC ACTIVATION OF CO₂”

Reproduced with kind permission by Juha Hurmalainen, Michael A. Land,
Katherine N. Robertson, Christopher J. Roberts, Ian S. Morgan, Heikki M. Tuononen,
Jason A.C. Clyburne.

Angewandte Chemie International Edition **2015**, *54*, 7484–7487.
Copyright © 2015 WILEY-VCH Verlag GmbH & Co. KGaA, Weinheim

Comment on “Crystallographic Snapshot of an Arrested Intermediate in the Biomimetic Activation of CO₂”**

Juha Hurmalainen, Michael A. Land, Katherine N. Robertson,
Christopher J. Roberts, Ian S. Morgan, Heikki M. Tuononen,* and
Jason A. C. Clyburne*

carbon dioxide · computational chemistry ·
structure elucidation · X-ray crystallography

In a recent article, “Crystallographic Snapshot of an Arrested Intermediate in the Biomimetic Activation of CO₂”, Ackermann et al. report the crystallographic characterization of an intermediate in the formation of tetra-*n*-butylammonium bicarbonate, [(*n*-C₄H₉)₄N]HCO₃, which displays a remarkably long C–OH bond of 1.563(6) Å.^[1] The paper immediately caught our attention as we are also interested in the chemical capture and conversion of CO₂.^[2] Recently we reported the complete characterization of a salt containing the cyanofornate anion, [NCCO₂][−], a simple adduct of cyanide and CO₂ which had long eluded characterization.^[3] Interestingly, some of the rarest adducts of CO₂ are, in fact, the simplest. For

instance, stable solid derivatives of simple coordination complexes of halides or pseudo halides with CO₂ are virtually unknown. Other than cyanofornate and bicarbonate, only the fluorocarbonate anion, [FCO₂][−], has been prepared.^[4] Naturally, a paper describing a very atypical geometry for the bicarbonate anion was of great interest to us.

The experimental work reported by Ackermann et al. can be summarized as follows. Gaseous CO₂ was bubbled through an aqueous solution of tetra-*n*-butylammonium hydroxide, [*n*Bu₄N]OH, until a neutral pH was reached. An anhydrous salt was then obtained by azeotropically dehydrating the reaction mixture using successive portions of diethyl ether. This yielded a white powder, which was spectroscopically (IR, Raman, and ¹H and ¹³C NMR) identified as tetra-*n*-butylammonium bicarbonate, [*n*Bu₄N]HCO₃. Slow evaporation of a saturated diethyl ether solution of the powder gave colorless crystals in an unreported yield. The data from a subsequent X-ray structural study was interpreted in terms of an unprecedented arrested anionic intermediate, [O₂C⋯OH][−]. The anion is described as being encapsulated within a hydrophobic host scaffold generated by the tetra-*n*-butylammonium, [*n*Bu₄N]⁺, cations. The scaffold holds two symmetry-related anions in a head-to-tail orientation with the two hydroxy groups separated by a long O⋯O distance of 4.71 Å. Owing to this structural arrangement and the lack of hydrogen-bond acceptors in the cation, the hydroxy groups are not involved in any secondary bonding interactions, which is rather surprising. However, the crystal structure shows several C–H moieties on the cation in close enough proximity to form weak C–H⋯O interactions with the anion. These interactions are postulated to help to stabilize the structure of the arrested intermediate, though no justification (other than structural data) is given.

The results reported by Ackermann et al. for [*n*Bu₄N]-[O₂C⋯OH][−] contrast with our experiences with cyanofornate.^[3] In our structure, the anion featured an sp–sp² carbon–carbon bond of normal length, 1.480(9) Å, even though it was readily cleaved in solvents of higher polarity, forming CO₂ and CN[−]. In a similar fashion, when trapped inside a hydrophobic pocket, bicarbonate would be expected to contain a regular C–OH bond unless distorted by strong inter-ionic interactions. The hydrophobic pocket discussed by Acker-

[*] J. Hurmalainen, M. A. Land, Dr. K. N. Robertson,
Prof. J. A. C. Clyburne
The Atlantic Centre for Green Chemistry
Department of Chemistry, Saint Mary's University
Halifax, Nova Scotia, B3H 3C3 (Canada)
E-mail: jason.clyburne@smu.ca

J. Hurmalainen, C. J. Roberts, Dr. I. S. Morgan, Dr. H. M. Tuononen
University of Jyväskylä, Department of Chemistry
Nanoscience Center
P.O. Box 35, FI-40014 University of Jyväskylä (Finland)
E-mail: heikki.m.tuononen@jyu.fi

[**] We thank the Natural Sciences and Engineering Research Council of Canada (through the Discovery Grants Program to J.A.C.C.) and the Academy of Finland (through its Research Fellowship to H.M.T.). J.A.C.C. acknowledges support from the Canada Research Chairs Program, the Canadian Foundation for Innovation, and the Nova Scotia Research and Innovation Trust Fund. H.M.T. acknowledges support from the Academy of Finland, the Foundation for Research of Natural Resources in Finland, and the University of Jyväskylä. This work was also supported in part by Encana Corporation (Deep Panuke Education & Training and Research & Development Fund), Springboard and the NSF Graduate Research Opportunities Worldwide Program (CJR). We are grateful to NMR-3 (Dalhousie University) for NMR data acquisition, Dr. Mark Obrovac (Dalhousie University) for X-ray powder data acquisition, and Dr. Christa Brosseau (Saint Mary's University) for Raman data acquisition. We also thank Dr. Phillip Jessop for his helpful insights. Metrical parameters for tetra-*n*-butylammonium acetate are available free of charge from the Cambridge Crystallographic Data Centre, under reference number CCDC 1036823.

Supporting information for this article is available on the WWW under <http://dx.doi.org/10.1002/anie.201411654>.

mann et al. is indeed structurally interesting but it offers no apparent explanation for the stabilization of the putative long C...O bond as only weak C-H...O contacts with the CO₂ end of the anion are present. In fact, the C...O bond length in [nBu₄N][O₂C...OH] is reminiscent of the C-C bond distance calculated by us for an isolated cyanofornate anion in vacuum, 1.544 Å (CCSD(T)/aug-cc-pVTZ). We therefore considered the possibility that the salt reported by Ackermann et al. could contain the common acetate anion, [O₂CCH₃]⁻, with a C-C bond of normal length. We contacted the corresponding authors of the original work and informed them about our concerns, but they felt it “unnecessary to revisit the chemistry at this time”. Since we could only access the CIF file for [nBu₄N][O₂C...OH] from the CCDC repository,^[5] a straightforward reinterpretation of the original crystallographic data was impossible. For this reason, we chose to crystallize tetra-n-butylammonium acetate, [nBu₄N][O₂CCH₃], and determine its structure using single-crystal X-ray diffraction. The results, supported by additional computational work, show that a more plausible explanation for the exceptional arrested intermediate reported by Ackermann et al. is the common acetate anion with a typical C-C bond length of 1.537(3) Å.

A fresh sample of [nBu₄N][O₂CCH₃] was purchased from Sigma-Aldrich and opened in an inert atmosphere. A single crystal was removed directly from the bottle and a complete X-ray crystallographic study (125 K) was performed on it as described in the Supporting Information. Once the low-temperature data collection was finished, a set of room-temperature data was also collected for the same crystal. In addition, a solution of [nBu₄N][O₂CCH₃] in dry acetonitrile was stirred for 24 h under argon in the presence of 3 Å molecular sieves. The solvent was then pumped off and the colorless precipitate was brought into an inert atmosphere. A saturated diethyl ether solution of the powder was allowed to evaporate for three days to produce colorless plate-like crystals. The structure of one of these crystals (123 K) was found to be identical to that determined from the crystal of the fresh sample and is not discussed further.

Table 1 shows a comparison of unit cell parameters for the structure described by Ackermann et al. to those obtained in this work for [nBu₄N][O₂CCH₃].

We are unsure of the actual data collection temperature for [nBu₄N][O₂C...OH] as conflicting information was found in the Supporting Information for the original paper and in the CIF file obtained from the CCDC.^[5] The systematic absences for all the data sets indicate that the space group for [nBu₄N][O₂CCH₃] is *P*2₁/*n* (No. 14), which is also the space group reported for [nBu₄N][O₂C...OH] by Ackermann et al. A comparison of the unit cell parameters (Ta-

Table 1: Unit-cell parameters for the structure described by Ackermann et al. compared to those obtained in this work for [nBu₄N][O₂CCH₃].

	<i>T</i> [K]	<i>a</i>	<i>b</i>	<i>c</i>	β	<i>V</i> [Å ³]
original work	unknown	10.755(2)	13.497(2)	13.948(2)	101.876(2)	1981.4(5)
this work	125	10.7273(12)	13.3080(15)	13.9495(15)	101.9615(13)	1948.2(6)
this work	297	10.8277(16)	13.799(2)	13.968(2)	101.1851(19)	2047.3(9)

ble 1) shows that the data are for closely related substances if not for the identical material.

During the refinement of the 125 K structure of [nBu₄N][O₂CCH₃], care was taken to make sure that all of the non-hydrogen atoms of the anion had been correctly assigned. To do this, in the anisotropic refinement, once all the atoms of the cation (including hydrogen atoms) had been modeled, each atom of the anion was studied individually in turn. For every atom, a cycle of refinement was carried out with that atom assigned sequentially as B, C, N, O, or F. The refinement statistics (*R*1, *wR*2, and *GoF*) were observed and the atom type giving the minimal values chosen as the correct fit for that position. Although this procedure is tedious and technical overkill for what is an essentially a pure crystalline salt, the results will be of interest when comparing our structural data with that reported by Ackermann et al. for [nBu₄N][O₂C...OH]. A summary of the most important results, for the C18 carbon of the terminal methyl group of the acetate anion, are summarized in Table 2. For our data, there is complete agreement with the anion being an acetate ion, as expected.

Next, the geometrical data for our O3 refinement (Table 2) was compared to the structural parameters reported by Ackermann et al. Geometrical parameters were determined to be significantly different if the difference (Δ) between the two was larger than three times the standard uncertainty (σ), that is, a 99.7% confidence interval. The bond lengths and angles reported for [nBu₄N][O₂C...OH] were taken from the Supporting Information of the original publication. We note, however, that the values reported in the CIF file obtained from the CCDC^[5] are, again, slightly different from those reported in the article.

Full data from the structural comparison is given in the Supporting Information. From the analysis, it is immediately evident that the two models are equivalent and represent the same structure. Only one bond in the entire model (the anion

Table 2: Statistical and other parameters for the anisotropic refinement of [nBu₄N][O₂CCH₃] at 125 K where the terminal C18 atom of the anion has been sequentially replaced by other second-row elements to judge the quality of the model.^[a]

X	B	C18	N	O3
<i>R</i> 1	0.0646	0.0555	0.0571	0.0678
<i>wR</i> 2	0.2290	0.1932	0.1955	0.2268
<i>GoF</i>	1.419	1.188	1.202	1.401
positive <i>Q</i> [e Å ⁻³]	0.81	0.47	0.41	0.66
negative <i>Q</i> [e Å ⁻³]	-0.20	-0.18	-0.32	-0.65
<i>U</i> _{eq}	0.03658	0.04773	0.06746	0.09659
C17-X distance [Å]	1.5364(34)	1.5374(28)	1.5416(28)	1.5421(33)

[a] The atom C18 corresponds to our refinement (complete except for the methyl hydrogen atoms on the anion), whereas O3 corresponds to a model, using our data, of the structure reported by Ackermann et al. (complete except for the proton on O3).

C17–O2 bond) is significantly different, for a reason not readily apparent to us. The crucial comparison between the C17...O3 bond in the two structures shows that there is no significant difference in the bond length and our model accurately replicates the large thermal motion of the O3 atom reported by Ackermann et al. We also note that all of the angles in the two models, including both the anion and the cation, are not significantly different. A similar comparison between our O3 model and the actual C18 refinement shows that the structural parameters are not considerably affected even in this case. This is clearly seen in Figure 1, which features an overlay of the thermal ellipsoid plots for $[n\text{Bu}_4\text{N}][\text{O}_2\text{CCH}_3]$ (our refinement) and $[n\text{Bu}_4\text{N}][\text{O}_2\text{C}\cdots\text{OH}]$ (data reported by Ackermann et al.). It is evident that the two structures are completely superimposable on one another, indicative of a common origin.

We concluded the structural comparison by considering the inter-ionic interactions in $[n\text{Bu}_4\text{N}][\text{O}_2\text{CCH}_3]$ and $[n\text{Bu}_4\text{N}][\text{O}_2\text{C}\cdots\text{OH}]$ (full analysis is given in the Supporting Information). Overall, a remarkably similar arrangement of anions in the pocket formed by the cations is observed in both structures. We also note that there is one C–H...O interaction of reasonable length (C1–H1A...O1) present in both structures that was not identified by Ackermann et al. The average difference in the $d(\text{H}\cdots\text{A})$ distances is only 0.06 Å and that of the $\chi(\text{DHA})$ angles is 4°. The head-to-tail orientation of the $[\text{O}_2\text{C}\cdots\text{OH}]^-$ anions in the structural analysis of Ackermann et al. lead to an O...O distance of 4.71 Å between the two hydroxy groups. In our refinement of $[n\text{Bu}_4\text{N}][\text{O}_2\text{CCH}_3]$, the shortest C18...C18#3 contact was found to be 4.665(4) Å, symmetry #3 being $-x+2, -y, -z+1$ (Figure 2). The two values are nearly equal, differing by only 0.04 Å over the rather large distance.

The detailed crystallographic analysis of $[n\text{Bu}_4\text{N}][\text{O}_2\text{CCH}_3]$ lends very strong support to our proposal that the structure of $[n\text{Bu}_4\text{N}][\text{O}_2\text{C}\cdots\text{OH}]$ reported by Ackermann et al. is, in fact, that of $[n\text{Bu}_4\text{N}][\text{O}_2\text{CCH}_3]$. However, since we

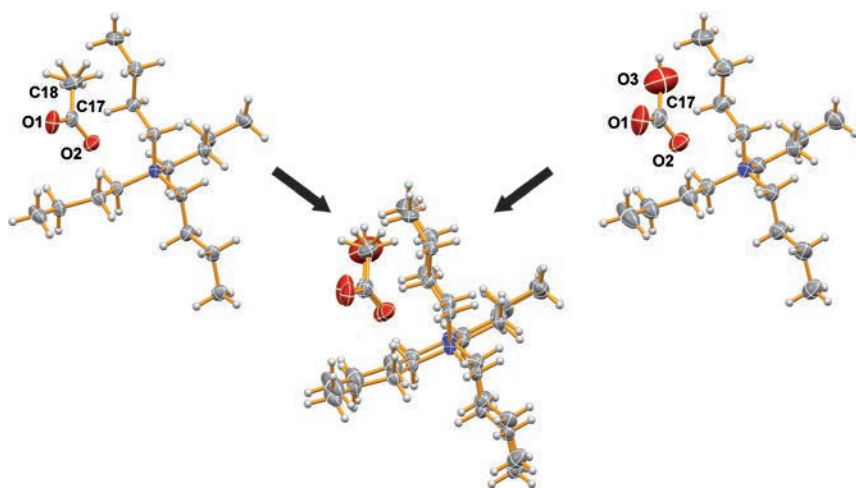


Figure 1. Thermal ellipsoid plots (50% probability) for $[n\text{Bu}_4\text{N}][\text{O}_2\text{CCH}_3]$ at 125 K (left, this work) and for the proposed $[n\text{Bu}_4\text{N}][\text{O}_2\text{C}\cdots\text{OH}]$ salt (right, data from Ackermann et al.), along with an overlay of the two structures (middle). The overlay has been left slightly offset to better highlight the structural similarities. All diagrams were prepared using the program Mercury CSD 3.3.1.^[6]

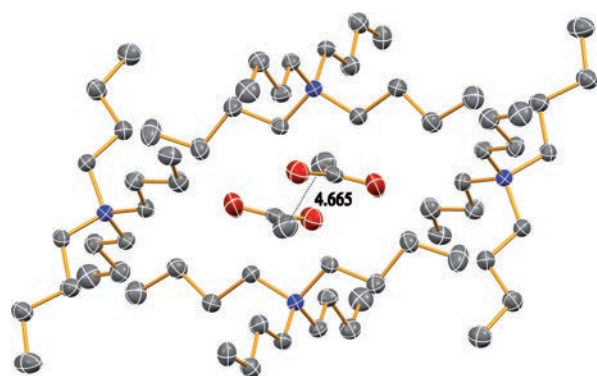


Figure 2. The pocket formed by $[n\text{Bu}_4\text{N}]^+$ cations, enclosing a pair of acetate anions, from the final structure of $[n\text{Bu}_4\text{N}][\text{O}_2\text{CCH}_3]$ at 125 K. Hydrogen atoms have been removed for clarity. The shortest C18...C18 contact in the structure, 4.665(4) Å, is shown.

have no access to the original crystallographic data, there remains a small possibility that the two compounds are in fact different and simply isostructural. For this reason, we performed geometry optimizations for bicarbonate and acetate anions in the gas phase as well as within the hydrophobic pocket formed by six $[n\text{Bu}_4\text{N}]^+$ cations.

First, the geometry of a free bicarbonate anion was optimized in the gas phase at the CCSD(T)-F12b/VTZ-F12 level of theory. Our results parallel those of Ackermann et al. and show that the optimized C–OH bond length is 1.433 Å while the OCO angle is 132.3°. Nearly the same set of values is obtained using dispersion corrected density functional theory (PBE1PBE-D3BJ/def-TZVP): $d(\text{C–OH}) = 1.437$ Å and $\chi(\text{OCO}) = 132.4^\circ$. In a similar fashion, the CCSD(T)-F12b/VTZ-F12 optimized geometry of an acetate anion ($d(\text{C–C}) = 1.552$ Å and $\chi(\text{OCO}) = 128.8^\circ$) is reproduced well at the computationally much less expensive PBE1PBE-D3BJ/def-TZVP level ($d(\text{C–C}) = 1.557$ Å and $\chi(\text{OCO}) = 129.1^\circ$). We therefore feel confident that the PBE1PBE-D3BJ/def-TZVP method can be safely used to optimize the structures of the anions in an environment mimicking the crystal structure as closely as possible.

The structure of the hydrophobic pocket, consisting of six $[n\text{Bu}_4\text{N}]^+$ cations and two anions, was extracted from the X-ray data. Full structural optimization of the anions, started from their crystallographic geometries, was then carried out within the environment provided by the $[n\text{Bu}_4\text{N}]^+$ cations, which were completely frozen to the places they adopt in the crystal structure. We note that no restraints to the location of the anions in the structures were enforced other than the overall C_i symmetry.

The optimization conducted for acetate inside the hydrophobic pocket shows that the metrical parameters of the anion are in good agreement with its gas phase geometry: $d(\text{C–C}) = 1.531$ Å and $\chi(\text{OCO}) = 126.2^\circ$. The result for the optimized bicarbonate anion is similar, $d(\text{C–C}) = 1.531$ Å and $\chi(\text{OCO}) = 126.2^\circ$.

OH) = 1.393 Å and $\angle(\text{OCO}) = 129.7^\circ$. This indicates that the weak C–H...O interactions are not able to support the long C...O bond in $[\text{nBu}_4\text{N}][\text{O}_2\text{C}\cdots\text{OH}]$. Consequently, even if $[\text{nBu}_4\text{N}][\text{O}_2\text{C}\cdots\text{OH}]$ were isostructural with $[\text{nBu}_4\text{N}][\text{O}_2\text{CCH}_3]$, the bicarbonate anion would be expected to have a conventional C–O bond.

In light of the crystallographic and computational data reported herein, we believe that the crystal structure of $[\text{nBu}_4\text{N}][\text{O}_2\text{C}\cdots\text{OH}]$ reported by Ackermann et al. is in fact that of $[\text{nBu}_4\text{N}][\text{O}_2\text{CCH}_3]$. There are also a number of other factors in the original publication that support the plausibility of our interpretation. First, even though a new structure was reported, no elemental analysis of the bulk powder (or the crystalline product) was provided. It is therefore impossible to judge the purity of the material although the reported spectroscopic data appears clean. Second, the paper by Ackermann et al. gives no experimental data that actually ties the reported crystal structure to the bulk powder. There is simply no way to know whether the chosen crystal is representative of the bulk sample. Third, the authors provide the following synthetic information: “The benchmark hydrogen carbonate salt **2** was prepared through a modified literature procedure, in which CO_2 was bubbled slowly through an aqueous solution of **1** (1.5 M $[\text{nBu}_4\text{N}]\text{OH}$) until a neutral pH value was attained.” We note that the synthetic reference provided by Ackermann et al. does not describe the preparation of $[\text{nBu}_4\text{N}]\text{HCO}_3$ but rather that of three $[\text{nBu}_4\text{N}]\cdot\text{ASM}\cdot\text{HCO}_3$ salts, where ASM is an “amine-based structural motif” ligand.^[7] Crystal structures of all three compounds are included in the reference and each of them contains conventional bicarbonate anions hydrogen bonded in a commonly observed dimeric arrangement.

In their published work, Ackermann et al. report that the hydrogen atom of the unusual $[\text{O}_2\text{C}\cdots\text{OH}]^-$ anion was located in the Fourier map, but that it was subsequently fixed to an ideal hydroxide geometry and refined using a riding model. To us it seems strange that such an important atom in the structure was not refined isotropically if it was clearly visible in the Fourier map. In fact, the data deposited by the authors in the CCDC^[5] contains an isotropically refined hydrogen atom; however, the reported U_{iso} value is a nonsensical 0.9(3). The authors do point out that the size and shape of the thermal ellipsoid of the hydroxide oxygen atom indicates rotational disorder. Based on our results, this ellipsoid becomes completely reasonable when using the acetate anion in the structural refinement (see Figure 1). The presence of a hydroxy group that is not engaged in hydrogen bonding is certainly not unprecedented, but it does raise significant concern as to whether the correct assignment has indeed been made. We also note that in our refinement of the acetate salt, the hydrogen atoms on the acetate methyl carbon were clearly visible in the Fourier map and could be refined isotropically. In fact, a disordered model for the methyl group was found to give the optimal fit.

Considering the chemistry involved in the preparation of the putative salt, $[\text{nBu}_4\text{N}][\text{O}_2\text{C}\cdots\text{OH}]$, the origin of an acetate anion seems puzzling. We can therefore see reasons for why alternative assignments of the crystallographic data were not considered. A possible source of acetate could be the

$[\text{nBu}_4\text{N}]\text{OH}$ reagent used, which does contain trace amounts of other cations and anions. Perhaps a more plausible explanation is the cleavage of diethyl ether during the distillation, which could have produced some ethanol that, in the presence of adventitious oxygen, could form acetate. The required oxygen may have been present in the original hydroxide solution. Alternatively, the diethyl ether might initially have been contaminated with a small amount of ethanol, the precursor to most commercial sources of diethyl ether. Additionally, adventitious oxygen in the diethyl ether could have initiated the formation of peroxides whose decomposition pathway includes acetic acid or one of its esters.^[8] Under the reported preparative conditions, these species could certainly be hydrolyzed and deprotonated to form acetate. In all of these scenarios, a small amount of the acetate salt could be present in the bulk powder and crystallize out from the ether solution. Our crystallization experiments clearly showed that $[\text{nBu}_4\text{N}][\text{O}_2\text{CCH}_3]$ is only sparingly soluble in ether and readily forms single crystals of excellent X-ray quality.

In summary, our detailed experimental evidence casts serious doubts on the claims made by Ackermann et al. in the Communication “Crystallographic Snapshot of an Arrested Intermediate in the Biomimetic Activation of CO_2 ”. We believe that the authors have synthesized and spectroscopically characterized powdered bicarbonate, $[\text{nBu}_4\text{N}]\text{HCO}_3$, and carried out an X-ray crystallographic study on a single crystal of acetate, $[\text{nBu}_4\text{N}][\text{O}_2\text{CCH}_3]$. We therefore consider that all extrapolations from the putative structural model proposed in the original study are invalid. Considering the general importance of the original publication, the activation of CO_2 under mild conditions and synthetic mimics to enzymatic functions, we feel it extremely important that the compound reported by Ackermann et al. is correctly identified.

How to cite: *Angew. Chem. Int. Ed.* **2015**, *54*, 7484–7487
Angew. Chem. **2015**, *127*, 7592–7595

- [1] S. L. Ackermann, D. J. Wolstenholme, C. Frazee, G. Deslongchamps, S. H. M. Riley, A. Decken, G. S. McGrady, *Angew. Chem. Int. Ed.* **2015**, *54*, 164–168; *Angew. Chem.* **2015**, *127*, 166–170.
- [2] L. J. Murphy, K. N. Robertson, R. A. Kemp, H. M. Tuononen, J. A. C. Clyburne, *Chem. Commun.* **2015**, *51*, 3942–3956.
- [3] L. J. Murphy, K. N. Robertson, S. G. Harroun, C. L. Brosseau, U. Werner-Zwanziger, J. Moilanen, H. M. Tuononen, J. A. C. Clyburne, *Science* **2014**, *344*, 75–78.
- [4] X. Zhang, U. Gross, K. Seppelt, *Angew. Chem. Int. Ed. Engl.* **1995**, *34*, 1858–1860; *Angew. Chem.* **1995**, *107*, 2019–2021.
- [5] The Cambridge Structural Database: F. H. Allen, *Acta Crystallogr. Sect. B* **2002**, *58*, 380–388.
- [6] Mercury 3.3.1: C. F. Macrae, I. J. Bruno, J. A. Chisholm, P. R. Edgington, P. McCabe, E. Pidcock, L. Rodriguez-Monge, R. Taylor, J. van de Streek, P. A. Wood, *J. Appl. Crystallogr.* **2008**, *41*, 466–470.
- [7] S. Dalapati, S. Jana, R. Saha, M. A. Alam, N. Guchhait, *Org. Lett.* **2012**, *14*, 3244–3247.
- [8] S. Di Tommaso, P. Rotureau, O. Crescenzi, C. Adamo, *Phys. Chem. Chem. Phys.* **2011**, *13*, 14636–14645.

Received: December 3, 2014
 Published online: June 3, 2015

DEPARTMENT OF CHEMISTRY, UNIVERSITY OF JYVÄSKYLÄ
RESEARCH REPORT SERIES

1. Vuolle, Mikko: Electron paramagnetic resonance and molecular orbital study of radical ions generated from (2.2)metacyclophane, pyrene and its hydrogenated compounds by alkali metal reduction and by thallium(III)trifluoroacetate oxidation. (99 pp.) 1976
2. Pasanen, Kaija: Electron paramagnetic resonance study of cation radical generated from various chlorinated biphenyls. (66 pp.) 1977
3. Carbon-13 Workshop, September 6-8, 1977. (91 pp.) 1977
4. Laihia, Katri: On the structure determination of norbornane polyols by NMR spectroscopy. (111 pp.) 1979
5. Nyrönen, Timo: On the EPR, ENDOR and visible absorption spectra of some nitrogen containing heterocyclic compounds in liquid ammonia. (76 pp.) 1978
6. Talvitie, Antti: Structure determination of some sesquiterpenoids by shift reagent NMR. (54 pp.) 1979
7. Häkli, Harri: Structure analysis and molecular dynamics of cyclic compounds by shift reagent NMR. (48 pp.) 1979
8. Pitkänen, Ilkka: Thermodynamics of complexation of 1,2,4-triazole with divalent manganese, cobalt, nickel, copper, zinc, cadmium and lead ions in aqueous sodium perchlorate solutions. (89 pp.) 1980
9. Asunta, Tuula: Preparation and characterization of new organometallic compounds synthesized by using metal vapours. (91 pp.) 1980
10. Sattar, Mohammad Abdus: Analyses of MCPA and its metabolites in soil. (57 pp.) 1980
11. Bibliography 1980. (31 pp.) 1981
12. Knuuttila, Pekka: X-Ray structural studies on some divalent 3d metal compounds of picolinic and isonicotinic acid N-oxides. (77 pp.) 1981
13. Bibliography 1981. (33 pp.) 1982
14. 6th National NMR Symposium, September 9-10, 1982, Abstracts. (49 pp.) 1982
15. Bibliography 1982. (38 pp.) 1983
16. Knuuttila, Hilikka: X-Ray structural studies on some Cu(II), Co(II) and Ni(II) complexes with nicotinic and isonicotinic acid N-oxides. (54 pp.) 1983
17. Symposium on inorganic and analytical chemistry May 18, 1984, Program and Abstracts. (100 pp.) 1984
18. Knuutinen, Juha: On the synthesis, structure verification and gas chromatographic determination of chlorinated catechols and guaiacols occurring in spent bleach liquors of kraft pulp mill. (30 pp.) 1984
19. Bibliography 1983. (47 pp.) 1984
20. Pitkänen, Maija: Addition of BrCl, B₂ and Cl₂ to methyl esters of propenoic and 2-butenic acid derivatives and ¹³C NMR studies on methyl esters of saturated aliphatic mono- and dichlorocarboxylic acids. (56 pp.) 1985
21. Bibliography 1984. (39 pp.) 1985
22. Salo, Esa: EPR, ENDOR and TRIPLE spectroscopy of some nitrogen heteroaromatics in liquid ammonia. (111 pp.) 1985

DEPARTMENT OF CHEMISTRY, UNIVERSITY OF JYVÄSKYLÄ
RESEARCH REPORT SERIES

23. Humppi, Tarmo: Synthesis, identification and analysis of dimeric impurities of chlorophenols. (39 pp.) 1985
24. Aho, Martti: The ion exchange and adsorption properties of sphagnum peat under acid conditions. (90 pp.) 1985
25. Bibliography 1985 (61 pp.) 1986
26. Bibliography 1986. (23 pp.) 1987
27. Bibliography 1987. (26 pp.) 1988
28. Paasivirta, Jaakko (Ed.): Structures of organic environmental chemicals. (67 pp.) 1988
29. Paasivirta, Jaakko (Ed.): Chemistry and ecology of organo-element compounds. (93 pp.) 1989
30. Sinkkonen, Seija: Determination of crude oil alkylated dibenzothiophenes in environment. (35 pp.) 1989
31. Kolehmainen, Erkki (Ed.): XII National NMR Symposium Program and Abstracts. (75 pp.) 1989
32. Kuokkanen, Tauno: Chlorocymenes and Chlorocymenenes: Persistent chlorocompounds in spent bleach liquors of kraft pulp mills. (40 pp.) 1989
33. Mäkelä, Reijo: ESR, ENDOR and TRIPLE resonance study on substituted 9,10-anthraquinone radicals in solution. (35 pp.) 1990
34. Veijanen, Anja: An integrated sensory and analytical method for identification of off-flavour compounds. (70 pp.) 1990
35. Kasa, Seppo: EPR, ENDOR and TRIPLE resonance and molecular orbital studies on a substitution reaction of anthracene induced by thallium(III) in two fluorinated carboxylic acids. (114 pp.) 1990
36. Herve, Sirpa: Mussel incubation method for monitoring organochlorine compounds in freshwater recipients of pulp and paper industry. (145 pp.) 1991
37. Pohjola, Pekka: The electron paramagnetic resonance method for characterization of Finnish peat types and iron (III) complexes in the process of peat decomposition. (77 pp.) 1991
38. Paasivirta, Jaakko (Ed.): Organochlorines from pulp mills and other sources. Research methodology studies 1988-91. (120 pp.) 1992
39. Veijanen, Anja (Ed.): VI National Symposium on Mass Spectrometry, May 13-15, 1992, Abstracts. (55 pp.) 1992
40. Rissanen, Kari (Ed.): The 7. National Symposium on Inorganic and Analytical Chemistry, May 22, 1992, Abstracts and Program. (153 pp.) 1992
41. Paasivirta, Jaakko (Ed.): CEOEC'92, Second Finnish-Russian Seminar: Chemistry and Ecology of Organo-Element Compounds. (93 pp.) 1992
42. Koistinen, Jaana: Persistent polychloroaromatic compounds in the environment: structure-specific analyses. (50 pp.) 1993
43. Virkki, Liisa: Structural characterization of chlorolignins by spectroscopic and liquid chromatographic methods and a comparison with humic substances. (62 pp.) 1993
44. Helenius, Vesa: Electronic and vibrational excitations in some

DEPARTMENT OF CHEMISTRY, UNIVERSITY OF JYVÄSKYLÄ
RESEARCH REPORT SERIES

- biologically relevant molecules.
(30 pp.) 1993
45. Leppä-aho, Jaakko: Thermal behaviour, infrared spectra and x-ray structures of some new rare earth chromates(VI). (64 pp.) 1994
46. Kotila, Sirpa: Synthesis, structure and thermal behavior of solid copper(II) complexes of 2-amino-2-hydroxymethyl-1,3-propanediol. (111 pp.) 1994
47. Mikkonen, Anneli: Retention of molybdenum(VI), vanadium(V) and tungsten(VI) by kaolin and three Finnish mineral soils. (90 pp.) 1995
48. Suontamo, Reijo: Molecular orbital studies of small molecules containing sulfur and selenium. (42 pp.) 1995
49. Hämäläinen, Jouni: Effect of fuel composition on the conversion of fuel-N to nitrogen oxides in the combustion of small single particles. (50 pp.) 1995
50. Nevalainen, Tapio: Polychlorinated diphenyl ethers: synthesis, NMR spectroscopy, structural properties, and estimated toxicity. (76 pp.) 1995
51. Aittola, Jussi-Pekka: Organochloro compounds in the stack emission. (35 pp.) 1995
52. Harju, Timo: Ultrafast polar molecular photophysics of (dibenzylmethine)borondifluoride and 4-aminophthalimide in solution. (61 pp.) 1995
53. Maatela, Paula: Determination of organically bound chlorine in industrial and environmental samples. (83 pp.) 1995
54. Paasivirta, Jaakko (Ed.): CEOEC'95, Third Finnish-Russian Seminar: Chemistry and Ecology of Organo-Element Compounds. (109 pp.) 1995
55. Huuskonen, Juhani: Synthesis and structural studies of some supramolecular compounds. (54 pp.) 1995
56. Palm, Helena: Fate of chlorophenols and their derivatives in sawmill soil and pulp mill recipient environments. (52 pp.) 1995
57. Rantio, Tiina: Chlorohydrocarbons in pulp mill effluents and their fate in the environment. (89 pp.) 1997
58. Ratilainen, Jari: Covalent and non-covalent interactions in molecular recognition. (37 pp.) 1997
59. Kolehmainen, Erkki (Ed.): XIX National NMR Symposium, June 4-6, 1997, Abstracts. (89 pp.) 1997
60. Matilainen, Rose: Development of methods for fertilizer analysis by inductively coupled plasma atomic emission spectrometry. (41 pp.) 1997
61. Koistinen, Jari (Ed.): Spring Meeting on the Division of Synthetic Chemistry, May 15-16, 1997, Program and Abstracts. (36 pp.) 1997
62. Lappalainen, Kari: Monomeric and cyclic bile acid derivatives: syntheses, NMR spectroscopy and molecular recognition properties. (50 pp.) 1997
63. Laitinen, Eira: Molecular dynamics of cyanine dyes and phthalimides in solution: picosecond laser studies. (62 pp.) 1997
64. Eloranta, Jussi: Experimental and theoretical studies on some

DEPARTMENT OF CHEMISTRY, UNIVERSITY OF JYVÄSKYLÄ
RESEARCH REPORT SERIES

- quinone and quinol radicals. (40 pp.) 1997
65. Oksanen, Jari: Spectroscopic characterization of some monomeric and aggregated chlorophylls. (43 pp.) 1998
66. Häkkänen, Heikki: Development of a method based on laser-induced plasma spectrometry for rapid spatial analysis of material distributions in paper coatings. (60 pp.) 1998
67. Virtapohja, Janne: Fate of chelating agents used in the pulp and paper industries. (58 pp.) 1998
68. Airola, Karri: X-ray structural studies of supramolecular and organic compounds. (39 pp.) 1998
69. Hyötyläinen, Juha: Transport of lignin-type compounds in the receiving waters of pulp mills. (40 pp.) 1999
70. Ristolainen, Matti: Analysis of the organic material dissolved during totally chlorine-free bleaching. (40 pp.) 1999
71. Eklin, Tero: Development of analytical procedures with industrial samples for atomic emission and atomic absorption spectrometry. (43 pp.) 1999
72. Väliisaari, Jouni: Hygiene properties of resol-type phenolic resin laminates. (129 pp.) 1999
73. Hu, Jiwei: Persistent polyhalogenated diphenyl ethers: model compounds syntheses, characterization and molecular orbital studies. (59 pp.) 1999
74. Malkavaara, Petteri: Chemometric adaptations in wood processing chemistry. (56 pp.) 2000
75. Kujala Elena, Laihia Katri, Nieminen Kari (Eds.): NBC 2000, Symposium on Nuclear, Biological and Chemical Threats in the 21st Century. (299 pp.) 2000
76. Rantalainen, Anna-Lea: Semipermeable membrane devices in monitoring persistent organic pollutants in the environment. (58 pp.) 2000
77. Lahtinen, Manu: *In situ* X-ray powder diffraction studies of Pt/C, CuCl/C and Cu₂O/C catalysts at elevated temperatures in various reaction conditions. (92 pp.) 2000
78. Tamminen, Jari: Syntheses, empirical and theoretical characterization, and metal cation complexation of bile acid-based monomers and open/closed dimers. (54 pp.) 2000
79. Vatanen, Virpi: Experimental studies by EPR and theoretical studies by DFT calculations of α -amino-9,10-anthraquinone radical anions and cations in solution. (37 pp.) 2000
80. Kotilainen, Risto: Chemical changes in wood during heating at 150-260 °C. (57 pp.) 2000
81. Nissinen, Maija: X-ray structural studies on weak, non-covalent interactions in supramolecular compounds. (69 pp.) 2001
82. Wegelius, Elina: X-ray structural studies on self-assembled hydrogen-bonded networks and metallosupramolecular complexes. (84 pp.) 2001
83. Paasivirta, Jaakko (Ed.): CEOEC'2001, Fifth Finnish-Russian Seminar: Chemistry and Ecology of Organo-Element Compounds. (163 pp.) 2001
84. Kiljunen, Toni: Theoretical studies on spectroscopy and

DEPARTMENT OF CHEMISTRY, UNIVERSITY OF JYVÄSKYLÄ
RESEARCH REPORT SERIES

- atomic dynamics in rare gas solids. (56 pp.) 2001
85. Du, Jin: Derivatives of dextran: synthesis and applications in oncology. (48 pp.) 2001
86. Koivisto, Jari: Structural analysis of selected polychlorinated persistent organic pollutants (POPs) and related compounds. (88 pp.) 2001
87. Feng, Zhinan: Alkaline pulping of non-wood feedstocks and characterization of black liquors. (54 pp.) 2001
88. Halonen, Markku: Lahon havupuun käyttö sulfaattiprosessin raaka-aineena sekä havupuun lahontorjunta. (90 pp.) 2002
89. Falábu, Dezső: Synthesis, conformational analysis and complexation studies of resorcarene derivatives. (212 pp.) 2001
90. Lehtovuori, Pekka: EMR spectroscopic studies on radicals of ubiquinones Q-*n*, vitamin K₃ and vitamiine E in liquid solution. (40 pp.) 2002
91. Perkkalainen, Paula: Polymorphism of sugar alcohols and effect of grinding on thermal behavior on binary sugar alcohol mixtures. (53 pp.) 2002
92. Ihalainen, Janne: Spectroscopic studies on light-harvesting complexes of green plants and purple bacteria. (42 pp.) 2002
93. Kunttu, Henrik, Kiljunen, Toni (Eds.): 4th International Conference on Low Temperature Chemistry. (159 pp.) 2002
94. Väisänen, Ari: Development of methods for toxic element analysis in samples with environmental concern by ICP-AES and ETAAS. (54 pp.) 2002
95. Luostarinen, Minna: Synthesis and characterisation of novel resorcarene derivatives. (200 pp.) 2002
96. Louhelainen, Jarmo: Changes in the chemical composition and physical properties of wood and nonwood black liquors during heating. (68 pp.) 2003
97. Lahtinen, Tanja: Concave hydrocarbon cyclophane B-prismands. (65 pp.) 2003
98. Laihia, Katri (Ed.): NBC 2003, Symposium on Nuclear, Biological and Chemical Threats – A Crisis Management Challenge. (245 pp.) 2003
99. Oasmaa, Anja: Fuel oil quality properties of wood-based pyrolysis liquids. (32 pp.) 2003
100. Virtanen, Elina: Syntheses, structural characterisation, and cation/anion recognition properties of nano-sized bile acid-based host molecules and their precursors. (123 pp.) 2003
101. Nättinen, Kalle: Synthesis and X-ray structural studies of organic and metallo-organic supramolecular systems. (79 pp.) 2003
102. Lampiselkä, Jarkko: Demonstraatio lukion kemian opetuksessa. (285 pp.) 2003
103. Kallioinen, Jani: Photoinduced dynamics of Ru(dcbpy)₂(NCS)₂ – in solution and on nanocrystalline titanium dioxide thin films. (47 pp.) 2004
104. Valkonen, Arto (Ed.): VII Synthetic Chemistry Meeting and XXVI Finnish NMR Symposium. (103 pp.) 2004

DEPARTMENT OF CHEMISTRY, UNIVERSITY OF JYVÄSKYLÄ
RESEARCH REPORT SERIES

105. Vaskonen, Kari: Spectroscopic studies on atoms and small molecules isolated in low temperature rare gas matrices. (65 pp.) 2004
106. Lehtovuori, Viivi: Ultrafast light induced dissociation of Ru(dcbpy)(CO)₂I₂ in solution. (49 pp.) 2004
107. Saarenketo, Pauli: Structural studies of metal complexing schiff bases, Schiff base derived *N*-glycosides and cyclophane π -prismands. (95 pp.) 2004
108. Paasivirta, Jaakko (Ed.): CEOEC'2004, Sixth Finnish-Russian Seminar: Chemistry and Ecology of Organo-Element Compounds. (147 pp.) 2004
109. Suontamo, Tuula: Development of a test method for evaluating the cleaning efficiency of hard-surface cleaning agents. (96 pp.) 2004
110. Güneş, Minna: Studies of thiocyanates of silver for nonlinear optics. (48 pp.) 2004
111. Ropponen, Jarmo: Aliphatic polyester dendrimers and dendrons. (81 pp.) 2004
112. Vu, Mân Thi Hong: Alkaline pulping and the subsequent elemental chlorine-free bleaching of bamboo (*Bambusa procera*). (69 pp.) 2004
113. Mansikkamäki, Heidi: Self-assembly of resorcinarenes. (77 pp.) 2006
114. Tuononen, Heikki M.: EPR spectroscopic and quantum chemical studies of some inorganic main group radicals. (79 pp.) 2005
115. Kaski, Saara: Development of methods and applications of laser-induced plasma spectroscopy in vacuum ultraviolet. (44 pp.) 2005
116. Mäkinen, Riika-Mari: Synthesis, crystal structure and thermal decomposition of certain metal thiocyanates and organic thiocyanates. (119 pp.) 2006
117. Ahokas, Jussi: Spectroscopic studies of atoms and small molecules isolated in rare gas solids: photodissociation and thermal reactions. (53 pp.) 2006
118. Busi, Sara: Synthesis, characterization and thermal properties of new quaternary ammonium compounds: new materials for electrolytes, ionic liquids and complexation studies. (102 pp.) 2006
119. Mäntykoski, Keijo: PCBs in processes, products and environment of paper mills using wastepaper as their raw material. (73 pp.) 2006
120. Laamanen, Pirkko-Leena: Simultaneous determination of industrially and environmentally relevant aminopolycarboxylic and hydroxycarboxylic acids by capillary zone electrophoresis. (54 pp.) 2007
121. Salmela, Maria: Description of oxygen-alkali delignification of kraft pulp using analysis of dissolved material. (71 pp.) 2007
122. Lehtovaara, Lauri: Theoretical studies of atomic scale impurities in superfluid ⁴He. (87 pp.) 2007
123. Rautiainen, J. Mikko: Quantum chemical calculations of structures, bonding, and spectroscopic properties of some sulphur and selenium iodine cations. (71 pp.) 2007
124. Nummelin, Sami: Synthesis, characterization, structural and

- retrostructural analysis of self-assembling pore forming dendrimers. (286 pp.) 2008
125. Sopo, Harri: Uranyl(VI) ion complexes of some organic aminobisphenolate ligands: syntheses, structures and extraction studies. (57 pp.) 2008
126. Valkonen, Arto: Structural characteristics and properties of substituted cholanoates and *N*-substituted cholanamides. (80 pp.) 2008
127. Lähde, Anna: Production and surface modification of pharmaceutical nano- and microparticles with the aerosol flow reactor. (43 pp.) 2008
128. Beyeh, Ngong Kodiah: Resorcinarenes and their derivatives: synthesis, characterization and complexation in gas phase and in solution. (75 pp.) 2008
129. Välishaari, Jouni, Lundell, Jan (Eds.): Kemian opetuksen päivät 2008: uusia oppimisympäristöjä ja ongelmalähtöistä opetusta. (118 pp.) 2008
130. Myllyperkiö, Pasi: Ultrafast electron transfer from potential organic and metal containing solar cell sensitizers. (69 pp.) 2009
131. Käkölä, Jaana: Fast chromatographic methods for determining aliphatic carboxylic acids in black liquors. (82 pp.) 2009
132. Koivukorpi, Juha: Bile acid-arene conjugates: from photoswitchability to cancer cell detection. (67 pp.) 2009
133. Tuuttila, Tero: Functional dendritic polyester compounds: synthesis and characterization of small bifunctional dendrimers and dyes. (74 pp.) 2009
134. Salorinne, Kirsi: Tetramethoxy resorcinarene based cation and anion receptors: synthesis, characterization and binding properties. (79 pp.) 2009
135. Rautiainen, Riikka: The use of first-thinning Scots pine (*Pinus sylvestris*) as fiber raw material for the kraft pulp and paper industry. (73 pp.) 2010
136. Ilander, Laura: Uranyl salophens: synthesis and use as ditopic receptors. (199 pp.) 2010
137. Kiviniemi, Tiina: Vibrational dynamics of iodine molecule and its complexes in solid krypton - Towards coherent control of bimolecular reactions? (73 pp.) 2010
138. Ikonen, Satu: Synthesis, characterization and structural properties of various covalent and non-covalent bile acid derivatives of N/O-heterocycles and their precursors. (105 pp.) 2010
139. Siitonen, Anni: Spectroscopic studies of semiconducting single-walled carbon nanotubes. (56 pp.) 2010
140. Raatikainen, Kari: Synthesis and structural studies of piperazine cyclophanes – Supramolecular systems through Halogen and Hydrogen bonding and metal ion coordination. (69 pp.) 2010
141. Leivo, Kimmo: Gelation and gel properties of two- and three-component Pyrene based low molecular weight organogelators. (116 pp.) 2011
142. Martiskainen, Jari: Electronic energy transfer in light-harvesting complexes isolated from *Spinacia oleracea* and from three

- photosynthetic green bacteria
Chloroflexus aurantiacus,
Chlorobium tepidum, and
Prosthecochloris aestuarii. (55
pp.) 2011
143. Wichmann, Oula: Syntheses,
characterization and structural
properties of [O,N,O,X']
aminobisphenolate metal
complexes. (101 pp.) 2011
144. Ilander, Aki: Development of
ultrasound-assisted digestion
methods for the determination of
toxic element concentrations in
ash samples by ICP-OES. (58 pp.)
2011
145. The Combined XII Spring
Meeting of the Division of
Synthetic Chemistry and XXXIII
Finnish NMR Symposium. Book
of Abstracts. (90 pp.) 2011
146. Valto, Piia: Development of fast
analysis methods for extractives
in papermaking process waters.
(73 pp.) 2011
147. Andersin, Jenni: Catalytic activity
of palladium-based nanostructures
in the conversion of simple
olefinic hydro- and
chlorohydrocarbons from first
principles. (78 pp.) 2011
148. Aumanen, Jukka: Photophysical
properties of dansylated
poly(propylene amine)
dendrimers. (55 pp.) 2011
149. Kärnä, Minna: Ether-
functionalized quaternary
ammonium ionic liquids –
synthesis, characterization and
physicochemical properties. (76
pp.) 2011
150. Jurček, Ondřej: Steroid conjugates
for applications in pharmacology
and biology. (57 pp.) 2011
151. Nauha, Elisa: Crystalline forms of
selected Agrochemical actives:
design and synthesis of cocrystals.
(77 pp.) 2012
152. Ahkola, Heidi: Passive sampling
in monitoring of nonylphenol
ethoxylates and nonylphenol in
aquatic environments. (92 pp.)
2012
153. Helttunen, Kaisa: Exploring the
self-assembly of resorcinarenes:
from molecular level interactions
to mesoscopic structures. (78 pp.)
2012
154. Linnanto, Juha: Light excitation
transfer in photosynthesis
revealed by quantum chemical
calculations and exciton theory.
(179 pp.) 2012
155. Roiko-Jokela, Veikko: Digital
imaging and infrared
measurements of soil adhesion
and cleanability of semihard and
hard surfaces. (122 pp.) 2012
156. Noponen, Virpi: Amides of bile
acids and biologically important
small molecules: properties and
applications. (85 pp.) 2012
157. Hulkko, Eero: Spectroscopic
signatures as a probe of structure
and dynamics in condensed-phase
systems – studies of iodine and
gold ranging from isolated
molecules to nanoclusters. (69
pp.) 2012
158. Lappi, Hanna: Production of
Hydrocarbon-rich biofuels from
extractives-derived materials. (95
pp.) 2012
159. Nykänen, Lauri: Computational
studies of Carbon chemistry on
transition metal surfaces. (76 pp.)
2012
160. Ahonen, Kari: Solid state studies
of pharmaceutically important
molecules and their derivatives. (65
pp.) 2012

DEPARTMENT OF CHEMISTRY, UNIVERSITY OF JYVÄSKYLÄ
RESEARCH REPORT SERIES

161. Pakkanen, Hannu: Characterization of organic material dissolved during alkaline pulping of wood and non-wood feedstocks (76 pp.) 2012
162. Moilanen, Jani: Theoretical and experimental studies of some main group compounds: from closed shell interactions to singlet diradicals and stable radicals. (80 pp.) 2012
163. Himanen, Jatta: Stereoselective synthesis of Oligosaccharides by *De Novo* Saccharide welding. (133 pp.) 2012
164. Bunzen, Hana: Steroidal derivatives of nitrogen containing compounds as potential gelators.(76 pp.) 2013
165. Seppälä, Petri: Structural diversity of copper(II) amino alcohol complexes. Syntheses, structural and magnetic properties of bidentate amino alcohol copper(II) complexes. (67 pp.) 2013
166. Lindgren, Johan: Computational investigations on rotational and vibrational spectroscopies of some diatomics in solid environment. (77 pp.) 2013
167. Giri, Chandan: Sub-component self-assembly of linear and non-linear diamines and diacylhydrazines, formylpyridine and transition metal cations. (145 pp.) 2013
168. Riisiö, Antti: Synthesis, Characterization and Properties of Cu(II)-, Mo(VI)- and U(VI) Complexes With Diaminotetraphenolate Ligands. (51 pp.) 2013
169. Kiljunen, Toni (Ed.): Chemistry and Physics at Low Temperatures. Book of Abstracts. (103 pp.) 2013
170. Hänninen, Mikko: Experimental and Computational Studies of Transition Metal Complexes with Polydentate Amino- and Aminophenolate Ligands: Synthesis, Structure, Reactivity and Magnetic Properties. (66 pp.) 2013
171. Antila, Liisa: Spectroscopic studies of electron transfer reactions at the photoactive electrode of dye-sensitized solar cells. (53 pp.) 2013
172. Kemppainen, Eeva: Mukaiyama-Michael reactions with α -substituted acroleins – a useful tool for the synthesis of the pectenotoxins and other natural product targets. (190 pp.) 2013
173. Virtanen, Suvi: Structural Studies Of Dielectric Polymer Nanocomposites. (49 pp.) 2013
174. Yliniemelä-Sipari, Sanna: Understanding The Structural Requirements for Optimal Hydrogen Bond Catalyzed Enolization – A Biomimetic Approach.(160 pp.) 2013
175. Leskinen, Mikko V: Remote β -functionalization of β' -keto esters (105 pp.) 2014
176. 12th European Conference on Research in Chemistry Education (ECRICE2014). Book of Abstracts. (166 pp.) 2014
177. Peuronen, Anssi: N-Monoalkylated DABCO-Based N-Donors as Versatile Building Blocks in Crystal Engineering and Supramolecular Chemistry. (54 pp.) 2014
178. Perämäki, Siiri: Method development for determination and recovery of rare earth elements from industrial fly ash. (88 pp.) 2014

DEPARTMENT OF CHEMISTRY, UNIVERSITY OF JYVÄSKYLÄ
RESEARCH REPORT SERIES

179. Chernyshev, Alexander, N.: Nitrogen-containing ligands and their platinum(IV) and gold(III) complexes: investigation and basicity and nucleophilicity, luminescence, and aurophilic interactions. (64 pp.) 2014
180. Lehto, Joni: Advanced Biorefinery Concepts Integrated to Chemical Pulping. (142 pp.) 2015
181. Tero, Tiia-Riikka: Tetramethoxy resorcinarenes as platforms for fluorescent and halogen bonding systems. (61 pp.) 2015
182. Löfman, Miika: Bile acid amides as components of microcrystalline organogels. (62 pp.) 2015
183. Selin, Jukka: Adsorption of softwood-derived organic material onto various fillers during papermaking. (169 pp.) 2015
184. Piisola, Antti: Challenges in the stereoselective synthesis of allylic alcohols. (210 pp.) 2015
185. Bonakdarzadeh, Pia: Supramolecular coordination polyhedra based on achiral and chiral pyridyl ligands: design, preparation, and characterization. (65 pp.) 2015
186. Vasko, Petra: Synthesis, characterization, and reactivity of heavier group 13 and 14 metallylenes and metalloid clusters: small molecule activation and more. (66 pp.) 2015
187. Topić, Filip: Structural Studies of Nano-sized Supramolecular Assemblies. (79 pp.) 2015
188. Mustalahti, Satu: Photodynamics Studies of Ligand-Protected Gold Nanoclusters by using Ultrafast Transient Infrared Spectroscopy. (58 pp.) 2015
189. Koivisto, Jaakko: Electronic and vibrational spectroscopic studies of gold-nanoclusters. (63pp.) 2015
190. Suhonen, Aku: Solid state conformational behavior and interactions of series of aromatic oligoamide foldamers. (68 pp.) 2016
191. Soikkeli, Ville: Hydrometallurgical recovery and leaching studies for selected valuable metals from fly ash samples by ultrasound-assisted extraction followed by ICP-OES determination. (107 pp.) 2016
192. XXXVIII Finnish NMR Symposium. Book of Abstracts. (51 pp.) 2016
193. Mäkelä, Toni: Ion Pair Recognition by Ditopic Crown Ether Based bis-Urea and Uranyl Salophen Receptors. (75 pp.) 2016
194. Lindholm-Lehto, Petra: Occurrence of pharmaceuticals in municipal wastewater treatment plants and receiving surface waters in Central and Southern Finland. (98 pp.) 2016
195. Härkönen, Ville: Computational and Theoretical studies on Lattice Thermal conductivity and Thermal properties of Silicon Clathrates (89 pp.) 2016
196. Tuokko, Sakari: Understanding selective reduction reactions with heterogeneous Pd and Pt: climbing out of the black box (85 pp.) 2016
197. Nuora, Piia: Monitapaustutkimus LUMA-Toimintaan liittyvissä oppimisympäristöissä tapahtuvista kemian oppimiskokemuksista (171 pp.) 2016

DEPARTMENT OF CHEMISTRY, UNIVERSITY OF JYVÄSKYLÄ
RESEARCH REPORT SERIES

198. Kumar, Hemanathan: Novel Concepts on The Recovery of By-Products from Alkaline Pulping (61 pp.) 2016
199. Arnedo-Sánchez, Leticia: Lanthanide and Transition Metal Complexes as Building Blocks for Supramolecular Functional Materials (227 pp.) 2016
200. Gell, Lars: Theoretical Investigations of Ligand Protected Silver Nanoclusters (134 pp.) 2016
201. Vaskuri, Juhani: Oppiennätyksistä opetussuunnitelman perusteisiin - lukion kemian kansallisen opetussuunnitelman kehittyminen Suomessa vuosina 1918-2016 (314 pp.) 2017
202. Lundell Jan, Kiljunen Toni (Eds.): 22nd Horizons in Hydrogen Bond Research. Book of Abstracts. (xx pp.) 2017
203. Turunen, Lotta: Design and construction of halogen-bonded capsules and cages. (xx pp.) 2017